2016

The Impact of Altered T Cell Receptor—Peptide-Major Histocompatibility Complex Interactions on Antigen Recognition and T Cell Function

Timothy T. Spear
Loyola University Chicago

LOYOLA UNIVERSITY CHICAGO

THE IMPACT OF ALTERED T CELL RECEPTOR—PEPTIDE-MAJOR HISTOCOMPATIBILITY COMPLEX INTERACTIONS ON ANTIGEN RECOGNITION AND T CELL FUNCTION

A DISSERTATION SUBMITTED TO

THE FACULTY OF THE GRADUATE SCHOOL

IN CANDIDACY FOR THE DEGREE OF

DOCTOR OF PHILOSOPHY

PROGRAM IN INTEGRATIVE CELL BIOLOGY

BY

TIMOTHY T. SPEAR

CHICAGO, IL

MAY 2016

ACKNOWLEDGEMENTS

I would like to thank Dr. Michael Nishimura for his continual guidance and support during my PhD training. His selfless mentorship and fervor for unique educational experiences is unparalleled. When I started my training, I never thought I would have the opportunity to do, see, and learn as much as I did, both inside and outside of the lab. His so-called “survival skills” I am sure will come in handy one day, if I ever learn to utilize them. I would also like to thank the members of the Nishimura lab past and present for both their assistance and constant source of entertainment. Specifically, Gina Scurti was invaluable, training me in numerous essential techniques for my project, including PBMC isolation, producer cell line generation, T cell transduction, immunomagnetic isolation, and functional assays. She also provided me with numerous lots of PBMC and TCR-transduced T cells as well as much needed advice. Sue Niccolai was also of huge help throughout my time in the lab and is the main reason why everything runs as smoothly as it does in our research group. Additionally, David Murray, Kendra Foley, and Erica Fleming were my partners in crime in the lab, continually offering their assistance, troubleshooting, and friendship.

Collaborations with Dr. Brian Baker and Dr. Hugo Rosen were instrumental in the development and execution of my dissertation studies. Dr. Lance Hellman, Timothy Riley, and Yuan Wang from the Baker lab were extremely helpful in contributing kinetic

and structural data. Dr. Rachel H. McMahan from the Rosen Lab contributed data regarding HCV-reactive T cell clones. I thank Drs. Baker and Rosen and the remaining members of my committee, Dr. Phong Le, Dr. Jose Guevara, and Dr. Stephanie Watkins, for their ongoing critical insight into my dissertation.

I would also like to thank the Integrative Cell Biology Program, the Graduate School, the MD/PhD Program led by Dr. Charles Hemenway and Dr. Andrew Dingwall, and the Stritch School of Medicine for their continual support in my educational training. Members of the Flow Cytometry Core Facility, especially Patricia Simms and Ashley Hess, were instrumental in the large amount of experimental design and data analysis that utilized flow cytometry. Statistical analysis was provided by Dr. Elizabeth Garrett-Mayer at the Medical University of South Carolina.

Funding for these studies was kindly provided by the National Cancer Institute of the National Institutes of Health. Grants P01 CA154778 (MIN) and F30 CA180731 (TTS) were of remarkable support. Lynn Walter was extremely helpful in applying for and managing our funding mechanisms.

I also owe a debt of gratitude to my parents Timothy and Sandra Spear as well as grandparents James and Mary Ellen Spear and John and Catherine Kinoff for their continual sacrifice, which provided me the opportunity for an advanced education. I thank my siblings Michael and Katherine for helping me maintain perspective on everything in life. I also thank my fiancée Elizabeth Santschi for always keeping me grounded and for your eternal patience. And to my new buddy, Niko, thank you for

always greeting me at the door when I come home, each time more excited than the last. Countless other friends, family, colleagues, and mentors over the years have all made an impact on my educational training and my life, and it has not gone without notice. Thank you.

TABLE OF CONTENTS

LIST OF TABLES

LIST OF FIGURES

LIST OF ABBREVIATIONS

^{o}C	Degrees Celsius
µl	Microliter
µg	Microgram
µM	Micromolar
2D	Two-dimensional
3D	Three-dimensional
ACT	Adoptive cell transfer
AF	Alexa Fluor
AICD	Activation induced cell death
ALL	Acute lymphoblastic leukemia
APC	Antigen presenting cell
APC	Allophycocyanin
BV	Brilliant Violet
C	Constant
CAIX	Carbonic anhydrase IX
CAR	Chimeric antigen receptor
CD	Circular dichroism
CD	Cluster of differentiation

CD8αβ	Full length CD8 heterodimer
CD8α'β'	Truncated CD8 heterodimer lacking intracellular lck-binding domain
CD34t	Truncated CD34 molecule lacking intracellular signaling domain
CDR	Complementarity determining region
CEA	Carcinoembryonic antigen
CLL	Chronic lymphocytic leukemia
CMV	Cytomegalovirus
CT	Computed tomography
CTA	Cancer-testis antigen
CTLA-4	Cytotoxic T-lymphocyte-associated protein 4
D	Diversity
DAA	Direct antiviral agent
DMEM	Dulbecco's Modified Eagle's Medium
DMSO	Dimethyl sulfoxide
DNA	Deoxyribose nucleic acid
DSF	Differential scanning fluorimetry
EBV	Epstein-Barr virus
ELISA	Enzyme-linked immunosorbent assay
ELISPOT	Enzyme-linked ImmunoSpot
EMEM	Eagle's Minimum Essential Medium
ER	Endoplasmic reticulum
Fab	Antigen binding fragment

FACS	Fluorescence-activated cell sorting
FBP	Folate binding protien
FBS	Fetal bovine serum
FITC	Fluorescein isothiocyanate
FLOCK	FLOw Clustering without K
FlowSOM	Self-Organizing Maps of Visualizing and Interpretation of Cytometry Data
FRET	Fluorescence resonance energy transfer
G	Gram
G418	Geneticin
GFP	Green fluorescent protein
gp	Glycoprotein
GVHD	Graft versus host disease
hAB	Human AB serum
HCC	Hepatocellular carcinoma
HCV	Hepatitis C virus
HCV1073 TCR	T cell receptor recognizing the Hepatitis C virus protein NS3:1073-1081 epitope
HCV1406 TCR	T cell receptor recognizing the Hepatitis C virus protein NS3:1406-1415 epitope
HIV	Human immunodeficiency virus
HLA	Human leukocyte antigen
HMW-MAA	High molecular weight melanoma associated antigen
HPV	Human papilloma virus

hr	Hour
HSV-tk	Herpes simplex virus thymidine kinase
iC9	Inducible caspase 9
ICOS	Inducible T cell costimulator
IFNα	Interferon-alpha
IFNγ	Interferon-gamma
IL-2	Interleukin-2
IL-4	Interleukin-4
IL-9	Interleukin-9
IL-17A	Interleukin-17A
IL-22	Interleukin-22
IMEM	Iscove's Modified Dulbecco's Medium
ImmPort	Immunology Database and Analysis Portal
IRB	Institutional review board
ITAM	Immunoreceptor tyrosin-based activation motif
ITIM	Immunoreceptor tyrosin-based inhibitory motif
J	Joining
J76	Jurkat76 cell
Kb	Kilobase, one thousand base pairs
KDR	Kinase insert domain receptor
LAK	Lymphokine activated killer
LB	Luria-Bertani

Lck	Lymphocyte-specific protein tyrosine kinase
LCL	Lymphoblastoid cell line
LTR	Long terminal repeats
M	Molar
mAb	Monoclonal antibody
MART-1	Melanoma antigen recognized by T cells 1
MDSC	Myeloderived suppressor cell
MHC	Major histocompatibility complex
min	Minute
mg	Milligram
mL	Milliliter
mM	Millimolar
MolMLV	Moloney murine leukemia virus
neo^r	Neomycin resistance gene
ng	Nanogram
nM	Nanomolar
NHEJ	Nonhomologous end joining
NHL	Non-Hodgkin's lymphoma
NK	Natural killer
NKG2D	Natural killer group 2, member D
NKp30	Natural killer cell p30-related protein
NS3	Nonstructural protein 3

PBL	Peripheral blood lymphocyte
PBMC	Peripheral blood mononuclear cell
PBS	Phosphate buffered saline
PBSA	Phosphate buffered saline with bovine serum albumin
PCR	Polymerase chain reaction
PD-1	Programmed cell death 1
PDB	Protein data bank
PE	Phycoerythrin
PEG	Percutaneous endoscopic gastrostomy
PerCP	Peridinin chlorophyll protein
pM	Picomolar
PMA	Phorbol 12-myristate 13-acetate
pMHC	Peptide-major histocompatibility complex
PSM	Probability state modeling
RAV	Resistance associated variants
RBV	Ribavirin
RCC	Renal cell carcinoma
REP	Rapid expansion protocol
rhIL-2	Recombinant human interleukin-2
rhIL-15	Recombinant human interleukin-15
RPMI	Roswell Park Memorial Institute
RS	Recombination signal

RT	Room temperature
SA	Splice acceptor
SAMEN	MolMLV-based *env* Splice acceptor-containing retroviral vector
scFv	Single-chain variable fragment
SD	Splice donor
sec	Second
siRNA	small interfering ribonucleic acid
SPADE	Spanning-tree Progression Analysis of Density-Normalized Events
SPICE	Simplified Presentation of Incredibly Complex Events
SPR	Surface plasmon resonance
SRL	Shared resource laboratory
SVR	Sustained viral response
TAP	Transporter associated with antigen processing
TCR	T cell receptor
TIL	Tumor infiltrating lymphocyte
TNFα	Tumor necrosis factor-alpha
t-SNE	t-distributed stochastic neighbor embedding
Tyro	Tyrosinase
V	Variable
VEGF	Vascular endothelial growth factor
VEGFR	Vascular endothelial growth factor receptor
VSV	Vesicular stomatitis virus

v/v	Volume by volume
WT	Wildtype
w/v	Weight by volume
ZAP70	Zeta-chain-associated protein kinase 70

ABSTRACT

Adoptive cell transfer (ACT) using T cell receptor (TCR) gene-modified T cells is an exciting and rapidly evolving field. Numerous basic science and clinical studies have demonstrated various levels of feasibility, safety, and efficacy using TCR-engineered T cells to treat cancer and viral infections. Although evidence suggests their use can be effective, how effective and how to improve these therapeutics are still remaining questions.

Because TCR affinity is thought to play the central role in defining T cell specificity and sensitivity, the field has adopted the theory that creating affinity-enhanced TCRs creates better functioning T cells; but, enhanced affinity creates the opportunity for cross-reactivity. TCR cross-reactivity against off-tumor/on-target or off-target antigens has caused serious adverse events, including death, in recent clinical trials using high affinity TCR-engineered T cells. However, the use cross-reactive TCRs could offer therapeutic benefit for diseases where targeted antigens are susceptible to mutation via genomic instability.

The proper choice and design of therapeutic TCRs mandate a broader understanding of the basic principles governing antigen recognition by a T cell. In light of what is known about TCRs and T cell function, numerous factors still need to be addressed. These include: (1) what kinetic or cellular parameters are most important in

facilitating antigen recognition; (2) how is T cell function affected by alterations in TCR-peptide-major histocompatibility complex (pMHC) interactions; (3) how can we structurally rationalize the cross-reactivity of a TCR; and (4) how might the cross-reactivity of a TCR augment or inhibit therapeutic efficacy. These biologic questions addressed in this dissertation utilize traditional and novel approaches to characterize TCR gene-modified T cells harboring an HLA-A2-restricted TCR cross-reactive against naturally occurring mutant HCV NS3:1406-1415 epitopes, serving as a model to study antigen recognition.

Overall, contrary to what is generally accepted in the field, we found that TCR-pMHC affinity is not necessarily the most important factor dictating antigen recognition. Other cellular parameters, including ligand density, TCR density, and co-receptor signaling greatly influenced recognition of altered pMHC ligands. Modifying any of these parameters changed functional responses, sometimes independent of affinity. Additionally, we found that the field's interpretation of antigen recognition may be narrowed and misguided when evaluation of T cell function is limited to a single cytokine. Functional phenotypes by seven-parameter flow cytometry revealed that T cell functional profiles are more complex than were previously believed. Evaluation of a single functional phenotype, such as IFNγ, did not accurately reflect the functional behavior of a T cell culture. Combining functional studies with structural analysis of the TCR-pMHC interface helps bring clarity to these unexpected results.

In summary, we have established a new working model highlighting the previously unappreciated and complex relationship between kinetic, cellular, and

structural parameters governing antigen recognition and T cell function. Together, our data suggest the field is oversimplifying the biology of T cells and the fundamentals of antigen recognition. This enhanced understanding will not only help steer rational, structure-guided design of TCRs to generate better functioning T cells for ACT, but will also impact the way in which we study other immune cell and receptor types, approach epitope discovery, and evaluate vaccine design. In this way, we have provided a new foundation in which to evaluate the design and implementation of novel immunotherapies.

CHAPTER ONE

REVIEW OF LITERATURE

Introduction

Immunotherapy is one of the most promising and innovative approaches to treat cancer, viral infections, and other immune-modulated diseases. Adoptive immunotherapy using gene-modified T cells is an exciting and rapidly evolving field. Exploiting knowledge of basic T cell biology and immune cell receptors has fostered innovative approaches to modify immune cell function. Novel and more efficient technologies have been developed to redirect T cell specificity by introducing designed receptors. The ability to engineer T cells to manifest desired phenotypes and functions is now a thrilling reality.

TCR-transduced T cells offer the ability to target a wide variety of self and nonself targets through the normal biology of a T cell. But to produce an optimally functioning gene-modified T cell, a firm understanding of the basic principles governing antigen recognition is required. Yet, many diseases targeted by such immunotherapies are genetically unstable, leading to immune escape. Investigation into how a T cell might be limited by changes in its target, affecting therapeutic efficacy, is also essential.

A potential solution to immune escape by antigen mutation is the use of cross-reactive TCRs given their ability to recognize a spectrum of related antigens. But the

potential for unwanted off-target reactivity, leading to adverse events in the clinic, warrants a closer examination into what factors govern T cell specificity. Conventionally, antigen recognition is thought to be dictated by the affinity between the TCR-pMHC interaction [1], but recent evidence suggests traditionally measured affinity interactions may not fully explain the complex relationship between T cell specificity and T cell reactivity [2]. Furthermore, current strategies used to randomly enhance the affinity of TCRs, hoping to improve their therapeutic efficacy [3, 4], may be too blinded. Thus, a greater understanding of antigen recognition by TCR-gene modified T cells may help lay the groundwork for more optimal therapeutic strategies.

The studies discussed in this dissertation explore structure-function relationships between a T cell receptor (TCR) and its peptide major histocompatibility complex (pMHC) ligand using hepatitis C virus (HCV) mutant epitopes as a model for genomic instability. A more complete appreciation of how altered TCR-pMHC affinity influences antigen recognition in light of genomic instability may aid in the rational design of TCRs for safer and more effective TCR-based immunotherapies.

TCR-Mediated Antigen Recognition

T cells play a central role in mediating cellular immunity. These multi-functional effector cells protect us from disease throughout our entire lives with their ability to recognize bacterial, viral, and cancer-associated antigens. The specificity of a T cell is mediated by the TCR, a cell surface heterodimer that facilitates target cell recognition [5]. There are two types of T cells, which can be distinguished by the TCRs expressed on

their surface. αβ T cells express a highly variable αβTCR whereas γδ T cells express a highly conserved γδTCR [6, 7]. TCRs mediate recognition of foreign or self-peptides bound to MHC molecule displayed by other cells [8-13]. This interaction between the TCR and its pMHC ligand plays a crucial role in determining the specificity and reactivity of an individual T cell. For the purpose of these studies, we will focus on αβ T cells/TCRs.

Cell surface expression of the TCR requires its association with the CD3 complex [14-19]. Upon TCR-pMHC engagement, a cascade begins with the initiation of a series of signaling events starting with the phosphorylation of ITAM's on the CD3 ζ chain, leading to full T cell activation and function [20]. The CD4 and CD8 co-receptors play a critical role in T cell activation and function by enhancing the binding of the TCR to the pMHC [21-24] and promoting the signaling by localizing lck to the TCR/CD3 complex [21, 25, 26] (Fig. 1). Consequently, a specific TCR-pMHC interaction (thought to be primarily driven by affinity) translates into a signaling cascade to facilitate functional recognition of the presence of pathogens or transformed cells. This complex process ultimately leads to target cell killing, or the secretion of pro-inflammatory cytokines that recruit and support other immune effectors, described in a later section. There are many important factors involved in antigen recognition and T cell function which should be thoroughly evaluated when considering how to generate the most effective anti-tumor T cells by introducing a foreign TCR.

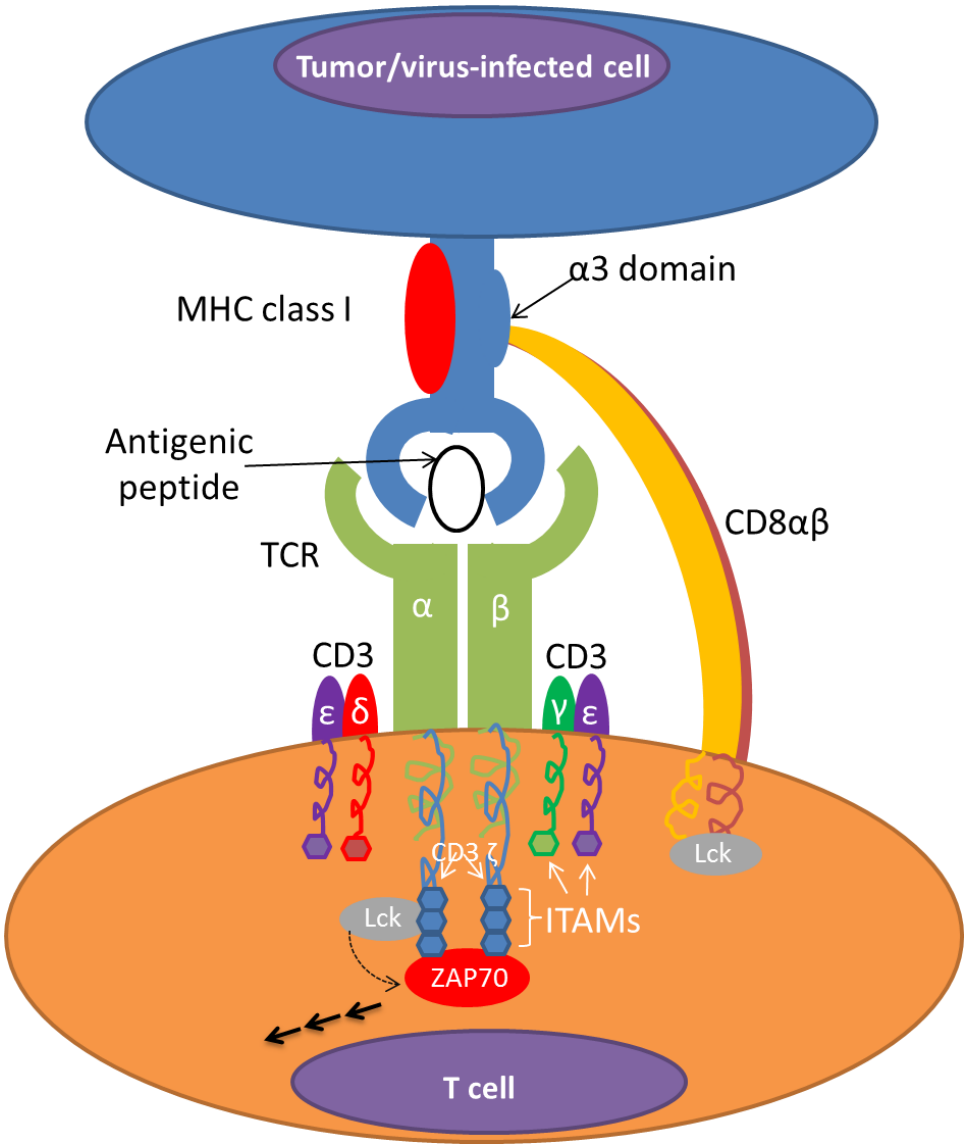

Figure 1. TCR-mediated target cell recognition. Depicted is the structure of an MHC class I-restricted TCR interacting with a tumor or virus-infected cell. TCR α and β chains are specific to both MHC and presented antigenic peptide. The TCR complexes with various CD3 components on the cell surface, and the CD8 co-receptor stabilizes the TCR-pMHC interaction while recruiting lck to facilitate TCR signaling. ITAMs are denoted as colored octagons. Lck = lymphocyte-specific protein tyrosine kinase; ZAP70 = zeta-chain-associated protein kinase 70; P=phosphate group; Black arrows=downstream signaling.

TCR Diversity

All higher vertebrates maintain a large and diverse repertoire of T cells capable of recognizing most of the pathogens we will ever encounter. This tremendous diversity is due to the extreme variability of the TCR expressed by each T cell. Each TCR chain consists of a variable (V) gene segment, a joining (J) region, a diversity (D) region in the β chain only, and a constant (C) region [27]. In the thymus, the different TCR α and β chains are generated randomly by germline rearrangements which bring together one of many Vα genes with one of many Jα regions for the TCRα chain or one of many Vβ genes, one of the two Dβ regions, and one of the thirteen Jβ regions for the TCRβ chain [28, 29]. The numerous arrangements of elements in each TCR chain together with the combinations of α and β chain pairing contribute to some of the TCR diversity observed in nature [7]. However, the majority of the diversity in TCRs expressed by mature T cell results from the addition and deletion of bases at the Vα-Jα, Vβ-Dβ, and, Dβ-Jβ junctions (known as N-region substitutions) which occurs during TCR gene rearrangement [7]. This hypervariable region of the TCR α chain or TCR β chain is the third complementarity determining region (CDR3). The TCR α and β chain CDR3s are considered to be the most important regions of the TCR for antigen recognition due to their length and sequence diversity. This combinatorial rearrangement of the TCR gene segments combined with N-region substitutions provides a theoretical estimate for 10^{15} different αβ TCRs in the T cell repertoire [27].

The random TCR rearrangements that lead to such a large potential TCR repertoire suggests we should have T cell immunity against most pathogenic peptides presented by MHC as well as self and nonself peptides presented by allo-MHC. Positive selection enables developing thymocytes expressing TCRs capable of binding antigen/self-MHC molecules in the thymus with the "correct" affinity to be protected from programmed cell death (positive selection). These positively selected T cells then complete T cell development resulting in a pool of mature T cells restricted only by self-MHC. In contrast, thymocytes expressing TCRs whose affinity for the host pMHC is too low (death by neglect) or too high (negative selection) are not protected from programmed cell death and do not complete T cell development, eliminating them from the pool of mature T cells [30]. The net effect of thymic selection is to save "immunologic space" for T cells that are beneficial to the host by eliminating T cells that are not self-MHC restricted and those that have the potential for autoimmunity. These are important factors to consider for TCR gene transfer studies given that most human tumor reactive T cells recognize normal, non-mutated self-antigens [31-33].

Given the extreme TCR diversity, two critical questions initially raised by the field are: (1) do we have a choice in TCRs that target a single pMHC, and (2) if we have a choice, does it matter which TCR we select to use for a given target. Early studies aimed to address these questions focused on the diversity of the TCR repertoire against a single target pMHC by testing the concept of restricted TCR V gene usage [34-39]. Because of clonal selection theory, it would make sense that our immune system would

select for one or a limited number of TCR rearrangements that “best” recognize a given peptide [40]. Using TCRs reactive against melanoma antigen MART-1 as a model, multiple studies found that the TCR diversity among MART-1 reactive T cell clones to be very high [35, 36]. More importantly, individual MART-1-reactive T cells clones recognized different subsets a panel of peptides with homology to the MART-1 peptide [41]. Furthermore, peptides recognized commonly by the different MART-1 reactive T cell clones were recognized by each clone with different efficiencies [41]. Diversity of TCR V gene usage is not a property unique to MART-1-reactive T cells [42]. Such findings indicate that each TCR can recognize a single antigen differently. Ultimately, how a T cell recognizes its target might make a difference in the effectiveness and the safety (cross-reactivity) of the resulting TCR gene-modified T cells *in vivo*.

TCR Affinity

TCR affinity has been traditionally thought to play a significant, if not the most important, role in determining the sensitivity of a T cell to antigen recognition[1] . Generally, the affinity of TCR for pMHC is lower than antibody/antigen interactions and generally occur between 1-100 μM [11, 30, 43]. As discussed earlier, TCRs have different affinities for the pMHC, the range of which is tightly regulated by thymic selection. There are several important facts to consider regarding the relationship between TCR affinity and T cell function. Contrary to the predictions of thymic selection, T cells reactive with self-antigens are not always deleted in the thymus since many are found in the periphery. In both animal and human systems, self-reactive T cells can be induced

to mediate tumor rejection and in some cases, autoimmunity. These T cells are generally CD8-dependent meaning they express TCRs with relatively low affinity for pMHC. Their anti-self-reactivity is generally limited until their physiology or the host environment is altered. Another key observation is that T cells derived from a single T cell clone can have varied T cell function [44]. Under certain circumstances, T cells can be very antigen reactive whereas in other circumstances they are weakly antigen reactive [44, 45]. Therefore, it is likely that the biology of a given T cell can dictate function and TCR affinity plays a less important role than previously thought.

There are several mechanisms, which can explain how the function of a T cell is influenced by its environment, regardless of the affinity of the TCR-pMHC interaction. It is well known that T cells become refractory to immune function resulting from the level of immune suppression in the tumor-bearing host [46-52]. Furthermore, reactive oxygen and nitrogen species in the tumor-bearing host can promote T cell death [53-58]. Interesting, none of these suppressive mechanisms require changes in TCR affinity to reduce immune function of a T cell. However, there are examples of immune suppression mechanisms that do seem to impact on TCR affinity. We know that one key role of CD8 is to stabilize the TCR-pMHC complex. It has been observed that the spatial relationship of the TCR and CD8 on the surface of a T cell can vary leading to differences in the relative stability of the TCR-pMHC complex [59]. Similarly, the ratio of the high affinity form of CD8 (CD8αβ) versus the low affinity form of CD8 (CD8αα) can vary on each T cell expressing the same TCR [60]. CD8αβ induces a higher functional avidity

than CD8αα, which translates to higher anti-tumor activity. Finally, myeloid-derived suppressor cells (MDSCs) have been shown to modify the TCR proteins by nitration of tyrosine residues leading to weaker binding to pMHC [61]. In all these suppressive mechanisms, the function of a T cell expressing a high affinity TCR could be as easily overcome as the function of a T cell expressing a low affinity TCR. The studies described in this dissertation aim to help shed light on this inconsistency.

T Cell Signaling and Function

As mentioned earlier, engagement of the TCR/CD3 complex with its pMHC ligand at the immunological synapse initiates a radiating and branching network of signaling cascades leading to T cell activation and function [62]. Precisely how the engagement of the TCR with its pMHC target tips the signaling balance in favor of T cell activation is still a matter of debate. Traditionally, TCR engagement is thought to promote lck-dependent phosphorylation of ITAMs of CD3ζ chains, resulting in recruitment and activation of ζ-chain associated protein 70 (ZAP70), which induces the assembly of the signal diversification and regulation components [63] (Fig. 1). Subsequent signaling events facilitate the hallmarks of T cell activation, including Ca^{2+} release, actin polymerization, integrin activation, proliferation, mobilization of transcription factors, cytokine secretion, and degranulation [62].

Ultimately, signal propagation results in a functional response, which can vary depending on the subset of T cell activated. When a naïve T cell is activated by an antigen presenting cell (APC), they acquire effector functions while differentiating into

various subtypes. Differentiation is often influenced by the cocktail of cytokines present in the milieu during antigen presentation [64]. These T cell subsets are subsequently identified by cell surface markers, transcription factors, and cytokine secretion profiles.

A well-characterized example of this is the Th1/Th2 dichotomy, where these $CD4^+$ T helper cell subpopulations are distinguished by their cytokine profiles. Th1 cells express transcription factor T-bet, produce mainly IFNγ, IL-2, and TNFα, and have functional importance in pro-inflammatory cell-mediated immunity, delayed-type hypersensitivity, and immune responses against certain protozoa. Conversely, Th2 cells express transcription factor GATA-3, secrete IL-4, -5, -6, -10, and -13, and promote non-inflammatory immediate immune responses and are essential in promoting B cell-mediate immunity. It is thought that these developmental routes and cytokine profiles of Th1 and Th2 are mutually antagonistic, giving rise to the model of polarization of the immune response [64].

Interestingly, a growing spectrum of additional T cell subset lineages has been defined by transcription factor expression and signature cytokine secretion. These include, but are not limited to, Th17 (ROR-γt$^+$; IL-17A and -22 secreting), Treg (Foxp3$^{+;}$ IL-10 and TGF-β secreting), and Th9 (IL-9 secreting) subsets [64]. $CD8^+$ cytotoxic lymphocytes (Tc) are similarly categorized into subsets based on cytokine profiles (Tc1, Tc2, Tc17, etc.). These $CD8^+$ subsets are hallmarked by cell-mediated killing by perforin/granzyme-mediated or Fas/Fas-ligand-mediated apoptosis. In this way, the

field generally accepts that T cells are functionally restricted by the subset into which they differentiate [64].

The impact of TCR-pMHC affinity on TCR signaling remains debated. One argument, the kinetic proofreading model [65], proposes that the TCR signaling cascade serves as a biochemical clock. This models predicts that very slight discrepancies in ligand engagement can cause time delays between successive steps of activation, resulting in a distinct kinetic attenuation. Because of the intricate radiation and branching of downstream pathways in TCR signaling, kinetic attenuation can produce different ratios of downstream signaling molecules, leading to substantially different cellular functions. Factors that influence this biochemical clock (unique to a given TCR-pMHC interaction) are thought to include TCR-pMHC dissociation rates, TCR clustering, and co-receptor accumulation in the immunological synapse [65, 66].

Overall, TCRs exhibit an enormous breadth of diversity, allowing for immune surveillance over countless self and nonself targets. Antigen recognition dictated by TCR specificity to its pMHC ligand initiates a complex, and not entirely understood, signaling pathway resulting in a host of cellular responses. Although TCR affinity plays a major role in dictating its specificity, the effect of slight alterations in TCR-pMHC interactions is not always reconciled with changes in T cell reactivity. An enhanced understanding of basic T cell biology will ultimately help improve the design of TCR-based therapeutics.

Adoptive Cell Therapy

In light of T cell-mediated immune surveillance, unfortunately most viruses and tumors have developed various mechanisms to evade the host immune system. Immune evasion can lead to weak or ineffective immune responses, resulting in chronic infections or malignancies. To address ineffective immune responses towards cancer, many therapeutic approaches are aimed at optimizing the anti-tumor potential of T cells. Immune-modulating strategies include directly promoting a T cell immune response by administration of IL-2 which is used in treatment against melanoma and renal cell carcinoma [67]. Conversely, other therapies lift restraints on T cell activation, known as checkpoint blockade. These tactics include targeting inhibitory receptors CTLA-4 or PD-1 with antagonist antibodies ipilimumab [68-70] and pembrolizumab [71, 72], respectively, which are currently approved to treat melanoma. Despite their recent success, cytokine administration and checkpoint blockade are not 100% effective; thus, combinatorial or novel therapeutic strategies need to be evaluated to improve cancer and viral immunotherapies.

One such novel immunotherapy known as adoptive cell transfer (ACT) involves the transfer of *ex vivo* activated and expanded antigen-reactive T cells or genetic modification to redirect their specificity prior to transfer. ACT gained its first success using lymphokine activated killer (LAK) cells [73] and later tumor infiltrating lymphocytes (TIL) [74, 75] or antigen stimulated autologous peripheral blood lymphocytes (PBL) [76-79]. The most promising of these early approaches utilized TIL

following harvest from tumor and short term *ex vivo* expansion and were pioneered by the Rosenberg group at the Surgery Branch of the National Cancer Institute. Animal models and studies in patients with melanoma demonstrated that TIL maintained tumor reactivity *in vitro*, having the capability to lyse tumor cells and secrete cytokines, such as IL-2, IFNγ, and TNFα [80, 81]. These cells also mediated objective clinical responses when grown *ex vivo* and infused back into patients [82].

Despite these promising but preliminary clinical results, for a variety of reasons TIL has not been a universal approach for ACT. For example, TIL production is a logistically and technically demanding process. Oftentimes primary tumors harboring TIL are previously resected as part of cancer treatment or are inaccessible depending on the tumor type and location. Additionally, the time it takes or the inability to expand available TIL to therapeutic numbers calls for an alternative cell-based approach for treating cancer or chronic viral infections [83, 84].

Recent technological advances have facilitated efficient expression of transgenes in T cells allowing for normal circulating PBL to be redirected targeting desired antigens. Genetically engineering T cells with chimeric antigen receptors (CARs), TCRs, and other receptor types have been shown to successfully redirect the specificity of T cells [85]. However, the ability to redirect a T cell to recognize a specific antigen is not enough to guarantee an effective immunotherapy. Antigen recognition needs to be coupled with efforts to ensure a T cell's functionality is specific, limiting off-target or off-tumor recognition. T cells should also be able to functionally persist long-term and be able to

traffic to and accumulate at the target site. Additionally, optimal gene-modified T cells should exhibit robust, multi-functional immune responses and resist mechanisms of anergy, exhaustion and immunosuppression. They should also be amenable to deletion on demand to diminish potential toxicity issues. While T cell engineering strategies show promise at the bench and have shown some clinical success at the bedside, many aspects of this type of therapy must be resolved before these effectors are safe and effective enough to become the standard of care.

CAR Gene Therapy

CAR design. CARs, the first class of antigen receptors we will discuss, have been widely examined for the use of redirecting T cell specificity. A CAR is simply described as combining the antigen binding capability of an antibody with the intracellular signaling-associated component of a TCR (Fig. 2). This unique juxtaposition allows for high affinity, three-dimensional epitope recognition by an immunoglobulin to be linked to the helper or effector responses of a T cell [86]. Specifically, the extracellular antigen-recognizing domain is generally derived from the antigen-binding fragment (Fab) of mouse monoclonal antibodies (mAbs) that have high affinity for specific antigens. Unlike the normal structure of the Fab fragment of a mAb, the Fab fragment in a CAR exists as a single-chain variable fragment (scFv) [86]. The scFv is linked via hinge and transmembrane domains to an intracellular signaling domain. This couples antigen recognition to immune cell signal transduction by phosphorylation of immunoreceptor tyrosine-based activation motifs (ITAMs). The first CAR, described by Eshhar and

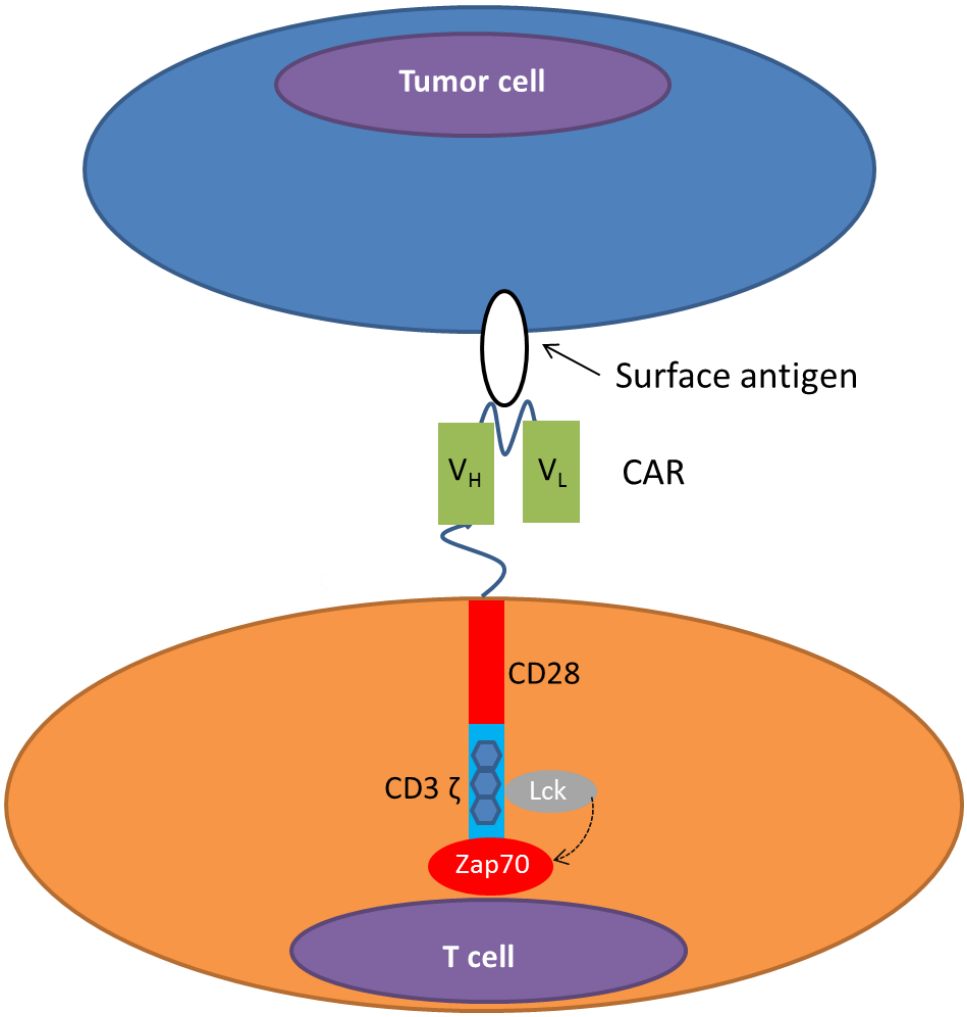

Figure 2. CAR-mediated target cell recognition. Structure of a 2nd generation CAR interacting with a tumor cell. A CAR consists of a single-chain variable fragment (scFv) composed of variable light (V_L) and heavy (V_H) chains linked via hinge, transmembrane domains, and intracellular signaling domains containing at least the γ chain of the FcR or the ζ chain of the TCR/CD3 complex. Specificity of the scFv region dictates MHC-independent recognition of a surface antigen. ITAMs of CD3ζ are denoted in blue octagons.

colleagues, linked the scFv to the signaling components of the FcRγ chain [87]. Subsequent CARs, however, have replaced FcRγ with ζ chain of the TCR/CD3 complex [88] to enhance signaling potential as the CD3ζ signaling domain contains three ITAMs as opposed to FcRγ's single ITAM. Overall, CARs' structural configuration allows for essentially any mAb to be engineered into a CAR. For targets where generating conventional antibodies in mice or other species is difficult, other techniques, including phage display, have been useful in generating the antigen-binding portion of the CAR [89, 90].

The use of a mAb as a ligand receptor facilitates recognition of intact proteins, carbohydrates, and lipids, alleviating the need for target antigens to be processed and presented by MHC molecules [86]. This would allow for CAR-mediated target recognition despite HLA downregulation or aberrant antigen processing mechanisms. Non-MHC-restriction also allows CAR to be used in patients of all HLA types [91]. This provides a distinct advantage compared to TCR-engineered T cells, which will be discussed in a later section. CAR function is also independent of many of the signaling molecules or co-receptors required for TCR signaling and do not require association with the CD3 complex for T cell activation and function [92]. As such, CARs contain all the minimal elements necessary to bind antigen and activate the T cell. Additionally, as a single chain construct, CAR are compact in relatively small vectors allowing it easy to make high titer virus for transduction. Furthermore, single chain CARs are not subject to

chain pairing competition or mispairing, unlike when introducing exogenous TCRs, described later [93].

However, there are some limitations using CAR-engineered T cells [94]. For example, CARs target surface antigens, rendering them ineffective against any intracellular target that would otherwise be processed and presented by MHC. Also, the mAb-antigen interaction is much stronger than a TCR-antigen interaction, which may negatively impact T cell function [95]. Additionally, used of murine-derived scFv cause concern for potential immunogenicity of these chimeric receptors [96], although efforts to reduce immunogenicity have been used by humanizing murine-derived scFv or generating scFv from human scFv phage display libraries [97]. Overall, CARs offer a unique approach to re-direct the specificity of T cells combining the antigen recognition capabilities of an antibody with T cell signaling components.

Generations of CARs. Over time, the design of CARs has been refined to provide better antigen recognition and a more efficient transfer of cellular signaling for T cell function and persistence. As mentioned previously, the signaling domain of FcRγ was swapped with that of CD3ζ because CD3ζ included a greater number of ITAMs (Fig. 3) leading to enhanced T cell function [88]. Additionally, the single chain antibody can be substituted for other receptors or a ligand of a receptor expressed on tumor cells. Such approaches include substituting the scFv region of a CAR for heregluin (a ligand for Her3 or Her4 receptors) [98], VEGF (anti-VEGFR2) [99], NKp30 (targeting B7-H6) [100] or the

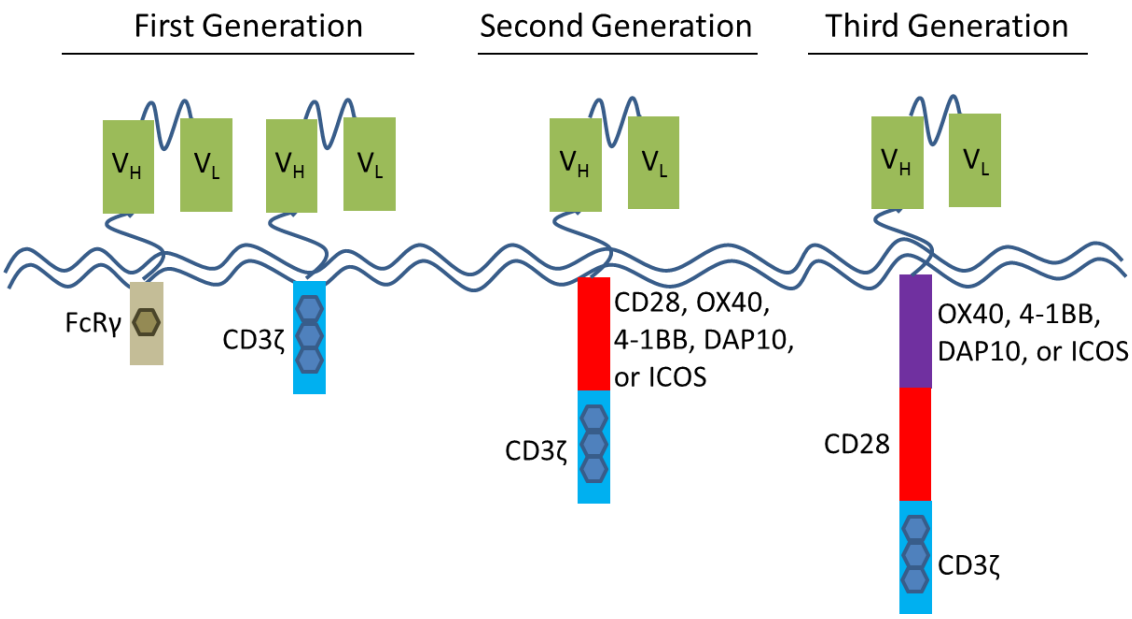

Figure 3. Generations of CARs. Comparison of co-stimulatory domains included in first (left), second (middle), or third (right) generation of CARs. ITAMs are denoted as colored octagons.

NKG2D receptor [101-103]. Moreover, multiple signaling domains have been added to the CD3ζ or FcRγ domains to augment activation and co-stimulation mimicking immunologic signal 2 during physiologic T cell activation [104]. Addition of co-stimulatory domains has led to subsequent "generations" of CARs.

"Second generation" CARs (Fig. 3) utilize one additional cytoplasmic domain of a co-stimulatory receptor, such as CD28, 4-1BB, DAP10, OX40, or ICOS, providing greater strength of signaling and persistence to the T cells [51, 105-117]. For example, one study investigating the requirements of CAR signaling cassettes found that in a mouse CEA^+ colorectal tumor xenograft model, CEA CAR-engineered T cells containing both CD3ζ and CD28 enhanced proliferation and IFNγ secretion compared to CD3ζ-only containing CARs [106]. The presence of CD28 was also required for efficient IL-2 secretion. Additionally, one group found that CD19-specific CARs containing CD3ζ and co-stimulatory cassette 4-1BB provided enhanced anti-leukemic efficacy and prolonged survival in tumor bearing mice compared to CD3ζ- or CD3ζ/CD28-containing CARs [113]. Together, these data suggest that the addition of co-stimulatory cassettes, including CD28 and 4-1BB, is required for complete T cell activation and that second generation CARs may provide enhanced therapeutic benefit.

A third generation of CARs (Fig. 3) were also developed using two co-stimulatory domains with an activating domain, conferring an even greater potency to redirected T cells [51, 115, 117-121]. For example, use of an ERBB2 CAR containing 4-1BB, CD28, and CD3ζ signaling moieties exhibited greater transgene persistence, increased cytokine

secretion, and enhanced lytic activity *in vitro* compared to ERBB2 CARs containing only CD3ζ and CD28 signaling cassettes [117]. Moreover, the third generation CAR better suppressed tumor growth in a xenogeneic mouse model compared to the second generation CAR. In light of enhanced performance by third generation CARs, it is unclear whether such strong co-stimulation would always be advantageous. One clinical report highlighting this point used a third generation trastuzumab-based CAR containing CD3ζ, CD28, and 4-1BB signaling moieties. Administration of anti-Her-2 third generation CAR-transduced autologous T cells was lethal in one patient after cytokine storm and fatal respiratory distress due to recognition of low levels of Her-2 on lung epithelia [122]. Thus, optimization of how many and which types of signaling domains included in CARs are necessary. Only then can we determine which combination is best for augmenting activation, sustained function and survival while minimizing anergy, premature death, and rapid exhaustion. Additionally, further efforts examining how antigen location and density, as well as CAR binding moiety, affinity, and sensitivity affect it T cell function may also optimize CAR design.

CAR targets. The first clinical trials using CARs targeted folate binding protein (FBP) for patients with ovarian cancer [123] and carbonic anhydrase IX (CAIX) for patients with renal cell carcinoma (RCC) [124]. Both CARs were first generation containing the FcRγ signaling domain. In both of these trials, no objective clinical responses were seen, nor were the gene-modified T cells able to persist long term. However, the potential for adverse events using CAR therapy was first recorded. In the

trial targeting $CAIX^+$ RCC, the phenomenon described as on-target/off-tumor effects was clearly evident. Patients treated with the CAIX CAR gene-modified T cells experienced grade 2-4 liver toxicity because the transduced cells recognized CAIX antigen expressed on the epithelial cells of the bile duct [124]. These results indicated administration of CAR T cells was feasible but could have unwanted off-tumor effects.

As subsequent generations of CARs were developed and more specific CAR targets were identified, we observed greater clinical success using CARs. Efforts targeting the pan-B cell antigen CD19 are the best examples of the proof-of-concept for CAR therapy. Initial trials targeting CD19-associated with relapsed indolent non-Hodgkin's lymphomas (NHL) and chronic lymphocytic leukemia (CLL) [125-131] demonstrated the safety of CAR T cells and modest clinical benefit. Later, patients with B cell acute lymphoblastic leukemia (B-ALL) receiving CD19-targeted CAR T cell treatment resulted in positive clinical outcomes with robust anti-tumor efficacy in two independent trials [132, 133].

The success of CD19-targeting CARs has relied on CD19's near universal expression on B cell malignancies and its limited expression on B cells. Its absence on bone marrow stem cells also limits off-target potential. Outcomes from this CD19 model additionally provided the practical limitations of initial CAR design and fostered the development of subsequent generations of CARs. Recently, a clinical trial using a second generation CD19-reactive CAR treated both children and young adults with chemotherapy-resistant B-precursor acute lymphoblastic leukemia [134]. In this trial,

CD19 CARs exhibited potent anti-leukemic activity and all grade 3 and 4 toxicities were reversible, suggesting second generation CARs can be relatively safe and effective. Other studies, however, have seen serious neurotoxicity associated with administration of CD19 CAR T cells [135], highlighting the remaining challenges in maximizing both the efficacy and safety with the use of CARs.

Although less serious than aforementioned on-target/off-tumor events, another drawback of the highly effective CD19 CAR campaign targeting B cell malignancies is the prolonged elimination of normal B lymphocytes and, thus, impairment of humoral immunity [125, 128, 130]. Although this can be mitigated by intravenous administration of gammaglobulin, B cell aplasia and hypogammaglobulinemia should still be recognized as on-target adverse events.

While CD19-targeted B cell malignancies have been the poster child advocating for CAR therapy, it is important to acknowledge another CAR target that has exhibited mixed clinical results. As mentioned earlier, the use of a third generation CAR based on the widely used mAb trastuzumab targeting Her-2 induced respiratory distress resulting in death in one treated patient with metastatic colon cancer [122]. It was discovered that low level Her-2 expression on normal lung epithelia caused this fatal side effect, characterized as a much more serious on-target/off-tumor adverse event than B cell aplasia. With this is mind, a modified CAR-based approach targeting Her-2 led to a more successful recent trial [136]. In this report, a dose-escalation study using a second-generation Her-2-specific CAR with a different scFv was used in patients with

recurrent/refractory Her-2^{+} sarcomas. This study also differed in that it did not use co-administration of high-dose IL-2 or lymphodepleting chemotherapy prior to transfusion. Transduced cells persisted for 6 weeks and trafficked to tumor sites without any evident toxicities. Some patients even exhibited stable disease or partial response. The stark contrast between these two trials highlights the importance of mAb and co-stimulatory cassette selection, target distribution, and host conditioning can have on the positive and negative outcomes in CAR clinical trials.

A wide variety of other CARs have been designed to target an array of antigens showing promise as potential cancer immunotherapies. Other targets evaluated *in vitro* and *in vivo* include but are not limited to EGFRvIII [137] for glioblastoma, GD2 [138, 139] for neuroblastoma, GD3 [140, 141], MAGE-1 [142], and HMW-MAA [143] for melanoma , CD20 [115, 119, 144-147], CD23 [148], CD30 [149-151] and others for hematologic malignancies, PSMA [107, 152] for prostate cancer, MUC-1 [120], Her-2 [19, 153], and CEA [154-156] for breast cancer, EGP-40 [157] for colorectal cancer, VEGF-R2 [99, 158] and KDR [159] for tumor neovasculature, and MUC16 [160] for ovarian cancer. Table 1 lists a sampling of active clinical trials using CARs and their respective targets.

CAR summary. Overall, CARs provide MHC-independent recognition of a variety of extracellular target types with a compact, single chain construct containing all the minimal elements necessary for T cell activation. For better or for worse, the design of CARs prevents any chance of receptor mispairing but circumvents the natural processes of T cell activation and dysregulation. While documentation of on-target/off-tumor

Table 1. Active clinical trials using CAR-engineered T cells.

Target Antigen	Associated Malignancy	CAR Generation	Clinical Trial ID#
CD19	Acute lymphoblastic leukemia	3rd (CD28:4-1BB)	NCT02186860
CD133	Various malignancies	1st	NCT02541370
CD171	Neuroblastoma	2nd (4-1BB) and 3rd (CD28: 4-1BB); transgene includes truncated EGFR	NCT02311621
CEA	CEA+ adenocarcinomas	2nd (CD28)	NCT01723306
EGFR	EGFR+ solid tumors	1st and 2nd (4-1BB)	NCT01869166
GD2	Neuroblastoma	3rd (CD28:OX40); transgene includes iC9	NCT02439788
GD2	GD2+ sarcomas	3rd (CD28-OX40); transgene includes iC9	NCT01953900
Her-2	Breast cancer	2nd (CD28)	NCT02547961
Her-2	Glioblasoma multiforme	2nd (CD28)	NCT01109095
Mesothelin	Pancreatic, ovarian, and mesothelioma	2nd (4-1BB)	NCT02159716

effects is well noted, off-target effects are not as readily seen because the antigen binding regions of CARs are generally derived from well-characterized monoclonal antibodies. However, several groups conducting clinical trials with CARs have recorded other serious adverse events including tumor lysis syndrome [130] and cytokine storm [128, 161, 162]. Overall, the majority of CAR studies have shown much promise for their clinical use. Continuing efforts are ongoing to improve clinical outcomes while minimizing adverse events.

TCR Gene Therapy

As the focus of these dissertation studies, we now introduce the concept, success, and limitations of TCR-gene modified T cells. These discussions serve as a prelude to identify what approaches can help us better understand antigen recognition by a T cell in order to improve TCR-based ACT. A schematic of TCR engineering of T cells for ACT (detailed in the following sections) is provided in Figure 4. Over the past 20 years, a myriad of TCRs have been cloned and characterized that recognize antigens, including but not limited to, EBV [163], gp100 [44, 164], HCV [165, 166], HPV [167], MART-1 [15, 34, 168], tyrosinase [169, 170], and unknown antigen reactivity [171]. To date, TCRs investigated for ACT have been limited to mostly MHC-I-restricted candidates. Although, more recent identification of direct tumor-recognizing MHC-II-restricted $CD4^+$ T cells [172] have provided the opportunity to generated MHC-II-restricted TCR-transduced T cells [173]. The sections below describe the design, use,

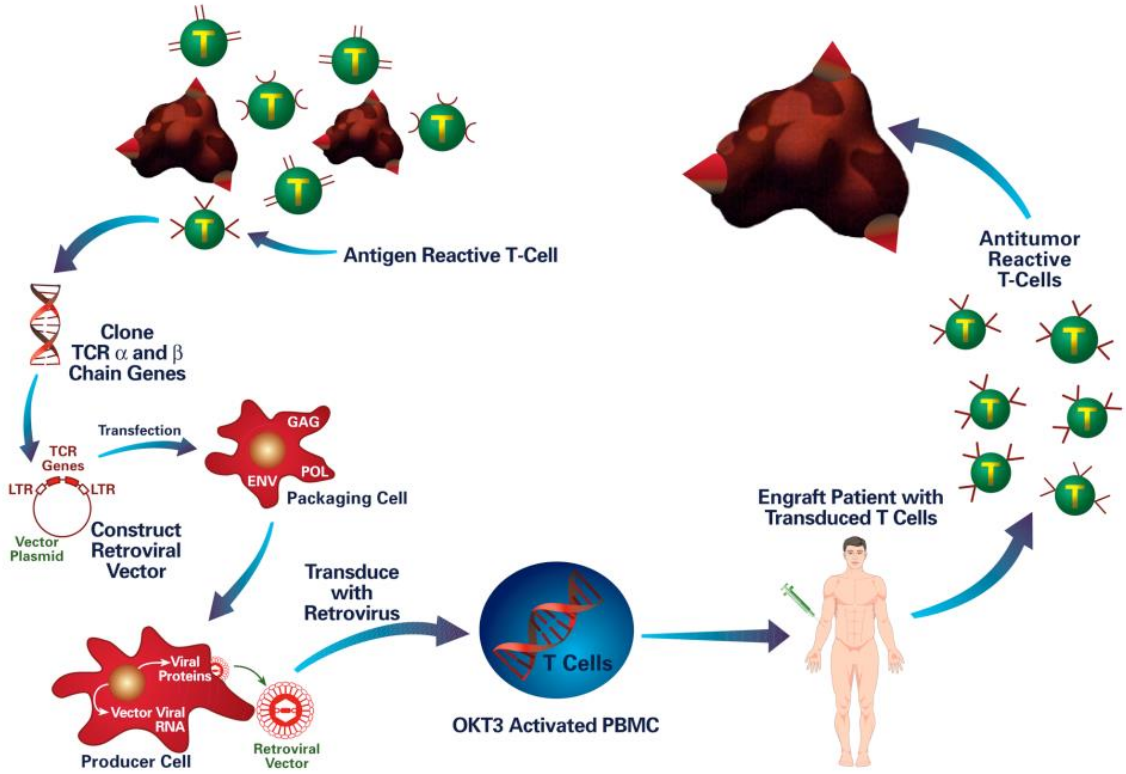

Figure 4. Adoptive cell transfer using TCR gene-modified T cells. Viral or cancer antigen-reactive T cell clones are isolated and expanded from TIL or peripheral blood to identify a therapeutic TCR candidate. TCR genes are identified and cloned into retroviral vectors. Packing and producer cell lines are engineered with this retroviral construct to produce high titer retrovirus used to transduce activated PBMC from an HLA-matched antigen positive patient. Transduced cells are expanded *ex vivo* with cytokine support and infused back into the patient. These autologous T cells with re-directed specificity provide new anti-viral or anti-tumor immunity.

success, and limitations of TCR-engineered T cells used in ACT. They provide a foundation for the biologic questions addressed in this dissertation.

TCR design. An important factor influencing the effectiveness of immunotherapeutic use of TCRs is the relationship between TCR-pMHC affinity and T cell function [1]. Antigen recognition depends on a productive interaction between a TCR and pMHC, and lower affinity interactions generally require the presence of the CD8 co-receptor to facilitate antigen recognition [2]. Thus, it might be predicted that T cells engineered with high affinity TCRs are better effectors than T cells engineered with lower affinity TCRs [15, 168, 169]. Various CD8-independent TCRs have been characterized that can transfer antigen recognition to $CD4^+$ cells in an MHC-I-restricted manner, providing helper cytokine support and enhanced tumor regression [165, 166, 169, 170, 174-181]. Naturally occurring high affinity, CD8-independent TCRs are relatively rare, however, and thus difficult to find. Rather than screening for such high affinity TCRs, various methods have been developed to affinity-enhance already characterized TCRs. These approaches are discussed in a later section. It is important to recognize, however, that T cells harboring higher affinity TCRs are more likely to undergo activation induced cell death (AICD) upon antigen encounter [182, 183], or induce off-tumor/on-target and off-tumor/off-target reactivity [184-186], counterproductive to their therapeutic intention.

It is also important to acknowledge that MHC-restriction of TCRs limits the number of patients that can be treated using a single TCR, and engineered T cells would

need to be HLA matched to patients. HLA class I expression has a tendency to be downregulated on tumor cells [187, 188], however, which may also serve as a barrier to effective therapy. Additionally, because TCRs require interaction with the CD3 complex, a TCR's expression and functionality is limited by available CD3 complex components. Competition for the CD3 complex with endogenous TCR limits functional transgene expression, although strategies discussed below may allow for improved association with CD3 by the introduced TCR.

TCR chain pairing. Because TCRs exist as heterodimers, TCR gene-modified T cells require two different genes, or chains, to be expressed to redirect specificity. Because expression of two individual genes may result in non-uniform chain expression, various approaches have been developed to address this. For example, the addition of viral 2A self-cleavage peptide sequences between the α and β chains within retroviral constructs allows for more uniform chain expression [189-191]. Additionally, codon optimization of the construct facilitates increased TCR expression [192, 193]. Both these approaches help augment introduced TCR expression without altering the TCR sequence itself.

Additionally, the presence of an endogenous TCR can induce chain mispairing between endogenous and introduced α and β chains. These interactions reduce the level of expression of functional introduced TCR [168, 194] and could lead to novel and unpredictable self-reactive TCRs (false pairing) with serious adverse events. Such off-target/off-tumor adverse events have been reported as a result of high affinity TCRs

recognizing unanticipated epitopes or as a result of TCR chain mispairing. Two recent studies demonstrate undesirable reactivity propagated from TCR mispairing between endogenous and introduced TCR α and β chains. One study recorded graft-versus-host-disease (GVHD) in a mouse model in five different TCR systems [195]. Another demonstrated the ability of engineered human T cells to develop MHC class I and II-restricted allo- and auto-reactivity through TCR chain mispairing [196]. However, to date, no evidence of GVHD has been seen in over 100 patients treated with this gene therapy approach [197].

A handful of approaches have been developed to address potential for TCR chain mispairing. One main strategic effort involves a host of modifications to the TCR construct, summarized in Figure 5. As mentioned previously, codon optimization of the TCR α and β genes can help promote efficient translation and surface assembly of the introduced receptor without altering the TCR sequence itself [192, 193]. Introduction of cysteine residues in the α and β constant regions has been shown to promote inter-chain disulfide bridge formation to limit mispairing [176]. Other approaches to help improve pairing, expression, and function of the introduced TCRs include the addition of leucine zippers at the end of the intracellular tails [174] and altering the glycosylation of the TCR [177]. Substituting human constant regions with portions of or the entire mouse constant regions also promotes proper pairing and enhanced surface expression [170, 198-202]. Specifically, elements of the murine constant regions do not efficiently interact with the human constant regions [200]. Additionally, the murine constant

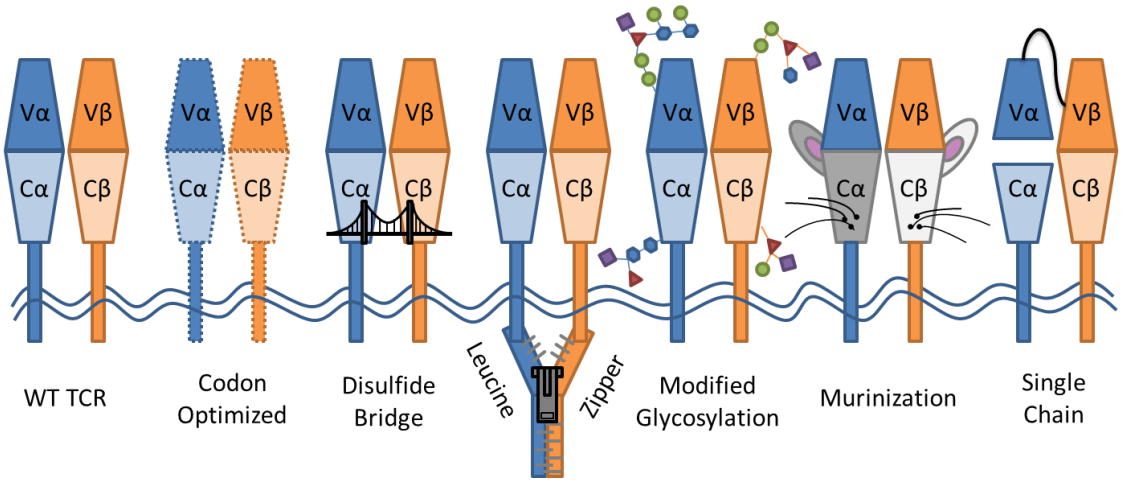

Figure 5. TCR modifications to limit mispairing and improve cell surface expression and function. Modifications of WT TCR structure (far left) include codon optimization, introduction of a disulfide bridge, addition of leucine zipper, modification of glycosylated residues, substitution with murine constant regions, or use of single chain Vα-Vβ-Cβ with a Cα chain. WT, wildtype; V, variable; C, constant.

region has a higher affinity for human CD3, which can favor the murinized receptor associating with limited surface CD3 [198]. Receptors with murine constant regions were also found to mediate higher levels of cytokine secretion *in vitro* [198, 199]. This technique poses additional problems, however, including immunogenicity and clearance of the engineered T cells as they express potentially antigenic domains in the transgene [199].

Another novel approach to alleviate mispairing was demonstrated by recent reports using single chain TCRs [200, 203]. One group engineered a recombinant TCR consisting of a single chain Vα-Vβ-Cβ and a Cα chain, which only paired with each other and not the endogenous TCR [200]. Another group used a stabilized Vα-Vβ single chain TCR linked to intracellular signaling domains (lck, CD28), which elicited functional activation of T cells in the absence of either the CD3 complex or co-receptors and circumvented mispairing with endogenous TCRs [203]. Efforts to limit mispairing have also focused on downregulating the endogenous TCR by via small interfering RNA (siRNA) [204] or using designer zinc-finger nucleases [205]. All of these alternate strategies share the same goal to reduce competition for the CD3 complex, allow for stable pairing of the introduced TCR, and minimize adverse events due to false pairing.

TCR targets*.* More than 20 years after TCR gene-modified T cells were first used to redirect T cell specificity in mice [206] this technology was first evaluated in humans targeting melanoma-associated antigens. TCR engineered T cells' first use in the clinic targeted HLA-$A2^{+}$/MART-1^{+} melanoma [207, 208]. These initial clinical studies

demonstrated that TCR gene-modified T cells were generally safe, well tolerated, and had the potential to be therapeutic in cancer patients. A later study targeting melanoma antigens MART-1 and gp100 demonstrated further clinical benefit using TCR-transduced T cells but highlighted the potential for adverse events [184]. Of note, the gp100-reactive TCR in this study was high affinity and of mouse origin, and many patients treated with this TCR exhibited toxicities in the eye and inner ear, displaying destruction of normal melanocytes. This well-characterized example of on-target/off-tumor effects first cautioned the use of high affinity TCRs. Fortunately, in this case such toxicities resolved naturally or with administration of topical steroids in almost all patients. These earliest studies suggested TCR gene-modified T cells were feasible with clinical benefit, but that the choice of TCR may be important to limit toxicities.

Since these early studies, however, identification of numerous TCR genes capable of recognizing tumor-associated antigens and improvements in TCR gene transfer technology have allowed for specificity redirection to target of a variety of other antigens and malignancies. These include, but not limited to, carcinoembryonic antigen (CEA), cancer-testis antigen (CTA) family members, and viral protein family members. Examples using TCR gene-modified T cells to target these families of antigens are described below.

CEA is overexpressed in a many epithelial cancers, allowing CEA-reactive TCRs to target a wide variety of malignancies. In fact, a recent clinical trial TCR gene-modified T cells to target CEA^+ colorectal cancer noted objective clinical response in a patient

bearing metastatic disease [186]. However, on-target/off-tumor adverse events, including inflammatory colitis, were documented in numerous patients as CEA has shared expression on normal tissues, including the colon. This example highlights therapeutic benefit as well as safety concerns using TCR-gene modified T cells targeting CEA.

The CTA family of antigens, including NY-ESO-1 and MAGE, are expressed by the normal testis and a host of human cancers including breast, bladder, colon, lung, melanoma, head and neck, gastric, ovarian, thyroid, neuroblastoma, synovial cell sarcoma, and prostate [209]. Clinical studies have shown T cells redirected to recognize NY-ESO-1 provided objective clinical response in patients with synovial cell sarcoma and melanoma without any evidence of previously reported adverse events [210]. A pair of clinical trials targeting another widely expressed CTA, MAGE-A3, recorded much more mixed results. The first clinical trial used a mouse-derived, high avidity TCR that was further modified by site directed mutagenesis in its CDR3 [211]. Targeting MAGE-A3, it cross-recognized MAGE-A9/A12. Although five out of nine patients experienced clinical regression of their cancers, one third of the patients experienced neurological toxicity. Two patients even died due to these adverse events. T cells cross-reactive against unknown expression of MAGE-A12 in the brain are believed to have caused this toxicity. Another clinical trial using an affinity-enhanced TCR targeting MAGE-A3 resulted in cardiogenic shock and death of the first two patients treated [212, 213]. While no MAGE-A3 expression was detected in cardiac tissue at autopsy, it was determined the

TCR designed with affinity-enhancing mutations in α and β CDR2s exhibited an unpredicted cross-reactivity to titin, a sarcomeric protein expressed in striated muscle. Interestingly, the parental TCR from which the engineered TCR was derived from was isolated from a patient without cardiac toxicity. This might attribute the adverse events in the clinical trial to the intentionally induced CDR2 mutations. Taken together, these studies are encouraging that TCR gene-modified T cells under the right circumstances can provide clinical benefit but also highlight the importance of TCR and target selection to minimize cross-reactivity by modified TCRs.

Viral proteins expressed on tumors compose a third family of antigens targeted by TCR-engineered T cells. Several groups have TCR-engineered T cells to target antigens, including CMV [214, 215], EBV [163, 216, 217], HIV [218-221], HCV [165, 166, 222], HPV [167, 223], and others. No clinical reports have yet been published testing virus-reactive TCR-transduced T cells in humans, however. Table 2 lists some of the active clinical trials using TCRs and their respective targets.

Use of high affinity TCRs in ACT. Discussed earlier, thymic selection generally excludes high affinity TCRs against tumor (self) antigens to occur normally in the periphery. But engineering T cells with high affinity TCRs circumvents normal thymic limitation and can generate high avidity tumor-reactive T cells. There are clear advantages to using a high affinity TCRs to engineer T cells for ACT. The ability to generate tumor-reactive MHC class I-restricted $CD4^+$ T cells is one major benefit using high affinity TCRs [169]. $CD4^+$ T cells' ability to produce helper cytokines upon antigen

Table 2. Active clinical trials using TCR-engineered T cells.

Target Antigen	Associated Malignancy	MHC Restriction	Clinical Trial ID#
gag	HIV	HLA-A2	NCT00991224
gp100	Melanoma	HLA-A2	NCT00509288
HPV E6	HPV-associated cancers	HLA-A2	NCT02280811
MAGE-A3	Various malignancies	HLA-A1	NCT02153905
MAGE-A3	Various malignancies	HLA-DP04	NCT02111850
NY-ESO-1	Various malignancies	HLA-A2	NCT02457650
Thyroglobulin	Thyroid cancer	HLA-A2	NCT02390739
Tyrosinase	Melanoma	HLA-A2	NCT01586403
WT1	Myelodysplastic syndrome, AML	HLA-A2	NCT02550535
WT-1	Non-small cell lung cancer, mesothelioma	HLA-A2	NCT02408016

stimulation offers the opportunity to provide MHC I-restricted T cell help at the tumor site [169, 224, 225]. Therefore, TCR transduced $CD4^+$ T cells might facilitate cross-priming or epitope spreading, leading to broad systemic anti-tumor immunity. Another application for a high affinity TCR involves engineering $CD4^+$ regulatory T cells [226]. Like helper T cells, MHC I-restricted regulatory T cells could help reduce the severity of autoimmune diseases [226]. Thus, the ability to use high affinity TCRs to target novel classes of MHC-I-restricted T cell subsets is a very attractive concept.

However, T cells expressing TCRs with extremely high affinity for pMHC can undergo activation-induced cell death (AICD) upon antigen encounter. AICD could lead to the destruction of the very effector cells that were intended to destroy a patient's cancer or virally infected cells [182, 183]. Additionally, high affinity TCRs are better at detecting low levels of antigen [227], and have even exhibited cross-reactivity to related antigens causing death in a clinical trial previously discussed [211]. T cells expressing high affinity TCRs can also lead to autoimmunity as observed in one transgenic mouse model [185] and two clinical trials [184, 186]. Given these observations, the proper use of high affinity TCR sfor effective anti-tumor immunity remains unresolved. Approaches used to design high affinity TCRs are discussed in a later section.

Other T cell Engineering Approaches

Other receptor types. While the use of CARs and TCRs to redirect the specificity of a T cell have been well documented, ongoing efforts to design other receptor types for gene modification hold therapeutic potential as well. For example, engineering T

cells to express the NKG2D receptor allows T cells acquire the reactivity of natural killer (NK) cells [101-103]. Another NK cell receptor that has been investigated for T cell engineering is NKp30, which recognizes the tumor-prone antigen B7-H6. A recent study combined the specificity of NKp30 and the signaling capability of CARs, designing a novel NKp30-based CAR replacing the scFv domain with the ligand-binding domain of NKp30 [100]. Adoptive transfer of the NKp30-CAR T cells allowed for non-MHC-restricted recognition of B7-H6 expressing RMA, a murine lymphoma, *in vivo*. Interestingly, NKp30-CARs T cells provided protection against subsequent challenge with wildtype (WT) RMA tumor cells. Similar efforts are examining the feasibility of replacing the scFV domain of CARs with other ligands or ligand-binding receptors described earlier. Exploring other approaches to engineer T cells with novel antigen receptors may help optimize the use of gene-modified T cells for ACT.

Another unique approach under investigation is dual-receptor-engineering of T cells. This strategy engineers T cells to co-express complementary CARs, TCRs or other receptors, each specific to a distinct target. This approach is thought to optimize T cell homing and tumor specificity while reducing toxic potential. Dual-specificity may also provide synergistic signaling as well as a means to combat downregulation or mutation of antigens in immune escape. One study validated this tactic by generating T cells co-expressing CARs reactive to MUC1 and ERBB2 targeting breast cancer cells *in vitro* [228]. They found that dual-targeted T cells killed $ERBB2^{+}$ targets efficiently, but T cell proliferation required engagement with both MUC1 and ERBB2 antigens because CARs

contained either CD3ζ or CD28 for ERBB2 and MUC1 specificity, respectively. Additionally, IL-2 production was modest in dual-CAR expressing cells compared to CAR T cells engineered with a single second generation CAR containing both CD3ζ and CD28. These data suggest generating dual-receptor engineered T cells is feasible but requires optimization to enhance T cell function.

Additionally, recent work has highlighted anti-specific inhibitory chimeric antigen receptors (iCARs) linked to a powerful acute inhibitory signaling domain, such as CTLA-4 and PD-1 [229]. T cells engineered with these iCARs were selectively limited in cytokine secretion, cytotoxicity, and proliferation compared to those engineered with an activating CAR targeting the same antigen. This dual-receptor approach provides an attractive opportunity to limit unwanted off-target responses.

Cytokine production. Another approach to modify or enhance the potency of receptor-engineered T cells is to further genetically modify T cells to secrete pro-inflammatory or pro-proliferative cytokines. This approach not only provides autocrine support to enhance T cell function, proliferation, and/or persistence, but also favorably alters the tumor microenvironment. This would enhance innate and cognate immune effector recruitment while limiting the systemic toxicity of exogenously delivered cytokines. For example, engineering melanoma-reactive T cells to express IL-2 resulted in continued cell growth in the absence of exogenous IL-2, which may a viable approach to help T cell persistence post-adoptive transfer [230]. A similar tactic demonstrated T cells modified to express IL-12 exhibited enhanced anti-tumor function and were better

able to resist immunosuppression by regulatory T cells [231, 232]. Similarly, engineering T cells to secrete IL-12 transformed myeloid cell within tumors from immunosuppressive to immunosupportive [233]. This strategy was even used in a recent phase I clinical trial where IL-12 secreting MUC-16 (ecto)-targeting CAR T cells were infused into patients with recurrent ovarian cancer [234]. In summary, the ability to additionally modify receptor-engineered T cells to provide cytokine support is an attractive approach that still needs more clinical validation to become mainstream.

Chemokine recognition. In addition to cytokine-engineered T cells, modifying them to express chemokine receptors can aid in migration patterns, increasing the efficiency of trafficking to and infiltration of tumors. Transferring genes encoding CCR4, CCR2B, or CXCR2, enabled T cells to home towards CCL17, CXCL1, and macrophage chemoattractant proteins [149, 235, 236]. Also, VEGFR-2-engineered T cells allowed T cells to find tumor-associated neovasculature in one study [237]. Additional efforts to improve T cell homing may include engineering T cells with certain integrins or their ligands [238] or by blocking inhibitors of migration like endothelin [239]. Further investigation is necessary, however, to prove clinical benefit.

Ways to Optimize Gene-Modified T cells.

Host conditioning. Lymphodepletion prior to ACT has been a point of interest to improve long-term persistence and function of transferred T cells. This host pre-conditioning strategy is thought to create space for the transferred T cells and eliminate competition for cytokines [240], remove competition at the surfaces of antigen

presenting cells [241, 242], and withdraw immunosuppressive regulatory T cells [243]. This evidence came from preliminary mouse studies that were followed up in the clinic by the Rosenberg group. They first noted that persistence and antitumor activity of transferred T cells *in vivo* was greatly increased with non-myeloablative lymphodepleting treatment using cyclophosphamide and fludarabine before adoptive transfer [244]. It is believed these changes in the host may lead to induction of a memory phenotype and enhance effector function. Systemic administration of cytokines, such as IL-2, post-ACT has also enhanced transferred T cell function and persistence [245, 246]. Post-conditioning with other cytokines including IL-15 or immunomodulatory therapies such as PD-1 and CTLA-4 blockade should also be considered.

Suicide switch. In light of on- or off-target toxicities, tumor lysis syndrome, and cytokine storm documented with the use of engineered T cells, it would be beneficial to preserve the ability to eradicate the transferred T cells, if needed. Such strategies aim at turning off antigen receptor expression or eliminating the engineered cells post-transfer by incorporating certain "suicide genes" into the transgene. A long-studied approach utilizes the herpes simplex virus-thymidine kinase (HSV-tk) gene. Its incorporation into the transgene vector makes engineered T cells susceptible to gancyclovir treatment [247, 248]. However, because HSV-tk is potentially immunogenic, its expression may create unwanted immune-mediated destruction of transferred T cells and decreased persistence [249, 250]. Another common approach and non-

immunogenic technique incorporates caspase 9 under an inducible promoter (iC9) to initiate apoptosis of transduced cells [251-254]. Additionally, studies incorporating CD20 [255] or EGFR [256] in transgene vectors generated transduced T cells susceptible to rituximab and cetuximab treatment, respectively. In short, incorporation of suicide switch mechanisms allow for novel ways to enhance the safety of engineered T cells by allowing simple means to specifically eliminate them *in vivo*.

Affinity maturation. As discussed earlier, TCR affinity is known to play a significant role in determining sensitivity of a T cell to antigen recognition. Therefore, it is logical to predict that higher affinity TCRs may provide better therapeutic candidates for reasons previously discussed. For example, the use of high affinity TCRs may better equip engineered T cells to combat immune suppression mechanisms that alter T cell function including MDSC-mediated nitration of TCR tyrosine residues, which can weaken TCR-pMHC binding [61]. Additionally gene transfer of high affinity TCRs can generate tumor-reactive MHC class I-restricted $CD4^+$ T cells, creating a novel population of T cell help at the tumor site [169, 224, 225]. Moreover, a population of reactive-$CD4^+$ T cells may facilitate cross-priming or epitope spreading allowing for a broad systemic anti-tumor response. For reasons discussed, however, identifying naturally occurring, high affinity tumor-reactive TCRs is feasible but challenging due the principles behind thymic selection [30].

One way to identify and clone high affinity TCRs is screening for CD8-independence against human MHC-restricted antigens in mice. It is documented that

mouse CD8 does not bind to the α3 domain of human MHC class I molecules [198, 257]. Thus, in a vaccinated HLA-A2 transgenic mouse model, isolated T cell clones reactive against human tumors *in vitro* would likely express high affinity TCRs. This approach has been used successfully to identify high affinity TCRs targeting CEA [258] and p53 [259]. Additionally, a recent approach has generated allo-restricted T cells using autologous dendritic cells (DCs). DCs are co-transfected with *in vitro* transcribed RNA encoding an allogeneic MHC molecule and a selected antigen [260], providing allo-stimulation. This procedure allows for novel allo-pMHC ligands to activate high avidity, allo-restricted, peptide-specific T cells as a source for high affinity TCRs. Together, these approaches provide great flexibility for obtaining high affinity and high avidity T cells as potential sources of TCRs for ACT.

While CD8-independent tumor cell recognition by a T cell clone should be a hallmark of a high affinity TCR, this has not always been true. One such example involved a gp100 reactive T cell clone designated T4H2 that was a $CD4^-/CD8^-$ T cell that efficiently recognized HLA-$A2^+$ $gp100^+$ human melanoma cells *in vitro* [44, 164]. However, when the T4H2 TCR was cloned and expressed in human T cells, it surprisingly required CD8 expression for tumor cell recognition [44]. Therefore, each TCR must be evaluated individually to ensure that a CD8-independent/high affinity TCR has been cloned.

More recently, TCRs have been genetically modified to improve their biophysical properties [210, 261-267]. Using yeast and phage display, TCRs have undergone

"evolution" to select for high affinity binding to pMHC [3, 4, 265, 268, 269] a technique also used in CAR design [89, 90]. Although it might be predicted that changes to the CDR3 would lead to the highest affinity TCRs, amino acid alterations in any of the three CDRs can contribute to enhanced TCR-pMHC affinities [262]. This was surprising because the CDR3 is responsible for the majority of TCR diversity and specificity.

What is troublesome about these affinity enhancement strategies is the randomness of introduced mutations. Yeast and phage display rely on purely random generations of high volumes of different clones, followed by screening for the highest biophysical interactions. Thus, there is no informed decision behind the selection of the TCR ultimately used. Such a "blind" approach is concerning when trying to predict therapeutic efficacy and safety in terms of potential on- or off-target toxicities. More appropriate may be a rational structure-guided design of high affinity TCRs. A relatively new concept, this approach allows for more control and understanding of the mechanism of TCR affinity improvement with the potential to consciously avoid adverse events related to off-target toxicities [266, 270]. Taken together, *in vitro* and *in vivo* studies with high affinity TCRs, described earlier, indicate that TCR affinity can make a difference in target recognition by TCR transduced T cells. But the overall effectiveness and safety of high affinity TCRs in patients remains unresolved. As such, each TCR may need to be carefully and individually evaluated for how its properties impact a T cell.

Genomic Instability and Cross-Reactive TCRs

Genomic instability plays a central role in allowing viruses and malignancies to escape immune surveillance [271, 272]. Mutated antigens enhance virulence by escaping HLA-restricted immune responses in viral infections including HBV [273-275], HCV [274, 276-279], HIV [280-282], EBV [283, 284], and choriomeningitis [285]. Similarly, a wide variety of cancers have displayed various mechanisms of immune escape including downregulation of MHC-I expression [187, 188], mutated or downregulated antigen processing proteins [286-288], and antigen loss or mutation [271, 289, 290]. These mechanisms pose a fundamental problem for antigen-specific TCR-engineered T cells that rely on proper processing and presentation of antigens by MHC for target recognition.

Immune escape is not only responsible for ineffective host immune responses, but also cause impaired development of preventative and therapeutic vaccines, and inherent or acquired resistance to novel treatment strategies including immunotherapies. Additionally, immunotherapies designed to elicit potent anti-tumor or anti-viral T cell responses like ACT, checkpoint blockade, and cytokine support all have potential to fail in light of these immune escape mechanisms. It is imperative to investigate novel therapeutic approaches designed to combat genomic instability.

One potential strategy, highlighted in this dissertation, utilizes cross-reactive TCR gene-modified T cells. Traditionally thought to have a lock-and-key specificity, the clonal selection theory proposed that individual lymphocytes are specific for a single pMHC,

and that alternative ligand recognition is unlikely [291, 292]. This “one-clonotype—one-specificity” paradigm has been challenged over the years. Based on sheer numbers, the notion of $>10^{15}$ potential foreign peptides (not including self) would require 10^{15} different mono-specific TCRs [293, 294]. This does not seem feasible in terms of immunologic space or sheer cellular mass. Additionally, the HLA locus is one of the most polymorphic and fastest evolving regions of the human genome, currently encoding more than 7,000 allelic variants [295]. Such HLA diversity is estimated to increase the variety of peptides displayed. Recent studies have suggested that there are less than 10^8 distinct TCRs in the human naïve T cell pool [296]. It is argued that the vast diversity of peptides and MHC alleles dwarfs that of TCR sequences, requiring TCRs to be able provide flexible immune coverage [294].

Elegant studies have since demonstrated a varied T cell repertoire can be selected by a single peptide [297] and that resulting T cells can be activated by unrelated peptide sequences [298]. The use of combinatorial peptide libraries also demonstrated cross-reactivity of individual T cell clones recognizing over a million different individual peptides presented by a single MHC molecule [299-301]. Though TCR cross-reactivity is no longer a novel concept, its mechanism, the control of antigen sensitivity, the biophysics of TCR-pMHC engagement, and its functional consequences are not yet fully understood.

A deeper understanding of what dictates the cross-reactive nature of a TCR (both structurally and functionally) will allow for a more informed approach to designing

therapeutics meant to combat mutating antigens and to limit cross-reactivity against self-antigens. Thus, engineering T cells with promiscuous TCRs serves not only as a potential therapeutic, but a tool to better understand and rationally design TCRs. In this way, immune effectors could be equipped with the ability to accommodate recognition of mutant antigens associated with immune escape.

Concluding Remarks

While the field of TCR gene transfer is still quite new, the use of TCR-transduced T cells represents a promising new approach for treating patients with cancer, viral infections, and their associated sequelae. TCR gene transfer also circumvents the hurdles of obtaining tumor reactive T cells associated with TIL therapy and other forms of adoptive T cell transfer. The use of viral vectors to engineer T cells with TCR genes enables us to generate populations of autologous T cells with limitless specificities. It is also clear that the TCR gene transfer approach is feasible and that the TCR transduced T cells can be delivered safely; and objective clinical responses in treated patients indicate that these genetically engineered T cells can be effective.

In light of recent clinical success, however, there remain many issues in optimizing the efficacy and safety of this type of immunotherapy. Ultimately, extensive studies are needed to determine if TCR-engineered T cells can deliver improvements in progression-free and overall survival when compared to the other therapies. Dependency on co-receptors, pairing competition, and predominantly low affinities of physiologic TCRs call for efforts to optimize their use in ACT. But strategies that “blindly”

affinity-enhance TCRs are worrisome because they lack the structural understanding required to anticipate efficacy and unwanted cross-reactivity. Generation of more efficient and safer TCRs warrants a more complete understanding of the basic biology of a TCR gene-modified T cell and what factors are truly important in defining antigen recognition and T cell function.

The goal of this dissertation is to better understand structure-function relationships between a high affinity, HCV-cross-reactive TCR (HCV1406 TCR) and naturally occurring mutant HCV pMHC ligands. We will compare changes in the kinetic, cellular, and structural components of TCR-pMHC interactions with the polyfunctional output by HCV1406 TCR gene-modified T cells. Taken together, these studies provide us with fundamental information to build a more suitable model to confront diseases with genomic instability and to better understand what factors govern antigen recognition by a T cell. As we learn more about how TCR behavior influences T cell function, we will be able to design more effective and safer TCR gene-modified T cells for ACT.

CHAPTER TWO

MATERIALS AND METHODS

Cell Lines and Media

All cell lines were obtained from the American Type Culture Collection (Rockford, MD), unless otherwise noted. All media were obtained from Corning Life Sciences (Corning, NY) unless otherwise noted. HEK293GP (human embryonic kidney packaging cell line expressing retroviral gag and polymerase proteins), COS (monkey kidney tumor, HLA-A2$^-$), HepG2 (human hepatocellular carcinoma, HLA-A2$^+$), and Huh-7 (human hepatocellular carcinoma, HLA-A2$^-$) cells lines were maintained in DMEM supplemented with 10% fetal bovine serum (FBS; Tissue Culture Biologics, Long Beach, CA). PG13 cells (stable viral producer cell line) were maintained in IMEM supplemented with 10% FBS. T2 (HLA-A2$^{+,}$ TAP-deficient antigen presenting cell), Jurkat (CD4$^-$CD8$^-$ T cell lymphoma), and Jurkat76 (CD4$^-$CD8$^-$TCR$^-$ T cell lymphoma) cell lines were maintained in RPMI 1640 medium supplemented with 10%. Jurkat76 cells were kindly provided by Dr. Miriam Heemskerk (Leiden University Medical Center, Leiden, Netherlands).

T Cells

All PBMC samples used for T cell transductions were obtained as apheresis products purchased from Key Biologics (Memphis, TN). Ficoll-Hypaque (Sigma-Aldrich, St. Louis, MO) density gradient centrifugation was used to isolate PBL-derived T cells

from PBMC of normal healthy donors. T cell clones isolated from HCV-infected individuals were generated from PBL samples collected from IRB-approved protocols at the University of Colorado Denver.

T cells were maintained in complete T cell medium consisting of AIM-V medium (Life Technologies, Grand Island, NY) supplemented with 5% heat-inactivated pooled human AB serum (hAB; Valley Biomedical, Inc., Winchester, VA), 300 IU/mL recombinant human IL-2 (rhIL-2; Novartis Pharmaceuticals Corporation, East Hanover, NJ) and 100 ng/mL recombinant human IL-15 (rhIL-15; Biological Resources Branch, National Cancer Institute, Bethesda, MD) at 37^{o}C in a humidified 5% CO_2 incubator. Prior to retroviral transduction, primary T cells were OKT3-activated for 3 days using 50 ng/mL anti-CD3 mAb (Miltenyi Biotec, Bergisch Gladbach, Germany), in complete T cell medium.

Cloning of HCV-Reactive T Cells from HCV^{+} Patients.

As mentioned above, HCV-reactive T cell clones were isolated from PBMC samples from chronically infected patients or those with spontaneously resolved infection collected under University of Colorado Denver IRB-approved protocols. HCV-reactive T cell clones were obtained from the Rosen Lab at the University of Colorado Denver. Briefly, T cells were Ficoll-Hypaque separated as described above and stained with PE-labeled HLA-A*0201 tetramer folded around HCV NS3:1406-1415 (KLVALGINAV) peptide (Beckman Coulter, Marseille, France). Cells were then sorted by flow cytometry on a FACSVantage (BD Biosciences, San Jose, CA), and cloned via limited dilution cloning as previously described [302]. Briefly, tetramer positive cells were plated at limiting

dilution (5, 10, and 100 cells/well) and cultured with $8x10^4$ and $1.6x10^4$ irradiated allogeneic PBMC and lymphoblastoid cell line (LCL), respectively in 250 µl/well of AIM-V medium supplemented with 5% hAB serum, 100 IU/mL rhIL-2, and 0.03 µg/mL purified anti-CD3 mAb (Miltenyi Biotec) in 96 well plates and incubated for 2 wk at 37°C and 5% CO_2. After 14-21 days, wells exhibiting growth were transferred to T-25 flasks and re-stimulated with $25x10^6$ and $5x10^6$ irradiated allogeneic PBMC and LCL, respectively, in 30 mL of AIM-V medium supplemented with 5% hAB serum, 100 IU/mL rhIL-2, and 0.03 anti-CD3 mAb. Cultures were analyzed by FACS 14 days later and used in functional assays.

Vectors

HCV NS3 Site Directed Mutagenesis

The WT HCV NS3 gene fused to GFP by a T2A self-cleaving viral sequence was synthesized by Genscript (Piscataway NJ) and provided in a pcDNAIII vector. To generate each variant HCV NS3:1406-1415 epitope within full length NS3, site directed mutagenesis (GeneArt Site Directed Mutagenesis System, Invitrogen, Grand Island, NY) was performed in the pcDNAIII vector using a series of primers (Table 3) synthesized by Integrated DNA Technologies (Coralville, IA). Variants 8S/9G/12L and 8S/9S/12L/14S required three and four rounds of site directed mutagenesis, respectively. Methylation, mutagenesis, and recombination were performed according to manufacturer's protocols. Methylation and PCR amplification was performed on a C1000 Thermal Cycler (Bio-Rad, Hercules, CA) under the following conditions: 20 min at 37°C (one cycle),

Table 3. Primers used for site-directed mutagenesis of HCV NS3 pCDNAIII vector variants.

Epitope	Forward primer(s): 5'→3'	Reverse primer(s): 5'→3'
V1408L	CTCGCCGCAAAGCTGCTCGCGTTGGGCATCA	TGATGCCCAACGCGAGCAGCTTTGCGGCGAG
A1409T	GCCGCAAAGCTGGTCACGTTGGGCATCAATG	CATTGATGCCCAACGTGACCAGCTTTGCGGC
I1412L	CTGGTCGCGTTGGGCCTCAATGCCGTGGCGT	ACGCCACGGCATTGAGGCCCAACGCGACCAG
I1412V	CTGGTCGCGTTGGGCGTCAATGCCGTGGCGT	ACGCCACGGCATTGACGCCCAACGCGACCAG
I1412N	TGGTCGCGTTGGGCAACAATGCCGTGGCGTA	TACGCCACGGCATTGTTGCCCAACGCGACCA
V1408S/	CTCGCCGCAAAGCTGAGCGCGTTGGGCATCAA	TTGATGCCCAACGCGCTCAGCTTTGCGGCGAG
A1409G/	CCGCAAAGCTGAGCGGGTTGGGCATCAATGC	GCATTGATGCCCAACCCGCTCAGCTTTGCGG
I1412L	CTGAGCGGGTTGGGCCTCAATGCCGTGGCGT	ACGCCACGGCATTGAGGCCCAACCCGCTCAG
V1408T	CTCGCCGCAAAGCTGACCGCGTTGGGCATCAA	TTGATGCCCAACGCGGTCAGCTTTGCGGCGAG
V1408S/	CTCGCCGCAAAGCTGAGCGCGTTGGGCATCAA	TTGATGCCCAACGCGCTCAGCTTTGCGGCGAG
A1409S/	GCCGCAAAGCTGAGCTCGTTGGGCATCAATG	CATTGATGCCCAACGAGCTCAGCTTTGCGGC
I1412L/	CTGAGCTCGTTGGGCCTCAATGCCGTGGCGT	ACGCCACGGCATTGAGGCCCAACGAGCTCAG
A1414S	TCGTTGGGCCTCAATTCCGTGGCGTACTACC	GGTAGTACGCCACGGAATTGAGGCCCAACGA

followed by 2 min at 94^{o}C (one cycle), followed by 20 sec at 94^{o}C, 30 sec at 57^{o}C, and 5 min at 68^{o}C (18 cycles), followed by 5 min at 68^{o}C (one cycle).

Mutated vectors were transformed into *Escherichia coli* DH5α-T1^{R} competent cells (Invitrogen) on LB ampicillin plates (25 g LB agar (Fisher, Hampton, NH) in 1 L de-ionized water supplemented with 100 µg/mL ampicillin (Sigma-Aldrich), and colonies were expanded in superbroth (32 g Tryptone (Fisher), 20 g yeast extract (Fisher), and 5 grams NaCl (Fisher) in 1 L de-ionized water) supplemented with 100 µg/mL ampicillin (Sigma-Aldrich). Plasmid DNA from recombinant clones was isolated using a Miniprep Plasmid Isolation Kit (Qiagen, Hilden, Germany) according to manufacturer's protocol and sequenced (Genewiz, South Plainfield, NJ) to confirm that correct mutation had been made and no other errors had occurred during the mutagenesis process. Final products were used to transfect COS/A2 cells or subcloned into a modified SAMEN retroviral vector (described below).

HCV TCR Retroviral Vectors

The original SAMEN retroviral vector described by Treisman and colleagues [303] has been modified from its original components in stepwise fashion to include TCR chain genes [170] and later a CD34t selection marker [304] for our TCR cloning purposes. Our modified SAMEN retroviral vectors contains the TCR α chain, P2A self-cleaving linker, TCR β chain, T2A self-cleaving-linker, and truncated CD34 molecule (CD34t) as a transgene expression marker (Fig 6a). Each HCV1406 TCR and HCV1073 TCR containing SAMEN retroviral vector was used to generate high titer produced cell lines used to

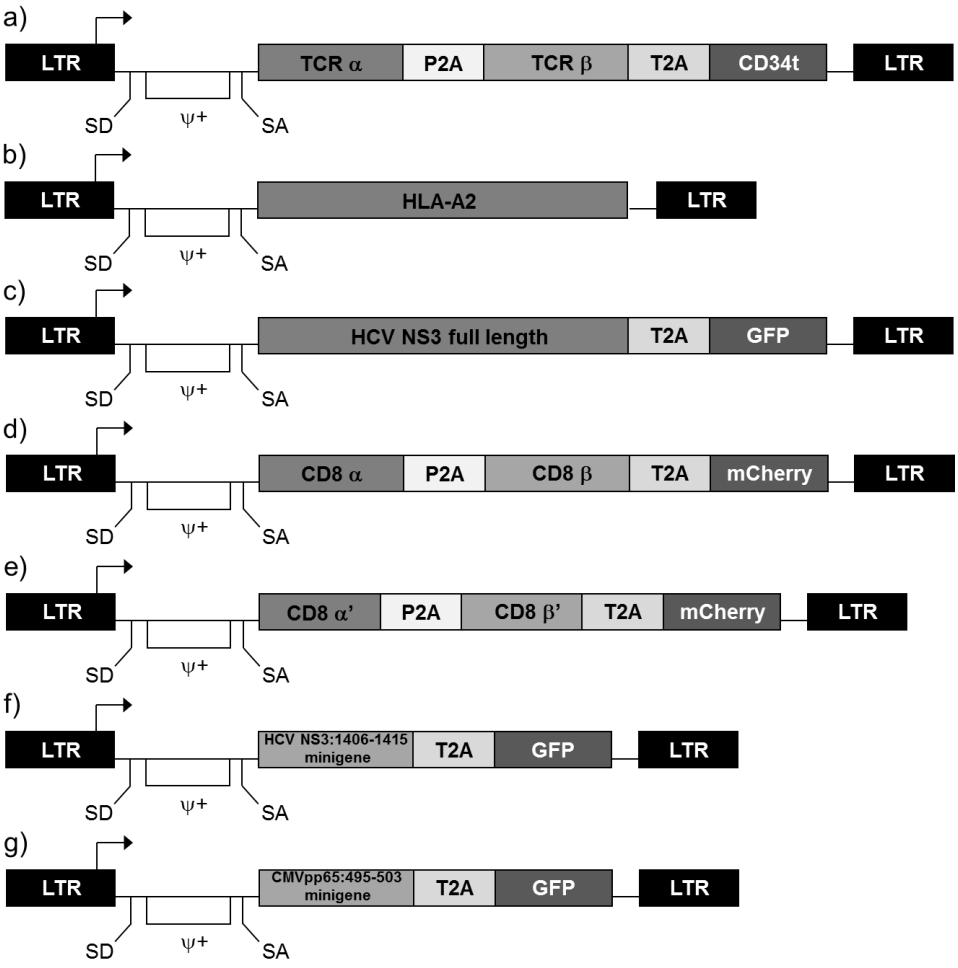

Figure 6. Structures of retroviral vectors used for gene transfer. A modified SAMEN retroviral backbone was used for transferring TCR, HLA-A2, HCV NS3, and CD8 genes to alternate effectors and targets. pMFG retroviral vectors were used to transduce HCV NS3:1406-1415 and CMVpp65:495-503 minigenes into tumor cell lines. **(a)** TCR retroviral vector containing the HCV1406 TCR or HCV1073 TCR α and β chain genes fused by a P2A self-cleaving peptide linker. A truncated version of the CD34 molecule (CD34t), which serves as a marker for transduction, was fused to the 3' end of the TCR β chain via a T2A self-cleaving peptide. **(b)** HLA-A2 encoding retroviral vector. **(c)** Full length HCV NS3 fused to GFP by T2A. **(d)** Full length CD8αβ genes or **(e)** truncated CD8α'β' lacking the intracellular lck-binding domain fused to an mCherry expression marker separated by P2A and T2A self-cleaving linkers, respectively. **V**ectors containing either **(f)** HCV NS3:1406-1415 epitope or **(g)** CMVpp65:495-503 minigenes in pMFG both fused to GFP by a T2A. LTR = long terminal repeat; ψ^+ = packaging signal; SD = splice donor; SA = splice acceptor.

harvest retroviral supernatants to transduce Jurkat cells and PBL-derived T cells (described in a later section).

Subsequent Retroviral Vector Construction Scheme

The structure of our modified SAMEN backbone offered the opportunity to swap in/out various other genes used for retroviral transduction-mediated delivery. NotI and BamHI restriction sites flank the 5' end of the TCR α chain and the 3' end of the CD34t cassette, respectively. This allowed for simple replacement of TCRα/TCRβ/CD34t with other genes/transduction makers with traditional cloning techniques using 5'-NotI/BamHI-3' compatible ends. The HLA-A2 gene was synthesized by GenScript and provided in the pUC57 vector engineered with 5' NotI and 3' BamHI restriction sites. HLA-A2 was subcloned out of the pUC57 vector into the modified SAMEN retroviral vector. Briefly, vector DNA was transformed into *Escherichia coli* TOP10 competent cells (Invitrogen) on LB ampicillin plates, and colonies were expanded in superbroth (supplemented with 100 μg/mL ampicillin (Sigma-Aldrich). Plasmid DNA from recombinant clones was isolated using a Miniprep Plasmid Isolation Kit (Qiagen) according to manufacturer's protocol and screened for the presence of each gene of interest by restriction enzyme digest analysis. Genes were digested with NotI and BamHI restriction enzymes (Thermo Scientific, Grand Island, NY) and products were separated on a 1% agarose gel. DNA bands corresponding to the correct length of HLA-A2 were excised from the gel and purified (Qiagen) according to manufacturer's protocol. Subsequently, gel-purified DNA was subcloned into the modified SAMEN retroviral

vector with compatible restriction sites. A ligation reaction containing T4 DNA ligase (New England Biolabs, Ipswich, MA) and T4 DNA ligase buffer (New England Biolabs) with vector DNA and insert DNA in a 1:5 vector:insert ratio was incubated overnight at 16^{o}C. Ligation products were transformed into competent *E. coli* and DNA was isolated (Qiagen). The final product was sequenced (Genewiz, South Plainfield, NJ) to ensure no errors had occurred during the cloning process.

Additionally, a pCR2.1 "shuttle vector" containing the sequence 5'-NotI/EcoRI/T2A/transduction marker/BamHI-3' was used to easily interchange genes with various transduction markers (CD34t, GFP, or mCherry) to be subcloned into SAMEN. CD8αβ, and CD8α'β' genes to be inserted into retroviral backbones were synthesized by GenScript provided in the pUC57 vector engineered with 5' NotI and 3' EcoRI restriction sites. Truncated CD8α'β' gene sequences have been previously described [305]. These genes were subcloned out of the pUC57 vector into pC2.1 shuttle vector containing mCherry with NotI and EcoRI restriction sites using methods described above. The resulting CD8-T2A-mCherry fragments were then excised from pCR2.1 and subcloned into the SAMEN vector using NotI and BamHI restriction sites using the same methodology. Final products were sequenced (Genewiz) to ensure no errors had occurred during the cloning process.

HCV NS3 retroviral vector. WT HCV NS3 gene fused to GFP by a T2A linker was synthesized by Genscript and provided in a pcDNAIII vector. Site directed mutagenesis was performed to generate variant 1406-1415 epitopes (described earlier). Each of

these subsequent sequences was subcloned from pcDNAIII into SAMEN in the same manner as pUC57 vectors described above.

Final SAMEN retroviral products included HLA-A2 fused to GFP by a T2A linker (Fig. 6b), HCV NS3 fused to GFP by a T2A linker (Fig. 6c), CD8α fused to CD8β fused to mCherry by P2A and T2A linkers, respectively (Fig. 6d), and CD8α' fused to CD8β' fused to mCherry by P2A and T2A linkers, respectively (Fig. 6e).

HCV and CMV minigene retroviral vectors. pMFG retroviral vectors containing CMVpp65:495-503 as well as WT and variant HCV NS3:1406-1415 minigenes fused to GFP by a T2A linker (also containing an additional *neo*^{r} cassette) were kindly provided by Zhang Yi in the Nishimura Lab (Fig. 6f-g). All above retroviral vectors were used to generate high titer producer cell lines used to transduce PBL-derived T cells, Jurkat cells, and multiple tumor cell lines.

Generation of High Titer Producer Cell Lines

Generation of stable producer PG13 cell lines was accomplished as follows. For each retroviral vector, 3 million 293GP cells were seeded in a 10 cm poly-D-Lysine coated tissue culture plate (Thermo Scientific). Cells were co-transfected with 20 μg retroviral vector DNA and 5 μg of a plasmid containing the vesicular stomatitis virus envelope gene in 50 μl Lipofectamine 2000 (Life Technologies). Media was replaced 6 hours post-transfection and viral supernatant was collected and 0.45 μm filtered after a 48 hr incubation at 37^{o}C in 5% CO_2. 2 million PG13 cells seeded in a 10 cm tissue culture plate were transduced over 72 hours using this fresh viral supernatant at 37^{o}C in 5%

CO_2. Transduction efficiency was analyzed by measuring CD34, GFP, or mCherry expression depending on the retroviral vector used. CD34, GFP, or mCherry positive cells were sorted for high and uniform expression using a FACSAria IIIu cell sorter (BD BioSciences), and the resulting high-tighter producer cell lines were maintained in IMEM supplemented with 10% FBS.

Preparation of retrovirus for transductions was accomplished by treating PG13 stable producer cell lines seeded overnight at $8x10^6$ cells/T-175 flask with sodium butyrate media (IMEM supplemented with 10% FBS, 1mM sodium butyrate (Sigma-Aldrich) and 10mM HEPES (Corning Life Sciences) for 8-10 hours. Media was replaced with IMEM supplemented with 10% FBS and fresh viral supernatants were harvested and 0.45 μm filtered the next day. Virus was used fresh or stored at -80^oC for later use.

Gene Delivery

HCV TCR Retroviral Transduction

T cells, Jurkat cells, and Jurkat76 cell lines were transduced by spinoculation as previously described [15, 305]. T cells derived from healthy donors were activated for 3 days prior to spinoculation using 50 ng/mL anti-CD3 monoclonal antibody (Miltenyi Biotec) in complete medium. 24-well flat-bottom non-tissue culture-treated plates (Thermo Fisher Scientific) were treated with 0.5 mL/well 30 μg/mL retronectin (Takara Bio, Otsu, Shiga, Japan) overnight at $4^{o-}C$. Plates were blocked with 0.5 mL/well 2% PBSA (bovine serum albumin (BSA; Fisher Scientific, Fair Lawn, NJ) in phosphate buffered saline (PBS; Corning Life Sciences)) for 30 min at room temperature (RT) and washed

with 2 mL/well PBS. 2 mL of fresh or frozen retroviral supernatant was added to each well and the plates were spun for 2 hr at 2,000xg at 32^{o}C and aspirated. 2 million activated T cells or Jurkat cell lines were gently added to the viral-coated plates in 1 mL of AIM-V/5% hAb, 600 IU/mL rhIL-2, and 200 ng/mL rhIL-15 and mixed with 1 mL filtered retroviral supernatant. The plates were spun again for 2 hr at 2,000xg at 32^{o}C and incubated overnight at 37^{o}C in 5%CO_2. After 24 hours, the transduced T cells were transferred to tissue-culture treated flasks. Three days later, transduction efficiency was determined by flow cytometry staining for CD34 using anti-CD34-APC mAb (Biolegend). Cultures were enriched for TCR-transduced T cells or Jurkat cells by positive selection using immunomagnetic beads labeled with anti-CD34 (Miltenyi Biotec) and maintained in complete medium. T cells may also have been selectively sorted for $CD4^+$ or $CD8^+$ transduced T cells using anti-CD4 or anti-CD8 immunomagnetic beads, respectively (Miltenyi Biotec). Purity of selection was confirmed by FACS analysis.

After immunomagnetic selection, TCR-transduced T cells were further expanded using a Rapid Expansion Protocol (REP). Briefly, $1x10^6$ T cells were cultured in an upright T-175 cell culture flask with $200x10^6$ irradiated (5000 rads) allogeneic PBMC in 150 mL of complete T cell medium supplemented with 30 ng/mL anti-CD3 mAb (Miltenyi Biotec). Cells were incubated at 37^{o}C in 5%CO_2 for 5 days and harvested for use in functional assays.

CD8αβ and CD8α'β' Retroviral Transduction

Jurkat and Jurkat76 cells were also transduced via spinoculation (methods described above) with a modified SAMEN retroviral vector containing human CD8αβ-mCherry or CD8α'β'-mCherry (Figs. 6d-e). $CD8^+$ cells were sorted for high and uniform expression by FACS using anti-CD8-PerCP/Cy5.5 mAb (Biolegend) and maintained in RPMI1640 supplemented with 10% FBS.

HLA-A2 Retroviral Transduction

A modified SAMEN retroviral vector containing HLA-A2 (Fig 6b) was used to transduce Huh-7 and COS cell lines. Huh-7 and COS cells were seeded in a 24-well tissue culture plate to yield 70-80% confluency. Two mL of 0.45 µm-filtered retroviral supernatants were applied to each well and incubated for 48 hr at 37^oC in 5% CO_2. Flow cytometry was used to confirm expression of HLA-A2 using an anti-HLA-A2-APC mAb (Biolegend, San Diego, CA). Positive cells were sorted for high and uniform expression of HLA-A2, and the resulting cell lines were maintained in DMEM supplemented with 10% FBS.

HCV NS3:1406-1415 Ninigene Retroviral Transduction

pFMG retroviral vectors containing WT or variant HCV NS3:1406-1415 minigenes (or the CMVpp65:495-503 epitope as a negative control) (Figs. 6f-g) were used to transduce HepG2 and Huh-7 in the same manner described above. HepG2 and Huh-7 cells were seeded in a 24-well tissue culture plate to yield 70-80% confluency. Two mL of 0.45 µm-filtered retroviral supernatants were applied to each well and incubated for

48 hr at 37^{o}C in 5% CO_2. Flow cytometry was used to confirm expression of minigenes by measuring GFP expression. Positive cells were sorted for high and uniform expression of GFP, and the resulting cell lines were maintained in DMEM supplemented with 10% FBS and 500 µg/mL G418 (Geneticin; Research Products International, Mount Prospect, IL).

Full length HCV NS3 DNA Transfection

COS and COS/A2 cells were transiently transfected to express the full length HCV NS3 protein with WT or variant 1406-1415 epitopes using pcDNAIII vectors encoding HCV NS3 linked to GFP by the self-cleaving viral sequence P2A. Cells were plated in a 24-well tissue culture plate to yield 70-80% confluency and were transfected with 3 µg DNA and 6 µl of Lipofectamine 2000 (Life Technologies) over 48 hours. Flow cytometry was used to confirm expression of full length HCV NS3 by measuring intracellular GFP levels.

Full length HCV NS3 Retroviral Transduction

Because HepG2 cells were resistant to lipid-based transfection, a modified SAMEN retroviral vector encoding HCV NS3-P2A-GFP was used to transduce HepG2 cells (Fig 6c). Cells were plated in a 24-well tissue culture plate to yield 70-80% confluency. Two mL of 0.45 µm-filtered retroviral supernatants were applied to each well and incubated for 48 hr at 37^{o}C in 5% CO_2. Flow cytometry was used to confirm expression of NS3 by measuring GFP expression. Positive cells were sorted for high and uniform expression of GFP, and the resulting cell lines were maintained in DMEM supplemented with 10% FBS.

Peptides

All peptides used in functional assays were purchased from Synthetic Biomolecules (San Diego, CA) at 95% purity. Peptides were stored in 100% dimethyl sulfoxide (DMSO; Sigma-Aldrich) at -80^{o}C at a concentration of 5 μg/μL. A complete list of all peptides used, their sequences, and their abbreviations as referred to in the text can be found in Table 4.

Alanine substituted peptides were used as stimulators against T cell clones isolated from infected HCV^{+} patients (Chapter 4) as well as PBL-derived T cells and Jurkat cell lines transduced to express the HCV1406 TCR (Appendix). An alanine scanner set for the HCV NS3:1406-1415 peptide, was generated by substituting an alanine at each residue position (1 through 10) except where an alanine natively occurs. In these cases (positions 4 and 9) an isoleucine was substituted for an alanine.

Naturally occurring mutant sequences for HCV NS3:1406-1415 and HCV NS3:1073-1081 epitopes were identified by searching the GenBank (http://www.ncbi.nlm.nih.gov/genbank/) using the WT nucleotide sequences. Sequence AAGCTGGTCGCGTTGGGCATCAATGCCGTG was used for HCV NS3:1406-1415, while sequence TGCATCAATGGGGTGTGCTGGACTGTC was used for HCV NS3:1073-1081. Of the 1,000+ sequences recovered for each, silent mutations were eliminated and 8 naturally occurring mutant epitopes were chosen for each that allowed for a spectrum of amino acid changes in position and class. These peptides (also listed in Table 4) were used for functional studies discussed in Chapters Four, Five, and Six.

Table 4. Peptide names, abbreviations, and sequences used for functional studies.

Peptide Name	Abbreviation	Sequence
Tyrosinase:368-376	Tyro	YMDGTMSQV
CMVpp65:495-503	CMV	NLVPMVATV
HCV NS3:1406-1415	HCV1406wt	KLVALGINAV
HCV NS3:V1408L	V1408L	KLLALGINAV
HCV NS3:A1409T	A1409T	KLVTLGINAV
HCV NS3:I1412L	I1412L	KLVALGLNAV
HCV NS3:I1412V	I1412V	KLVALGVNAV
HCV NS3:I1412N	I1412N	KLVALGNNAV
HCV NS3:V1408S/A1409G/I1412L	8S/9G/12L	KLSGLGLNAV
NS3:V1408T	V1408T	KLTALGINAV
HCV NS3:V1408S/A1409S/I1412L/A1414S	8S/9S/12L/14S	KLSSLGLNSV
HCV NS3:K1406A	K1406A	ALVALGINAV
HCV NS3:L1407A	L1407A	KAVALGINAV
HCV NS3:V1408A	V1408A	KLAALGINAV
HCV NS3:A1409I	A1409I	KLVILGINAV
HCV NS3:L1410A	L1410A	KLVAAGINAV
HCV NS3:G1411A	G1411A	KLVALAINAV
HCV NS3:I1412A	I1412A	KLVALGANAV
HCV NS3:N1413A	N1413A	KLVALGIAAV
HCV NS3:A1414I	A1414I	KLVALGINIV
HCV NS3:V1415A	V1415A	KLVALGINAA
HCV NS3:1073-1081	HCV1073wt	CINGVCWTV
HCV NS3:I1074V	I1074V	CVNGVCWTV
HCV NS3:I1074L	I1073A	CLNGVCWTV
HCV NS3:V1077A	V1077A	CINGACWTV
HCV NS3:C1078F	C1078F	CINGVFWTV
HCV NS3:V1081N	V1081N	CINGVCWTN
HCV NS3:T1080S	T1080S	CINGVCWSV
HCV NS3:V1081A	V1081A	CINGVCWTA
HCV NS3:T1080S/V1081I	80S/81I	CINGVCWSI

*All peptides were acquired at 95% purity from Synthetic Biomolecules (San Diego, CA).

Proteins

MHC class I protein was kindly generated by members of the Baker Lab at the University of Notre Dame. Recombinant MHC-I was used for peptide-MHC thermal denaturation studies as well as TCR-pMHC binding affinity measurements. Briefly, recombinant HLA-A*0201 heavy chain and β-2 microglobulin were expressed as inclusion bodies in *Escherichia coli* [306]. Expression of HCV1406 TCR was performed similarly. TCR and MHC folding and assembly from inclusion bodies was performed according to standard procedures [307]. Protein was purified using ion exchange followed by size-exclusion chromatography.

Cytokine Release Assay

Antigen reactivity by HCV1406 TCR or HCV1073 TCR transduced T cells and Jurkat cell lines was measured in cytokine release assays as previously described [168]. Briefly, HCV^+ tumor cells or peptide-loaded T2 cells were routinely used as stimulators. T2 cells were pulsed with 10 μg/mL peptide for 2 hrs prior to co-culture. Titration of HCV1406 TCR reactivity used peptide concentrations ranging from 10 – 0.00001 μg/mL. $1x10^5$ responder and stimulator cells were co-cultured in a 1:1 ratio in 96-well U-bottom tissue culture plates in 200 μL complete medium. Ten ng/mL phorbol 12-myristate 13-acetate (PMA; Sigma-Aldrich) was added to Jurkat cell co-cultures to enhance sensitivity to stimulation. Co-cultures were incubated at 37^oC for 20 hrs and supernatants were harvested. The amount of IFNγ or IL-2 released by 10^5 T cells or Jurkat cells, respectively, was measured via ELISA (R&D Systems, Minneapolis, MN).

Immunofluorescence Staining Reagents

A table summarizing all immunofluorescence staining reagents can be found in Table 5. Sections below describe the applications for various reagents used.

Immunofluorescence Antibodies

Fluorochrome-conjugated antibodies were used to detect T cell surface markers (CD3, CD4, CD8), transduced or endogenous TCRs, and CD34 as a marker for transduction. Additionally, TCR-transduced T cells were analyzed for activation markers CD25 and CD69 and inhibitory markers PD-1 and TIM-3 to characterize a representative population of TCR-transduced PBL-derived T cells. In functional assays, TCR-transduced T cells were also stained for lytic marker CD107a and intracellular cytokines IFNγ, TNFα, IL-2, IL-4, IL-17A, and IL-22. Pairing of fluorochromes to antibodies was determined by established staining profiles of each antibody to allow for detection of bright, dim, and negative populations. Spectral overlap between fluorescent dyes was also considered.A summary of antibodies, selected fluorochormes, and their manufacturers are listed in Table 5.

Dextramers and Tetramers

APC-labeled HLA-A*0201 dextamer folded around WT HCV NS3:1406-1415 (KLVALGINAV) (Immundex, Copenhagen, Denmark) was used as a surrogate for TCR expression as commercially available antibodies do not bind HCV1406 TCR very well. The NIH Tetramer Core Facility at Emory University (Atlanta, GA) kindly provided a panel of monomers and tetramers used for tetramer binding experiments. The core provided

Table 5. Reagents and manufacturers used for immunofluorescence.

Use	Reagent	Clone	Conjugated Fluorochrome	Manufacturer
Transduced T Cell Culture Characterization (Chapter Three)	anti-CD3	SK7	APC/Cy7	Biolegend[§]
	anti-CD4	161A1	FITC	Biolegend
	anti-CD8	SK1	AF[†] 700	Biolegend
	anti-CD34	581	PerCP/Cy5.5	Biolegend
	anti-CD25	BC96	BV[‡] 711	Biolegend
	anti-CD69	FN50	PE/Cy7	Biolegend
	anti-PD-1	EH12.2H7	BV 421	Biolegend
	anti-TIM-3	F38-2E2	BV 605	Biolegend
	KLVALGINAV/HLA-A*0201 Dextramer	N/A	APC	Immudex[¶]
	anti-TCR Vβ13.6	N/A	PE	Beckman Coulter[‖]
T Cell Surface Markers (Remaining Chapters)	anti-CD3	UCHT1	APC/Cy7	Biolegend
	anti-CD4	RPA-T4	PE/Cy7	Biolegend
	anti-CD34	561	PE	Biolegend
	anti-CD107a	H4A3	BV 510	Biolegend
Polyfunctionality Assay-Specific Surface Markers	anti-CD3	UCHT1	APC/Cy7	Biolegend
	anti-CD4	RPA-T4	PE/Cy7	Biolegend
	anti-CD8	SK1	FITC	Biolegend
	anti-CD34	581	AF 700	Biolegend
	anti-CD107a	H4A3	BV 510	Biolegend
Intracellular Cytokines	anti-IFNγ	4S.B3	BV 421	Biolegend
	anti-TNFα	Mab11	BV 711	Biolegend
	anti-IL-2	MQ1-17H12	PerCP/Cy5.5	Biolegend
	anti-IL-4	8D4-8	AF 647	Biolegend
	anti-IL-17A	BL168	BV 570	Biolegend
	anti-IL-22	BG/IL22	PE	Biolegend

[†]AF, Alexa Fluor [‡]BV, Brilliant Violet; [§]Biolegend, San Diego, CA; [¶]Immudex, Copenhangen, Denmark; [‖]Beckman Coulter, Marseille, France

Table 5. Reagents and manufacturers used for immunofluorescence (cont'd).

Use	Reagent	Clone	Conjugated Fluorochrome	Manufacturer
Tetramer Staining and Dissociation Experiments	KLVALGINAV/ HLA-A*0201	N/A	APC (supplied as a monomer)	NIH Tetramer Core Facility[#]
	KLLALGINAV/ HLA-A*0201	N/A	APC	NIH Tetramer Core Facility
	KLVTLGINAV/ HLA-A*0201	N/A	APC	NIH Tetramer Core Facility
	KLVALGLNAV/ HLA-A*0201	N/A	APC	NIH Tetramer Core Facility
	KLVALGVNAV/ HLA-A*0201	N/A	APC	NIH Tetramer Core Facility
	KLVALGNNAV/ HLA-A*0201	N/A	APC	NIH Tetramer Core Facility
	KLSGLGLNAV/ HLA-A*0201	N/A	APC	NIH Tetramer Core Facility
	KLTALGINAV/ HLA-A*0201	N/A	APC	NIH Tetramer Core Facility
	KLSSLGLNSV/ HLA-A*0201	N/A	APC	NIH Tetramer Core Facility
	YMDGTMSQV/ HLA-A*0201	N/A	APC	NIH Tetramer Core Facility
	Streptavidin	N/A	APC	Prozyme**

[#]NIH Tetramer Core Facility at Emory University, Atlanta, Georgia; **Prozyme, Hayward, CA

HLA-A*0201 monomers folded around WT HCV NS3:1406-1415 (KLVALGINAV) or tyrosinase:368-376 (TMDGTMSQV) at 2.0 mg/mL. They also provided APC-labeled HLA-A*0201 tetramers folded around WT and variant HCV NS3:1406-1415 peptides at 1.5 mg/mL. A full description of tetramers and monomers provided is listed in Table 5.

Monomer Tetramerization

HLA-A*0201 monomers (folded around HCV NS3:1406-1415 and tyrosinase:368-376) supplied at 2.0 mg/mL were tetramerized by adding 13.9 µL of 2.1 mg/mL streptavidin-APC (Prozyme, Hayward, CA) at RT 10 times in 10 minute intervals. At the end of 10 additions of streptavidin-APC, monomers were fully tetramerized with a slight excess of streptavidin-APC.

Tetramer Binding Experiments

Saturating concentrations of WT and variant HCV NS3:1406-1415 tetramers were evaluated for HCV1406 TCR transduced Jurkat or Jurkat76 cells and HCV1406 TCR-transduced Jurkat as well as Jurkat76 cells engineered to co-express full length CD8αβ. Cell lines were incubated with each tetramer, concentrations ranging from $1x10^{-7}$ to $1x10^{-12}$, and either anti-CD34/AF700 (Biolegend) (for Jurkat cells) or anti-CD3-APC/Cy (Biolegend) (for Jurkat76 cells) in 2% PBSA/0.2% sodium azide (Sigma-Alrich) on ice for at least 2 hr in the dark. Because it has been shown the presence of anti-CD8 antibodies can alter tetramer binding [308-310], cells were not co-stained for CD8. Rather, the presence of CD8 was measured by transgene marker mCherry. Cells were washed and resuspended in ice-cold 2% PBSA/0.2% sodium azide, and analyzed for bound

fluorescent tetramers using an LSRFortessa flow cytometer (BD Biosceinces). Fluorescence of the non-TCR-transduced cells was used for background subtraction to determine specific binding to TCR-transduced cells. Specific tetramer binding for each concentration of tetramer was calculated for each cell line as follows:

$CD8^+$ Jurkat: $\%Tetramer^+CD34^+mCherry^+ - \%Tetramer^+CD34^-mCherry^+$

$CD8^-$ Jurkat: $\%Tetramer^+CD34^+mCherry^- - \%Tetramer^+CD34^-mCherry^-$

$CD8^+$ Jurkat76: $\%Tetramer^+CD3^+mCherry^+ - \%Tetramer^+CD3^-mCherry^+$

$CD8^-$ Jurkat76: $\%Tetramer^+CD3^+mCherry^- - \%Tetramer^+CD3^-mCherry^-$

Bi-Functional T cell Reactivity Assay

Percentages of IFNγ producing and/or lytic HCV1406 TCR -transduced T cells was measured in an intracellular IFNγ/surface CD107a-detection assay. $3x10^5$ responder and $3x10^5$ stimulator cells were co-cultured in a 1:1 ratio in 96-well U-bottom tissue culture plates in 200 µL complete medium. Five µL anti-CD107a mAb, 5.0 ng/mL brefeldin-A, and 2.0 nM monensin (all Biolegend) were added at the start of co-culture. Co-cultures were incubated at 37^oC for 5 hours, and cells were stained for immunofluorescence against cell surface antigens for 20 minutes at RT. Subsequently, cells were fixed in Fixation Buffer (Biolegend) for 20 min, washed 3 times in Permeabilization and Wash Buffer (Biolegend), and counterstained for intracellular IFNγ for 20 min at RT. Data were acquired using an LSRFortessa flow cytometer (BD Biosciences). $CD34^+$ events (transduced T cells) were gated into $CD4^+CD8^-$ or $CD4^-CD8^+$ populations using FlowJo vX (TreeStar, Ashland, OR). Percentages of $CD107a^+IFN\gamma^-$ (lytic only), $CD107a^+IFN\gamma^+$ (lytic

and cytokine-secreting), $CD107a^{-}IFN\gamma^{+}$ (cytokine-secreting only), or $CD107a^{-}IFN\gamma^{-}$ (non-reactive) cells were calculated for both $CD34^{+}CD4^{+}CD8^{-}$ and $CD34^{+}CD4^{+}CD8^{-}$ T cell populations and frequencies were converted into pie charts.

Polyfunctional T Cell Lysis and Multi-Intracellular Cytokine Assay

In similar methods described above, HCV^{+} tumor cells or peptide-loaded T2 cells were put into co-culture with HCV1406 TCR-transduced PBL-derived T cells. $3x10^{5}$ responder and $3x10^{5}$ stimulator cells were mixed in a 1:1 ratio in 96-well U-bottom tissue culture plates in 200 µL complete medium. Five µL anti-CD107a mAb, 5.0 ng/mL brefeldin-A, and 2.0 nM monensin (all Biolegend, San Diego, CA) were added at the beginning of the co-culture. Co-cultures were incubated at $37^{o}C$ for 5 hours, and cells were stained for cell surface antigens for 20 minutes at RT. Subsequently, cells were incubated in Fixation Buffer (Biolegend) for 20 min, washed 3 times in Permeabilization and Wash Buffer (Biolegend), and stained for intracellular cytokines for 20 min at RT. Cells were washed, resuspended in Cell Staining Buffer (Biolegend), and analyzed by flow cytometry. Samples were acquired using a LSRFortessa flow cytometer (BD Biosciences). Staining profiles were gated and analyzed using FlowJoX software (TreeStar, Ashland, OR).

Multi-Dimensional Flow Cytometry Data Analysis

Seven-parameter functional analysis by flow cytometry yields datasets far too complex to analyze in traditional flow cytometry analysis software such as FlowJo. We evaluated a series of software packages in their ability to visualize and interpret our

complex, high dimensional data assessing T cell polyfunctionality. Some of the requirements of these tools are to be able to represent rare and high frequency populations, visualize the data at a single cell level, preserve the relationships and geometry of the data, and provide an interpretable view of the data for publication or presentation. The programs available ranged from all manual gating to unsupervised gating, and analysis algorithms contained clustering, dimension reduction, hierarchy extraction and/or t-Distributed Stochastic Neighbor Embedding (tSNE).

In order to uniformly evaluate the different analysis methods, the same set of polyfunctional T cell stimulation data was analyzed in each approach. Below we present detailed methods, highlighting representative graphical output for each tool evaluated. We also provide commentary on the general benefits and drawbacks and the feasibility of (or lack thereof) in generating meaningful interpretation of changes in T cell polyfunctionality. For consistency, we use the same experimental dataset for the comparison of each tool, and for simplicity, we illustrate only comparisons of negatively (tyrosinase:368-376) or positively (WT HCV NS3:1406-1415) peptide-stimulated HCV TCR-transduced $CD8^+$ T cells. It is pointed out where additional comparisons between $CD8^+$ and $CD4^+$ T cells as well across variant peptide or tumor stimulation conditions would be easily interpreted in subsequent analytical approaches or would make the data more complicated to discern a biological message. In summary, the goal of these comparative evaluations was to generate simple and meaningful graphical output

evaluating changes in HCV1406 TCR-transduced T cell polyfunctional phenotypes in response to variant HCV NS3:1406-1415 peptide and tumor stimulations.

Gating Strategy

Lymphocyte populations were discerned by FSC vs. SSC comparison, and events were gated on $CD4^+CD8^-$ or $CD4^-CD8^+$ populations. $CD4^+$ or $CD8^+$ T cells were then gated on $CD34^+$ expression to define our transduced cell populations. These $CD4^+CD8^-CD34^+$ or $CD4^-CD8^+CD34^+$ were subsequently used as starting points for subsequent analysis using the remaining software strategies. Functional parameters included CD107a, IFNγ, TNFα, IL-2, IL-4, IL-17A, and IL-22.

GemStone

GemStone, available through Verity Software House (Topsham, ME), uses probability state modeling (PSM) to represent a set of cellular progressions or "Cell Types", originally engineered to analyze and visualize multidimensional cellular populations [311]. The basis of PSM is creating a model consisting of different Cell Types, which are defined by the user. Using the information available for each of the Cell Types, parameter profiles are then created, and these Cell Types are used as progression steps in the model. Relationships between parameters may be discovered and transitional cell types may also be defined. As a model is built, complexity may be added and then tested with the data to be analyzed.

Major benefits of PSM analysis include accounting for population overlap, simple clustering routines, and identifying populations without giving biological

interrelationships. Additionally, gates are not drawn using GemStone so there is neither subjectivity nor operator variability. While gating defines positive and negative, GemStone allows for transitional populations and can allow for up- and down-regulation of markers. One disadvantage, however, is that design of templates used for analysis requires knowledge of some biology of the system.

A TriCOM is a tool contained within GemStone that is used to show different phenotypes and activation states (Fig. 7). TriCOM analysis displays concentric pie charts for each level of co-expressed parameters. Multiple parameters in a single cell population are represented by multiple colors within a single wedge.

For our purposes, the TriCOMs showed a distinct visualization of cytokines present at each order of staining, but the concentric pie charts became much harder to read when analyzing higher orders of staining (≥3 parameters). For example, the proportions of cells expressing only one cytokine each are relatively easily interpreted (Fig. 7, bottom pie chart). It becomes less clear, however, when trying to resolve populations greater than three parameters or looking at two parameter positive cells that occur in low frequencies. Overall, while TriCOMs are useful tools that clearly visualize phenotypes, they can become difficult to read at greater than three parameters or for low frequency populations. Additionally, making comparisons across multiple treatment groups would require a large number of TriCOMs with so many functional parameters evaluated.

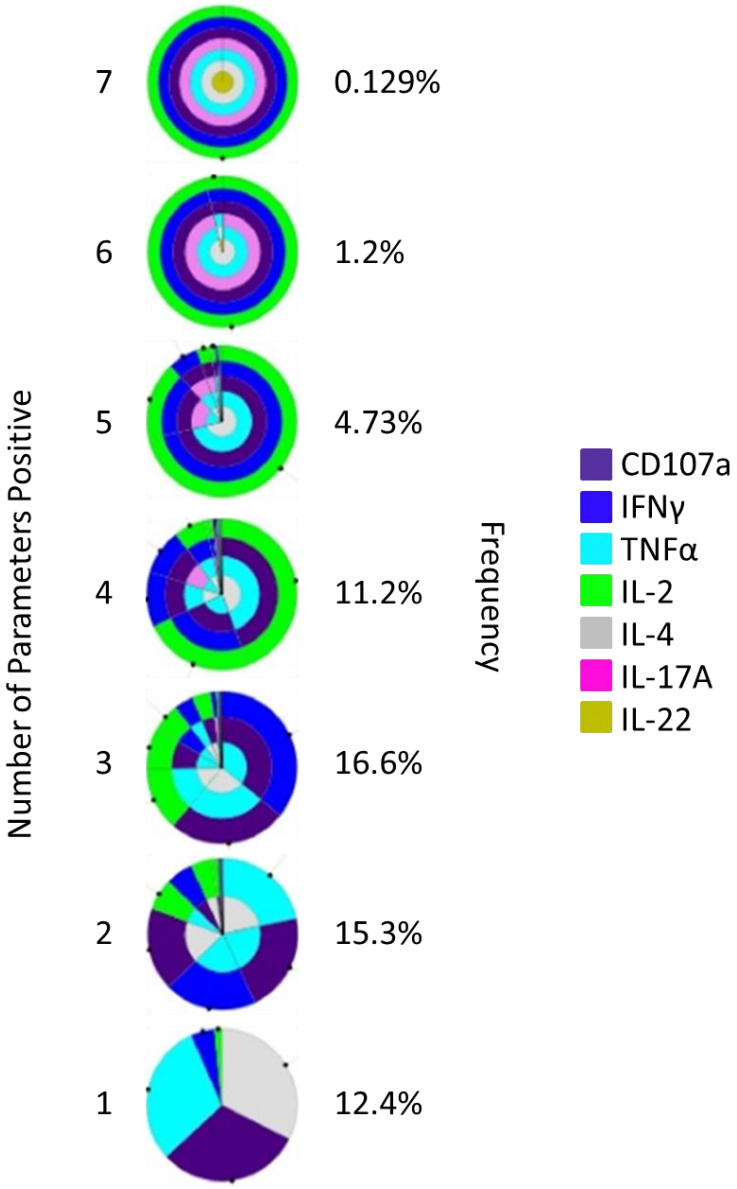

Figure 7. GemStone TriCOM analysis. TriCOMs display percentage of $CD8^+$ HCV1406 TCR-transduced T cells positive for combinations of functional markers in concentric pie charts. The bottom pie chart represents frequency of cells positive for only 1 marker, and each pie chart above it represents an additional level of staining up to 7 simultaneous markers (top pie chart). Functional phenotypes are represented by a single wedge with multiple colors. Frequency of cells in each category is shown to the right of each pie chart. Phenotypes at each level are coded by the colors that make up each wedge. Purple=CD107a, Blue-IFNγ, Turquoise=TNFα, Green=IL-2, Gray=IL-4, Pink=IL-17A, Gold=IL-22.

Spanning-Tree Progression Analysis of Density-Normalized Events

Spanning-tree Progression Analysis of Density-Normalized Events (SPADE) was created to aid in visualization and analysis of multi-parameter data. This algorithm, available through Cytobank (Mountain View, CA; http://www.cytobank.org), is designed to extract a hierarchy from high-dimensional cytometry data in an unsupervised manner. This enables multiple cell types to be visualized in a branched tree structure [312]. SPADE contains 4 modules: i) Density-dependent down-sampling, which allows rare as well as abundant populations to be represented equally; ii) Agglomerative clustering, which separates the down-sampled data into groups containing cells with similar phenotypes; because the rare cells are represented equally, a node for these cells can be created; iii) A minimum spanning tree is created which connects all of the clusters with a minimal edge length; iv) Each data file is up-sampled, with the cells being mapped to the appropriate cluster. The clusters are then organized and displayed as a two dimensional tree. SPADE has been most useful for studies looking at cell populations with mixed lineages or tracking distinct cellular progressions [312-315]. Clusters form nicely when certain markers are mutually exclusive from others or if there is a clear progression of cellular phenotypes. After spanning-trees are generated, other markers can be analyzed for their intensity within these nodes, but only one a time.

The major benefits of SPADE are that the user does not need to know a hierarchical order before analysis and that rare cell types are identifiable. It is also scalable with increasing numbers of parameters. As such, investigators can infer likely

cellular processes and hierarchies without needing predetermined hierarchies. The spanning tree is only limited by choice of markers used in an experiment and the subsets used for building a tree. The major limitation of SPADE, however, is that data are represented as clusters rather than individual cells so single cell resolutions is lost. And if spanning trees fail to cluster, few useful conclusions can be made.

For our purposes, a SPADE-derived spanning-tree was not optimal in determining a cellular progression of T cell polyfunctionality. Cytokine phenotypes did not cluster, and instead of a tree, a web-like pattern was generated. Although it is clear there are visual differences between spanning-trees of tyrosinase versus WT NS3:140601415 peptide-stimulated TCR-transduced T cells (Fig. 8), SPADE-generated spanning-trees were not useful in easily determining phenotypes of each individual node. Addition of parameters that would cluster naive, memory, activating, or inhibitory T cell markers would create more nodal or mutually exclusive populations but would limit our ability to evaluate as many cytokines.

Self-Organizing Maps of Visualizing and Interpretation of Cytometry Data

Self-Organizing Maps of Visualizing and Interpretation of Cytometry Data (FlowSOM) also focuses on clustering as well as being a visualization aid [316]. An R-based program available through BioConductor (Seattle, WA), this algorithm consists of four steps. First, the data is read. Data can be compensated, transformed and gated and then exported by FlowJo, or these functions may be performed using FlowSOM itself within R. Second, a self-organizing map is built which is an artificial neural network,

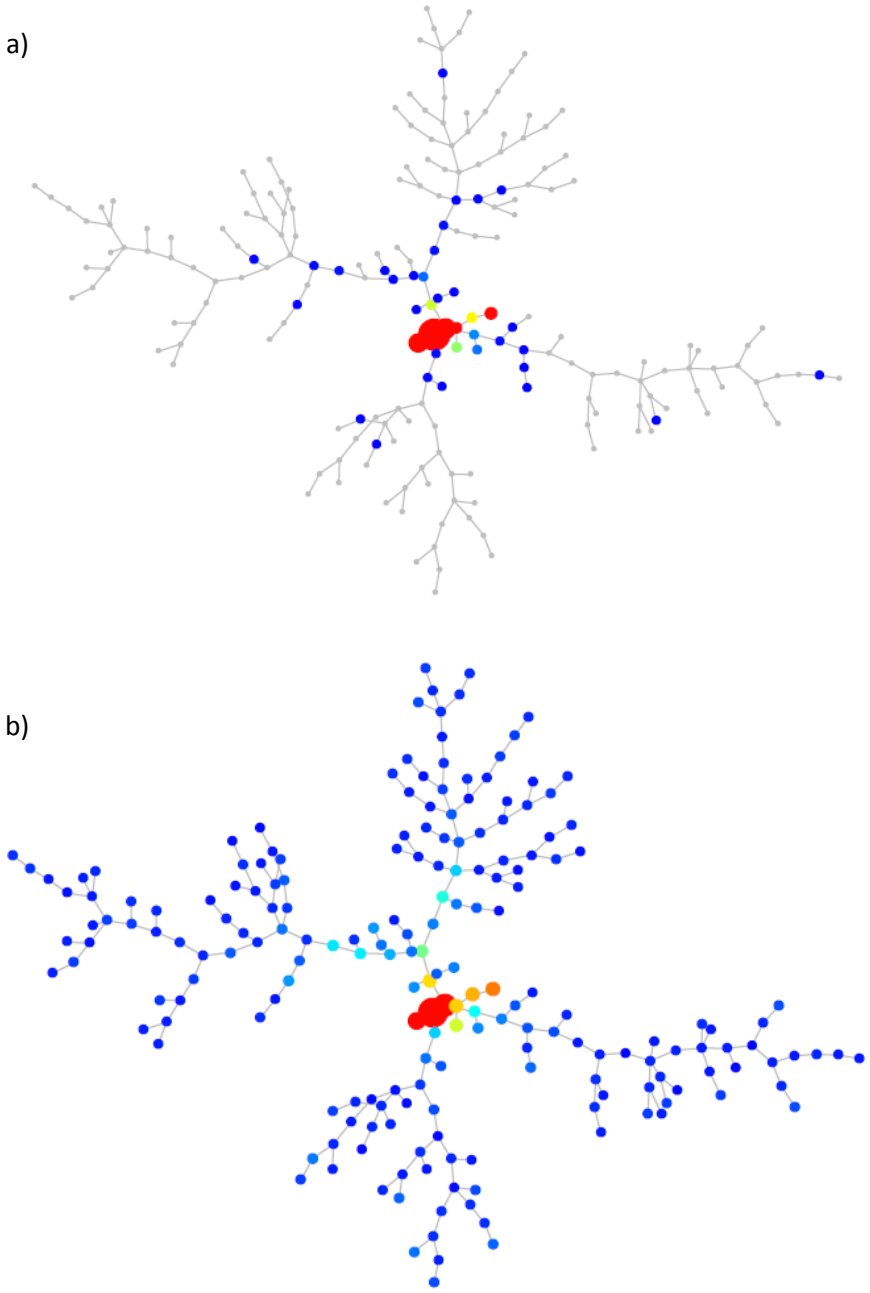

Figure 8. Graphical output provided by clustering tool SPADE. SPADE-generated spanning trees represent phenotypic clustering of $CD8^+$ HCV1406 TCR-transduced T cells after co-culture stimulation **(a)** tyrosinase:368-376 or **(b)** WT HCV NS3:1406-1415 peptides. Colored nodes refer to cell density. Cytokine profiles of each node are unable to be graphically displayed.

containing a grid of nodes. These nodes represent a single point in multidimensional space. Cells are then classified to the nearest node, and the grid places nodes that closely resemble each spatially proportionally. Third, a minimal spanning tree is built connecting the nodes that are most similar to each other in minimal branches. Lastly, metaclustering calculates the expected number of nodes if there is a much larger amount of clusters than the expected number of cell types. After this process, the data may be visualized either as a minimal spanning tree, similar to SPADE, or as a grid. Each node is coded as a pie chart with information about the phenotype of cells in that node.

The benefits of using FlowSOM is that even though this is an R-based program, using the provided documentation only a minimal understanding of R will allow you to successfully use this program. The program also does not tax the memory usage of a desktop computer, and the output is very detailed. Each node of the minimal spanning tree contains colored wedges corresponding to the measured functional parameters.

Similar to our analysis in SPADE, there are clear visual differences between NS3:1406-1415 peptide stimulation compared to negative control tryosinase (Fig. 9). However, the identification of nodal phenotypes was difficult to interpret. Overall, clustering tools can be very useful for when tracking distinct cellular progressions or measuring changes in mixed cell populations with distinct lineages. But when looking at a subset of T cells without mutually exclusive markers present, clustering tools are not optimal to make these multi-dimensional analyses.

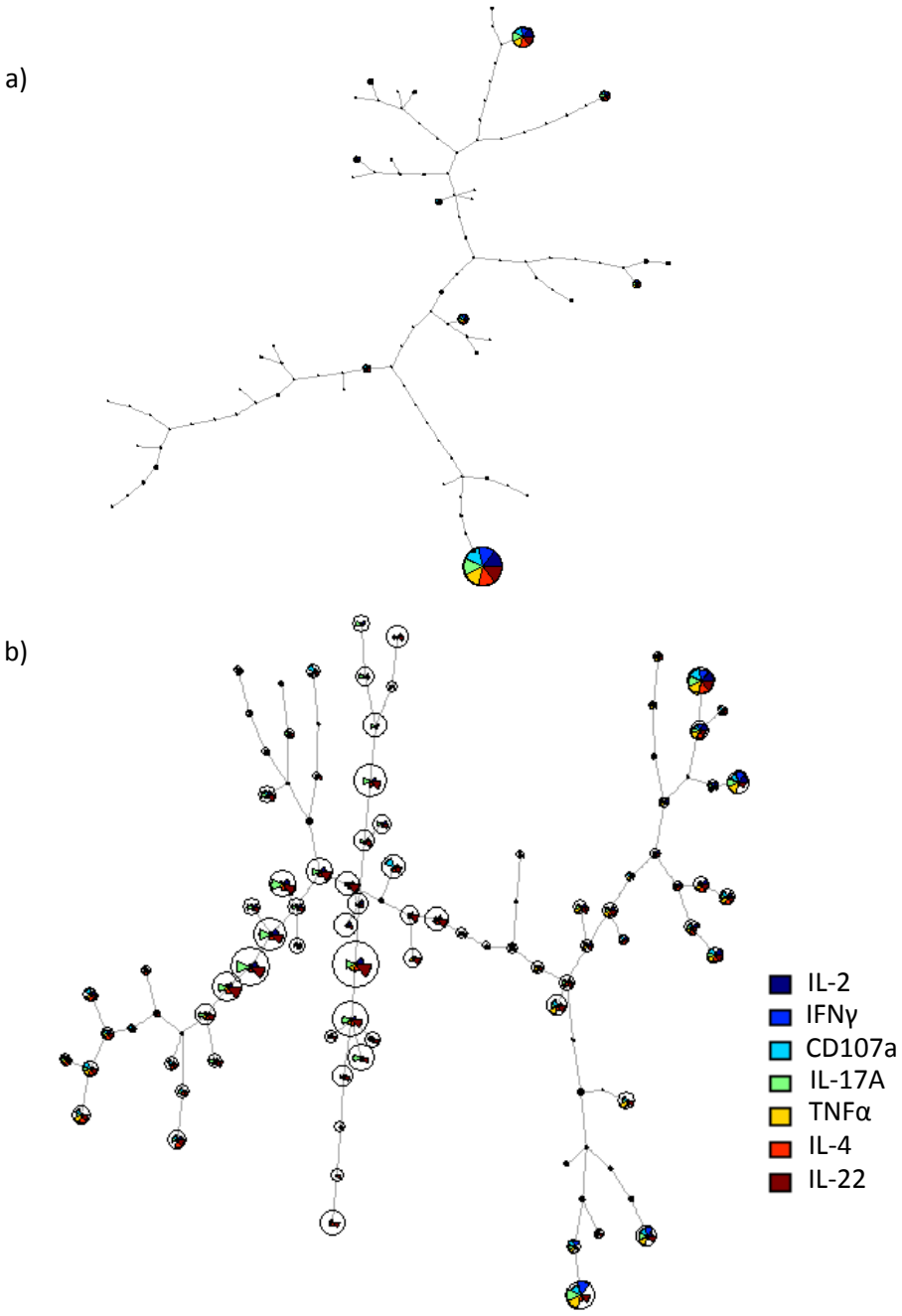

Figure 9. Graphical output provided by clustering tool FlowSOM. FlowSOM-generated minimal spanning trees represent phenotypic clustering of $CD8^+$ HCV TCR-transduced T cells after co-culture stimulation with **(a)** tyrosinase:368-376 or **(b)** WT HCV NS3:1406-1415. Size of each node corresponds to cell density. Colored pie wedges refers to cytokine(s) produced by each nodal population.

viSNE

viSNE, also available through Cytobank, is a tool for the visualization of high-dimensional single-cell data. Analysis places a cell in a two-dimensional map but preserves the separation between types. This mapping takes advantage of the inherent structure of the data where different types are in separate regions in high-dimensional space. viSNE uses a nonlinear dimensionality reduction algorithm which is based on t-Distributed Stochastic Neighbor Embedding (t-SNE) [317]. t-SNE calculates a distance matrix in high dimensional space, which is transformed into a similarity matrix. Low dimensional similarities are calculated using Student's t-distribution. viSNE generates a representation of this data that is similar to a biaxial plot and retains the geometry of the populations. The data is represented as cells in high-dimensional data space and does so without relying on traditional gating strategies. viSNE can also discretely and automatically separate cells based on subtype, provided they exist. The *cyt* feature allows for coloring of cells based on selected expression markers. The data appears as a cloud biaxial plot with a specific geometry. Differences in populations can be seen as changes in the geometry, and events may be colored to determine which parameter or parameters have changed.

A major benefit with using viSNE is that comparisons are made in high dimensional space. When there are populations that do not resolve when examined in 2 or 3 dimensions, viSNE can overcome that obstacle. viSNE is also unsupervised and does not require in depth knowledge of the system being investigated. A limitation of viSNE is

that low-dimensional mapping cannot represent all of the information in high dimensional space as viSNE only captures the most dominant structures. Additionally, plots become too crowded when more than 30,000 cells are shown.

For our purposes, viSNE was able to detect distinct changes in our populations when examining cytokines or CD107a singly (Fig. 10), but determination of polyfunctional populations required cumbersome mental overlap of the plots. For example, while it is evident that IFNγ^{+} cells reside in the top right corner of its corresponding *cyt* map, it is logical to conclude that TNFα directly overlays much of this area. IL-2 also seemingly occupies much of the cyt map where TNFα is positive as well, but that IL-4 but is limited in its overlap with IFNγ. While these observations support what FlowJo-generated dotplots suggest, making conclusive arguments by mentally overlapping multiple plots is difficult. This would be even more challenging when comparing multiple T cell subsets or across multiple stimulation conditions. While others have shown a *cyt* plots with color gradients coding for the number of cytokines present using t-SNE within R [318], viSNE is currently unable to spatially compare multiple cytokines in the same plot for our analysis.

FLOw Clustering without K

FLOw Clustering without K (FLOCK) is an unsupervised algorithm analysis publically available through Immunology Database and Analysis Portal (ImmPort; http://www.immport.org), sponsored by the NIAID, for open use by the immunology research community. FLOCK computationally determines the number of unique

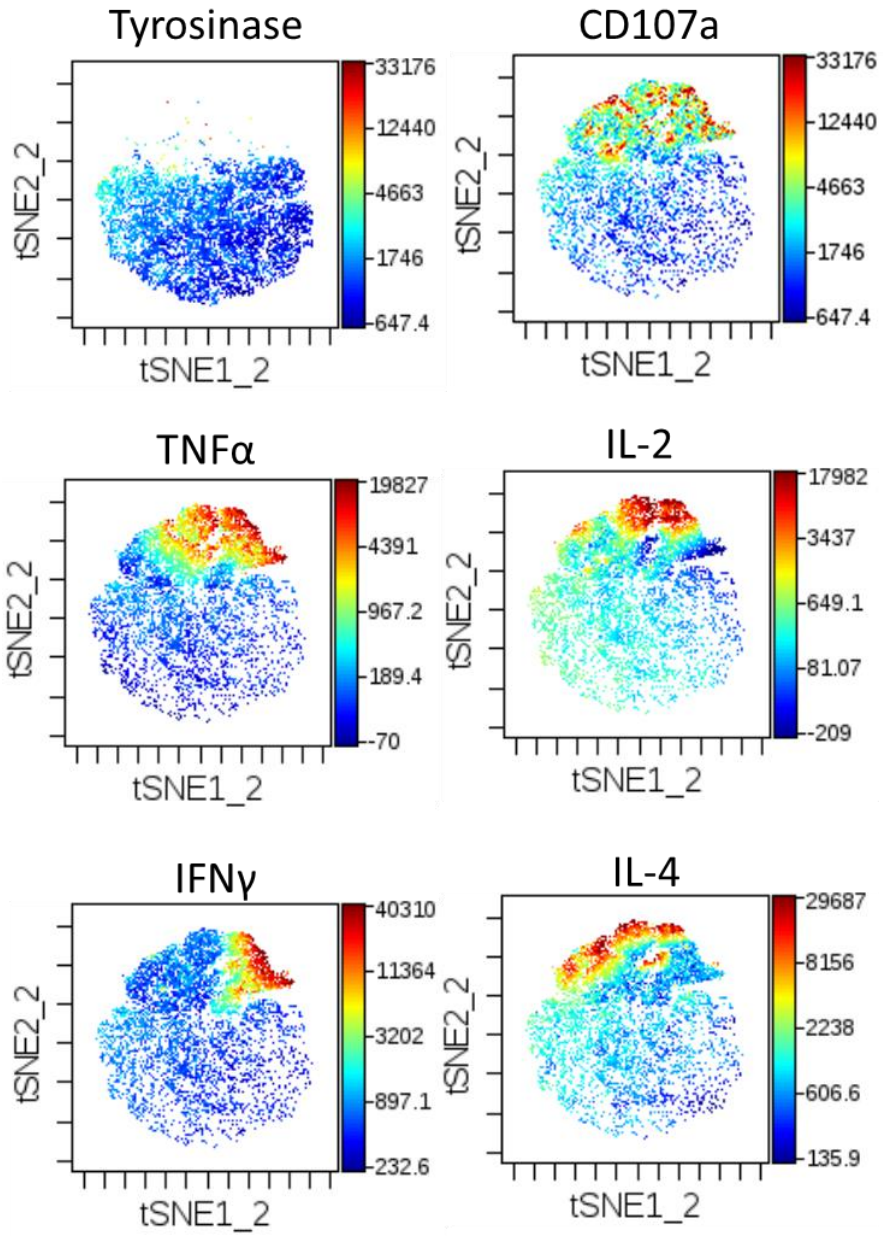

Figure 10. viSNE-generated *cyt* maps. *cyt* maps displaying collected events in a tyrosinase peptide stimulation (top left panel) or HCV peptide stimulation (remaining panels) for expression of CD107a, IFNγ, TNFα, IL-2, and IL-4. Scale (blue to red) corresponds to strength of parameter fluorescence (low to high, respectively).

populations in high dimensional flow data using a rapid binning approach and maps across independent samples [319]. Relying on predetermined gating of populations of interest, it color-codes various populations within a matrix of biaxial plots. FLOCK can calculate many useful summary statistics through cross-sample analysis to compare differences across treatment groups, and is a model-independent approach to multi-parameter analysis.

There are 5 steps in this analysis algorithm. i) Data preprocessing: Compensated FCS files were converted to tab-delimited text files using a FlowJo export function. The data consisted of a table of rows and columns defined by cells and measured parameters, respectively. The columns are normalized so that the balance of each parameter is normalized. ii) Grid-based density clustering: Data is portioned into equally sized bins, and partitioning is applied to all dimensions in the dataset simultaneously. Each dimension is portioned into the same number of bins, resulting in partitions of *n*-dimensional space called hyperregions. Each hyperregion is assessed to determine the number of events in the region. If events exceed a specific threshold, the hyperregion is called dense. iii) Centroid generation: Hyperregions are grouped together if they are adjacent to each other in *n*-dimensional space, each called a dense hyperregion group. The centroids representing all events in each dense hyperregion group are then determined. iv) Event assignment: After centroids are determined, each event is assigned to its closest centroid. The centroids are updated based on the newly assigned events, and the cluster membership is computed again with the new centroids. This

procedure, after a few iterations, is regarded as a modified K-means determination. FLOCK quickly converges to a stable result during the centroid recalculation, and unique populations are identified. The visualization module of FLOCK contains two-dimensional dot plots with each population colored uniquely. Expression profiles of a population are presented to indicate the approximate expression level of each marker of a population as negative, low, or high.

Major advantages of FLOCK are that any up-front gating can be performed using FlowJo, which is a familiar tool, and FLOCK's ease of use. Data can be easily uploaded, and after answering a few questions an analysis is requested with a subsequent notification after it has been completed.

For our purposes, FLOCK was able to identify distinct populations based on intensity of staining for each pair-wise comparison of functional parameters (Fig. 11). For example, the red population (Pop. 1) corresponds to the third most prevalent population consisting of IL-2 low, IFNγ negative, CD107a low, IL-17A low, TNFα negative, IL-4 low, and IL-22 low expressing $CD8^+$ T cells. In this way, FLOCK adds greater resolution to individual polyfunctional populations but at the expense of graphical clarity. To be able to track changes in polyfunctional populations across variant epitope stimulations would require eight additional matrices per T cell subset analyzed. Overall, the ability to visualize each population with corresponding quantitative data is a very nice and useful aspect of FLOCK. But large-scale comparative analysis requires too many plots for clear evaluations.

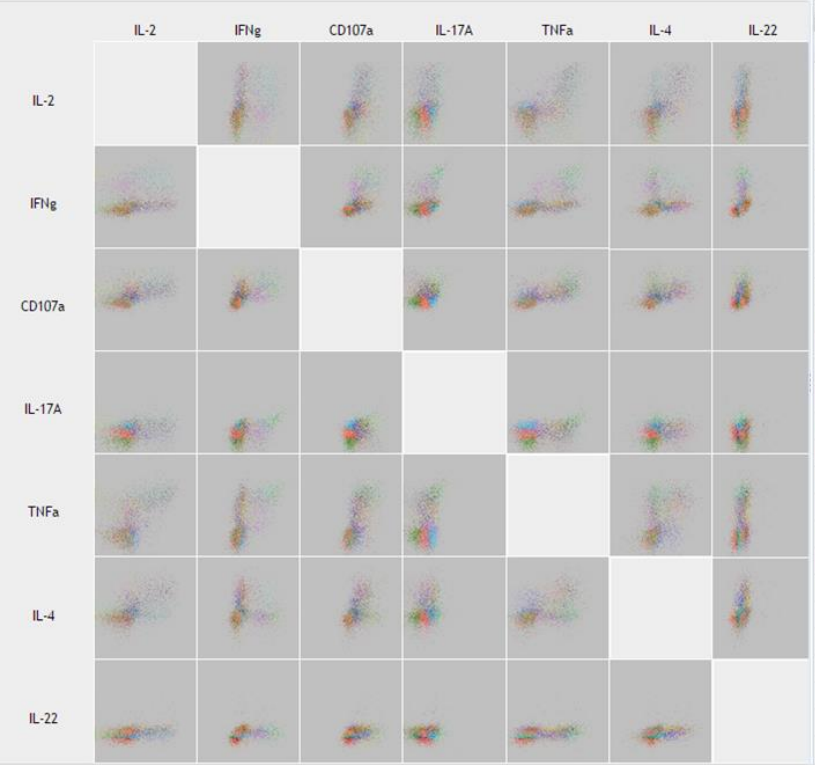

Key: 1=negative, 2=low, 3=positive, 4=high

Pop.	Color	IL-2	IFNg	CD107a	IL-17A	TNFa	IL-4	IL-22	Proportion %
1		2	1	2	2	1	2	2	7.3
2		1	3	3	3	3	2	2	2.13
3		2	1	2	1	1	2	2	7.26
4		2	1	2	2	2	3	2	3.94
5		2	1	3	2	2	2	2	2.22
6		2	2	2	2	2	2	2	7.91
7		2	1	2	1	2	2	2	6.66
8		2	1	2	2	1	2	2	7.96
9		2	2	2	2	3	2	2	3.45
10		1	1	2	2	3	2	2	2.22
11		2	1	2	2	3	2	2	3.61
12		2	1	2	2	3	3	2	3.23
13		4	2	2	2	3	2	4	0.31
14		3	2	3	2	3	3	2	2.1
15		2	3	3	3	3	2	2	1.58
16		2	2	3	1	3	2	2	1.32
17		3	3	3	3	3	2	2	2.04
18		4	1	2	2	3	3	2	2.65
19		2	1	2	2	1	2	2	9.95
20		2	2	3	2	3	3	2	4.12
21		3	3	2	3	3	2	2	2.08
22		4	2	3	2	3	3	2	3.29
23		3	2	3	2	3	2	2	3.75
24		2	1	3	1	2	2	2	3.21
25		3	2	3	1	3	3	2	2.62
26		4	3	3	3	4	3	2	3.12

Figure 11. Quantitative multidimensional dotplots generated in FLOCK. FLOCK analysis displays pairwise comparisons using a matrix of dotplots to display the relationship of expression among the 7 functional parameters. Color-coded populations for various combinations of markers are accompanied with frequency percentages and description of staining intensity. 1=negative fluorescence; 2=low fluorescence; 3=positive fluorescence; 4=high fluorescence.

Simplified Presentation of Incredibly Complex Evaluations

Simplified Presentation of Incredibly Complex Evaluations (SPICE) uses large FlowJo datasets to graphically normalize data. Preprocessing of the data is performed using both FlowJo and Pestle. After sequential gating in FlowJo, Pestle offers data formatting and background subtraction of multivariate datasets, which are import into SPICE for graphical and statistical analyses. While background subtraction can result in below zero values, SPICE has a threshold approach which will minimize systematic bias and can maximize the amount of information that can be gained from positive measurements [320]. SPICE also offers the ability to statistically compare the distributions for all parameters. A χ^2 measurement uses a nonparametric partial permutation (Monte Carlo simulation) to determine the differences between samples. Visualization of data includes pie charts, bar graphs, and cool plots, a type of heat map.

The major benefits of using Pestle/SPICE are the ease of use, readily available software and its range of simple visualization of data. A major drawback of SPICE analysis, however, is that the data is initially manipulated in FlowJo, which means a significant amount of subjectivity is present. Another potential drawback is the software is currently only offered for Apple Mac™ usage.For our purposes, tandem analysis in Pestle/SPICE most clearly displayed polyfunctional phenotypes of TCR-transduced T cells. A complete interpretation of SPICE-generated data is provided in Chapter Six.

Hierarchical Clustering Analysis

This approach was made popular in the era of gene expression microarray data analysis where both tissue samples and genes would be clustered to identify genes that could distinguish between tissue subtypes. The frequencies of the 128 possible combinations of seven parameters (generated in FlowJo) are formed into a 128xk matrix where k is the number of different conditions to be compared (e.g. k = 7 if there are 7 different peptide conditions included). The row corresponding to the frequency of cells with no parameters is removed, leaving a matrix of 127xk. Next, the correlation matrix of the 127 patterns is calculated, creating a 127x127 matrix representing the similarity of patterns across the cells under the different peptides. The correlation matrix is then used to perform agglomerative ("bottom up") hierarchical clustering in which patterns that are most similar to each other (i.e. have the highest correlation) are put into one cluster, and clusters that are similar are merged. There are many references that provide details of the algorithm and specify the different options the user is required to choose (i.e., similarity metric, and distance metric between clusters (called the "linkage"), agglomerative vs. divisive clustering) to fully generate the dendrogram (i.e., the tree-structure) [321]. For our purposes, we used correlation as our similarity metric, average linkage, and agglomerative clustering. Graphical representations are included with discussion of the data in Chapter Six. A comparison of all multi-dimensional flow cytometry data analysis strategies evaluated for T cell polyfunctionality is summarized in Table 6.

Table 6. Summary of approaches used to analyze antigen-specific polyfunctional T cell responses.

Software	Analysis Strategy	Advantages	Disadvantages	Graphical Display	Available Through:*
FlowJo	Basic flow cytometry software package; Manual, sequential gating	Popular, widely used software; output can be imported into other multidimensional software tools	Limited in scope for analyzing >2 dimensions. Time consuming and subjective gating	Histograms and dot plots	TreeStar (P)
GemStone	Probability state modeling; template driven analysis	Accounts for population overlap and simple clustering routines; lack of gating eliminates subjectivity and operator variability	Templates require knowledge of some biology of the system; TriCOMs visually hard to interpret and compare ≥3 parameters	TriCOMs	Verity Software House (P)
SPADE	"Spanning-tree Progression Analysis of Density-Normalized Events"; unsupervised clustering extracts cellular hierarchy	No prior knowledge of hierarchical order needed; scalable; better for mutually exclusive markers and mixed lineage populations	Represents data as clusters rather than individual cells; does not appropriately analyze if data does not lend itself to clustering	Spanning trees	Cytobank (F/P)
FlowSOM	"Self-Organizing Maps of Visualizing and Interpretation of Cytometry Data"; R-based clustering tool	Similar to SPADE; while R-based, only requires minimal understanding of R to effectively use	Similar to SPADE; difficultly detailed data to compare across multiple treatment groups	Minimal spanning trees or grids	Bioconductor (F)

***(P) = software for purchase; (F) = freeware; (F/P) = freeware with additional purchasable options

Table 6. Summary of approaches used to analyze antigen-specific polyfunctional T cell responses (cont'd)

Software	Analysis Strategy	Advantages	Disadvantages	Graphical Display	Available Through:*
viSNE	Nonlinear dimensionality reduction algorithm based on t-Distributed Stochastic Neighbor Embedding (t-SNE)	Unsupervised and does not require in depth knowledge of the system; preserves cell separation and retains prior gating information	Low-dimensional mapping cannot represent all the information in high dimensional space; *cyt* maps require visual overlay to make multi-dimensional comparisons	*cyt* maps	Cytobank (F/P)
FLOCK	"FLOw Clustering without K"; unsupervised rapid binning	Up-front gating relies on familiar FlowJo; delineates populations based intensity of expression profiles; cross-sample statistical analysis	Difficult to demonstrate differences between populations with very complex matrices	Color-coded dot plots	ImmPort (F)
Hierarchical Clustering Analysis	Agglomerative "bottom up" clustering tool	Uses FlowJo generated population frequencies; can show response relatability across treatment groups	Subjective gating generates bias;	Dendogram / heat map	R (F)
SPICE	"Simplified Presentation of Incredibly Complex Data"; quantitatively compares discrete phenotypic profiles in a mixture; uses FlowJo output with formatting tool Pestle	Ease of use and clear visualization of complex datasets; offers background subtraction and permutation statistical analysis	manual gating within FlowJo affords significant amount of subjectivity	Pie charts, bar graphs, "cool plots"	NIAID (F)

***(P) = software for purchase; (F) = freeware; (F/P) = freeware with additional purchasable options

In Vivo Xenograft Model

Prior to tumor challenge, *scid/beige* mice (n=5 per treatment group) were given 2Gy total body irradiation. 10^7 HCV NS3:1406-1415 minigene$^+$ or HCV$^-$ HepG2 cells were injected subcutaneously in 0.1 cc saline. Generally, palpable tumors formed within 7 days after tumor challenge. Once palpable tumors formed, mice were adoptively transferred 10^6 or 10^7 HCV1406 TCR-transduced T cells, 10^7 tyrosinase-reactive TIL 1383I TCR-transduced T cells, or no T cells. Tumor volume was measured every three days through day 70 post tumor challenge. A Wilcoxon rank sum test was used to determine significant difference in tumor burden between treatment groups.

Circular Dichroism Spectroscopy

Thermal denaturation of peptide/MHC complexes was performed by Yuan Wang in the Baker Lab at the University of Notre Dame as described previously [322, 323]. Briefly, proteins were dissolved in 20 mM phosphate, 75 mM NaCl, pH 7.4 at a concentration of 10 μM. Circular dichroism (CD) spectroscopy was performed on a Jasco J815 instrument (Jasco, Inc., Easton, MD). Temperature was increased from 10 °C to 100 °C at an increment of approximately 1 °C/min, monitoring at a wavelength of 218 nm. Data analysis was performed in OriginPro 9.0. Because unfolding is irreversible, the resulting derivative curve was processed with a single peak fitting algorithm to fit the peak to a Gaussian function to determine the T_m and its standard error.

Surface Plasmon Resonance

TCR-pMHC binding affinity between HCV1406 TCR and WT or mutant HCV NS3:1406-1415/HLA*0201 was measured by the Baker Lab at the University of Notre Dame via surface plasmon resonance (SPR). SPR was performed using a Biacore 3000 instrument (GE Healthcare) in 10 mM HEPES, 150 mM NaCl, 3 mM EDTA and 0.005% surfactant P20 (pH 7.4). The TCR was covalently coupled to a CM5 sensor chip via standard amine coupling. Equilibrium experiments were performed by injecting 70 µl of multiple concentrations of the pMHC complex at a flow of 5 µl/min. Injected concentrations ranged from 0.5 µM to 200 µM. The responses at equilibrium were determined by averaging the signal over the final 10 s of the injection and subtracting the responses from identical injections over a mock surface. Experiments were performed at 25^{o}C. All injections were repeated three times. Fitting was performed with Biaevaluation 3.0.1 using a 1:1 binding model.

Modeling of TCR-pMHC Complexes

Computational modeling experiments were performed by Timothy Riley in the Baker lab at the University of Notre Dame. TCR-pMHC structural models were constructed using a template-based approach described recently [324]. Briefly, sequences for the HCV1406 and HCV1073 TCRs were aligned and compared to a panel of HLA-A2 restricted TCRs with known TCR-pMHC structures to serve as model templates. A template TCR was selected if the TCR alignment indicated strong sequence similarity and/or minor loop length changes. The DMF5-MART-1/HLA-A2 TCR-pMHC

complex [325] was selected as the template for the HCV1406 complex and the B7-Tax/HLA-A2 complex [326] was chosen for HCV1073. Using PyRosetta, a python toolkit for the Rosetta protein design suite [327, 328], the given TCR sequences and peptides were mapped onto the three-dimensional coordinates of the template TCRs and peptides in the TCR-pMHC complexes. Repacking the amino acid sidechains and an energetic minimization of the CDR loops/peptides generated initial models of the target TCRs.

Further design work performed in Rosetta followed a steepest descent design where many independent decoy structures were generated for each modeling stage. Each model underwent one stage for low resolution docking, one stage for high resolution docking, and multiple stages for CDR loop modeling. Using the energy scoring function Talaris2013 [329], the lowest scoring decoys from each stage were chosen for the next step. Following generation of an initial TCR-pMHC model, 10,000 decoys were generated with fully randomized pMHC and TCR docking orientations coupled with a low resolution rigid body energy minimization move. Since many decoys generated in this stage were low scoring, preference was given to structures with docking angles similar to the template. After the low resolution docking stage, loop randomization and modeling was performed as previously described with generation of 100 decoys for each CDR loop [330]. The first round of loop modeling was followed by generation of 10,000 decoys with 3 Å, 8° rigid body perturbations and docked in high resolution. The final stages consisted of sequentially modeling each modified CDR loop

until Rosetta scores were no longer decreasing between stages. The final model of HCV1406 required 19 stages and HCV1073 required only 12 stages due to a high template similarity (See Appendix). Structural analysis was performed with PyMol and Discovery Studio.

Determination of HCV1406 TCR— NS3:1406-1415/HLA-A*0201 Crystal Structure

Crystal structure determination was performed by Yuan Wang in the Baker Lab at the University of Notre Dame. Crystals of the HCV1406 TCR—WT HCV NS3:1406-1415/HLA-A2 complex were grown in 13% (v/v) PEG 3350, 0.1M Sodium cacodylate, pH 6.1, 0.2M ammonia sulfate and 3% (w/v) 1,5-diaminopentane dihydrochloride at a protein concentration of 6mg/mL at 20°C. Crystallization was performed by hanging drop vapor diffusion. For cryoprotection, crystals were transferred into 20% glycerol/80% mother liquor for 30s and immediately frozen in liquid nitrogen. Diffraction data were collected at 22ID (SER-CAT) beamlines at the Advanced Photon Source, Argonne National Laboratories, Argonne, IL. Rigid body refinement followed by TLS refinement was performed with program Phenix [331] and Refmac5 [332]. Evaluation of models and fitting to map were performed with program COOT [333]. The model was checked in WHATIF and MolProbity to evaluate the structure during the refinement. Atomic positioning was verified with a simulated annealing composite OMIT map calculated in Phenix. The structure has been deposited into Protein Data Bank (PDB ID 4ZEZ).

Ethics Statement

All recombinant DNA and retroviral transduction work was done under approved Medical University of South Carolina, University of Chicago, University of Colorado Denver, University of Notre Dame, and Loyola University of Chicago Institutional Biosafety Committee (IBC) protocols. All applicable international, national, and/or institutional guidelines for the care and use animals were followed. All animal studies were conducted under approved Medical University of South Carolina (MUSC) Institutional Animal Care and Use Committee (IACUC) protocols. The University of Colorado Denver institutional review board (IRB) approved the study for the collection of PBMC samples to generate HCV-reactive T cells clones, as described above. All adult subjects were provided written informed consent. All other human materials used were either established, de-identified tumor cell lines or PBMC purchased from commercial sources.

CHAPTER THREE

TCR GENE-MODIFIED T CELLS CAN EFFICIENTLY TREAT ESTABLISHED HEPATITIS C-ASSOCIATED HEPATOCELLULAR CARCINOMA: A PROOF OF CONCEPT

Rationale

As described earlier, many groups have reported that retroviral vectors containing TCR genes can be used to redirect the specificity of PBL-derived T cells to recognize tumor cells [15, 34, 165, 168, 169, 259, 334, 335]. Recent clinical success with TCR gene-modified T cells to treat malignancies such as melanoma encourages the investigation of using this approach to treat other malignancies and viral infections [210, 211, 336]. Available technology to TCR-gene modify T cells allows for the generation of therapeutic autologous T cells with new anti-viral and anti-tumor immunity, provided an effective TCR against a viral/tumor antigen has been identified and target cells can be recognized.

While the bulk of the studies in this dissertation focus on TCR cross-reactivity against mutagenic HCV epitopes, it is both prudent and logical to first firmly characterize basic T cell reactivity against its wildtype (WT) cognate ligand. Such fundamental information would also be imperative when evaluating the therapeutic potential of any TCR. In this chapter, we discuss the rationale behind the original selection of this TCR and how its gene transfer into PBL-derived T cell facilitates recognition of HCV^+ tumor targets *in vitro* and *in vivo,* providing potential therapeutic benefit.

As with any candidate for TCR gene therapy, there needs to be a rationale behind both the target and receptor selection. HCV is a model target for exploring the potential use of such adoptive transfer techniques to treat virally-infected cells and tumor cells. HCV infects approximately 130-150 million people globally [337] and chronic infection can lead to associated liver diseases including cirrhosis and hepatocellular carcinoma (HCC). These diseases are a leading cause of liver transplantation in the United States and Europe [338, 339]. Although standard combined therapy of pegylated-IFNα and ribavirin (RBV) have had some success, there has been much greater clinical responses when treating HCV^+ patients with newly FDA-approved NS3/4A protease inhibitors boceprevir, telaprevir, and simeprevir [340-342]. Despite this recent success, the rapidly mutating HCV genome can generate drug resistant variants, which might lead to virologic breakthrough or relapse [343-345]. Moreover, many patients who may be cured of HCV infection by these novel drugs may have already developed associated disease or malignancies that cannot be treated effectively by these anti-viral agents. These issues combined with hindered preventative and therapeutic vaccine development [346, 347] warrants exploration of other novel methods to treat HCV infection and its associated disease such as HCC.

The TCR we have selected as a candidate to treat HCV-associated HCC recognizes HCV NS3:1406-1415, a highly antigenic and mutagenic epitope of the helicase/protease NS3, restricted by HLA-A2, and is referred to here as HCV1406 TCR. We have previously shown that this HCV1406 TCR was isolated from a T cell clone found in an HCV^+ $HLA\text{-}A2^-$

patient who received an HLA-A2$^+$ liver allograft [302] and that we can genetically engineer Jurkat cells with HCV1406 TCR to recognize HCV$^+$ targets [165]. In the sections described below, we demonstrate that transduced PBL-derived T cells can recognize naturally processed HCV NS3 protein in HCC cell lines *in vitro* and can inhibit the growth of established HCV$^+$ tumors *in vivo*. These results indicate that HCV1406 TCR-engineered T cells may serve as a potential immunotherapy to treat HCV-associated HCC. Moreover, these studies provide the basis of WT ligand reactivity and provide a foundation of cross-reactive antigen recognition studies in subsequent chapters.

HCV1406 TCR-Transduced T Cells Can Recognize Naturally Processed HCV NS3

Although we have shown that TCR-transduced Jurkat cells can recognize HCV NS3:1406-1415 peptide-loaded T2 cells and minigene-expressing tumor cells [165], it is critical to establish that TCR gene-modified primary T cells can recognize both peptide-loaded targets and HCV$^+$ tumors to validate its potential use in ACT and provide a foundation for WT antigen reactivity.

The best system to assess TCR-transduced T cell recognition of HCV antigen would be to use HCV-infected primary liver cells or liver tumor cells, but human liver containing HCC cells infected with HCV were not available for our experiments. As an alternative, we engineered HepG2 cells to express HCV NS3:1406-1415 as a minigene. Anti-CD3-activated PBL-derived T cells transduced with HCV1406 TCR for *in vitro* experiments were enriched for TCR transgene expression using anti-CD34 immunomagnetic beads. The enriched populations are routinely ≥95% CD34$^+$ post

magnetic sort. Both $CD4^+$ and $CD8^+$ TCR-transduced T cell populations ($CD3^+CD34^+$) post immunomagnetic selection are highly activated ($CD25^+CD69^+$) with low levels of exhaustion markers PD-1 and TIM-3. Due to poor staining with available Vβ11 antibodies, dextramer binding is shown to measure expression of the introduced TCR. Dextramer staining also allows us to identify properly paired introduced TCR. Representative immunofluorescence analysis for experimental HCV1406 TCR-transduced T cells is shown in Figure 12a. T cells transduced to express HCV1406 TCR secreted large amounts of IFNγ when stimulated by HepG2 cells ($HLA\text{-}A2^+$) either pulsed with HCV NS3:1406-1415 peptide or expressing the HCV minigene (Fig. 12b). Similarly, TCR-transduced T cells recognized Huh-7 cells ($HLA\text{-}A2^-$) only when transfected to express the HCV minigene and HLA-A2. Thus, we have shown for the first time that HCV1406 TCR-transduced PBL-derived T cells can recognize HCV^+ tumor targets.

Because HCV antigen expression as a minigene is not naturally processed for presentation, we wanted to test HLA-A2-restricted recognition of naturally processed and presented HCV NS3:1406-1415 derived from a larger protein (full length NS3) to more accurately reflect physiologic conditions. COS/A2 cells were transiently transfected with a pcDNAIII vector encoding the full length HCV protein NS3 linked to GFP. Typical transfections yielded 40-60% GFP expression (Figure 13a). These HCV TCR-transduced T cells were capable of recognizing the naturally processed HCV NS3 in an HLA-A2-dependent manner (Fig. 13b). Robust IFNγ secretion was observed when stimulated with COS/A2/NS3 but not any other cell lines. Additionally, HepG2 cells

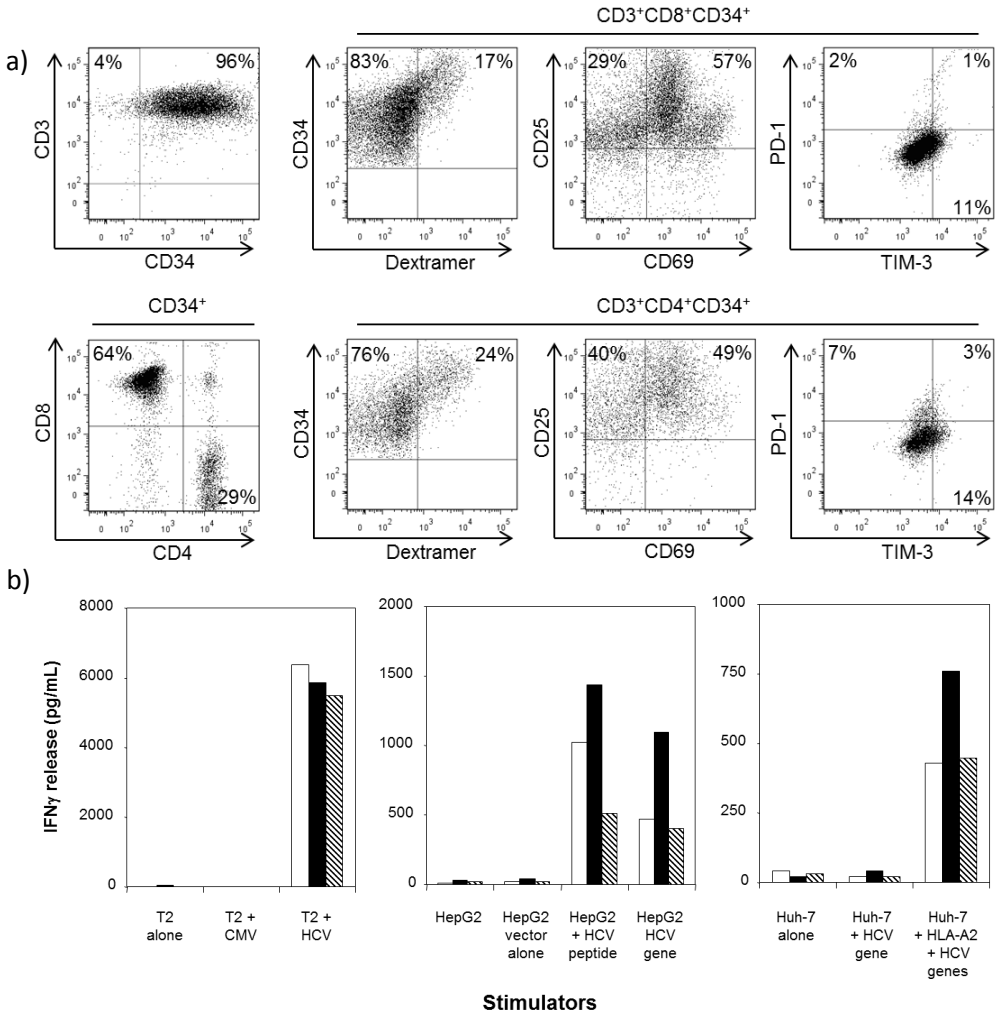

Figure 12 HCV1406 TCR-transduced T cell recognition of HCV$^+$ hepatocellular carcinoma cells. PBL from three normal donors were transduced with the HCV1406 TCR retroviral vector and enriched for CD34t expressing cells using anti-CD34 immunomagnetic beads. **(a)** Representative populations of CD34-enriched TCR-transduced T cells. TCR-transduced T cells were analyzed for HCV NS3:1406-1415 dextramer binding and markers of activation (CD25, CD69) or exhaustion (PD-1, TIM-3). **(b)** HCV1406 TCR-transduced T cells from three representative normal donors (Donor A (white bars), Donor B (black bars), Donor C (striped bars)) were co-cultured with various stimulators. (left panel) T2 cells alone or loaded with NS3:1406-1415 peptide or control CMVpp65 peptide; (middle panel) HepG2 cells (HLA-A2$^+$) alone, pulsed with HCV peptide or expressing the HCV minigene; (right panel) Huh-7 cells (HLA-A2$^-$) alone or expressing the HCV minigene±HLA-A2. IFNγ secretion was assessed as a single-point ELISA by Yi Zhang (University of Chicago).

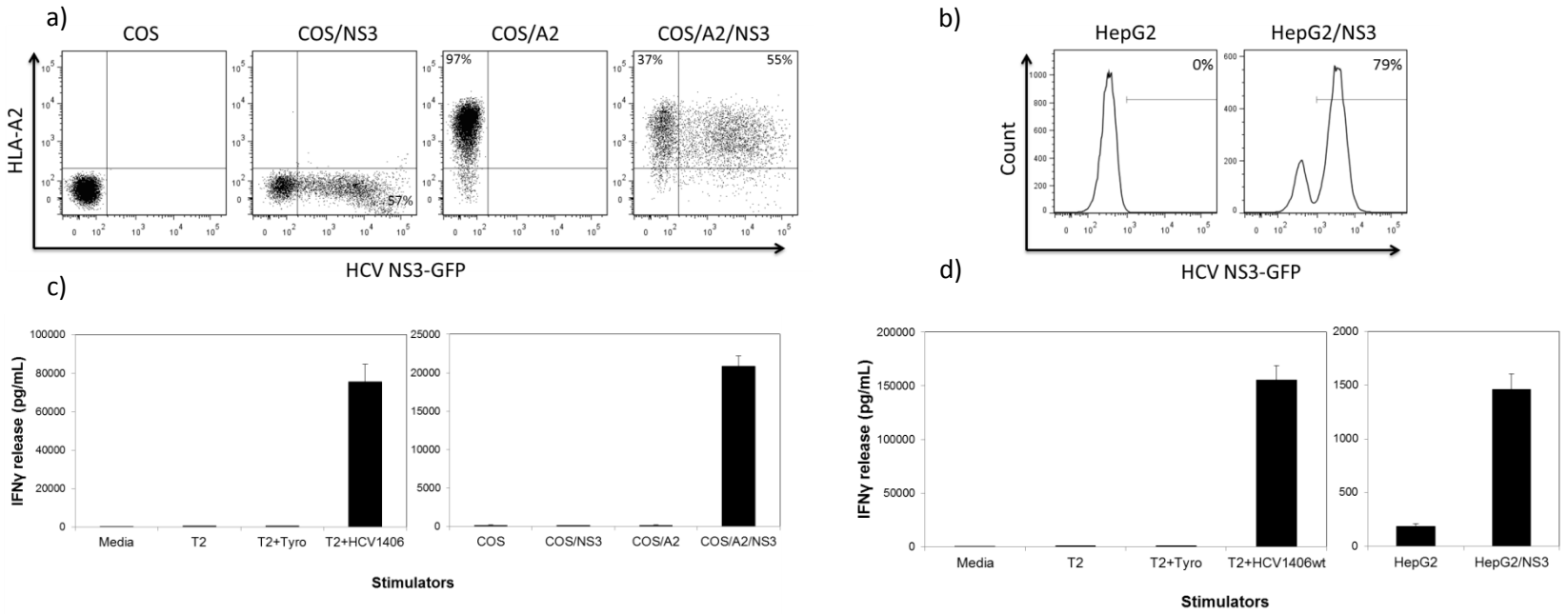

Figure 13. HCV1406 TCR transduced T cells can recognize naturally processed HCV NS3:1406-1415 antigen. PBL from a normal donor was transduced with the HCV1406 TCR retroviral vector and immunomagnetically enriched for CD34t expressing cells. **(a)** COS and COS/A2 cells were transiently transfected with pcDNAIII expression vector harboring HCV NS3-GFP and analyzed for transfection efficiency. **(b)** HepG2 cells were transduced with a retroviral vector encoding HCV NS3-GFP and were analyzed for transfection efficiency. Transduced T cells were stimulated with T2 cells loaded with HCV NS3:1406-1415 or tyrosinase:368-376 peptides and **(c)** COS±HLA-A2 cells or **(d)** HepG2 cells engineered to express full length HCV NS3 protein. The amount of IFNγ released (average ± standard deviation of triplicate wells) was measured by ELISA.

transduced to express NS3 (Fig. 13c) also stimulated substantial IFNγ secretion by HCV1406 TCR-transduced T cells (Fig. 13d). These data indicate that HCV1406 TCR gene-modified T cells can recognize naturally processed HCV NS3 antigen, meaning they may have therapeutic potential against HCV-associated HCC.

HCV NS3:1406-1415 Recognition by HCV1406 TCR-Transduced PBL Is CD8-Indpendent

To verify CD8-independent recognition of both peptide and tumor, we purified TCR-transduced $CD4^+$ and $CD8^+$ T cells from a bulk culture and stimulated each T cell subset with peptide-loaded and HCV^+ tumor targets. Figure 14 demonstrates that CD8-independent recognition is conserved against peptide-loaded or HCV^+ tumor targets as both purified $CD4^+$ and $CD8^+$ TCR-transduced T cells secreted robust amounts of IFNγ when stimulated by HCV-loaded T2 cells and HCV^+ HepG2 cells. Moreover, our HCV TCR-transduced T cells displayed lytic behavior as measured by CD107a surface expression against peptide-loaded targets and HCV^+ HepG2 cells (Fig. 15). Counterstaining for intracellular IFNγ also revealed that reactive T cells can be lytic, IFNγ -producing, or both. $CD4^+$ and $CD8^+$ T cells also exhibited distinct heterogeneous functional phenotypes. Therefore, we are able to generate both $CD8^+$ and $CD4^+$ effectors, potentially offering MHC class I-restricted helper function against this HCV antigen *in vivo*.

HCV TCR-Transduced T cells Mediate the Regression of Established HCV^+ HCC *In Vivo*

While our *in vitro* data firmly demonstrates that both $CD4^+$ and $CD8^+$ TCR-transduced T cells can be lytic and produce IFNγ, it is necessary to validate *in vivo*

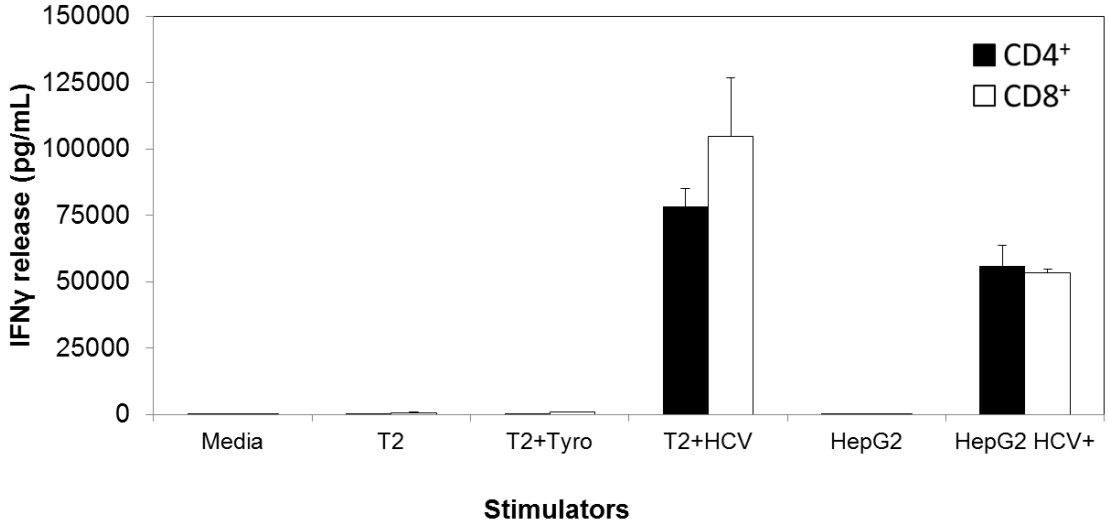

Figure 14. Recognition of HCV NS3:1406-1415 by HCV1406 TCR-transduced PBL-derived T cells is CD8-independent.. HCV1406 TCR-transduced PBL were immunomagnetically purified into $CD4^+$ (black bars) or $CD8^+$ (white bars) populations. Stimulators included T2 cells pulsed with 10 μg/mL of HCV NS3:1406-1415 peptide or control tyrosinase:368-376 peptide as well as HepG2 engineered to express the HCV NS3:1406-1415 minigene. The amount of IFNγ release (average ± standard deviation of triplicate wells) was measured by ELISA.

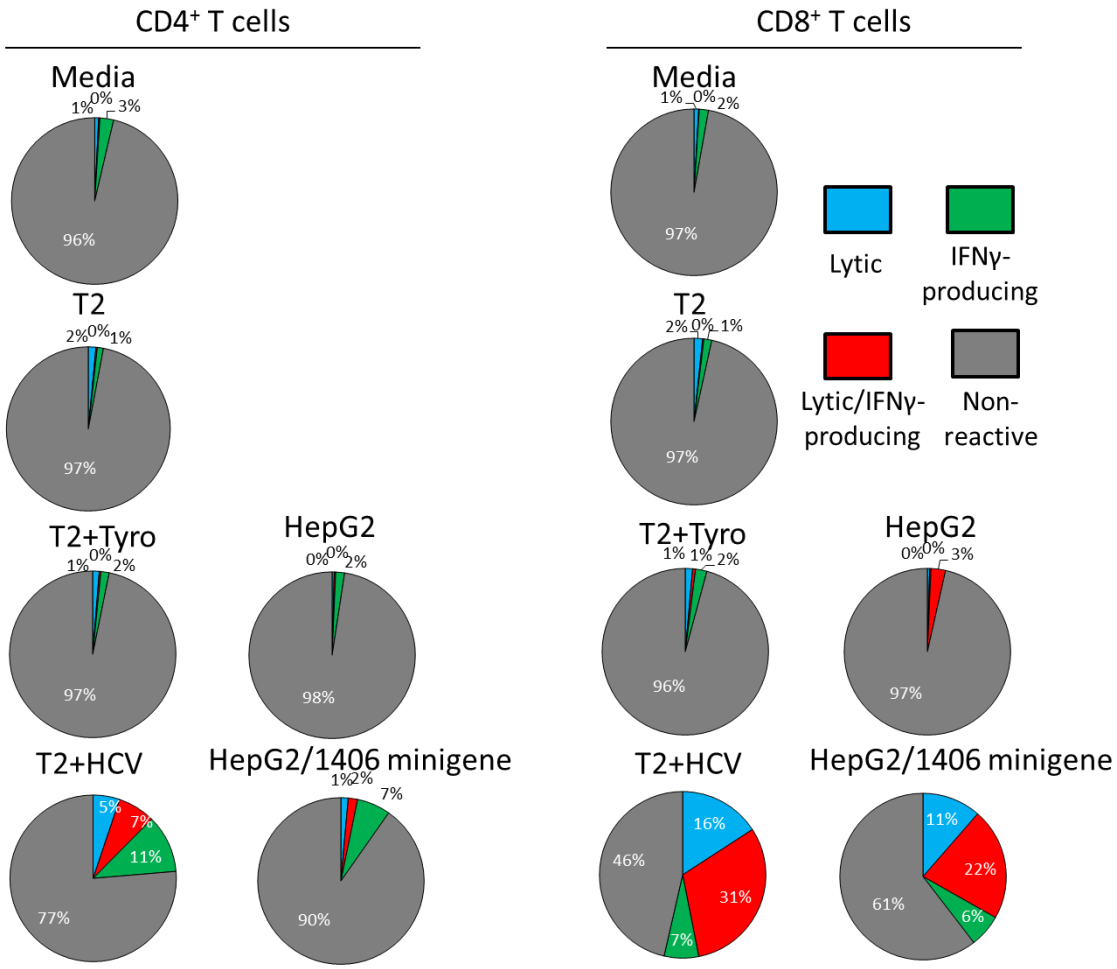

Figure 15. Lytic and IFNγ-producing ability of HCV1406 TCR transduced T cells reactive against HCV NS3:1406-1415. T2 cells pulsed with HCV NS3:1406-1415 or tyrosinase:368-376 and HCV$^+$ HepG2 cells were used as targets and co-cultured with transduced PBL. Cells were immunofluoresnce stained for CD3, CD4, CD8, CD34, CD107a, and intracellular IFNγ. Gating and data analysis was performed in FlowJo. Pie charts reflect reactivity of TCR-transduced (CD34$^+$) CD4$^+$ (left) or CD8$^+$ (right) T cells. Pie chart percentages are represented as CD107a$^+$IFNγ$^-$ (lytic only=blue), CD107a$^+$IFNγ$^+$ (lytic and cytokine-secreting=red), CD107a$^-$IFNγ$^+$ (IFNγ -producinng only=green), or CD107a$^-$ IFNγ$^-$ (non-reactive=gray).

recognition of HCV^+ tumors in a xenograft mouse model to establish therapeutic potential. We established HCC tumors in *scid/beige* mice (n=5 per treatment group) by subcutaneous injection of HCV^+ or HCV^- HepG2 cells. Once the tumors were palpable (day 7 post injection), transduced T cells were adoptively transferred. HCV^+ tumor-bearing mice exhibited reduced tumor growth after adoptive transfer of 10^7 HCV TCR-transduced T cells but not when treated with tyrosinase-reactive TIL 1383I TCR-transduced T cells or a lower dose (10^6) of HCV TCR-transduced T cells (Fig. 16). It is important to note that in the experiment presented HCV^+ HepG2 tumors in untreated mice grew at a slower rate after day 30 than in other HCV^+ tumor-bearing mice groups. We attribute this to experimental variation since other experiments demonstrated more uniform HCV^+ tumor growth in other treatment groups (Zhang, unpublished). Regardless, the change in tumor burden at day 70 between HCV TCR-transduced T cell-treated HCV^+ and HCV^- HepG2-tumor bearing mice exhibited significance with a *p*-value of 0.02 as determined by Wilcoxin Rank Sum Test. In at least one instance, HCV^+ tumors harvested from 10^7 HCV TCR-transduced T cells exhibited antigen loss, which could explain why tumors were not completely eliminated even though displaying a statistically significant reduction in tumor burden (Zhang, unpublished). Taken together, these data further support the HCV^+ HCC recognition capability by HCV1406 TCR-transduced T cells and the potential for HCV1406 TCR-transduced T cells to be used in patients.

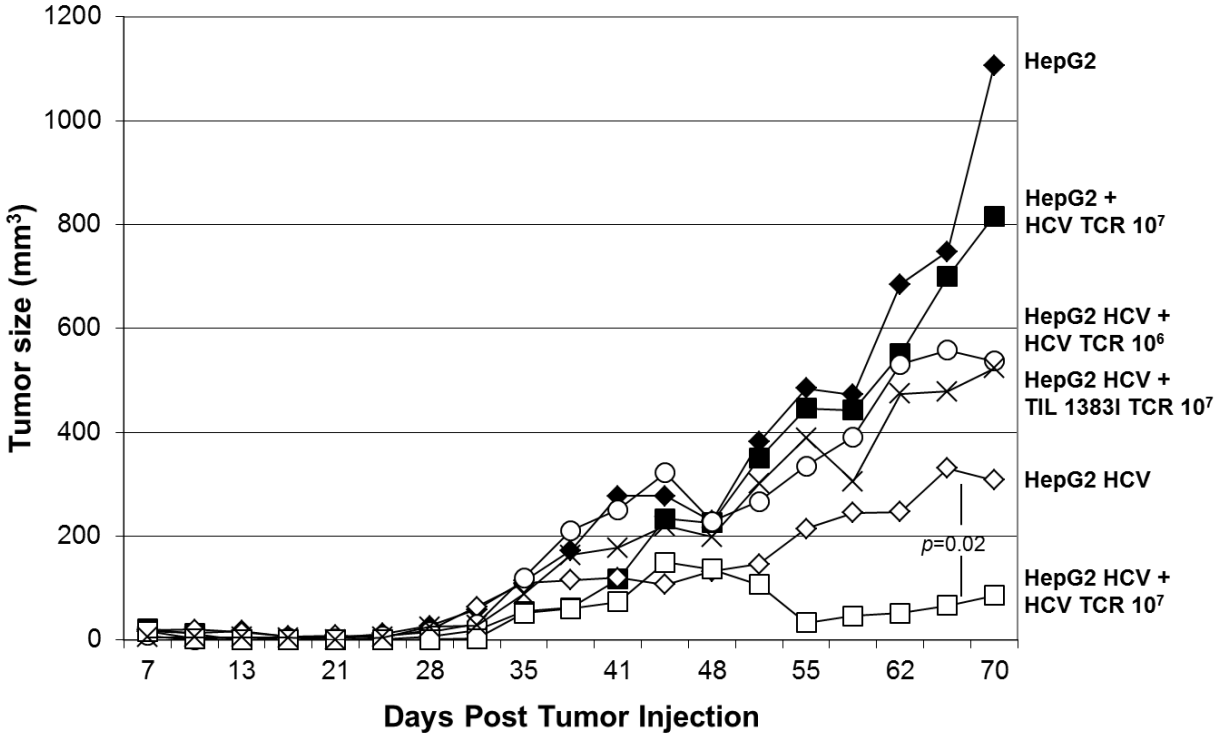

Figure 16. HCV1406 TCR-transduced T cells inhibit the growth of established HCV$^+$ hepatocellular carcinoma tumors *in vivo*. Parental HepG2 (black) or HCV$^+$ HepG2 (white) tumors were established in *scid/beige* mice (n=5 per treatment group). Mice were given no T cells (diamonds), 10^7 TIL 1383I TCR-transduced T cells (circles), or 10^6 (x's) or 10^7 (squares) HCV1406 TCR-transduced T cells on day 7 post tumor challenge. Statistically significant differences in tumor growth over 70 days was determined using the Wilcoxon rank sum test, p=0.02. These data were generated by Yi Zhang (University of Chicago).

Significance

HCV1406 TCR-transduced T cells demonstrated their ability to recognize HCV NS3:1406-1415 peptide-loaded targets as well as naturally processed antigen presented by HCV^+ HCC cells. Furthermore, in our xenograft model, HCV^+ tumor-bearing mice exhibited tumor regression after adoptive transfer of HCV1406 TCR-engineered human T cells. These data suggest that HCV1406 TCR-transduced T cells may provide therapeutic benefit against HCV infection and/or its associated disease, such as HCC.

Of interest is the phenotypic heterogeneity observed in TCR-transduced T cells reactive against peptide-loaded targets and naturally processed HCV^+ tumors. While both $CD4^+$ and $CD8^+$ T cells are capable of recognizing these targets, they expressed IFNγ and CD107a in different proportions. While most reactive $CD4^+$ T cells secreted IFNγ in response to these targets, some cells exhibited cytolytic activity as indicated by CD107a expression. Conversely, a greater number of $CD8^+$ T cells exhibited a lytic phenotype; those that secreted IFNγ were more likely to simultaneously express CD107a as well. These data support other reports that $CD4^+$ T cells can exhibit cytolytic activity [348-351] and provide insight into the heterogeneous behavior of T cells expressing the same TCR. Interestingly, not all $CD34^+$ T cells produced IFNγ or expressed CD107a. As shown in Figure 12, there is a range of CD34 expressed on TCR-transduced T cells, and only a subset of $CD34^+$ TCR-transduced T cells bound dextramer (indicating properly paired HCV1406 TCR). Perhaps, there is a minimal amount of $CD34^+$ (TCR transgene) expression necessary to facilitate TCR engagement with pMHC, activating a functional response.

This could explain why not all $CD34^+$ T cells were reactive against HCV targets. Additionally, $IFN\gamma^-CD107a^-CD34^+$ T cells may be producing other cytokines not evaluated in these experiments and are not actually "non-reactive". The influence of TCR density on antigen recognition as well as evaluating reactivity by other cytokines is addressed in subsequent chapters.

Taken together, we have established a proof-of-principle that we can generate HCV1406 TCR gene-modified $CD4^+$ and $CD8^+$ PBL-derived T cells capable of recognizing and inhibiting the growth of HCV^+ tumor targets. They may provide a useful tool to treat patients with HCV-associated diseases, such as HCC. While important observations for a potential immunotherapeutic candidate, these data also lay the groundwork for subsequent cross-reactive characterization of this TCR in light of HCV's genomic instability.

Several groups have reported that mutations in the HCV genome can lead to HCV antigen escape variants [279, 352-356]. In this way, it is speculated that HCV can evade the immune response resulting in disease progression. Although it is not clear to what extent antigen loss actually leads to disease progression, especially in HCC, TCR gene transfer may provide an opportunity to treat patients with HCV antigen escape variants should a TCR exhibit cross-reactive behavior against prevalent variants. The next chapter describes cross-reactive behavior of TCRs against mutagenic HCV antigens, serving as a model to combat diseases of genetic instability.

CHAPTER FOUR

HEPATITIS C VIRUS-CROSS-REACTIVE TCR GENE-MODIFIED T CELLS: A MODEL FOR IMMUNOTHERAPY AGAINST DISEASES WITH GENOMIC INSTABILITY

Rationale

As described in Chapter One, the genomic instability of cancers and viruses can serve as a mechanism for immune escape, leading to HLA downregulation, alterations in antigen processing, antigen loss, and antigen mutation [187, 188, 271, 288, 289]. Contributing to poor host immune responses, such mechanisms of immune escape pose barriers for the development of preventative and therapeutic vaccines and impair the design of effective immunotherapies. Therefore, it is important to investigate novel treatment approaches designed to combat genomic instability.

The HCV genome contains several regions that are genetically unstable and mutate readily [357, 358], making HCV an excellent model for genomic instability. Immune escape variants may be potential therapeutic targets for HCV infection and its associated disease. Despite the recent clinical success of FDA-approved protease inhibitors [359, 360], the very genomic instability that allows for immune escape could generate acquired resistant variants to these novel drugs [361, 362]. Therefore the use of cross-reactive TCRs targeting mutagenic epitopes may be advantageous in this instance.

We chose to use HCV as our TCR cross-reactivity model for a variety of reasons. First, we have the available reagents to assess T cell reactivity against mutant HCV epitopes. We have previously cloned multiple high-affinity HCV-reactive TCRs capable of transferring reactivity to both $CD4^+$ and $CD8^+$ PBL-derived T cells [165, 166]. Additionally, we have selected panels of naturally occurring and epidemiologically relevant immunogenic epitopes to assess cross-reactivity of a pair of HCV-reactive TCRs. More importantly, HCV is epidemiologically significant with a worldwide prevalence of 3% [337]. Strong evidence suggests that the immune system plays a key role in mediating viral clearance [357], but that weak or ineffective immune responses can lead to chronic infections [363-365]. A hallmark of HCV, and most relevant to this study, is its high rate of replication coupled with the lack of proofreading ability of its polymerase [366, 367]. This genomic instability is thought to lead to immune escape variants that evade T cell recognition [274, 276-278, 357, 358]. However, T cells' ability to cross-recognize mutated epitopes has been previously associated with viral control [368, 369], suggesting TCR cross-reactivity may be advantageous for viral clearance. Additionally, while ineffective immune responses may be partially caused by low avidity T cells [365, 370], it has been suggested that high avidity T cells can also quell HCV immune escape by selective pressure [365]. So in diseases with genomic instability, such as HCV, it would optimal to generate T cells with both high avidity and cross-reactivity [365].

In this chapter, we examined whether T cells harboring cross-reactive TCRs might offer a therapeutic solution in instances of genomic instability, using HCV as a model.

We demonstrated cross-reactivity of two TCRs against immunogenic and mutagenic NS3:1406-1415 and NS3:1073-1081 epitopes in TCR-gene-modified T cells. Our approach includes: (1) functional studies demonstrating cross-reactive profiles; (2) epidemiological data supporting the relevance of mutant epitopes targeted in these studies; (3) TCR-pMHC structural modeling to rationalize how TCR structural properties accommodate recognition of certain mutated epitopes; and lastly, we (4) provide preliminary clinical evidence suggesting cross-reactive TCR may facilitate HCV viral clearance. Together, this approach serves as a model to address diseases with genomic instability and highlights the potential benefit of cross-reactive TCRs. A better understanding of such TCRs' promiscuous behavior may allow for exploitation of these properties to develop novel adoptive T cell-based therapies.

HCV1406 TCR Is Cross-Reactive Against Naturally Occurring

HCV NS3:1406-1415 Mutant Epitopes

We have previously reported on an HLA-A2-restricted, HCV NS3:1406-1415-reactive TCR from an allo-specific $CD8^+$ T cell clone isolated from an HCV^+ $HLA\text{-}A2^+$ patient who received an $HLA\text{-}A2^-$ liver allograft [302]. In Chapter Three, we described our ability to transfer CD8-independent reactivity against HCV peptide-targets and HCV^+ HCC cells to both Jurkat cells and primary T cells [165, 371]. Because this TCR lacked any selective pressure against A2-restricted antigens during development or in the periphery, we wanted to test any potential diversity in recognition against altered but physiologically relevant HCV ligands. In this manner, HCV1406 TCR served as an optimal

candidate to assess cross-reactivity against diseases of genomic instability. We identified a variety of naturally occurring mutant epitopes with a GenBank search using the nucleotide sequence for the WT HCV NS3:1406-1415 epitope KLVALGINAV. Results were filtered for silent mutations and a panel of selected mutant epitopes with amino acid substitutions varying in both position and class is listed in Table 7. HCV1406 TCR-transduced PBL-derived T cells from three representative normal healthy donors were generated as previously described [304], and enriched for transduced cells as described in Chapters Two and Three.

Cross-recognition of naturally occurring mutant HCV NS3:1406-1415 epitopes was tested by stimulating bulk cultures of HCV1406 TCR-transduced T cells with T2 cells loaded with WT or mutant NS3:1406-1415 peptides in IFNγ release assays (Fig. 17). Of the eight naturally occurring mutants tested, seven induced robust IFNγ production by TCR-transduced T cells similar to or greater than that of WT peptide stimulation. We generally classify “reactive” peptides as those that elicit at least 200 pg/mL and twice above background IFNγ levels. Only T2 cells loaded with variant V1408S/A1409G/I1412L (subsequently referred to as 8S/9G/12L) were not recognized by a bulk culture of all three donors T cells. Of note, Donor B exhibited substantially less IFNγ secretion across all peptide stimulation conditions and did not recognize mutants A1409T, I1412N, and V1408S/A1409S/I1412L/A1414S (subsequently referred to as 8S/9S/12L/14S). A peptide titration from 1 μg/mL – 0.00001 μg/mL suggested Donor B had an overall lower functional avidity against the WT peptide (Fig. 18). Further analysis of Donor B’s

Table 7. HCV NS3:1406-1415 and NS3:1073-1081 mutant epitope sequences and epidemiological frequencies.

Epitope	Sequence	Genotype	Frequency (%)*
HCV NS3:1406-1415	KLVALGINAV	1a	43.46
V1408L	KL**L**ALGINAV	1b	0.31
A1409T	KLV**T**LGINAV	1a	1.31
I1412L	KLVALG**L**NAV	1a	1.63
I1412V	KLVALG**V**NAV	1a/1b	31.7/0.31
I1412N	KLVALG**N**NAV	N/A†	N/A
8S/9G/12L	KL**SG**LG**L**NAV	1a/1b	0.65/42.81
V1408T	KL**T**ALGINAV	1a	1.63
8S/9S/12L/14S	KL**SS**LG**L**N**S**V	1b	0.31
HCV NS3:1073-1081	CINGVCWTV	1a/1b	90.2/41.59
I1074V	C**V**NGVCWTV	1a/1b	1.31/45.57
I1074L	C**L**NGVCWTV	1b	0.61
V1077A	CING**A**CWTV	1a	0.98
C1078F	CINGV**F**WTV	1a	0.33
V1081N	CINGVCWT**N**	N/A	N/A
T1080S	CINGVCW**S**V	1a	0.33
V1081A	CINGVCWT**A**	1a	0.33
80S/81I	CINGVCW**SI**	1a	0.98
Tyrosinase:368-376	YMDGTMSQV	N/A	N/A

*Frequencies based on the 918 collected HCV genome sequences in the Los Alamos HCV Sequence Database (http://hcv.lanl.gov/content/index). †N/A: Epitope not found in database.

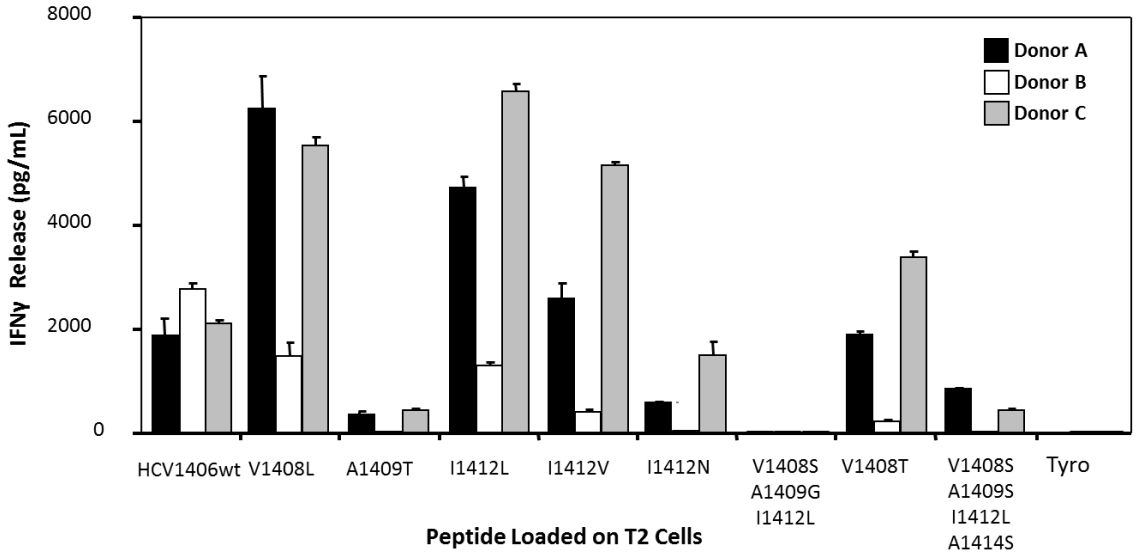

Figure 17. HCV1406 TCR-transduced PBL are cross-reactive against naturally occurring HCV NS3:1406-1415 variants. HCV1406 TCR-transduced PBL from three representative donors (A, black bars; B white bars; C gray bars) were co-cultured with T2 cells pulsed with 10 µg/mL of WT or mutant HCV NS3:1406-1415 peptides or tyrosinase:368-376 as a control. IFNγ secretion was measured by ELISA. Mean and standard deviation of triplicate measurements are shown. All variants that qualified as reactive in the text secreted at least 200 pg/mL IFNγ and twice above background. These data were generated by Gretchen Lyons in the Nishimura Lab (University of Chicago).

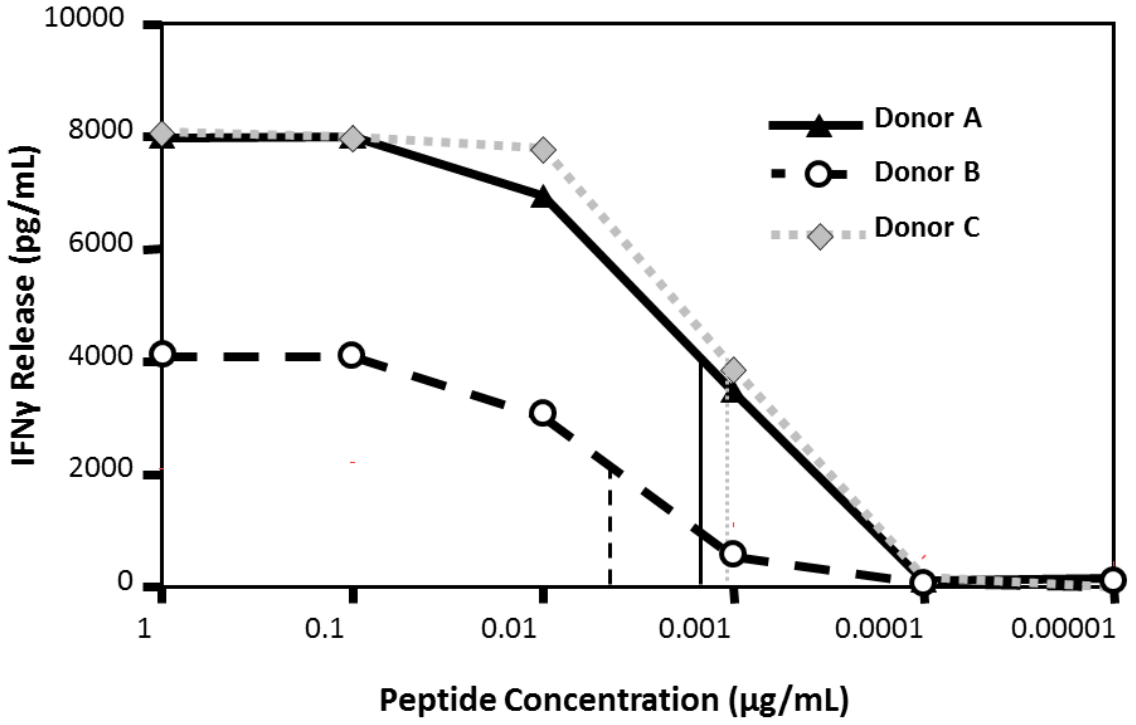

Figure 18. Relative avidity of HCV1406 donors A and B against WT HCV NS3:1406-1415. HCV1406 TCR-transduced PBL were co-cultured with peptide-loaded T2 cells in concentrations ranging from 1 - 0.00001 µg/mL. IFNγ secretion was measured by ELISA. Mean and standard deviation of triplicate measurements are shown. Relative avidity curves and estimated EC_{50} values of Donors A (solid, black triangles) B (dashed, white circles), and C (dotted, gray diamonds) are shown. These data were generated by Gretchen Lyons in the Nishimura Lab (University of Notre Dame).

transduced T cells revealed 87% $CD4^+$ with only 10% $CD8^+$ T cells. Comparatively, Donors A and C had much higher levels of $CD8^+$ T cells compared to $CD4^+$ T cells at 32% $CD4^+$ / 61% $CD8^+$ and 14% $CD4^+$ / 72% $CD8^+$, respectively (data not shown). Together, these observations suggest that some mutant epitopes may require CD8 to be recognized, even though we have previously shown recognition of the WT antigen is CD8-independent.

Some but Not All NS3:1406-1415 Mutant Epitopes Require the CD8 Co-Receptor

The data described above suggest that T cells may require CD8 to cross-recognize some but not all HCV NS3:1406-1415 epitopes. To test this hypothesis, we evaluated the cross-reactivity of HCV1406 TCR-transduced Jurkat cells (natively $CD8^-$ [165, 305]) or Jurkat cells we engineered to express the α and β genes of CD8. Transduced cells were stimulated with peptide-loaded T2 cells, and subsequent IL-2 release was measured by ELISA (Fig. 19). Transduced $CD8^-$ Jurkat cells recognized WT NS3:1406-1415 and mutants V1408L, and I1412V with similar or greater IL-2 secretion than $CD8^+$ Jurkat cells. Interestingly, recognition of I1412L and V1408T was also CD8-independent but $CD8^-$ Jurkat cells released only 25-50% as much IL-2 compared to $CD8^+$ Jurkat cells. In contrast, IL-2 production after stimulation with T2 cells loaded with mutants A1409T, I1412N, 8S/9S/12L/14S was restricted to $CD8^+$ Jurkat cells. These observations suggest that certain amino acid substitutions may lower the affinity of the TCR-pMHC interaction enough to require stabilization by CD8 to facilitate recognition. These data are supportive of transduced PBL cross-reactivity shown in Figure 18 where

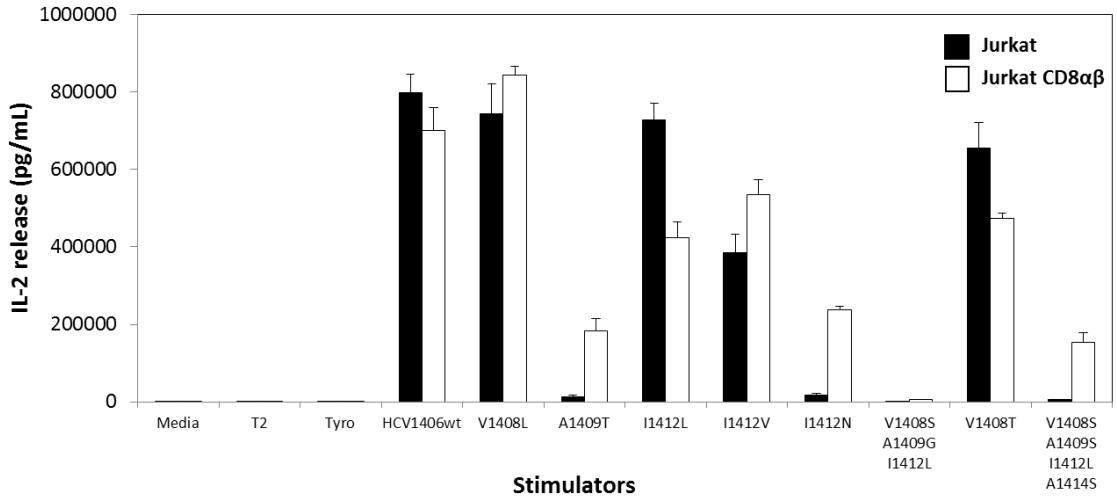

Figure 19. Recognition of some but not all mutant HCV NS3:1406-1415 peptides require the CD8 co-receptor. Peptide-loaded T2 cells were co-cultured with HCV1406-transduced Jurkat cells (CD8 negative, black bars; CD8 positive, white bars). IL-2 secretion was measured by ELISA. Mean and standard deviation of triplicate measurements are shown. All variants that qualified as reactive in the text secreted at least 200 pg/mL IL-2 and twice above background.

Donor B (with only 10% $CD8^+$ T cells) was very weakly/non-reactive against these same three mutant peptides. Although Donor B still contains a low frequency a $CD8^+$ T cells, it may require a greater number to achieve detectable levels of secreted IFNγ above background and comparable to that of other more strongly recognized variants. Additionally, peptide titration experiments down to 0.0001 μg/mL demonstrated that different mutations had differential impacts of functional avidity, but that avidity was enhanced by presence of CD8 (Fig. 20). Yet, even at low levels of antigen (1-10 nM) Jurkat cells were responsive to multiple antigens, which may be important for maintaining enough cross-reactive immune pressure to help prevent immune escape.

It is important to consider that amino acid substitutions could disrupt peptide–MHC binding, destabilizing the overall protein complex, which could alter antigen recognition [372]. We determined that a lack of or weaker peptide binding to MHC cannot account for an absent an attenuated response of any of the NS3:1406-1415 variants because all epitopes bound similarly to HLA-A2 as measured by their thermal stability via CD spectroscopy (Table 8). Together, these data suggest that the HCV1406 TCR is cross-reactive against a variety of naturally occurring HCV NS3:1406-1415 variants, but some mutations require CD8 for recognition and/or maximum cytokine response.

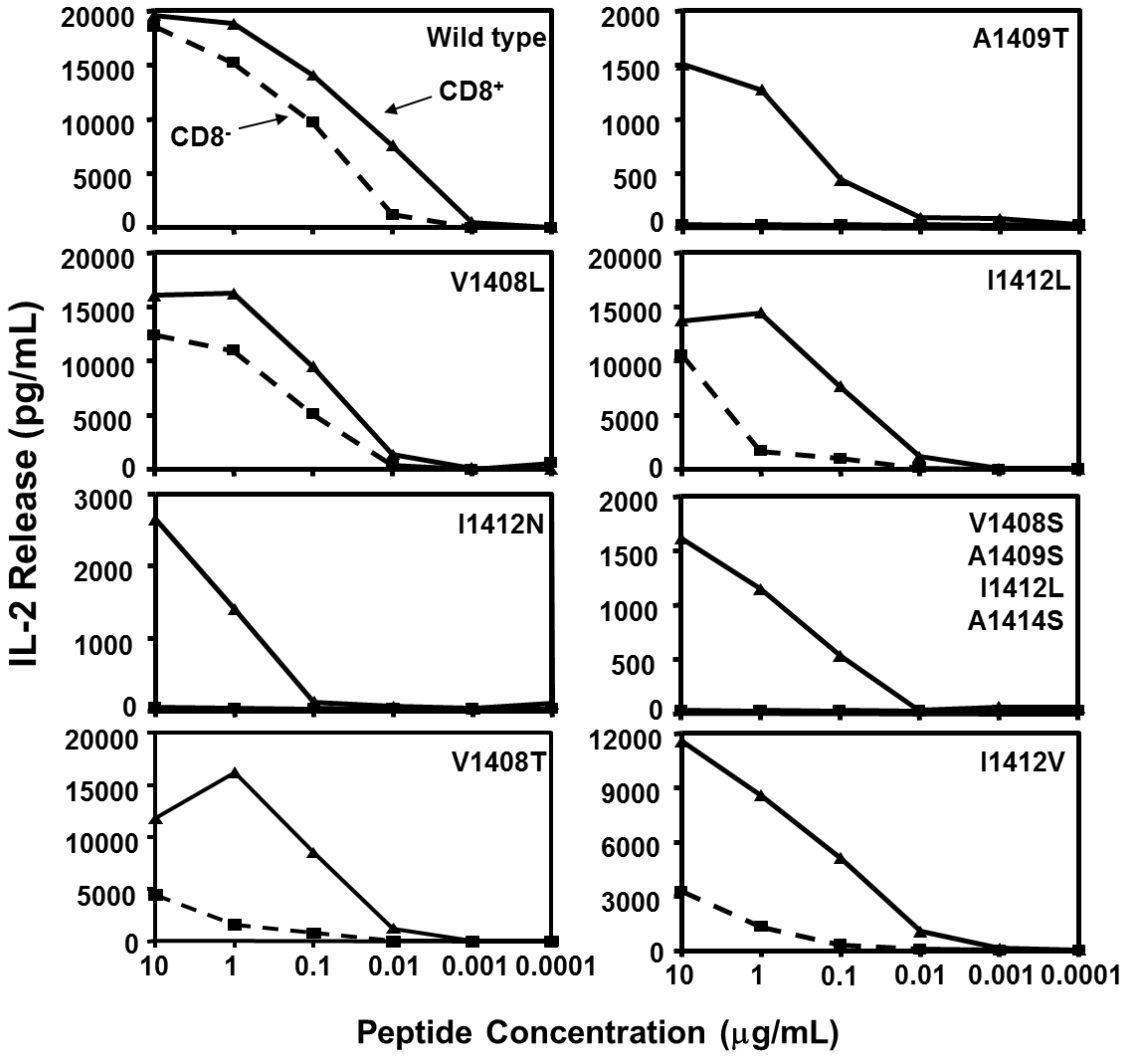

Figure 20. Influence of the CD8 co-receptor on the functional avidity of HCV1406 TCR-transduced Jurkat cells against naturally occurring mutant HCV NS3:1406-1415 variants. HCV1406 TCR-transduced Jurkat cells were co-cultured with peptide-loaded T2 cells in concentrations ranging from 1 - 0.0001 μg/mL. IL-2 secretion was measured by ELISA. Relative avidity curves values of $CD8^+$ (solid, triangles) $CD8^-$ (dashed, squares) Jurkat cells are shown. These data were generated by Gretchen Lyons in the Nishimura Lab (University of Notre Dame).

Table 8. The apparent T_m values of HCV NS3:1406-1415/HLA-A2 variants as measured by circular dichroism spectroscopy.

Epitope	T_m (^oC)*
WT	64. 9±0.1
V1408L	60.7±0.3
A1409T	64.6±0.1
I1412L	58.1±0.3
I1412V	58.4±0.3
I1412N	59.3±0.1
8S/9G/12L	62.0±0.1
V1408T	69.2±0.2

*Average of three independent experiments ± standard error. These measurements were kindly provided by Yuan Wang in the Baker Lab (University of Notre Dame).

Cross-Reactivity against Naturally Occurring Mutant

HCV Epitopes Is Not Limited to HCV1406 TCR

While we have clear evidence that the HCV1406 TCR demonstrates cross-reactivity against mutant epitopes, it is possible that this is because this TCR is HLA-A2 restricted but was identified in an HLA-A2$^-$ host, and by definition cross-reactive [302]. To better generalize the phenomenon of TCR cross-reactivity, we assessed the cross-reactivity of a second TCR reactive against a second immunodominant HCV epitope NS3:1073-1081. This HLA-A2-restricted TCR was isolated from an HLA-A2$^+$ host with chronic HCV infection. We previously showed T cells transduced with the HCV1073 TCR recognized both peptide-loaded targets and human HCC cells expressing the WT antigen [166]. HCV1073 TCR is not allo-restricted, and thus, a complementary TCR used to characterize cross-reactivity.

A panel of naturally occurring HCV NS3:1073-1081 mutant epitopes was identified in the same manner described above (Table 7) and used to established cross-reactivity of HCV1073 TCR-gene modified T cells. Remarkably, a strong cross-reactive profile was seen in primary T cells from three healthy donors engineered to express the HCV1073 TCR (Fig. 21). T2 cells loaded with utant peptides I1074V, I1074L, T1080S, and T1080S/V1081I (subsequently referred to as 80S/81I) stimulated robust IFNγ release by HCV1073 TCR-transduced T cells. Interestingly, mutant V1081A stimulated weak cytokine release (just over our threshold of 200 pg/mL and twice background) in all three donors, and V1081N was weakly reactive in two out of three donors. Mutant

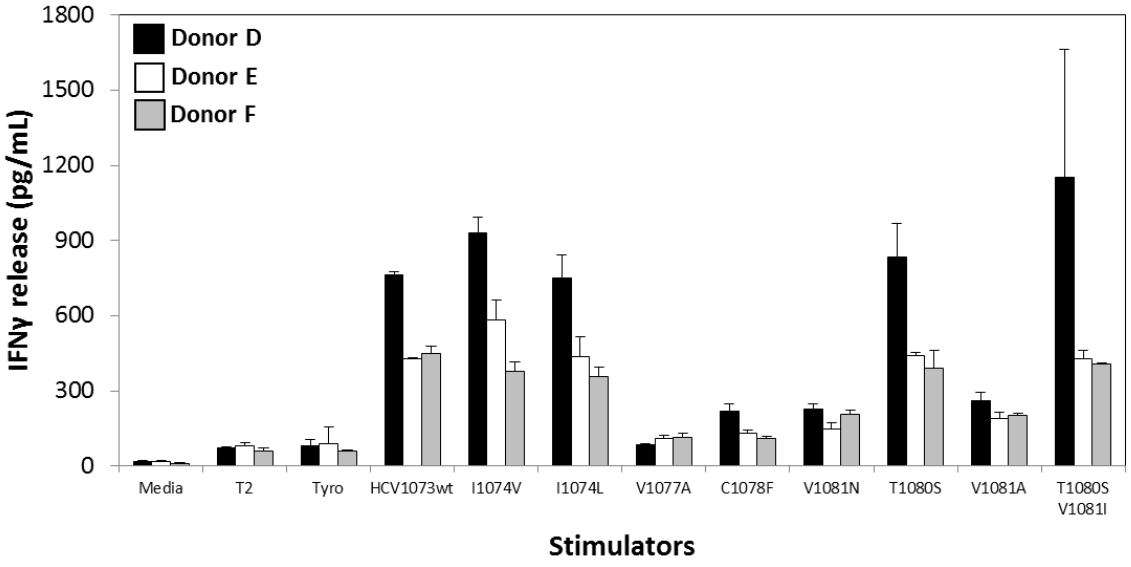

Figure 21. HCV1073 TCR is also cross-reactive against naturally occurring HCV NS3:1073-1081 mutants. HCV1073 TCR-transduced PBL of three representative donors (Donor D, black bars; Donor E, white bars; Donor F, gray bars) were co-cultured with T2 cells loaded with 10 µg/mL WT or mutant HCV NS3:1073-1081 peptides or tyrosinase:368-376 peptide as a control. IFNγ secretion was measured by ELISA. Mean and standard deviation of triplicate measurements are shown. Mean and standard deviation of triplicate measurements are shown. All variants that qualified as reactive in the text secreted at least 200 pg/mL IFNγ and twice above background.

epitope C1078F, however, only stimulated very weak IFNγ release in one donor, and mutant peptide V1077A was not recognized by any donors. In summary, we have identified an additional HCV-reactive TCR isolated from a second host exhibiting broad cross-reactivity against naturally occurring mutants of a second immunodominant HCV epitope.

HCV NS3:1073-1081 Naturally Occurring Mutants Are Less CD8-Dependent

To test CD8-dependent recognition of mutant HCV NS3:1073-1081 peptides, we engineered $CD8^-$ and $CD8^+$ Jurkat cells with the HCV1073 TCR and stimulated them with peptide-loaded T2 cells (Fig. 22). Both $CD8^-$ and $CD8^+$ HCV1073 TCR-transduced cells secreted similar or greater amounts of IL-2 to some but not all mutant peptides compared to WT. $CD8^-$ Jurkat cells secreted substantial amounts of IL-2 against mutant peptides I1074V, I1074L, V1070S, 80S/81I, and to a lesser extent mutant V1081A. This suggests that the HCV1073 TCR may exhibit flexibility to accommodate changes in some peptides without needing CD8 to stabilize the TCR-pMHC interaction. Interestingly, co-expression of CD8 does not seem to greatly enhance the reactive potential against these five mutant epitopes. Additionally, $CD8^+$ TCR-transduced Jurkat cells were also weakly reactive against V1081N, suggesting that this peptide modification requires either CD8-driven affinity-enhancement or augmented signaling to be recognized. In summary, we have shown that HCV1073 TCR can facilitate CD8-independent recognition of multiple naturally occurring mutant HCV NS3:1073-1081 mutant epitopes.

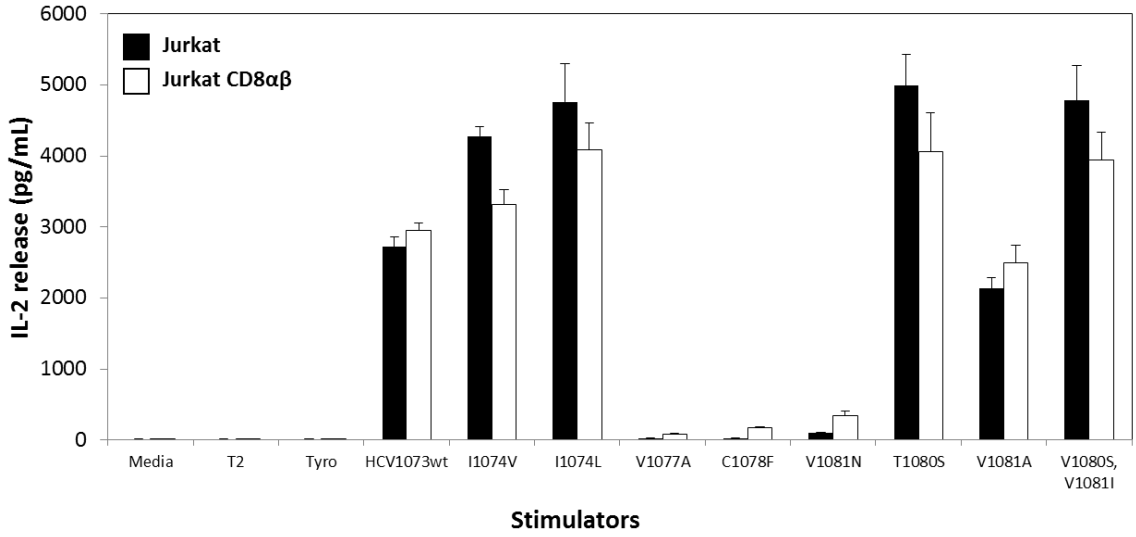

Figure 22. HCV NS3:1073-1081 naturally occurring mutants are less CD8-dependent. $CD8^-$ (black bars) or $CD8^+$ (white bars) HCV1073 TCR-transduced Jurkat76 cells were co-cultured overnight with peptide-loaded T2 cells. The average and standard deviation of triplicate measurements of IL-2 release by ELISA is shown. All variants that qualified as reactive in the text secreted at least 200 pg/mL IL-2 and twice above background.

HCV NS3:1406-1415 and NS3:1073-1081 Mutant Epitopes Are Epidemiologically Relevant

We know that the mutant HCV NS3:1406-1416 and NS3:1073-1081 epitopes studied here are naturally occurring because they were identified in the GenBank. However, our cross-reactive TCRs would only be clinically advantageous if the mutant epitopes recognized were highly prevalent in infected individuals. To evaluate the prevalence of these mutations, we searched the Los Alamos HCV Sequence Database, which contains 918 HCV genome sequences recorded worldwide in a variety of known viral genotypes. Using the QuickAlign search tool, we examined the database for epitope frequency of both NS3:1406-1415 and NS3:1073-1081 using KLVALGINAV or CINGVCWTV, respectively, as the reference peptide sequence. Frequencies of recorded altered sequences were generated and sorted by known HCV genotype. Table 7 illustrates the predominant frequency and genotype(s) of these naturally occurring mutant immunodominant epitopes.

In the United States, HCV genotypes 1a and 1b make up greater than 75% of prevalent infections and the most common genotypes worldwide [373]. Interestingly, for the NS3:1406-1415 epitope, the WT sequence KLVALGINAV makes up only 43.46% or genotype 1a frequencies in this database, and mutant I1412V makes up an additional 31.7% of recorded genome sequences ranking as the second most common recorded epitope sequence. Of note, both of these epitopes are recognized independently of CD8 expression, allowing for both $CD4^+$ and $CD8^+$ transduced T cells to recognize these

HCV^+ targets. While the nine total epitope sequences studied here account for 42.38% of all recorded sequences in the Los Alamos HCV Sequence Database, they comprise 80.38% of the recorded genotype 1a sequences. Inclusion of these mutant epitopes recognized by this TCR nearly doubles the amount of recorded sequences recognized by $CD8^+$ effectors from only 43.46%, representative of only the WT epitope. This suggests HCV1406 TCR could provide enhanced coverage against observed HCV NS3:1406-1415 variants most applicable to the United States. However, this TCR does not recognize variant 8S/9G/12L, which is the dominant epitope of genotype 1b at 42.81%, suggesting the HCV1406 TCR may not be as effective in genotype 1b-infected individuals.

Comparing HCV1073 TCR cross-reactivity with epidemiological frequencies also suggests that a second cross-reactive TCR may have clinical benefit. While genotype 1a HCV NS3:1073-1081 epitope is well conserved with 90.2% of the recorded genomes have the WT CINGVCWTV sequence, genotype 1b is dominated by the I1074V mutant (45.57%); WT comprises only 41.59% of recorded sequences. In total, the various epitope sequences studied here account for 64.28% of total sequences in the database, but they provide coverage of 94.46% and 89.3% of genotypes 1a and 1b, respectively (most relevant to the United States' and Europe's viral prevalence [373]). The ability for HCV1073 TCR to mediate CD8-independent recognition includes upwards of 90% of the recorded epitope sequences in both genotypes 1a and 1b instead of being limited to 41.59% of recorded cases in genotype 1b. Thus, our HCV model suggests there could be

clinical benefit in using cross-reactive TCRs if mutant epitopes in the TCR recognition patterns are highly prevalent.

Computational Modeling of TCR-pMHC Structures Rationalizes Biological Outcomes

To generate structural hypotheses for the cross-reactivity of the HCV1073 and HCV1406 TCRs, we generated models of the two TCR-pMHC complexes using a template-based approach that combines loop and peptide modeling with low and high resolution docking procedures. We previously demonstrated this modeling procedure can reliably reproduce key structural features such as interface contacts and TCR docking modes [324]. After identifying appropriate template structures, the TCRs and peptides were computationally morphed and several rounds of structural and energetic refinement were applied. The TCR-pMHC complexes were subsequently subjected to multiple rounds of fully randomized low resolution docking, high resolution interface refinement, and restrained high resolution docking (See Appendix). Both TCRs are predicted to engage with binding modes typical for class I-restricted TCRs [374] (Fig. 23a). In the model of the HCV1406 TCR-pMHC complex, the NS3:1406-1415 peptide is predicted to adopt a conformation similar to that in the known pMHC crystal structure (Protein Databank (PDB) identification 3MRM) (Fig. 23b). Detailed interpretation of structure-based assessment of each TCR's cross-reactivity is described below.

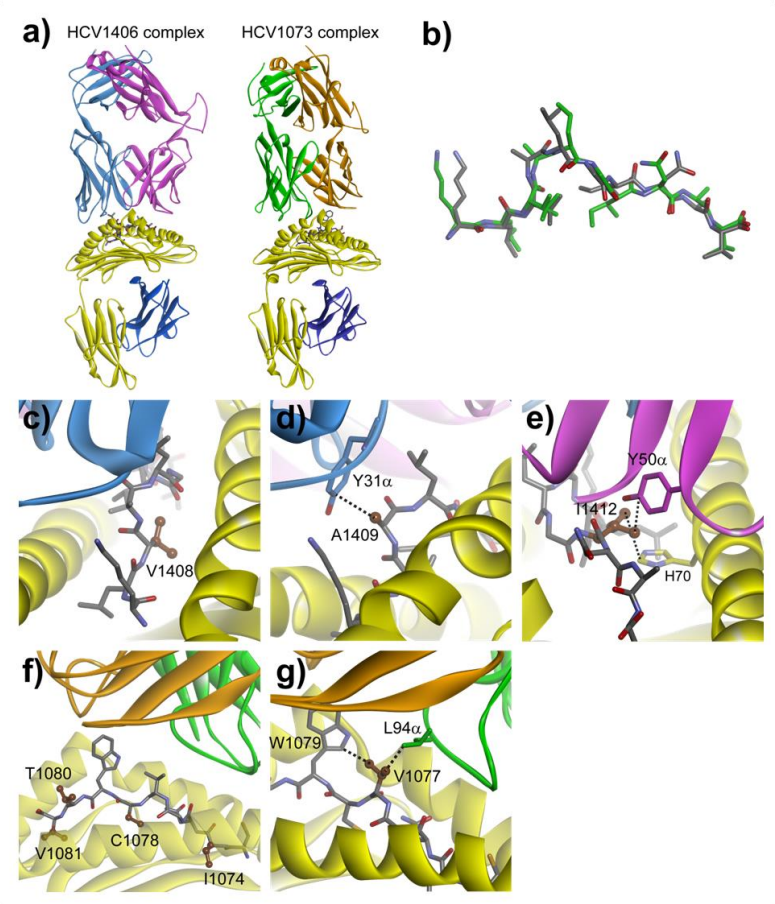

Figure 23. Computational models of the HCV1406 and HCV1073 TCR-pMHC complexes rationalize receptor cross-reactivity. (a) Overview of the modeled complexes, showing the traditional TCR binding mode. **(b)** The conformation of the peptide in the model of the HCV1406 complex (grey) is predicted to be very similar to the conformation seen in the unligated peptide/HLA-A2 complex (green). **(c)** V1408 of the NS3:1406-1415 peptide occupies a large space near the HLA-A2 α1 helix, with no contacts predicted from the TCR. **(d)** A1409 of NS3:1406-1415 is predicted to interact with Y31 of CDR1α. **(e)** I1412 of NS3:1406-1415 is predicted to interact with Y50 of CDR2α, as well as H70 of the HLA-A2 α1 helix. **(f)** I1074 and V1081 of the NS3:1073-1081 peptide occupy the P2 and P9 pockets of HLA-A2 as expected. C1078 is predicted to face downward towards the base of the peptide binding groove. T1080 is predicted to be fully exposed, with no contacts to the TCR. **(g)** V1077 of NS3:1073-1081 is predicted to interact with L94 of CDR3α as well as W1079 of the peptide. These data were kindly provided by Timothy Riley in the Baker Lab (University of Notre Dame).

Structure-Based Assessment of HCV1406 Cross-Reactivity

In the model of the HCV1406 TCR-pMHC complex, the NS3:1406-1415 peptide is predicted to adopt a conformation very similar to that in the known pMHC crystal structure (PDB 3MRM) (Fig. 23b). The side chain of V1408 is directed down towards the base of the HLA-A2 α1 helix, in a loosely-packed region with sufficient space to accommodate other side chains (Fig. 23c). There are no TCR atoms in proximity to contact the WT valine or a mutant leucine, serine, or threonine. The region is solvent exposed, ensuring a serine or threonine would be able to satisfy hydrogen bonding requirements. The model is thus consistent with the observation that the V1408L and V1408T mutant peptides are recognized as equally well as the wild type epitope. In contrast to V1408, A1409 is directed towards the TCR, contacting Y31 of CDR1α (Fig. 23d). Substitution with a threonine would require TCR and/or peptide rearrangements to resolve atomic clashes and satisfy the threonine hydrogen bonding needs. This would likely weaken TCR binding and could account for the weaker potency and loss of CD8 independence seen with the A1409T mutant peptide.

The side chain of I1412 of NS3:1406-1415 is directed towards the HLA-A2 α1 helix, but interacts with Y50 of CDR2β as well as H70 of HLA-A2 (Fig. 23e). Substitution with leucine would be predicted to retain these interactions, accounting for the high level of reactivity with the I1412L peptide. The I1412V peptide, however, would lose interactions with HLA-A2, likely resulting in weaker peptide binding and/or peptide conformational changes. Some combination of either of these could account for the

weaker potency of the I1421V peptide. Substitution with asparagine would require more drastic structural alterations, accounting for the even weaker potency of the I1412N mutant peptide.

For the NS3:1406-1415 V1408S/A1409G/I1412L triple mutant, as V1408S and I1412L should be well-tolerated, the loss of activity may be attributable to the loss of interactions Y31α stemming from the A1409G mutation (Fig. 23d). Additionally, substitution of A1409 with glycine may render the peptide more dynamic, further reducing TCR binding by raising the entropic penalty for binding [375]. The latter explanation may explain the weakened but not eliminated potency of variant 8S/9S/12L/14S. Mutants V1048S, I1412L, and A1414S should all be tolerated as described above. On the other hand, substitution of A1409 to serine rather than glycine would be expected to impact interactions with Y31α, but still retain peptide rigidity. A summary of these structural interpretations of functional responses is listed in Table 9.

Structure-Based Assessment of HCV1073 Cross-Reactivity

The model of the HCV1073 complex provides for similar structural interpretations as with the HCV1406 complex. The side chain of the P2 I1074 of the NS3:1073-1081 peptide is predicted to occupy the HLA-A2 P2 pocket as is typical for a peptide bound to HLA-A2 [376, 377], with sufficient room for a valine and leucine (Fig. 23f). Although some effect on peptide binding affinity is anticipated, the lack of any TCR contacts to this position coupled with the relatively conserved mutations can explain the strong activity of the I1074V and I1074L mutant peptides. A similar interpretation is

Table 9. Summary of predicted structural consequences of the HCV NS3:1406-1415 and NS3:1073-1081 mutations.

Epitope	Structural Interpretation	Figure	Potency –CD8	Potency +CD8
HCV NS3:1406-1415				
V1408L	No changes in TCR/MHC/peptide contacts	23C	++	++
V1408T	No changes in TCR/MHC/peptide contacts	23C	++	++
A1409T	Altered TCR contacts, rearrangements needed for hydrogen bonding	23D	-	+
I1412L	No changes in TCR/MHC/peptide contacts	23E	++	++
I1412V	Loss of MHC contacts, altered peptide conformation	23E	+	+
I1412N	Loss of MHC contacts and introduction of polar group requiring changes in peptide conformation	23E	-	+
8S/9G/12L	Loss in TCR contacts, greater peptide dynamics from introduction of glycine	23C-E	-	-
8S/9S/12L/14S	Loss in TCR contacts	23C-E	-	+
HCV NS3:1073-1081				
I1074V	Conservative P2 anchor substitution	23F	++	++
I1074L	Conservative P2 anchor substitution	23F	++	++
V1077A	Loss of and alteration in TCR contacts	23G	-	-
C1078F	Altered MHC contacts and peptide conformation	23F	-	-
V1081N	Substantially weaker peptide binding from inappropriate P9 anchor	23F	-	+
T1080S	No changes in TCR/MHC/peptide contacts	23F	++	++
V1081A	Weaker peptide binding from P9 anchor substitution	23F	+	+
80S/81I	No change in TCR/MHC/peptide contacts	23F	++	++

possible for mutant V1081A, as the valine at P9 occupies the HLA-A2 PΩ pocket (Fig. 23f). Substitution of an alanine here is likely to have a greater effect on peptide binding, explaining the reduced activity of the V1081A mutant.

The model shows the P6 cysteine of the NS3:1073-1081 peptide vectored down towards the base of the HLA-A2 binding groove (Fig. 23f), as commonly seen with peptides bound to class I MHC proteins [377]. Substitution to a bulky amino acid such as phenylalanine is likely to substantially alter peptide conformation and likely weaken peptide binding to HLA-A2, explaining the loss of activity of the C1078F peptide. The P8 threonine is predicted to be fully exposed (Fig. 23f), with no interactions with the TCR, and hence a serine substitution here is expected to be well tolerated, explaining the full potency of the conservative T1080S mutant. Similar explanations hold for the fully active T1080S/V1081I double mutant.

The model shows the P5 valine of NS3:1073-1081 pointing directly up into the TCR-pMHC interface, packing against L94 of CDR3α (Fig. 23g). This valine also packs against the P7 tryptophan of the peptide, which interacts with multiple residues of the TCR β chain. In addition to removing interactions with CDR3α, replacement of the valine with alanine could have knock-on effects on the position of the tryptophan, further impacting TCR interactions with the peptide. A combination of these effects may explain the loss of activity seen with mutant V1077A. A summary of these structural interpretations is also reported in Table 9. Together, we can begin to

rationalize how various amino acid substitutions can alter functional responses by HCV1406 TCR- and HCV1073 TCR-transduced T cells.

HCV Cross-Reactive TCRs May Be Clinically Advantageous to Help Prevent Chronic Infection

It has been suggested that a major cause of chronic HCV infection is the ability of the virus to escape immune surveillance with a rapidly mutating genome [279, 352-356]. Therefore, it would be logical to predict that infected individuals with more cross-reactive TCRs might facilitate clearance of HCV infection or prevent chronic infection better than those with a more restricted repertoire of HCV-reactive TCRs. Such an observation would also support the claim that cross-reactive TCRs may be therapeutically beneficial in diseases exhibiting genomic instability. A very preliminary set of experiments to detect any such clinical evidence of this theory examined recognition capability of T cells isolated from chronically infected patients and from those who spontaneously resolved infection. After raising HCV NS3:1406-1415 tetramer positive T cell clones from both types of patients, reactivity of multiple clones was tested against an alanine scanner set of the HCV NS3:1406-1415 peptide and a variety of naturally occurring mutants. Based on a limited number clones evaluated, T cells isolated from chronically infected patients tended to have a similar and limited cross-reactive profile. Conversely, representative clones isolated from patients who spontaneously resolved infection tended to have a much more varied and diverse response against both alanine-substituted peptides and naturally occurring mutant

epitopes. Reactivity profiles from two representative clones of each patient cohort are shown in Figure 24. While not an exhaustive characterization or a conclusive study, these observations support the hypothesis that cross-reactive TCRs may have play a beneficial role in combating HCV and other diseases with genomic instability.

Significance

Immune evasion by viruses and cancer cells has been a critical barrier to mounting effective host immune responses and has been problematic for the development of successful immunotherapies including ACT. A combination of viral/cancer genomic instability and immense selective pressure by successful immune effectors can lead to these escape variants. Finding a way to harness the immune system's ability to selectively eliminate its targets while maintaining flexibility to combat genomic instability, a driving force behind immune escape, is the ultimate therapeutic goal for these diseases.

Overall, in our HCV model for genomic instability, we have characterized CD8-independent recognition of multiple naturally occurring mutant epitopes for two HCV-cross-reactive TCRs. The reported prevalence of mutant epitopes adds clinical relevance to potential therapeutic use of either or both of these receptors in ACT. Furthermore, preliminary experiments testing cross-reactivity of T cell clones raised from chronically infected versus spontaneously resolved patients support the hypothesis that HCV-cross-reactive TCRs could have an impact on clearance of HCV infection or its associated disease. Our structural modeling also provides a context for altered T cell responses. An

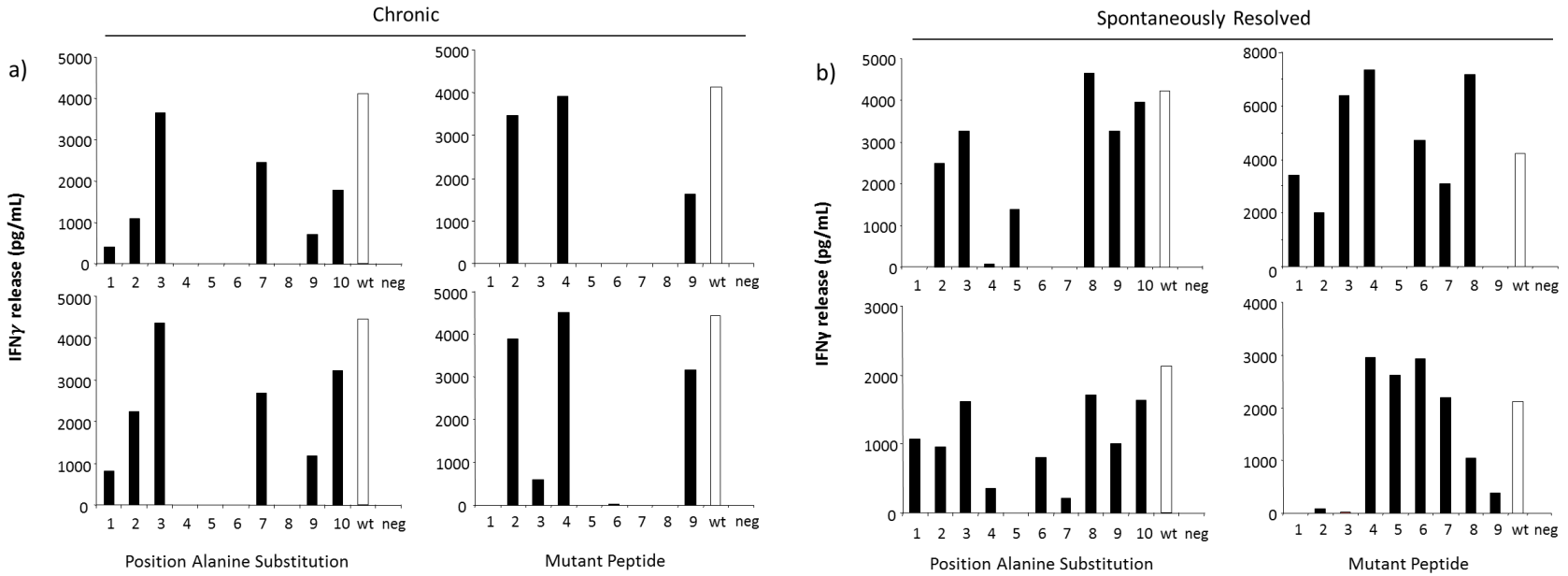

Figure 24. T cell clones raised from patients with spontaneously resolved HCV infection have a more diverse cross-reactivity than those isolated from chronically infected HCV patients. HLA-A2*01/HCV NS3:1406-1415 tetramer positive T cell clones raised from (a) chronically HCV-infected patients or (b) patients who spontaneously resolved HCV infection were co-cultured with T2 cells pulsed with 10 µg/mL of WT HCV NS3:1406-1415 peptide (white bars), HCV NS3:1406-1415 peptides with alanine substitutions at positions 1 through 10 (black bars; left panels), a variety of naturally occurring mutant epitopes (black bars; right panels) or tyrosinase:368-376 peptide as a control. Two representative clones from each cohort are shown. IFNγ secretion was measured by ELISA. Peptides: 1-V1408L, 2-V1408T, 3-A1409T, 4-A1409V, 5-I1412L, 6-I1412V, 7-8S/9G/12L, 8-8S/9S/12L, 9-8S/9S/12L/14S. These data were kindly provided by the Rosen Lab (University of Colorado Denver).

improved structural understanding of how amino acid substitutions impact the pMHC topography and subsequently T cell function will be helpful. Nonetheless, our approach serves as an important model for identifying and designing cross-reactive TCR-based immunotherapies for diseases with genomic instability, including HCV. Studies aimed to address what kinetic, biological, and structural factors influence antigen recognition, TCR cross-reactivity, and T cell function are addressed in the following chapters.

CHAPTER FIVE

ASSESSING THE IMPORTANCE OF TCR-pMHC AFFINITY ON ANTIGEN RECOGNITION BY HCV1406 TCR GENE-MODIFIED T CELLS

Rationale

In Chapter Four, we discussed how two TCRs exhibited cross-reactivity against naturally occurring mutant HCV epitopes and how TCR cross-reactivity may be advantageous for treating diseases with genomic instability. Additionally, structural modeling of the TCR-pMHC interface helped rationalize altered antigen recognition (or lack thereof). But modeling does not identify the mechanism(s) responsible for the changes in the pMHC ligand that might alter T cell function. Although speculation revolves around which parameters best explain a productive or non-productive TCR-pMHC interaction, TCR-pMHC affinity is generally thought to play the most central role [1].

A better understanding of how a TCR engages with the pMHC complex and how that interaction activates a T cell could help manipulate TCR gene-modified T cells to enhance therapeutic efficacy and limit off-target toxicities. Our HCV model allows us to evaluate antigen recognition of a single TCR against a series of naturally occurring mutant epitopes with varied TCR-pMHC affinities. In this chapter, we begin our investigation into which parameters influence antigen recognition by comparing altered TCR-pMHC binding affinities with functional responses. We also address how other

factors, including the CD8 co-receptor, pMHC ligand density, and TCR density affect recognition of altered pMHC ligands and TCR cross-reactivity.

We have chosen to focus the remainder of these structure-function studies on the HCV1406 TCR. Structure-function studies using the HCV1073 TCR would not be feasible because the HCV NS3:1073-1081 epitope contains two cysteine residues (**C**INGV**C**WTV). This peptide and its mutants have the propensity for oxidization and forming disulfide bridges. These properties make NS3:1073-1081 peptides extremely challenging to generate reliable peptide-MHC and TCR-pMHC binding measurements and would be troublesome for additional kinetic or structural evaluations. For these reasons, the remaining kinetic, functional, and structural studies will focus on HCV1406 TCR.

TCR-pMHC Affinity Trends with but Does Not Completely Dictate Antigen Recognition

Most investigators in the field believe that the critical feature of a TCR-pMHC interaction is its affinity [1]. Our model using WT and naturally occurring mutant HCV NS3:1406-1415 peptides enables us to examine how TCR-pMHC interactions with varying affinities impact T cell function. By surface plasmon resonance (SPR), we measured the equilibrium K_D of HCV1406 TCR with all NS3:1406-1415 pMHC except 8S/9S/12L/14S—HLA-A2 (Table 10). We determined that HCV1406 TCR bound WT HCV NS3:1406-1415/HLA-A2 at the highest affinity of all pMHC with an average of 16.8 μM. Although functionally a high affinity TCR exhibiting CD8-independent target recognition,

Table 10. TCR-pMHC binding affinities for HCV1406 TCR—HCV NS3:1406-1415/HLA-A2 variants as measured by surface plasmon resonance.

Epitope	K_D (μM)*
WT	16.8±0.3
I1412L†	32.4±0.7
V1408T†	45.9±0.6
V1408L†	60.1±5.2
I1412V†	63.4±3.0
A1409T‡	119.7±9.2
I1412N‡	168.0±17.6
8S/9G/12L‡	169.3±23.4

*average K_D of three independent experiments ± standard error. These measurements were kindly provided by Yuan Wang in the Baker Lab (University of Notre Dame).
†"moderate affinity"
‡"lower affinity"

the affinity measurement of HCV1406 TCR-WT pMHC interaction falls short of a traditional high affinity K_D. Traditional high affinity interactions are classified in the nM or <10 μM range and low affinity TCRs are generally >300 μM; but we are arbitrarily categorizing the remaining TCR-pMHC interactions as "moderate" and "lower" as a point of comparison to WT. TCR-pMHC interactions containing variants I1412L (32.4 μM), V1408T (45.9 μM), V1408L (60.1 μM), and I1412V (63.4 μM) exhibited relatively similar measurable affinities (within a two-fold range). We categorized these variants in a "moderate affinity" range compared to WT. TCR-pMHC interactions containing variants A1409T, I1412N, and 8S/9G/12L were approximately one log fold higher K_D than the WT peptide, measuring in a similar range we called "lower affinities": 120 μM, 168 μM, and 169 μM, respectively. Although the TCR- 8S/9S/12L/14S–MHC interaction could not be measured by SPR, its amino acid substitutions would predict it to fall into the "lower affinity" range. Taken together, we have established multiple ranges of measurable affinities (comprised of various amino acid substitutions) to compare the influence of TCR-pMHC affinity on T cell function.

We discussed in Chapter Four that recognition of some but not all mutant HCV NS3:1406-1415 peptides required the CD8 co-receptor. Thus, we wanted to evaluate whether changes in TCR-pMHC affinity correlate with CD8-dependence. Figure 25 demonstrates WT and variant HCV NS3:1406-1415 peptide recognition of PBL-derived HCV1406 TCR-transduced $CD4^+$ and $CD8^+$ T cells ranked by affinity (decreasing left to right). Recall, we normally define "reactive" T cells as producing >200 pg/mL IFNγ and at

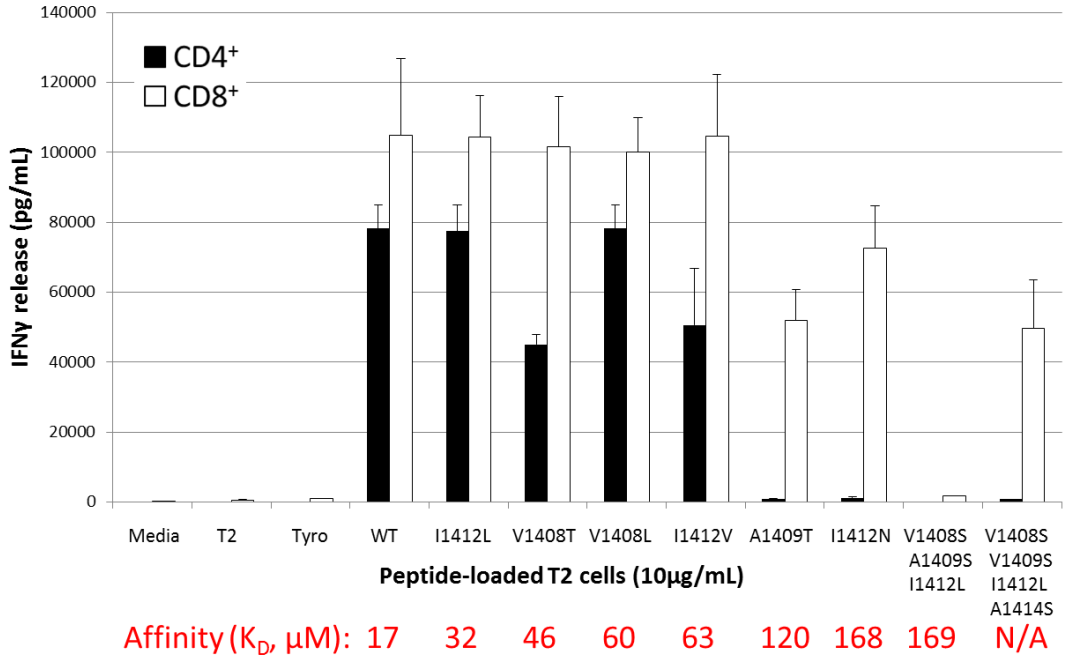

Figure 25. Reorganization of cross-reactivity by decreasing affinity reveals an inverse trend. PBL from a normal donor were transduced with the HCV1406 TCR retroviral vector. TCR-transduced cells were enriched using anti-CD34 immunomagnetic beads and subsequently isolated into $CD4^+$ and $CD8^+$ populations. T cells were co-cultured with T2 cells pulsed with 10 µg/mL of WT or mutant HCV NS3:1406-1415 peptides or tyrosinase:368-376 as a control. IFNγ secretion was measured by ELISA. Mean and standard deviation of triplicate measurements are shown. All variants that qualified as reactive in the text secreted at least 200 pg/mL IFNγ and twice above background and at least >5% of WT cytokine release. Affinities of TCR-pMHC interactions are shown in red.

least twice above background (tyrosinase stimulation). However, in the case of HCV1406 where TCR-transduced T cells and Jurkat cells can secrete cytokine > 40,000 ng/mL, reactive ligands must also exceed 5% of WT cytokine response. Interestingly, the IFNγ secretion patterns are distinctly different between $CD4^+$ and $CD8^+$ TCR-transduced T cells. Both $CD4^+$ and $CD8^+$ TCR-transduced T cells were reactive against T2 cells loaded with WT (17 μM) and the four variant ligands that fall into our "moderate affinity" range (32-63 μM). $CD8^+$ T cells routinely exhibited comparable averages of IFNγ secretion against all five of these peptides. This suggests there may be an upper limit at which a higher affinity no longer augments cytokine secretion. While $CD4^+$ T cells responded with similar magnitudes of IFNγ secretion against WT, I1412L, and V1408L, they reproducibly secreted up to 50% less IFNγ against V1408T, and I1412L. This is surprising because decreased function is not consistent with decreased affinity.

However, none of the "lower affinity" pMHC variants (A1409T, I1412N, 8S/9G/12L, and 8S/9S/12L/14S) were recognized by $CD4^+$ T cells, suggesting that a threshold for CD8-independece exists somewhere between 63 and 120 μM. However, variant 8S/9G/12L was not recognized by either $CD4^+$ or $CD8^+$ T cells, despite having virtually identical TCR-pMHC affinity as CD8-dependent mutant I1412N (169 μM compared to 168 μM). While we observed antigen recognition trends with affinity, these data do not support TCR-pMHC affinity as the defining characteristic dictating antigen recognition. With that in mind, it is prudent to explore other potential factors

including co-receptors, antigen density, or TCR density that may contribute to T cell recognition of altered peptide ligands.

CD8-Dependent TCR Cross-Reactivity Relies on the Recruitment of Lck

Although we observed a relationship between CD8-dependence and TCR-pMHC affinity, it was uncertain how CD8 was actually permitting or enhancing functional recognition of some mutant peptides. One way the CD8 co-receptor facilitates antigen recognition is through stabilization of the TCR-pMHC complex, thus enhancing the affinity of the TCR-pMHC interaction [378]. TCR-pMHC stabilization by CD8 helps justify differences in the recognition of mutant peptides between HCV1406 TCR-transduced $CD4^+$ and $CD8^+$ T cells (segregated by "moderate" and "lower" affinities). However, CD8 can also bind the src kinase, lck [379]. Recruitment of lck to the TCR/CD3 complex helps facilitate the initiation of the TCR signaling cascade [26]. It has previously been suggested that a T cell's sensitivity to antigen stimulation can be more dependent on the signaling capacity of CD8 rather than its affinity-enhancement, especially among high affinity TCRs [305]. To determine the influence of affinity-enhancement versus signaling augmentation by CD8 on TCR cross-reactivity, we engineered Jurkat cells (natively $CD8^-$) to express full length CD8αβ, or a truncated form (CD8α'β'), lacking the intracellular lck-binding domain. CD8-transduced cells were sorted to have roughly equivalent expression of CD8 (Figure 26a). Examining the reactivity of these CD8-engineered Jurkat cells against each of the mutant peptides allowed us to separate the importance of affinity enhancement and signaling augmentation by CD8.

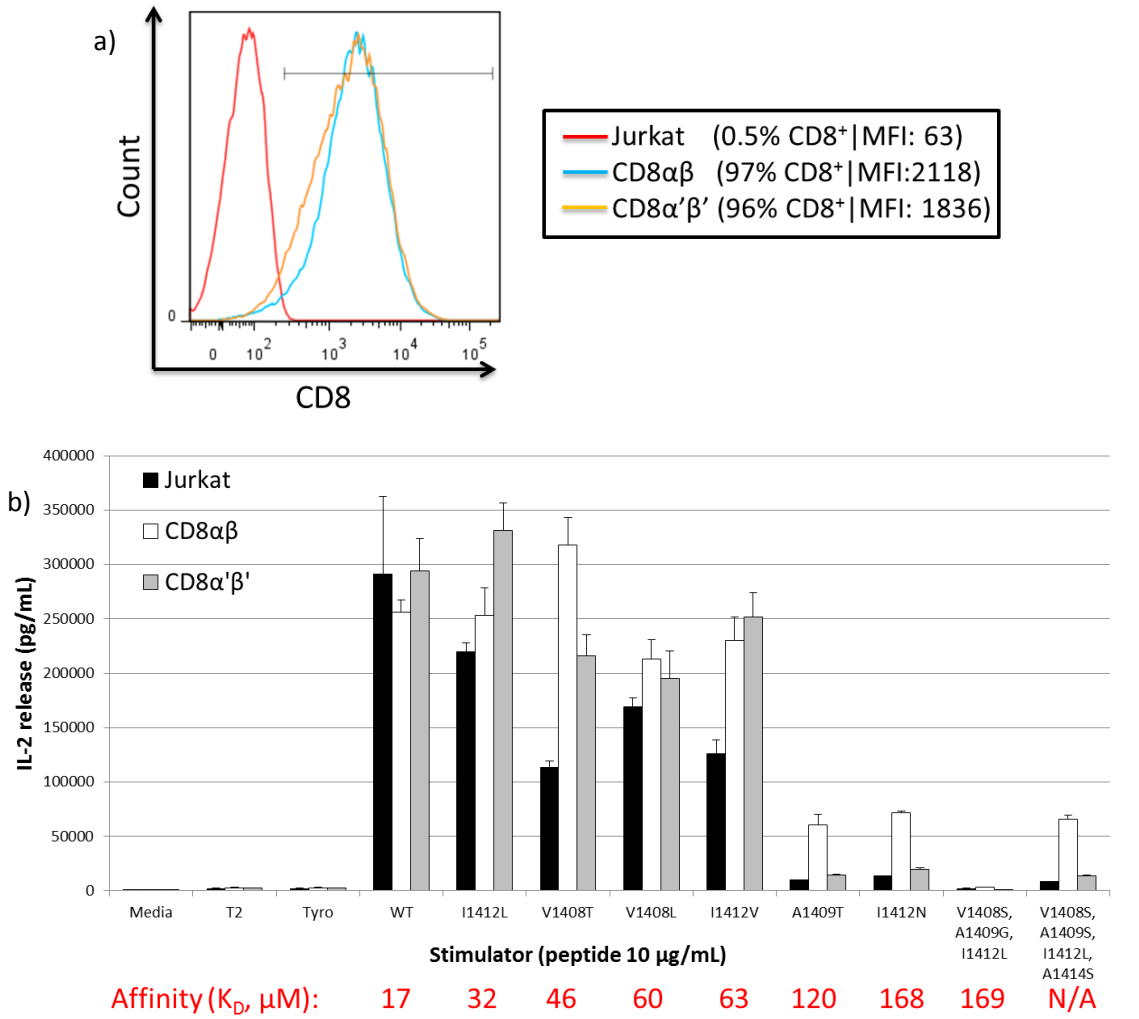

Figure 26. CD8 co-receptor signaling components are required for reactivity against CD8-dependent ligands. (a) Jurkat cells were transduced to express either full length CD8αβ or truncated CD8α'β' lacking the intracellular lck-binding domain. **(b)** Each group was transduced with a retrovirus encoding the HCV1406 TCR. After anti-CD34 immunomagnetic enrichment, these cells were co-cultured with T2 cells loaded with HCV NS3:1406-1415 (WT and variants) peptide or tyrosinase:368-376 peptide as a negative control. IL-2 secretion by Jurkat cells was measured by ELISA. Mean and standard deviation of triplicate measurements are shown. All variants that qualified as reactive in the text secreted at least 200 pg/mL IL-2 and twice above background and >5% of WT reactivity. Affinities of TCR-pMHC interactions are shown in red. These data are representative of three independent experiments.

HCV1406 TCR-transduced Jurkat cells stimulated with WT HCV NS3:1406-1415 peptide-loaded T2 cells reproducibly resulted in minimal differences in IL-2 secretion among CD8 negative, CD8αβ, or CD8α'β' cells (Fig. 26b). The previously characterized CD8-independent ligands, I1412L, V1408T, V1408L, and I1412V stimulated robust IL-2 release from all three Jurkat cell lines. Of note, the presence of CD8 (full length or truncated) did not seem to always augment cytokine release against all of these "moderate affinity" variants. This observation contradicts what we and others have found whereby the presence of CD8αβ can augment cytokine release in TCR-transduced T cells [305]. Perhaps there is an upper limit to CD8 help if the TCR-pMHC interaction is maximally efficient at inducing T cell activation. Jurkat cells lacking CD8 are again not reactive (by our established criteria) against "lower affinity" ligands A1409T, I1412N, 8S/9G/12L, or 8S/9S/12L/14S. The introduction of full length CD8αβ, however, rescues reactivity against all mutant peptides except 8S/9G/12L. Interestingly, Jurkat cells expressing truncated CD8α'β' were minimally or non-reactive reactive against these "lower affinity" variants, suggesting that TCR-pMHC stabilization is not sufficient and that the intracellular lck-binding domain is also required for T cell activation. These results also support the claim that TCR-pMHC affinity is not necessarily the determining factor in antigen recognition. We have also highlighted the important role of CD8 signaling on facilitating or enhancing antigen recognition of multiple mutant peptides.

Antigen Density Influences Cross-Reactive Responses

Clinical reports of on-target/off-tumor or off-target effects by TCR-transduced T cells used in ACT have been attributed to recognition of low levels of antigen by high affinity TCRs [122, 184, 186]. We also acknowledge that evaluating reactivity against peptide-loaded T2 cells is not necessarily a physiological representation of the antigen density a T cell might encounter on a virally-infected cell or tumor. For these reasons, the effect of antigen density on recognition of WT and naturally occurring mutant peptides by a TCR is an important point to consider for anti-tumor responses and potential cross-reactivity.

Therefore, we established multiple levels of antigen density arbitrarily defined as highest, lowest, and intermediate (Fig. 27). T2 cells are TAP-deficient and incapable of presenting endogenously processed antigen, which allows for saturating levels of exogenously loaded peptide. Peptide-pulsed T2 cells serve as our highest ligand density and have been used in reactivity assays thus far. To achieve an arbitrarily lower level of antigen density, we engineered a panel of HepG2 cells expressing WT and variant HCV NS3:1406-1415 epitopes each as a minigene fused to GFP by a 2A linker. Transduced cells were sorted for high and uniform GFP expression (Fig. 28a). We define minigene^{+} HepG2 cells as lower antigen density because they require the internal expression of epitopes with minimal antigen processing, but compete with endogenously processed peptides for available MHC-I. To establish an intermediate density of antigen between peptide-loaded T2 cells and antigen-expressing HepG2 cells, we exogenously loaded

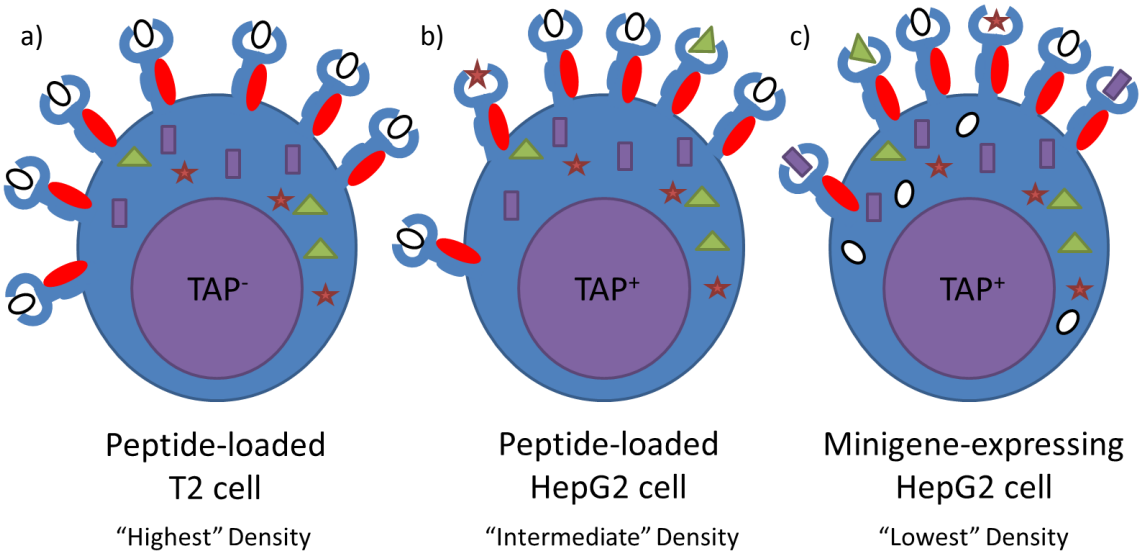

Figure 27. A model for pMHC ligand density. (a) T2 cells are TAP-deficient and incapable of presenting endogenously processed antigens (green triangles, red stars, purple rectangles). Exogenously loading with HCV NS3:1406-1415 peptide (white ovals) saturates available surface MHC-I with antigen. **(b)** HepG2 cells are TAP^+ and present internally processed antigens on MHC-I. Exogenously loading with high concentrations of HCV NS3:1406-1415 peptide can compete out endogenous antigen presented on MHC-I, but are presented at a lower density than peptide-loaded T2 cells. **(c)** HepG2 cells engineered to express HCV NS3:1406-1415 epitopes as minigenes require internal expression and minimal antigen processing and compete with endogenously processed peptides for MHC-I. HCV minigene-expressing HepG2 cells present HCV NS3:1406-1415 peptide at the "lowest" density of our three systems. HCV1406 TCR-transduced T cells were stimulated with each of these arbitrarily defined densities of pMHC ligand to assess the impact of ligand density on antigen recognition and TCR cross-reactivity.

HCV NS3:1406-1415 peptides on HepG2 cells. While peptides are not internally expressed, the loaded antigen still has to compete out occupied surface MHC-I on TAP^+ HepG2 cells for effective presentation to T cells. These three antigen expression-presentation systems allow for an arbitrary evaluation of the influence of antigen density on the cross-reactivity of a single TCR.

We previously showed that $CD4^+$ TCR-transduced T cells recognized WT and all "moderate affinity" mutants, while $CD8^+$ TCR-transduced T cells recognized all but mutant 8S/9G/12L. (Fig. 25) Changes in the amount of cytokine released by "reactive" T cells reproducibly differed by no greater than two-fold when stimulated with variant pMHC ligands. Interestingly, the antigen recognition pattern varied much more at a lower density of antigen, consistent with the results of a peptide titration presented earlier (Fig. 20). Not unexpected, peptide-loaded HepG2s were better recognized than minigene-expressing HepG2 cells (Fig. 28b). WT peptide recognition did not differ dramatically, but a decrease in antigen density had the greatest impact on "moderate" and "lower affinity" interactions. HepG2 cells expressing I1412L, V1408T, and V1408L minigenes stimulated nearly 20-fold less IFNγ secretion compared to peptide-loaded HepG2 cells. Interestingly, despite nearly identical affinity to V1408L, expression of I1412V as a minigene abrogated recognition by our defining criteria. Additionally, "lower affinity" ligands A1409T, I1412N, and 8S/9S/12L/14S exogenously loaded onto HepG2 cells were non-reactive defined by our criteria (<5% WT reactivity response), but still elicited hundreds more pg/mL IFNγ secretion compared to minigene-expressing cells.

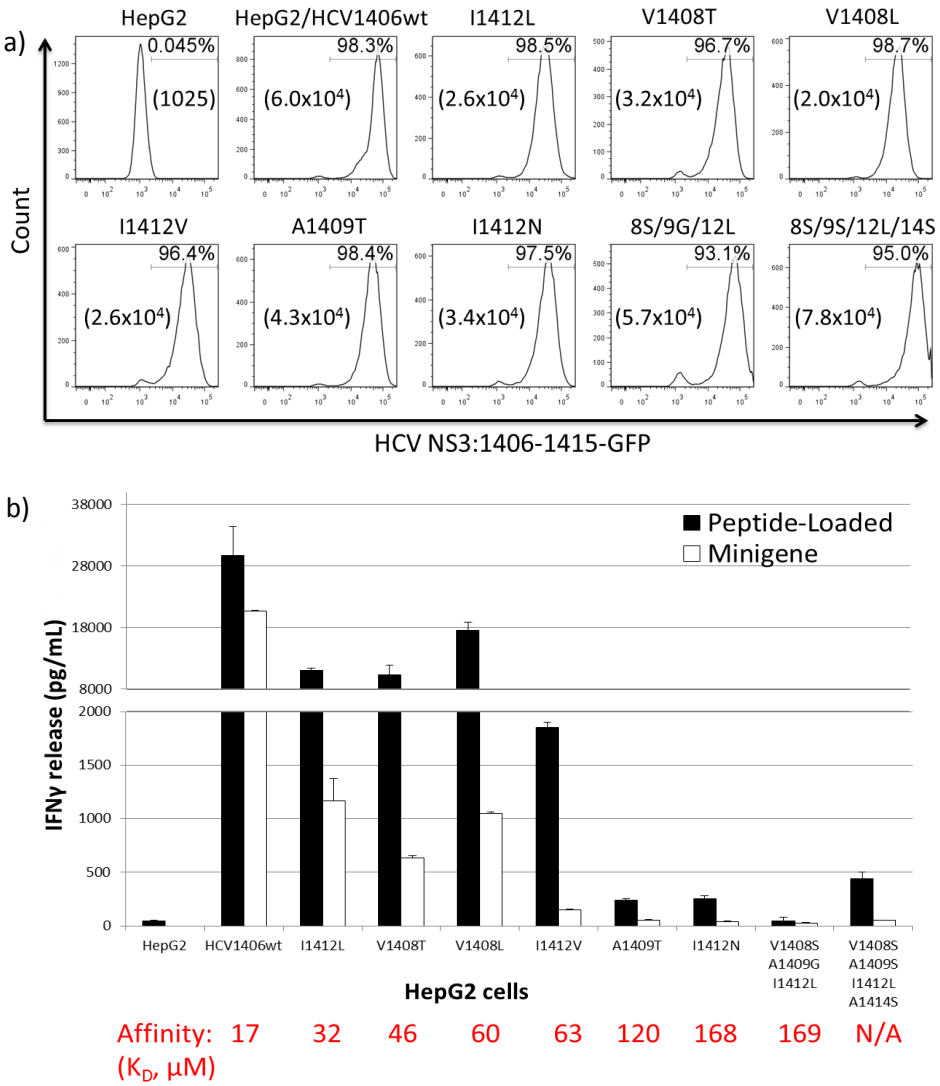

Figure 28. HCV1406 TCR cross-reactivity is substantially diminished in the context of HCV$^+$ tumor cells. (a) HepG2 cells were transduced with retroviral vectors encoding HCV NS3:1406-1415 variants as minigenes fused to GFP by a T2A linker. Cells were sorted for high and uniform expression of GFP. MFI are shown in parenthesis. **(b)** PBL from a normal donor were transduced with the HCV1406 TCR retroviral vector and enriched for CD34t expressing using anti-CD34 immunomagnetic beads. CD34$^+$ T cells co-cultured for 18 hr with WT or mutant HCV NS3:1406-1415 peptide-loaded or minigene-expressing HepG2 cells . IFNγ secretion was measured by ELISA. Mean and standard deviation of triplicate measurements are shown. All variants that qualified as reactive in the text secreted at least 200 pg/mL IFNγ and twice above background and at least >5% of WT reactivity. SPR-measured affinities of TCR-pMHC interactions are shown below in red. These data are representative of three independent experiments.

These results suggest the density of antigen plays an important role in facilitating antigen recognition and T cell activation.

To evaluate if the CD8 co-receptor impacts antigen recognition in light of decreased antigen density, we stimulated HCV1406 TCR-transduced $CD4^+$ or $CD8^+$ T cells with “intermediate density" peptide-loaded HepG2 cells (Fig. 29a) or “lower density” minigene-expressing HepG2 cells (Fig. 29b). We found that $CD4^+$ T cells were most susceptible to changes in antigen density. For example, we previously demonstrated that TCR-transduced $CD4^+$ T cells were highly reactive against WT and all “moderate affinity” antigen-loaded T2 cells. Differences in magnitude of IFNγ secretion were reproducibly no more than 2-3 fold (Fig. 25). Interestingly, mutant peptides (V1408T and I1412V) loaded on HepG2 cells (a lower density of antigen compared to T2) stimulated less than 750 pg/mL of IFNγ, while WT and V1408L stimulated over 60,000 and 20,000 pg/mL of IFNγ, respectively. Additionally, the presence of the CD8 co-receptor compensated for intermediate densities of “moderate affinity” ligands, but “lower affinity” mutant ligands stimulated nearly 60-fold less IFNγ secretion. Only two-fold differences were observed between “moderate” and “lower” affinity ligands in T2 cell stimulations (Fig. 25). These observations suggest that even antigen densities between peptide-loaded targets (tumor cells vs T2 cells) can have a profound effect on antigen recognition. Also, differences in cytokine secretion are not always reconciled by differences in TCR-pMHC affinity.

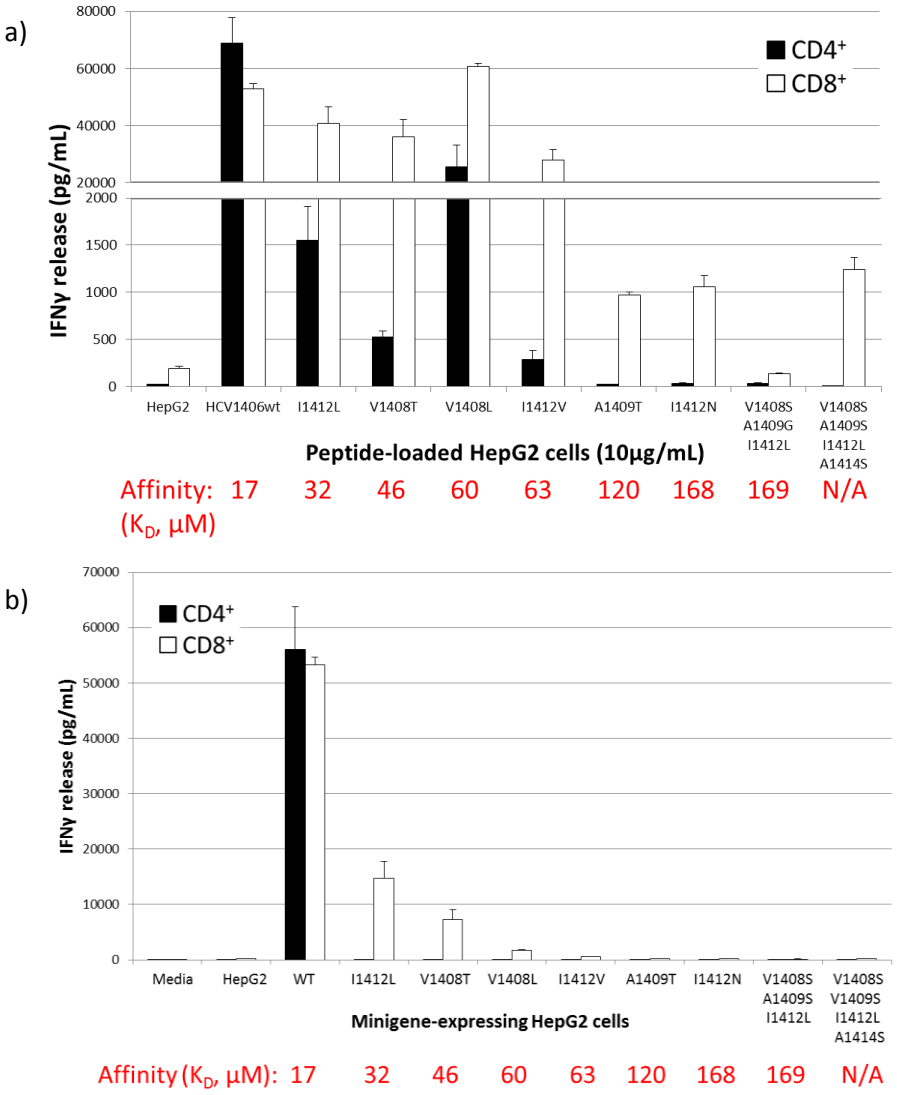

Figure 29. HCV1406 TCR CD4$^+$ T Cells are more susceptible to changes in ligand density. (a) HepG2 cells exogenously loaded with 10 µg/mL WT or variant HCV NS3:1406-1415 peptides or HepG2 cells engineered to express WT and variant HCV NS3:1406-1415 minigenes were co-cultured with PBL-derived T cells transduced with the HCV1406 TCR retroviral vector. (b) HCV1406 TCR-transduced PBL were immunomagnetically isolated into CD4$^+$ or CD8$^+$ populations and co-cultured with HepG2 cells loaded with WT or variant HCV NS3:1406-1415 peptides. IFNγ secretion after 18 hr co-culture was measured by ELISA. Mean and standard deviation of triplicate measurements are shown. All variants that qualified as reactive in the text secreted at least 200 pg/mL IFNγ and twice above background and at least >5% of WT reactivity. SPR-measured affinities of TCR-pMHC interactions are shown below in red. These data are representative of three independent experiments.

In our lowest antigen density system, minigene-expressing HepG2 cells elicited reproducibly similar amounts of IFNγ release from both $CD4^+$ and $CD8^+$ TCR-transduced T cells. However, only "moderate affinity" mutant pMHC could be recognized at lowest densities and now required the presence of CD8. In summary, recognition of lower affinity ligands seems to be affected more dramatically by changes in antigen density. However, CD8 can facilitate recognition of higher affinity antigens at lower densities. These data suggest that antigen density plays a critical role in antigen recognition of altered ligands.

TCR Transgene Levels Influence IFNγ Production Independent of Affinity

Given that antigen density influences antigen recognition and TCR cross-reactivity, it would be logical to predict that TCR density may also impact T cell recognition of altered ligands. The composition of our retroviral vector used to gene-modify T cells provides a useful tool to answer this question. As discussed previously, our TCR retroviral vector contains a CD34t cassette as a marker of transduction efficiency. While useful for enriching transduced T cell populations for *in vitro* studies and clinical treatment, our CD34t marker also allows us to assess relative TCR expression without staining for the TCR with an antibody or tetramer, which can influence the outcome of functional assays [380-382].

We evaluated the impact of TCR density on antigen recognition and TCR cross-reactivity by HCV1406 TCR-transduced PBL by relating intracellular IFNγ production with TCR transgene levels. HCV1406 TCR-transduced T cells were stimulated with WT and

mutant HCV NS3:1406-1415 peptide-loaded T2 cells and analyzed for intracellular IFNγ production by flow cytometry. We also stained T cells for surface markers CD4 and CD8 and our transduction marker CD34t. We have previously shown that increased levels of CD34 relate to increased tetramer binding (Foley unpublished, [304]), suggesting that CD34 serves as a good correlate for TCR expression. This approach enabled us able to relate the various levels of TCR transgene with intensity of cytokine production. Figure 30 displays representative CD34 vs IFNγ dotplots and our gating strategy used to assess IFNγ production in High, Medium, and Low CD34-expressing $CD4^+$ or $CD8^+$ TCR-transduced T cells. Mean fluorescence intensity (MFI) of intracellular IFNγ was calculated in each CD34 expression gate for both $CD8^+$ (Fig. 31a) and $CD4^+$ T cells (Fig. 31b).

In TCR-transduced $CD8^+$ T cells, IFNγ production was positively associated with TCR transgene expression. CD34 Hi-expressing $CD8^+$ T cells exhibited the greatest intensity of IFNγ, and all peptide but 8S/9G/12L stimulated similar levels of IFNγ staining in the CD34 Med and CD34 Low populations. However, only CD34 Hi-expressing $CD4^+$ T cells produced high IFNγ levels above background against all CD8-independent peptides. The WT epitope, as well as mutant peptides I1412L and V1408L, stimulated modest IFNγ production in CD34 Med- and CD34 Low-expressing cells. Despite having similar affinities to I1412L and V1408L, however, mutants V1408T and I1412V only stimulated substantial amounts of IFNg production in CD34 Hi-expressing T cells. Together, these data suggest that TCR transgene expression influences antigen recognition, but that the

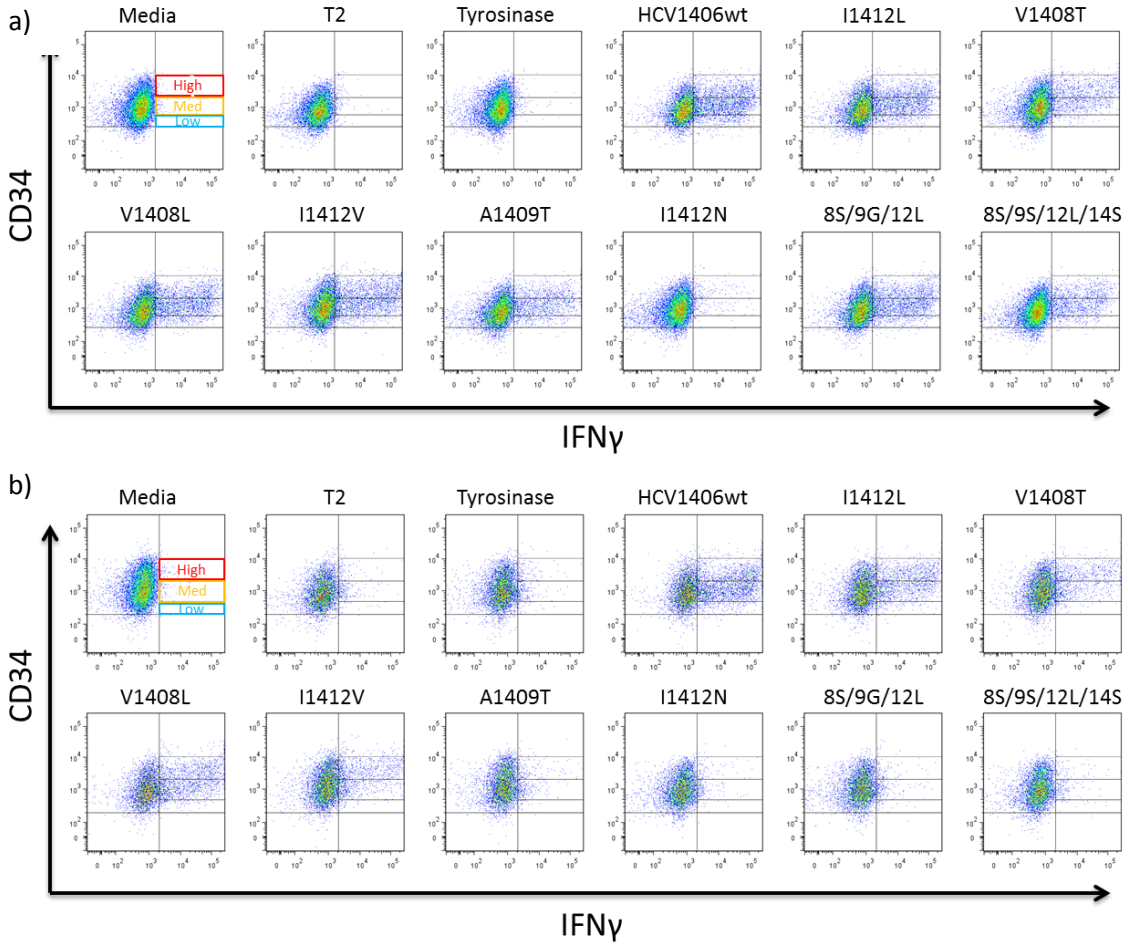

Figure 30. Gating strategy used to establish the relationship between TCR transgene expression and IFNγ production. PBL from a normal donor were transduced to express HCV1406 TCR and enriched for TCR-transduced cells using anti-CD34 immunomagnetic beads. T cells were co-cultured with peptide-loaded T2 cells for 5 hr and IFNγ production was assessed by intracellular cytokine staining. Representative immunofluorescence and gating of surface CD34 vs intracellular IFNγ for **(a)** $CD8^+$ and **(b)** $CD4^+$ TCR-transduced T cells. $CD34^+$ populations were subgated to delineate CD34 high, medium, and low expressing populations. Mean fluorescence intensity (MFI) of intracellular IFNγ was calculated for each CD34-expressing population.

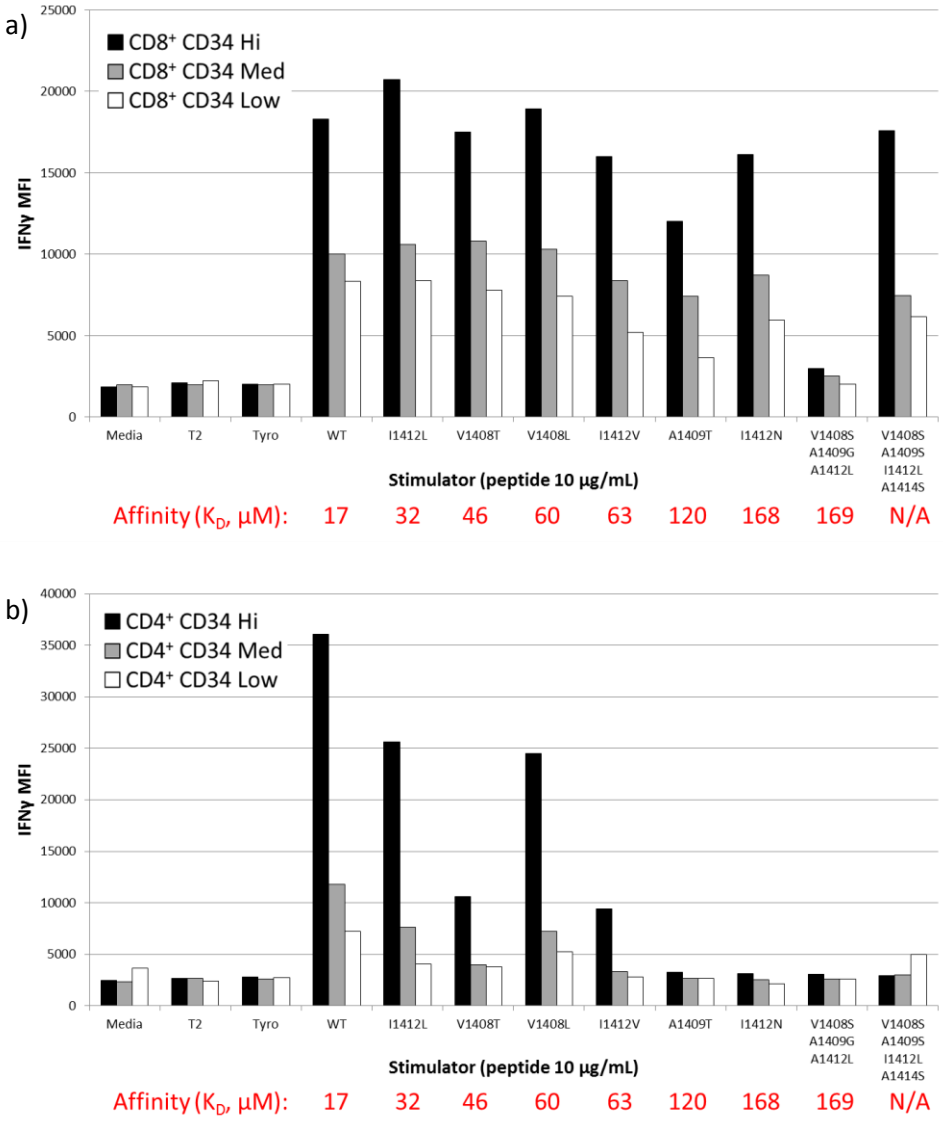

Figure 31. IFNγ production is positively associated with TCR transgene expression but high expression is required for CD4$^+$ T cells to produce IFNγ. PBL from a normal donor were transduced to express HCV1406 TCR and enriched for transduced cells using anti-CD34 immunomagnetic beads. T cells were co-cultured with peptide-loaded T2 cells for 5 hr and evaluated for IFNγ production by intracellular cytokine staining. Mean fluorescence intensity (MFI) of IFNγ production in CD34 high (black), medium (gray), and low (white) expression populations are shown in **(a)** CD8$^+$ and **(b)** CD4$^+$ TCR-transduced T cells. These data are representative of three independent experiments with three different donors each.

relationships between TCR-pMHC affinity, TCR density, CD8, and the intensity of cytokine production remain ill-defined.

Elimination of TCR Pairing Competition Enhances Cross-Reactivity

In an effort to better understand the interplay between TCR density, CD8 co-receptor function, and TCR cross-reactivity, we designed a panel of Jurkat cells equipped to delineate these contributions. Jurkat cells, like PBL-derived T cells, express an endogenous TCR. Consequently, TCR chains introduced into Jurkat cells have the potential to mispair with the endogenous TCR chains and also compete for association with CD3, limiting the density of functional introduced TCRs. Conversely, a variant Jurkat cell line, Jurkat76, lacks an endogenous TCR [383] (Fig. 32a). Introduction of a TCR into Jurkat76 cells eliminates the opportunity for both TCR chain mispairing and competition for CD3. Therefore, Jurkat76 cells serve as a system with optimal density of the introduced TCR. We also engineered Jurkat76 cells (natively $CD8^-$) to express full length CD8αβ, or truncated CD8α'β' lacking the intracellular lck-binding domain (Figs. 32b-c). Comparing functional responses between Jurkat and Jurkat76 cell lines may provide better insight into the impact of both TCR density and CD8 on antigen recognition and TCR cross-reactivity. A schematic of this model is provided in Figs 32d-e.

As described earlier, we observed CD8-dependence in Jurkat cells in light of TCR pairing competition between endogenous and introduced TCRs (Fig. 33a). We evaluated the effect of TCR chain pairing competition on cross-reactivity by peptide-stimulating our engineered Jurkat76 cell lines (Fig. 33b). Jurkat76 cells with and without CD8

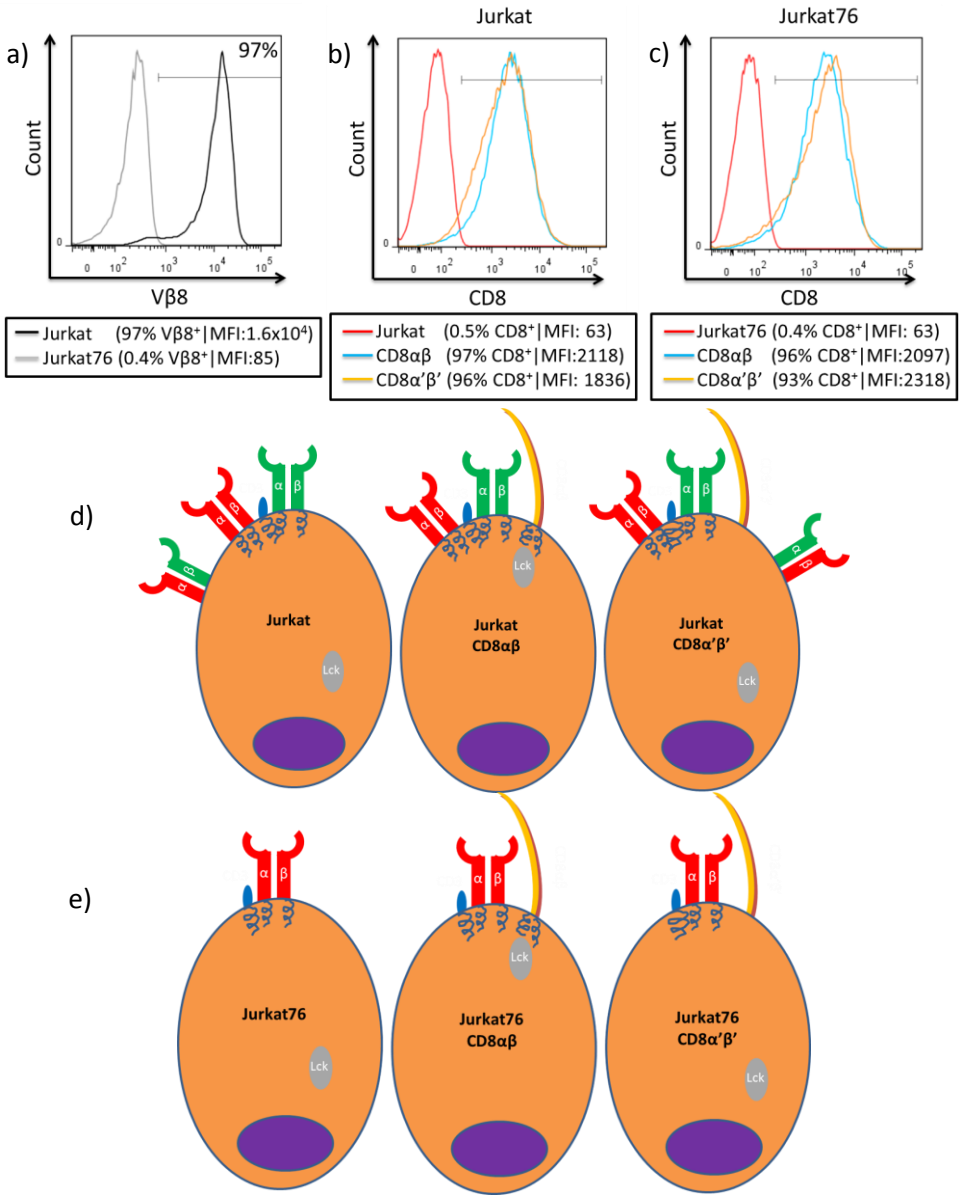

Figure 32. A Jurkat model for TCR chain pairing and CD8 signaling. (a) Jurkat cells express an endogenous TCR (measured by Vβ8 expression) while Jurkat76 cells lack an endogenous TCR. Both **(b)** Jurkat and **(c)** Jurkat76 cells were engineered to express full length CD8αβ or a truncated version (CD8α'β') lacking the intracellular lck-binding domain. **(d)** Introduced TCRs (red) can mispair with endogenous TCRs (green) and compete to associate with CD3 (blue) in Jurkat cells. **(e)** TCR pairing competition is absent in Jurkat76 cells. Introduction of full length CD8αβ stabilizes the TCR-pMHC interaction and facilitates TCR/CD3 signaling by recruiting lck. Introduction of CD8α'β' uncouples signaling from TCR-pMHC stabilization.

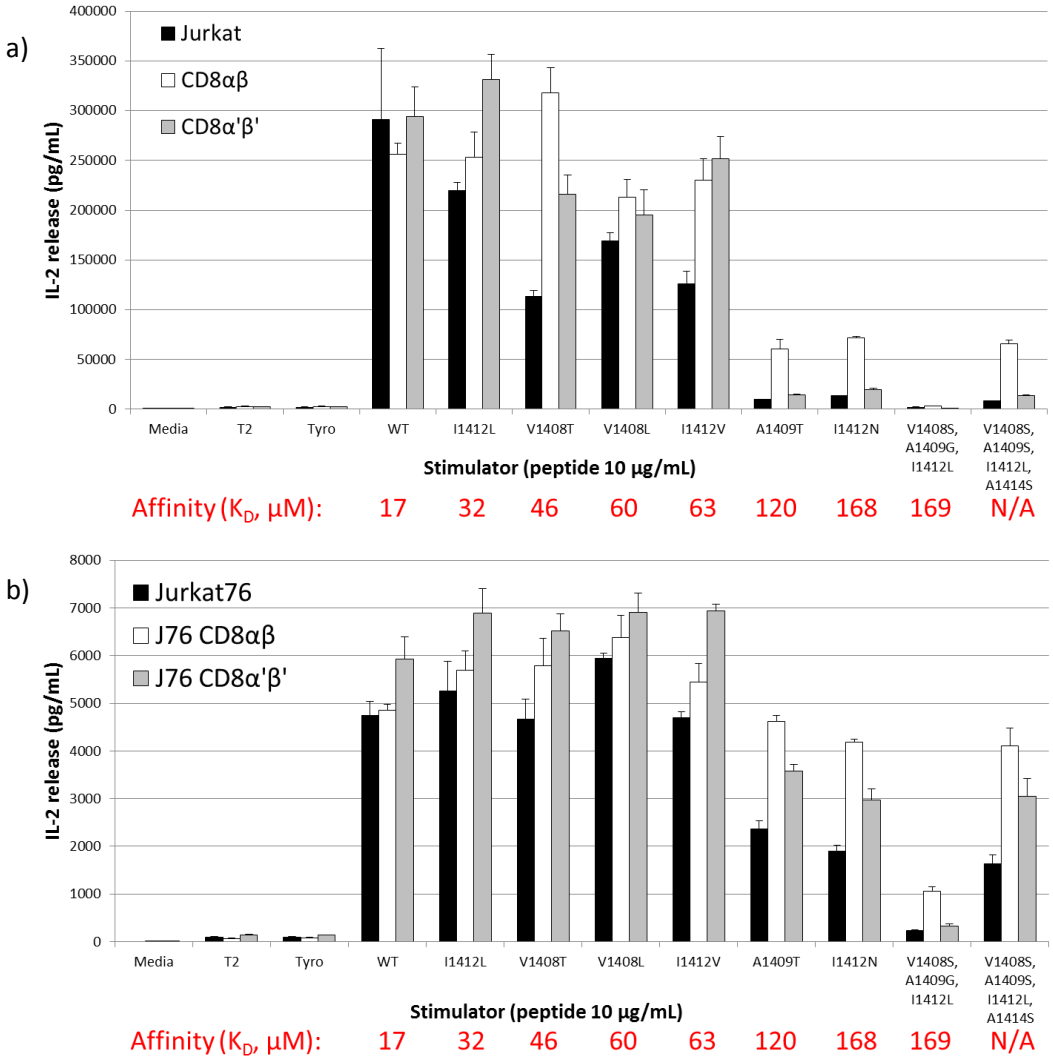

Figure 33. Absence of TCR pairing competition alleviates CD8-dependence. (a) Jurkat and **(b)** Jurkat76 cells (lacking an endogenous TCR) were transduced to express either full length CD8αβ or truncated CD8α'β'. Each group was transduced with a retrovirus encoding the HCV1406 TCR. After anti-CD3 immunomagnetic enrichment, Jurkat cells were co-cultured with peptide-loaded T2 cells. IL-2 release by Jurkat cells was measured by ELISA. Mean and standard deviation of triplicate measurements are shown. All variants that qualified as reactive in the text secreted at least 200 pg/mL IFNγ and twice above background and at least >5% of WT reactivity. SPR-measured affinities of TCR-pMHC interactions are shown in red. These data are representative of three independent experiments.

variants demonstrated similar levels of IL-2 release against WT or “moderate affinity” ligands. In contrast, mutants V1408T and I1412V, which exhibited a reproducibly lower reactivity in TCR-transduced $CD8^-$ Jurkat cells, had comparable cytokine release to WT in in all Jurkat76 cells. Overall, the lack of an endogenous TCR had minimal impact on recognition of ligands with moderate affinities (17 μm – 64 μM). Surprisingly, eliminating TCR pairing competition (enhancing TCR density) facilitated the recognition of “lower affinity” ligands A1409T, I1412N, and 8S/9S/12L/14S by $CD8^-$ Jurkat76 cells. CD8α’β’ Jurkat76 cells also recognized “lower affinity” mutant pMHC, with IL-2 secretion levels falling between $CD8^-$ and CD8αβ Jurkat76 cells’. Together, these data suggest that in the presence of TCR chain pairing competition, both the stabilization and signaling functions of CD8 are required. However, increased TCR expression in the absence of TCR chain pairing competition reduces the importance of the CD8 signaling component.

Most unexpectedly, we observed IL-2 secretion by CD8αβ Jurkat76 when stimulated with variant 8S/9G/12L. Countless experiments in WT Jurkat cells, numerous PBL donors, and even the parent T cell clone from which this TCR originated consistently showed no reactivity (Figs. 17,19,25-26,28-31). While the lack of recognition of 8S/9G/12L by the parent T cell clone seems puzzling, the most plausible explanation is that the parent clone underwent aberrant allelic exclusion during development and expressed two productively rearranged TCR α chains [165]. Thus, the parent clone exhibited endogenous TCR pairing competition and sub-optimal TCR density. Overall, it

is clear that limiting or enhancing TCR expression can have dramatic effects on antigen recognition and TCR cross-reactivity.

We also performed a peptide titration to determine if the elimination of TCR pairing competition alters the requirement of CD8 for enhanced functional avidity. We evaluated IL-2 release by Jurkat76 cells in response to peptide-stimulation, concentrations ranging from 10 – 0.0001 μM (Fig. 34). Based on similarly estimated EC_{50} values, functional avidity seemed to be independent of CD8 TCR-pMHC stabilization and lck recruitment upon stimulation with WT and "moderate affinity" mutants I1412L, V1408T, V1408L, and I1412V. "Lower affinity" ligands A1409T, 8S/9G/12L, and 8S/9S/12L/14S depended more on CD8 signaling in order to achieve maximum magnitude of cytokine release, but maintained relatively similar functional avidities compared to CD8α'β' Jurkat76 cells. We previously showed that in TCR-transduced Jurkat cells (Fig. 20), functional avidity of $CD8^-$ Jurkat cells was modestly reduced in WT and V1408L stimulation, but all other "moderate affinity" ligands had very low functional avidity with estimated EC_{50} values ranging between 10-1 μM. In the absence of TCR chain pairing, the estimated EC_{50} values were only a log-fold lower for $CD8^-$ Jurkat76 cells (Fig. 34) suggesting that CD8 not as important for high functional avidity with enhanced TCR density.

We also evaluated the impact of TCR density (as a function of TCR chain pairing) on antigen recognition by comparing the ability of HCV1406 TCR-transduced Jurkat and Jurkat76 cells to bind tetramers. A panel of tetramers containing WT or mutant HCV

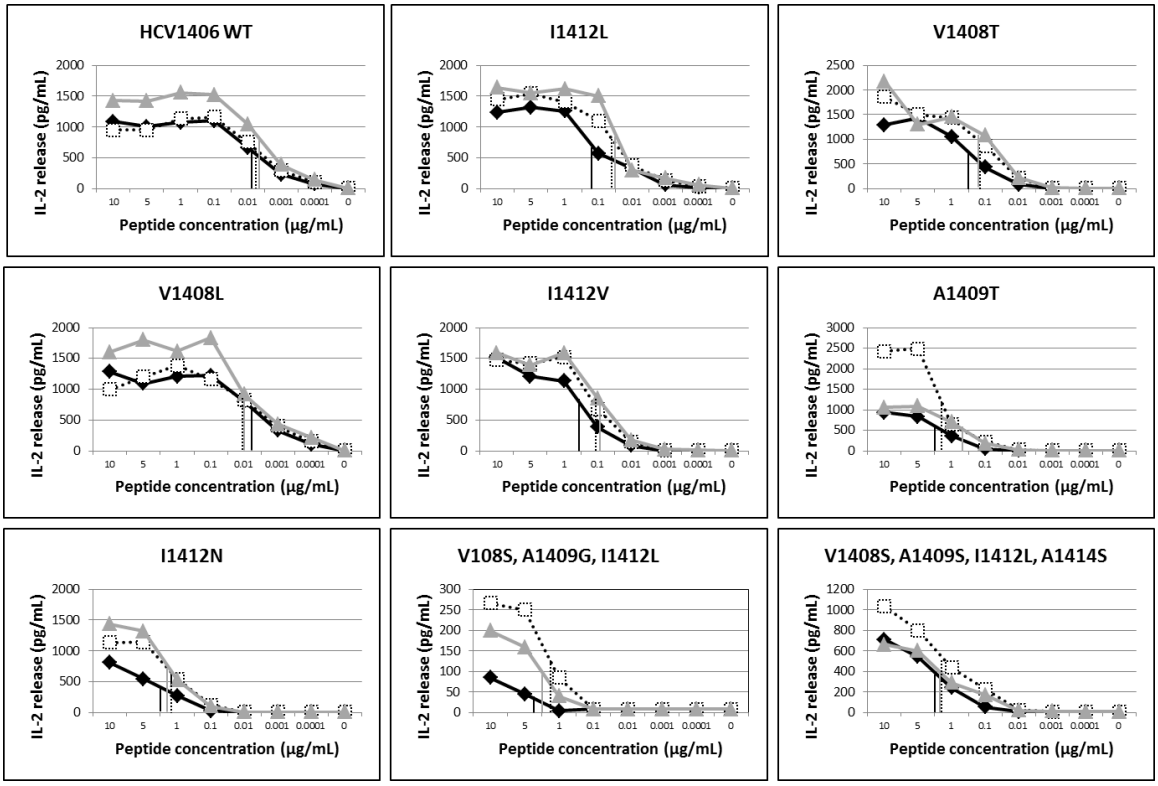

Figure 34. CD8 signaling is not necessarily required for enhanced functional avidity in the absence of TCR chain pairing competition. Jurkat76 cells (black diamonds) were transduced to express either full length CD8αβ (white squares) or truncated CD8α'β' (gray triangles). Each group was transduced with a retrovirus encoding the HCV1406 TCR and co-cultured with T2 cells loaded with peptides at various concentrations. IL-2 release by Jurkat cells was measured by ELISA. Means of triplicate measurements are shown. Compare to Figure 20 for functional avidity of Jurkat±CD8 cells. These data are representative of three independent experiments.

NS3:1406-1415 epitopes folded around HLA-A2 was kindly provided by the NIH Tetramer Core Facility at Emory University (Atlanta, Georgia). Tetramers containing mutant epitope 8S/9G/12L were not provided by the Core. We performed a steady-state binding assay with each tetramer, concentrations ranging from 10^{-7} – 10^{-12} M, and calculated the specific staining by HCV1406 TCR-transduced Jurkat or Jurkat76 cells by subtracting %Tetramer^{+} non-transduced cells from %Tetramer^{+} transduced cells. Often, non-TCR-transduced Tetramer^{+} populations were due to non-specific tetramer binding by CD8 [384]. TCR-transduced Jurkat cells were identified using the CD34 marker in our retroviral vector. Jurkat76 cells endogenously express CD34, so TCR-transduced cells were instead identified by the expression of CD3; Jurkat76 cells will only express surface CD3 when a TCR is expressed on the surface.

Steady-state tetramer binding curves are shown in Figures 35-36 representing Jurkat76 or Jurkat cells, respectively. HCV1406 TCR-transduced Jurkat76 cells bound WT tetramer very efficiently, with nearly 90% of TCR-transduced CD8^{+} Jurkat76 cells bound to tetramer (Fig. 35). A lower percentage of TCR-transduced cells, however, bound tetramers containing mutant epitopes at saturating concentrations, and decreases in tetramer binding generally trended with decreases in TCR-pMHC affinity. The presence of CD8 enhanced the EC_{50} of tetramers only one log-fold or less throughout. Interestingly, the presence of TCR chain pairing in HCV1406 TCR-transduced Jurkat cells affected the ability to bind tetramer (Fig. 36). Vertical axes are scaled to 100% tetramer bound TCR-transduced Jurkat cells for easy comparison to Jurkat76 cells (Fig. 35). Nearly

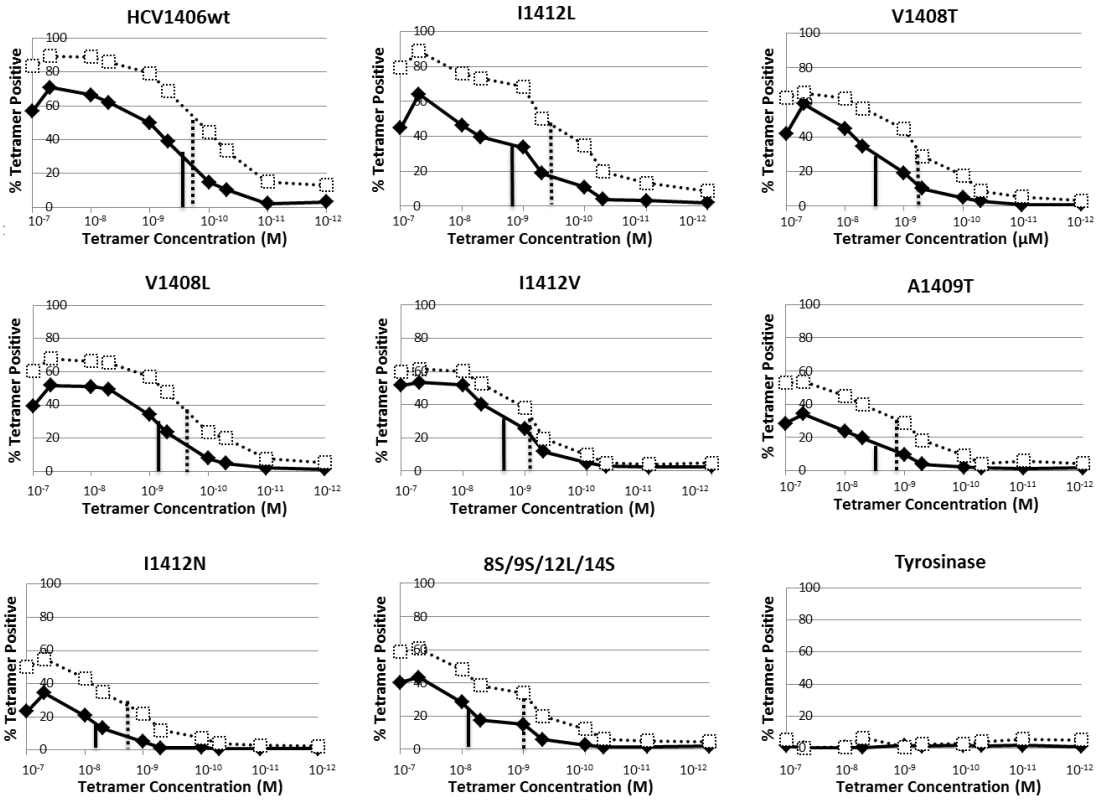

Figure 35. Steady-state binding of WT or mutant HCV NS3:1406-1415 tetramers by HCV1406 TCR-transduced Jurkat76 cells. Jurkat76 cells (black diamonds) were transduced to express full length CD8αβ (white squares). Both groups were transduced with a retrovirus encoding the HCV1406 TCR and stained with tetramers containing WT or mutant HCV NS3:1406-1415 epitopes at concentrations ranging from 10^{-7} – 10^{-12} M. Cells were counterstained for CD3 and analyzed for mCherry expression (CD8). Specific tetramer binding by HCV1406 TCR-transduced Jurkat76 cells was calculated as %$CD3^{+}Tetramer^{+}$ - %$CD3^{-}Tetramer^{+}$. These data are representative of two independent experiments.

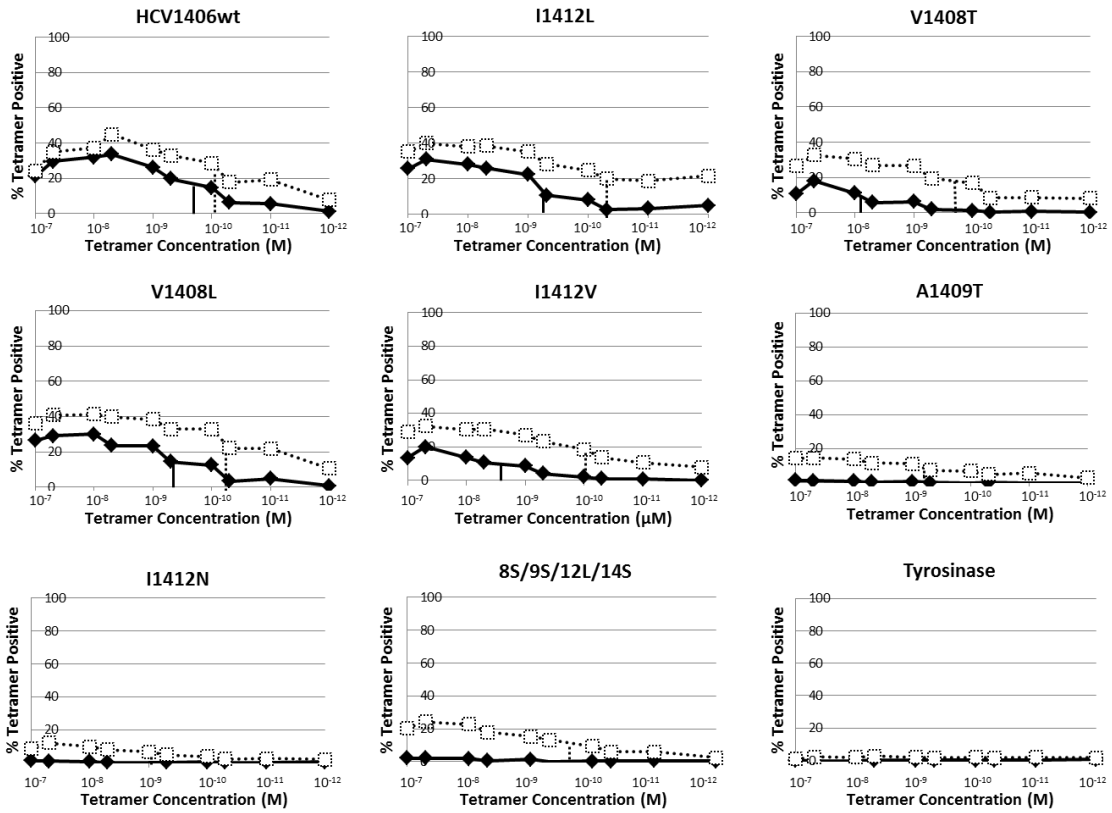

Figure 36. Steady-state binding of WT or mutant HCV NS3:1406-1415 tetramers by HCV1406 TCR-transduced Jurkat cells. Jurkat cells (black diamonds) were transduced to express full length CD8αβ (white squares). Both groups were transduced with a retrovirus encoding the HCV1406 TCR and stained with tetramers containing WT or mutant HCV NS3:1406-1415 epitopes at concentrations ranging from 10^{-7} – 10^{-12} M. Cells were counterstained for CD3 and analyzed for mCherry expression (CD8). Specific tetramer binding by HCV1406 TCR-transduced Jurkat cells was calculated as %$CD34^{+}Tetramer^{+}$ - %$CD34^{-}Tetramer^{+}$. These data are representative of two independent experiments.

50% fewer TCR-transduced Jurkat cells bound tetramer than Jurkat76 cells for each tetramer evaluated. Additionally, while tetramers containing mutant peptides A1409T, I1412N, and 8S/9S/12L/14S bound both $CD8^-$ and $CD8^+$ Jurkat76 cells (ranging from 40-60% at saturating concentrations), they bound only 20% or less of HCV1406 TCR-transduced $CD8^+$ Jurkat cells, and did not bind $CD8^-$ Jurkat cells. These differences in tetramer binding are consistent with functional assays shown in Figure 33, further suggesting that TCR chain pairing competition can have a substantial impact on antigen recognition and TCR cross-reactivity.

The relationship between TCR expression levels and tetramer binding was also evaluated for HCV1406 TCR-transduced Jurkat76 (Fig. 37a) and Jurkat (Fig. 37b) cells. For simplicity, staining of WT, V1408L, I1412V, and I1412N tetramers are shown at limited concentrations. Please see The Appendix for all tetramers and concentrations evaluated for both Jurkat cell lines. In HCV1406 TCR-transduced Jurkat76 cells, a linear relationship existed between CD3 (TCR) expression and WT tetramer binding at saturating concentrations (10^{-7} M). As the concentration of tetramer decreased, the relationship became less linear, and the ability to bind tetramer was more dependent on higher levels of TCR expression. Dependence on higher TCR density was exaggerated when evaluating TCR vs tetramer staining of lower affinity ligand I1412N (168 μM, compared to WT 17 μM). At saturating concentrations (10^{-7} M) the distribution of CD3 and tetramer positive cells suggests a higher threshold of TCR is necessary for tetramer binding. Furthermore, it is clear that a higher density of TCR is required to bind I1412N

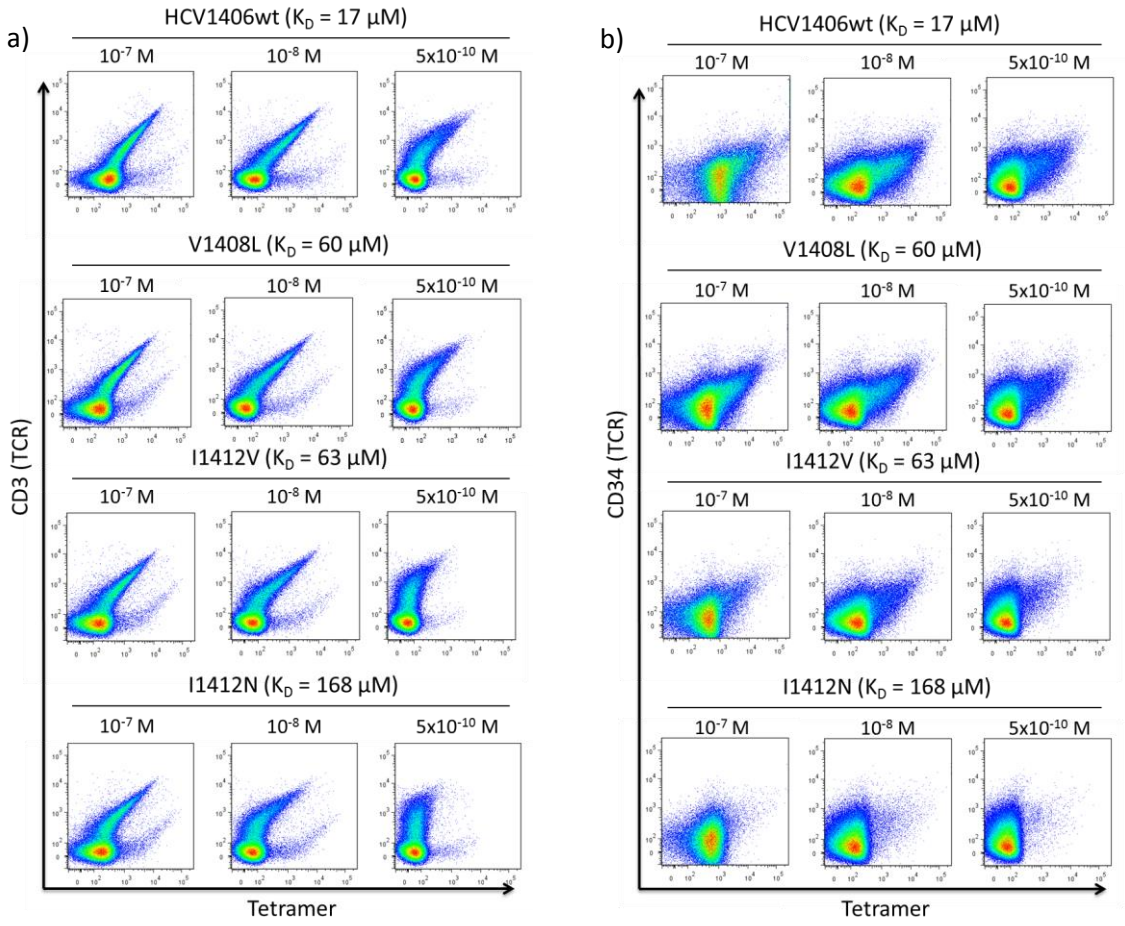

Figure 37. Influence of TCR-pMHC affiity and TCR chain pairing competition on tetramer binding. (a) Jurkat76 or **(b)** Jurkat cell lines were transduced to express full length CD8αβ. Both groups were transduced with a retrovirus encoding the HCV1406 TCR and stained with tetramers containing WT or mutant HCV NS3:1406-1415 epitopes at concentrations ranging from 10^{-7} – 10^{-12} M. Cells were also stained for CD3 or CD34. The relationship between TCR density and tetramer binding was evaluated using CD3 (Jurkat76 cells) or CD34 (Jurkat cells) as a surrogate marker for TCR transgene expression.

tetramer at lower concentrations compared to WT tetramer. Interestingly, TCR expression and tetramer binding between mutant ligands V1408L and I1412V were not consistent despite nearly identical affinity measurements (60 and 63 μM, respectively). For comparison, fewer HCV1406 TCR-transduced Jurkat cells bound tetramers compared to Jurkat76 cells and the distributions of TCR-transduced cells binding tetramers are remarkably different in the presence of TCR chain pairing competition (Fig. 37b). This is also reflected in the lower overall percentages of TCR-transduced Jurkat cell bound to tetramer shown in Figure 36.

In summary, both tetramer binding and functional studies suggest that TCR density plays a critical role in antigen recognition. When TCR density is high enough, it can allow for CD8-independent antigen recognition, despite a log-fold change in TCR-pMHC affinity. This evidence further supports that the ability of a T cell to recognize antigen does not solely depend on TCR-pMHC affinity.

Significance

The ability to fully understand what factors govern antigen recognition by T cells and TCR cross-reactivity may help improve TCR-based therapeutics. While affinity is generally accepted as the most important factor dictating antigen recognition, the field is relying on affinity-enhancement of TCRs to presumably augment their efficacy in TCR gene-modified T cells. Therefore, it is critical to evaluate the true importance of affinity. Appreciating how TCR antigen recognition is affected by TCR-pMHC affinity will help

modulate the field's approach in optimizing affinities to enhance or limit cross-reactivity of TCRs.

The data described in this chapter surprisingly suggest that TCR-pMHC affinity may not be the most important influence on antigen recognition. While decreases in T cell reactivity (especially in $CD8^-$ T cells) trended with decreases in TCR-pMHC affinity, cytokine release were not always proportional to changes in affinity. Additionally, mutant peptides with similar or equal affinities sometimes elicited substantially different IFNγ or IL-2 release. Other cellular parameters, including ligand density, TCR density, and CD8 co-receptor signaling, greatly impacted antigen recognition and functional avidity. Additionally, modification of any of these parameters altered functional response, sometimes independent of TCR-pMHC affinities. Collectively, these data suggest that TCR-pMHC affinity is not necessarily the driving force behind T cell function.

Through this point, we have admittedly evaluated T cell function based on the release of a single cytokine. We also acknowledge the potential for T cells to act as multi-functional effector cells. Thus, the evaluation of one cytokine may not accurately reflect changes in overall T cell function. In the next chapter, we aim to evaluate the polyfunctionality of T cells and to relate changes in polyfunctional phenotypes to alterations in TCR-pMHC interactions.

CHAPTER SIX

ANALYSIS OF POLYLFUNCTIONAL PHENOTYPES BY CROSS-REACTIVE HCV1406 TCR GENE-MODIFIED T CELLS

Rationale

We have suggested that affinity may not necessarily play the most central role in determining antigen recognition. In fact, it is clear that T cell function relies on a complex relationship between TCR-pMHC affinity, CD8 signaling, antigen density, and TCR density. We have defined the importance of these interactions by evaluating IFNγ or IL-2 release by HCV1406 TCR-transduced PBL and Jurkat cells, respectively. While standard assays in the field measure the production of a single cytokine to define T cell reactivity [385-393], it is important to acknowledge that T cells are multi-functional effectors.

Historically, effector T cells have been classified into type 1 (Th1, Tc1) or type 2 (Th2, Tc2) T cells based on the production of signature cytokines (i.e. IFNγ, IL-2, and TNFα for type 1; IL-4 and IL-13 for type 2) [394]. These functional profiles have also been related to therapeutic efficacy of individual T cell populations [395-399]. In general, a T cell population that has a type 1 phenotype is considered to have better anti-tumor efficacy than T cells with a type 2 phenotype [395, 396]. However, both type 1 and type 2 responses have been shown to play important roles in viral infections [400-402]. More recently, other T cell subsets have been implicated in facilitating anti-tumor or anti-viral

responses. For example, IL-9-producing $CD4^+$ T cells (Th9 cells) facilitated $CD8^+$ CTL-mediated anti-tumor immunity in a melanoma mouse model [403]. Furthermore, the presence of T cell subsets producing IL-17 (Th17, Tc17) or IL-22 has been recently associated with spontaneous HCV viral clearance [404]. The presence of multiple T cell subsets secreting varying combinations of cytokines suggest the evaluation of a single type 1 cytokine may not accurately characterize the reactivity of a T cell culture.

In fact, investigators have shown that in patients with advanced stage IV malignant melanoma who received a therapeutic vaccine, analysis of intracellular IFNγ induction in PBL-derived T cells showed no correlation in survival advantage [405]. However, evaluation of an additional cytokine (IL-2) by flow cytometry found an association in clinical outcome. Namely, there was enhanced survival in patients with induction of $IL\text{-}2^+IFN\gamma^-$ T cells. These studies support the hypothesis that evaluation of a single pro-inflammatory cytokine may hinder the proper biologic evaluation of T cells in a given experimental system. Flow cytometry-based approaches staining for multiple intracellular cytokines offer alternatives to more appropriately evaluate the true biology of a T cell culture and differential T cell responses. In this chapter, we describe how the inclusion of more than one functional parameter when evaluating antigen recognition can change or enhance the biologic message. We also evaluate how alterations in TCR-pMHC interactions can influence polyfunctional T cell responses.

Evaluating Bi-Functional HCV1406 TCR-Transduced T Cells

While single cytokine release assays are standard in the field, we wanted to begin our assessment of multi-functional T cell populations by simultaneously evaluating IFNγ production and cytolytic activity by HCV1406 TCR-transduced T cells. Target cell lysis is important in facilitating anti-tumor and anti-viral immunity [406] and thus a reasonable second functional parameter in evaluating antigen reactivity. Although CD107a is a surrogate marker for degranulation [406], traditional chromium release assays would prevent us from simultaneously measuring cytokine production and correlating with lytic behavior on a per-cell basis. In this way, we simultaneously measured intracellular IFNγ production and surface CD107a expression to assess the impact of variant HCV NS3:1506-1415 pMHC on T cell function.

Heterogeneity of Bi-Functional $CD4^+$ and $CD8^+$ T Cell Responses Is Not Evident In Bulk Culture Analysis

We first characterized bi-functional responses of HCV1406 TCR-transduced T cells against WT HCV NS3:1406-1415 peptide-loaded T2 cells. Figure 38 displays percentages of lytic-only ($CD107a^+IFN\gamma^-$), IFNγ producing-only ($CD107a^-IFN\gamma^+$) or bi-functional ($CD107a^+IFN\gamma^+$) phenotypes. T cells were analyzed as a bulk culture or gated on $CD4^+CD8^-$ or $CD4^-CD8^+$ TCR-transduced T cells. Assessing bulk culture reactivity suggests of the 49% of TCR-transduced T cells that are reactive, with nearly equal proportions only producing IFNγ (15%), only being lytic (15%), or are bi-functional (20%). Subsequent gating on $CD4^+$ or $CD8^+$ T cells revealed how proportionally different these

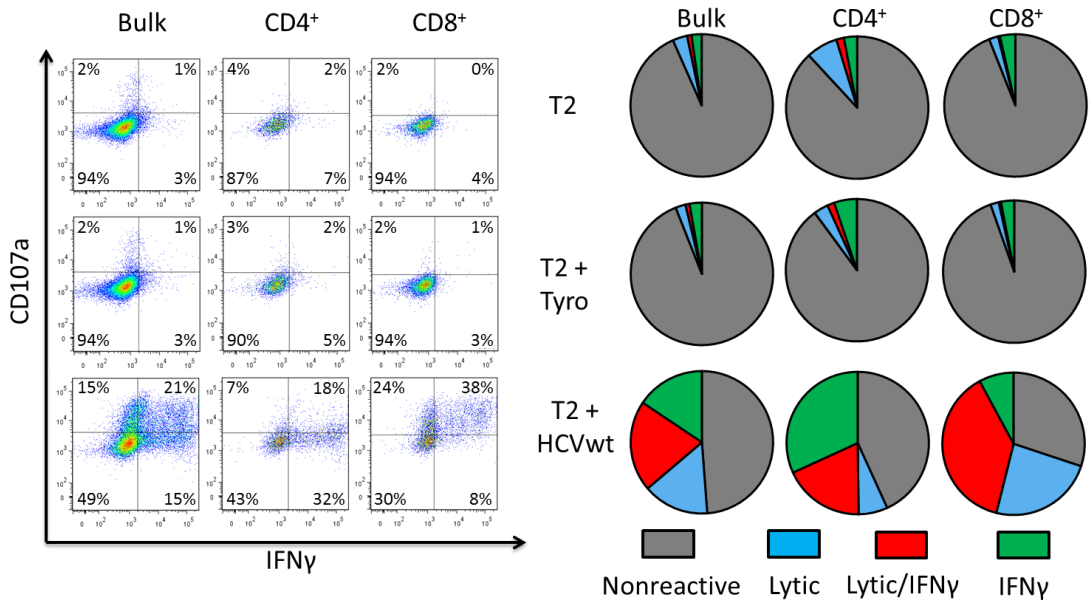

Figure 38. Bi-functional T cell reactivity assay demonstrates T cell subset heterogeneity. PBL from a normal donor were transduced with a retroviral vector encoding the HCV 1406 TCR. HCV TCR-transduced T cells were co-cultured for 5 hours with T2 cells loaded with tyrosinase:368-376, HCV NS3:1406-1415, or no peptide in the presence of monensin, brefeldin-A, and anti-CD107a. Co-cultures were then stained for T cell surface markers and IFNγ. **(a)** TCR-transduced T cells were identified by $CD34^+$ phenotype (Bulk culture, left panel) and subsequently gated as $CD4^+CD8^-$ (CD4, middle panel) or $CD4^-CD8^+$ (CD8, right panel). Each population was evaluated with a biaxial comparison of CD107a and intracellular IFNγ. **(b)** Percentages of each CD107a vs IFNγ quadrant were converted into pie charts. $CD107a^+$ $IFN\gamma^-$ (lytic-only, blue); $CD107a^+IFN\gamma^+$ (bi-functional lytic and IFNγ producing, red); CD107a-IFNγ+ (IFNγ producing-only, green); $CD107a^-IFN\gamma^-$ (nonreactive, gray). Pie charts reflect a minimum of 2,000 cells (average 4,000 cells). These data are representative of a single donor from three independent experiments using three different donors each.

subsets behave. This representative example shows that of $CD4^+$ T cells, 32% only produce IFNγ, 7% are only lytic, but 18% exhibit dual functions. Conversely, $CD8^+$ T cells are predominantly bi-functionally lytic and IFNγ-producing (38%), but with smaller populations being only lytic or only producing IFNγ (24% and 8%, respectively). Additionally, the fact that there were a higher percentage of non-reactive $CD4^+$ T cells supports our previous claim that the presence of CD8 can impact overall function. Together, this analysis provides a unique perspective on T cell function than evaluation of either IFNγ or lysis alone.

Bi-Functional T Cell Populations Are Disproportionately Affected by Alterations in pMHC

We have previously shown that the magnitude of IFNγ release differs between mutant peptide stimulations. We subsequently evaluated whether changes in TCR-pMHC interactions could affect T cell function as measured by both IFNγ and CD107a. Figure 39 displays percentages of lytic-only ($CD107a^+IFN\gamma^-$), IFNγ producing-only ($CD107a^-IFN\gamma^+$) or bi-functional ($CD107a^+IFN\gamma^+$) TCR-transduced $CD4^+$ or $CD8^+$ T cells after stimulation with naturally occurring mutant HCV NS3:1406-1415 peptides. Mutant peptides are grouped into “moderate affinity” (middle column) and “lower affinity” (right column) in decreasing affinity (top to bottom). Representative flow cytometry data are provided in The Appendix.

We observed again that $CD4^+$ T cell functional responses are restricted to variant ligands I1412L, V1408T, V1408L, and I1412V. We defined reactivity in these assays when

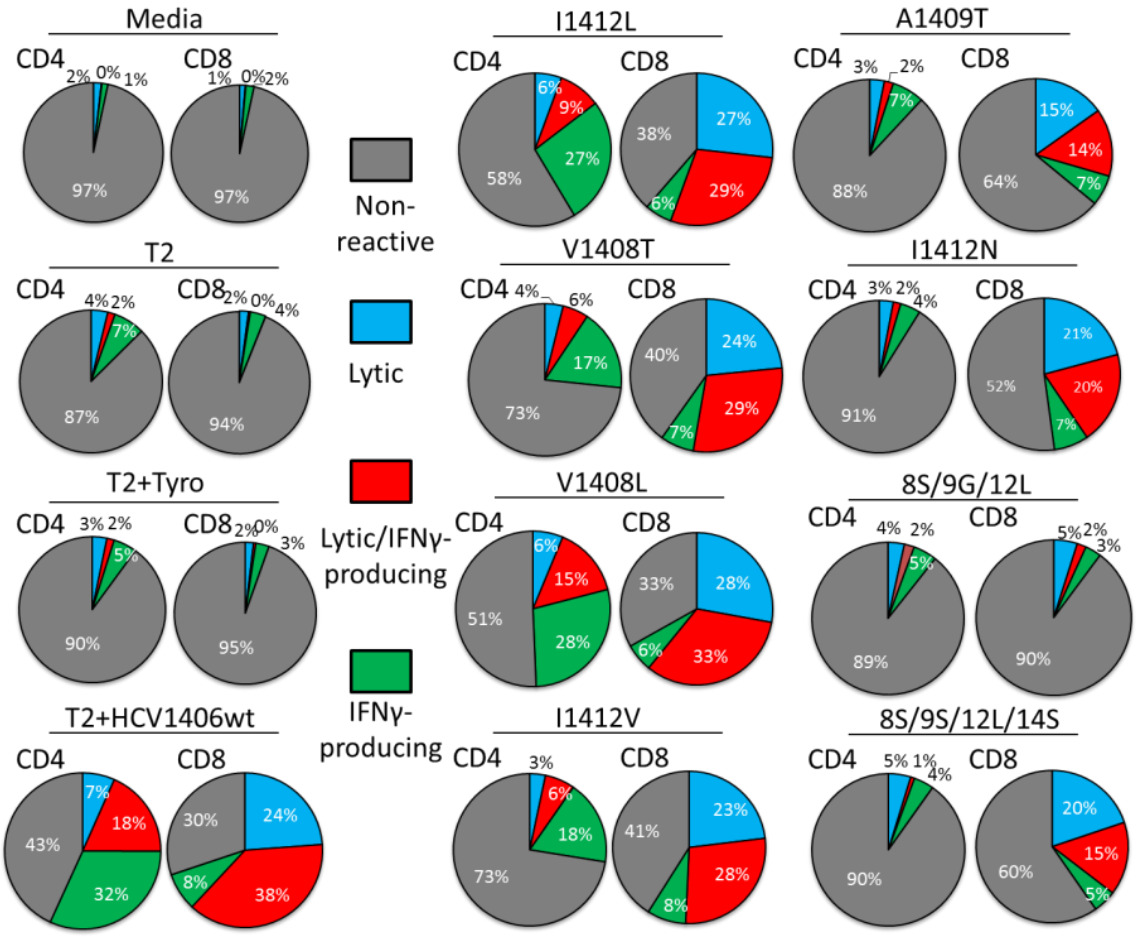

Figure 39. HCV1406 TCR-transduced CD4$^+$ and CD8$^+$ T cells have varying bi-functional responses against naturally occurring mutant HCV NS3:1406-1415 peptides. HCV1406 TCR-transduced PBL were co-cultured for 5 hr with T2 cells loaded with WT and mutant HCV NS3:1406-1415 peptides or tyrosinase:368-376 peptide as a control, T cells were analyzed by flow cytometry for T cell surface markers, CD107a expression, and intracellular IFNγ. Percentages lytic and/or IFNγ producing TCR-transduced CD4$^+$ (left pie) or CD8$^+$ T (right pie) cells are displayed as pie charts for corresponding stimulation conditions. Variant peptides are grouped into "moderate affinity" (middle column of each panel) and "lower affinity" (right column of each panel) in decreasing order of affinity (top to bottom). Pie charts reflect a minimum of 2,000 cells (average 4,000 cells). Reactivity is defined by greater than twice the percentage of total reactive cells against background (tyrosinase) stimulation. These data are representative of a single donor from three independent experiments using three different donors each.

the total percentage of functional cells was greater than twice background (tyrosinase) stimulation. It was clearly evident that alterations in TCR-pMHC interactions affected the overall percentage of reactive cells. While 57% of TCR-transduced $CD4^+$ T cells stimulated with WT peptide were reactive, this amount decreased when T cells were stimulated by any of the mutant peptides. Interestingly, however, the decrease in reactive T cells was not necessarily proportional to the decrease in TCR-pMHC affinity as V1408L (46 μM)-stimulated T cells exhibited nearly twice as many reactive T cells when stimulated by V1408T (60 μM) peptide-loaded T2 cells. Additionally, mutant I1412V stimulated nearly 50% less reactive T cells than V1408L, despite having nearly identical affinities (63 and 60 μM, respectively).

Remarkably, when the overall percentage of reactive T cells was reduced, the bi-functional population disproportionately decreased compared to either mono-functional population. For example, when $CD4^+$ T cells were stimulated with I1412L compared to WT peptide-loaded targets, the mono-functional lytic-only population was modestly reduced by 15% (7% compared to 6%) and the IFNγ-only population was reduced by 16% (32% compared to 27%). However, bi-functional cells decreased by 51% (18% compared to 9%) (Table 11). Interestingly, a reduction in bi-functional populations sometimes occurred despite comparable affinities. V1408L and I1412V have measurable TCR-pMHC affinities of 60 and 63 μM, respectively. Yet, their bi-functional responses compared to WT were drastically different. Compared to WT stimulation, V1408L peptide-loaded T2 cells elicited 95% as many lytic-only cells, 89% as many IFNγ-only

Table 11. Percent of WT reactivity in mono- and bi-functional populations upon stimulation with HCV NS3:1406-1415 mutant peptides.

Epitope	$CD4^+$ TCR-Transduced T Cells			$CD8^+$ TCR-Transduced T Cells		
	Lytic only	IFNγ only	Lytic/IFNγ	Lytic only	IFNγ only	Lytic/IFNγ
WT	100	100	100	100	100	100
I1412L	84.7	84.3	48.7	112.3	73.3	75.5
V1408T	58.4	54.4	29.8	98.3	90.1	76.9
V1408L	94.6	89.3	79.7	116.9	75.7	86.6
I1412V	50.1	56.2	34.5	96.9	104.7	72.5
A1409T*	47.0	21.7	10.5	63.8	81.7	37.5
I1412N*	45.0	13.6	8.7	87.4	92.9	51.6
8S/9G/12L*†	52.5	15.9	11.5	20.6	42.4	5.0
8S/9S/12L/14S*	71.8	13.3	4.5	83.3	62.2	40.8

*Non-reactive against $CD4^+$ T cells; †Non-reactive against $CD4^+$ or $CD8^+$ T cells
Percentages reflect the ratio of mutant:WT antigen stimulations for each functional phenotype. WT is normalized at 100%. These data are representative of a single donor from three independent experiments using three different donors each.

producing cells, and an 80% decrease in bi-functional populations. However, I1412V with essentially the same affinity as V1408L stimulated roughly 50% fewer mono-functional cells, and curbed the presence of bi-functional cells by nearly two thirds compared to WT stimulation (Table 11). Together, these data suggest that alterations in TCR-pMHC interactions can disproportionately alter bi-functional T cell responses.

Similar trends in altered responses held true for $CD8^+$ T cells as well. Stimulation with I1412L peptide-loaded targets elicited a modest change in overall reactivity from 70% to 62% total reactive T cells. Interestingly, the entire 8% decrease in overall reactivity is lost in the bi-functional population. This trend is even more dramatic when comparing TCR-transduced $CD8^+$ T cells against "lower affinity" ligands (A1409T, I1412N, and 8S/9S/12L/14S). When $CD8^+$ T cells were stimulated by the WT antigen, bi-functional populations were roughly 50% greater than lytic only cells. But when the TCR-pMHC interaction is at a lower affinity, the proportion of bi-functional $CD8^+$ T cell was less than or equal to lytic-only cells. As mentioned, a summary of each phenotype's percent change compared to WT stimulation, emphasizing a larger percent change in bi-functional populations, can be found in Table 11. Overall, these findings support the hypothesis that alterations in TCR-pMHC interactions (sometimes independent of affinity) elicit varied functional responses. These data also suggest that when measuring two functional parameters simultaneously, blunted T cell reactivity disproportionately affects bi-functional T cells and is not necessary influenced by changes in TCR-pMHC affinity.

Recognition of Naturally Processed NS3 Is Restricted to HCV1406 TCR-Transduced CD8$^+$ T Cells

The data described above compare changes in bi-functional phenotypes in light of high antigen density (peptide-loaded T2 cells). In the last chapter, we provided evidence that antigen density played a role dictating antigen recognition. Here, we establish a new "lowest antigen density" model using COS/A2 cells engineered to expressing the full length NS3 protein with WT or mutant 1406-1415 epitopes (Fig. 40). In NS3$^+$ COS/A2 cells, the 1406-1415 epitope must be naturally processed before competing with endogenous peptides for available MHC-I. This system allows us to measure the effects of even lower antigen density on T cell bi-functionality.

Figure 41 illustrates that reactivity against WT naturally processed antigen is limited to CD8$^+$ T cells. Recall, we previously defined that for an antigen to be arbitrarily reactive, the total percentage of functional cells must be greater than twice background (here, COS/NS3) stimulation. Compared to HCV minigene$^+$ HepG2 cells, which stimulated both CD4$^+$ and CD8$^+$ TCR-transduced T cells (Figs. 14,29), COS/A2 cells express a lower density of antigen. These data suggest that CD8 is most necessary at lowest levels of antigen density, which would be predicted based on the function of CD8.

Interestingly, naturally processed mutant epitope recognition was also restricted to HCV1406 TCR-transduced CD8$^+$ T cells. Only V1408T, V1408L, and I1412V qualified as reactive, despite I1412L exhibiting the lowest TCR-pMHC affinity out of this group of

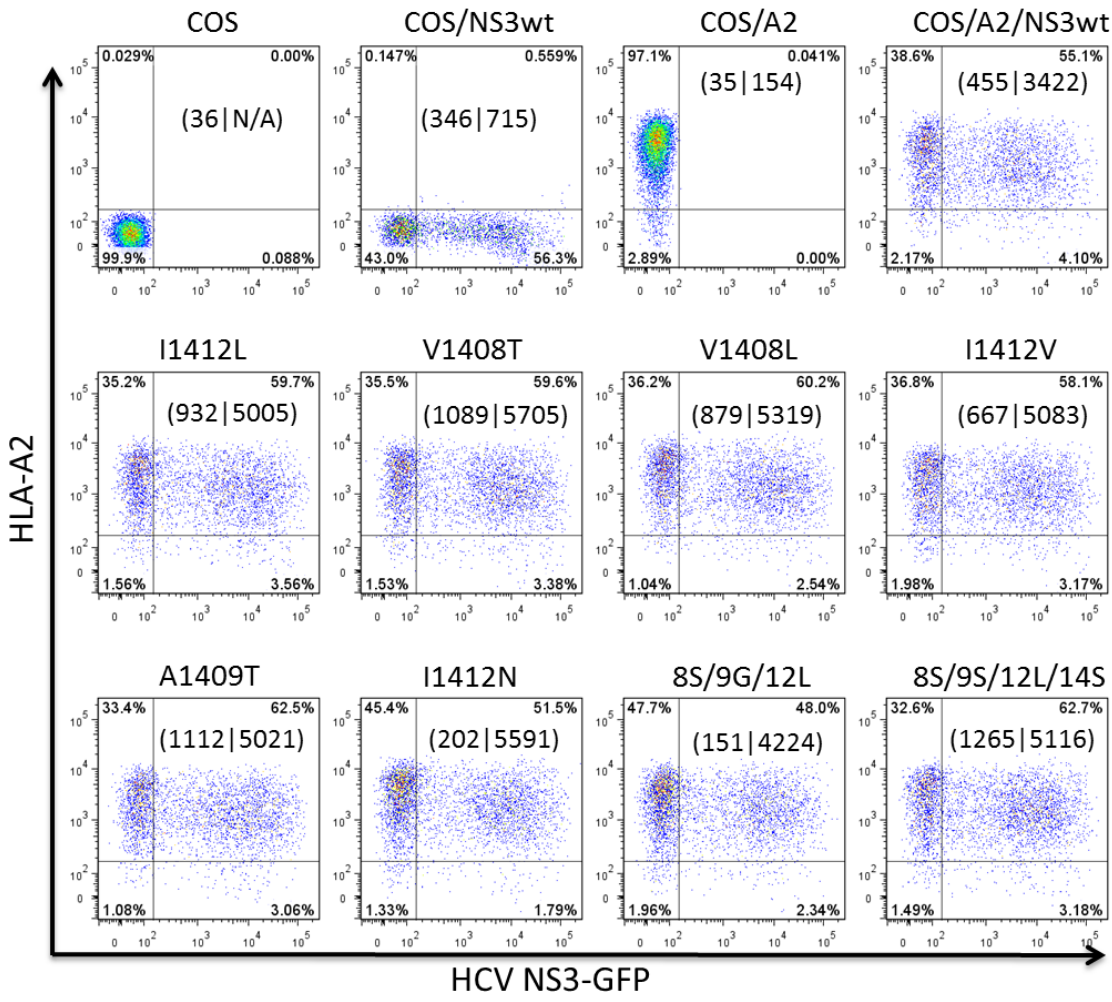

Figure 40. Generation of COS/A2 expressing naturally processed HCV NS3 with WT and naturally occurring mutant NS3:1406-1415 epitopes. COS cells and COS/A2 cells were transfected with a pcDNAIII vector encoding full length HCV NS3 protein containing WT or variant NS3:1406-1415 epitopes fused to GFP by a T2A linker. Representative transfection efficiency as measured by GFP expression is shown. Mean fluorescence intensity of each total population (MFI-1) and the GFP^+ population (MFI-2) are listed as: (MFI-1|/MFI-2).

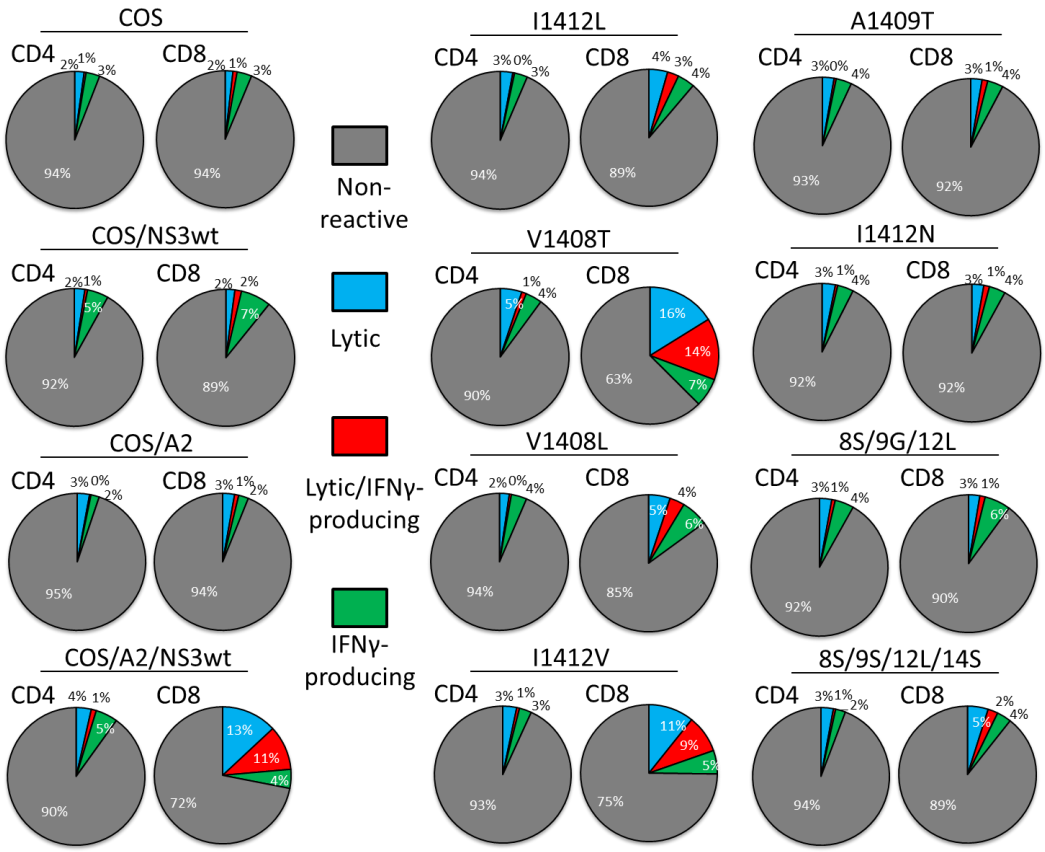

Figure 41. HCV1406 TCR-transduced CD4$^+$ and CD8$^+$ T cells have limited bi-functional reactivity against HCV NS3:1406-1415 naturally processed antigen. HCV1406 TCR-transduced PBL were co-cultured for 5 hr with COS/A2 cells transiently transfected to express full length WT HCV NS3 or HCV NS3 with various mutant 1406-1415 epitopes. T cells were analyzed by flow cytometry for T cell surface markers, surface CD107a expression, and intracellular IFNγ. Percentages lytic and/or cytokine producing TCR-transduced CD4$^+$ (left pie) or CD8$^+$ (right pie) T cells are displayed as pie charts for corresponding stimulation conditions. Variant peptides are grouped into "moderate affinity" (middle column of each panel) and "lower affinity" (right column of each panel) in decreasing order of affinity (top to bottom). Pie charts reflect a minimum of 2,000 cells (average 4,000 cells). Reactivity is defined by greater than twice the percentage of total reactive cells against background (tyrosinase) stimulation. These data are representative of a single donor from three independent experiments using three different donors each.

mutant ligands. Additionally, mutant V1408T elicited a greater percentage of reactive cells compared to WT antigen (37% compared to 28%). These data provide further evidence that TCR-pMHC affinity may not be the most critical influence on T cell function.

A Decrease in Ligand Density Preferentially Diminishes Bi-Functional Responses

A dramatic decrease in bi-functional T cells was also evident when comparing peptide versus naturally processed antigen stimulations (Fig. 42). Over half (38% out of 70%) of total reactive TCR-transduced $CD8^+$ T cells were bi-functional when stimulated with WT peptide-loaded T2 cells. But when stimulated with naturally processed antigen, bi-functional populations were reduced to 29% of the peptide-elicited response. Lytic-only and IFNγ-only populations were only reduced by 54% and 50%, respectively. This trend is consistent for the remainder of reactive naturally processed antigens (summarized in Table 12). These data not only support the claim made in the previous chapter that decreased ligand density impacts antigen recognition, but that a decrease in antigen density also contributes to a preferential loss of bi-functional T cell responses.

A Two-Parameter Analysis Enhances Our Understanding of Antigen Recognition over a One-Parameter Evaluation

As mentioned earlier, traditional techniques used to assess T cell reactivity usually rely on the evaluation of a single pro-inflammatory cytokine secreted by a mixed culture of lymphocytes. Interestingly, we found that evaluation of a single cytokine measured by ELISA is limited in its interpretation. Decreases in the magnitude of a

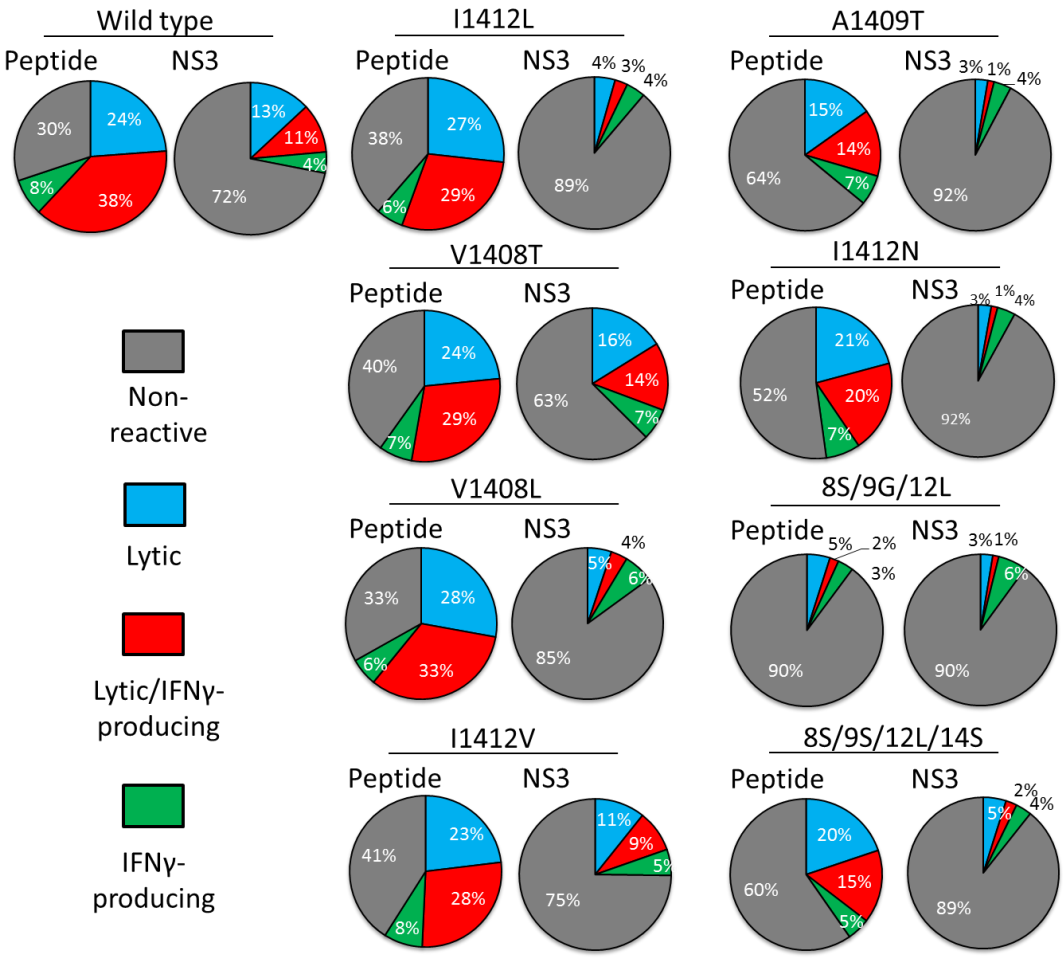

Figure 42. A decrease in HCV NS3 ligand density preferentially decreases bi-functional HCV1406 TCR-transduced CD8$^+$ T cells. HCV1406 TCR-transduced PBL were co-cultured for 5 hr with T2 cells loaded with WT and mutant HCV NS3:1406-1415 peptides ("Peptide", left pie) or COS/A2 cells transiently transfected to express full length WT HCV NS3 or HCV NS3 with mutant 1406-1415 epitopes ("NS3", right pie). Cells were analyzed by flow cytometry for T cell surface markers, CD107a expression, and intracellular IFNγ. Percentages of lytic and/or cytokine producing TCR-transduced CD8$^+$ T cells are displayed as pie charts for each stimulation conditions. Variant peptides are grouped into "moderate affinity" (middle column of each panel) and "lower affinity" (right column of each panel) in decreasing order of affinity (top to bottom). Pie charts reflect a minimum of 2,000 cells (average 4,000 cells). Reactivity is defined by greater than twice the percentage of total reactive cells against background (tyrosinase) stimulation. These data are representative of a single donor from three independent experiments using three different donors each.

Table 12. Percent of peptide-stimulated reactivity in mono- and bi-functional populations upon stimulation with HCV NS3 naturally processed antigen.

Epitope	$CD8^+$ TCR-Transduced T Cells		
	Lytic only	IFNγ only	Lytic/IFNγ
WT	54.9	56.8	27.6
I1412L	16.5	70.5	9.4
V1408T	69.1	94.6	49.5
V1408L	18.3	106.2	10.7
I1412V	46.5	67.1	32.2
A1409T	17.5	57.6	9.5
I1412N	13.5	52.4	6.8
8S/9G/12L*	53.4	182.7	67.0
8S/9S/12L/14S	24.6	69.6	15.3

*Non-reactive; Percentages reflect the ratio of naturally processed antigen:peptide stimulation for each functional phenotype. These data are representative of a single donor from three independent experiments using three different donors each.

response suggest that either there are less overall reactive T cells, or that an equal number of reactive T cells are producing less cytokine. This confusion can be resolved by two-parameter analysis using flow cytometry (Fig. 43a). Additionally, IFNγ ELISAs fail to identify that in dampened cytokine release, $CD8^+$ T cells contribute to almost all of the cytokine production (Fig. 43b). By simultaneously measuring intracellular IFNγ and surface CD107a, we also demonstrated that HCV1406 TCR-transduced $CD4^+$ and $CD8^+$ T cells display different proportions of mono- and bi-functional populations in light of changes in the TCR-pMHC interaction as well as antigen density. Taken together, comparing magnitudes of a single cytokine release within a bulk T cell culture may oversimplify changes in reactivity. However, even a two-parameter assessment using CD107a and IFNγ may not most accurately depict the impact of altered TCR-pMHC interactions on T cell function. Therefore, the addition of more markers will likely better reflect the functional phenotypes in a T cell population.

Seven-Dimensional Comparisons Provide Complicated Analysis

We expanded our assessment of altered TCR-pMHC interactions' impact on T cell function by using multi-dimensional flow cytometry to measure six intracellular cytokines (IFNγ, TNFα, IL-2, IL-4, IL-17A, IL-22) and lytic marker CD107a. A multi-functional evaluation such as this may better reflect the changes in functional phenotypes of a T cell population than one or two parameters. We wanted to be able to compare differences in polyfunctional profiles between transduced $CD4^+$ and $CD8^+$ T cells across various HCV NS3:1406-1415 peptide and HCV^+ tumor stimulation conditions.

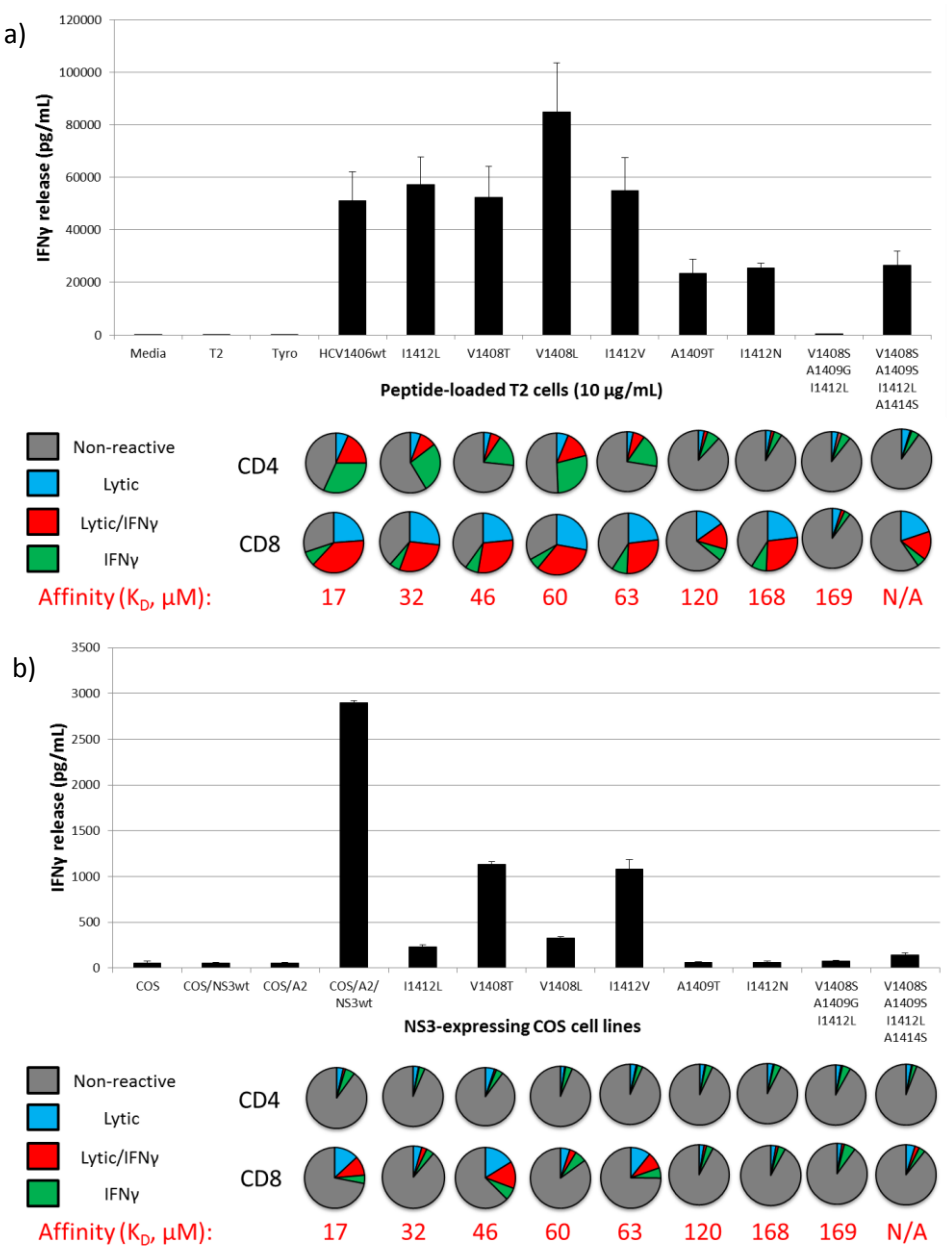

Figure 43. Comparing bulk-culture single cytokine release assay versus two-parameter FACS-based analysis provides a much different functional interpretation. IFNγ cytokine release analyzed by ELISA by a bulk (mixed $CD4^+$ and $CD8^+$ HCV1406 TCR-transduced T cell) culture is compared with bi-functional reactivity assessed by flow cytometry. Affinity measurements for TCR-pMHC interactions are displayed below pie charts in red **(a)** Reactivity against peptide-loaded T2 cells. **(b)** Reactivity against naturally processed antigen.

The analysis of seven functional parameters after gating on our lymphocyte population markers generated 128 possible combinations of positivity/negativity for these functional markers. Compounding the analysis were multiple peptide or tumor stimulation conditions between two T cell subsets ($CD4^+$ and $CD8^+$). This yielded a grossly complex dataset that was difficult to analyze with basic flow cytometry software.

For example, practical limitations in FlowJo, a standard software for flow cyotmetry analysis, generally restrict the visualization of data to one or two parameters at a time. Analysis of seven functional parameters required a matrix of 21 pairwise dotplots for a single stimulation condition (Fig. 44). Although this matrix is limited in its scope, we can deduce simple observations. Figure 44 displays a representative example of pairwise comparisons in $CD8^+$ TCR-transduced T cells stimulated with WT HCV NS3:1406-1415 peptide-loaded T2 cells. All seven functional markers are present, but in varying proportions. While a limited number of TCR-transduced cells produced IL-17A and IL-22 (7.2% and 2.4%, respectively), larger proportions were positive for TNFα, CD107a, IL-4, IFNγ, and IL-2 (ranging from 42% to 20% in decreasing order). Evaluating two parameters simultaneously revealed interesting expression patterns. For example, pairwise comparisons between IL-2 and TNFα demonstrated that 90% of $IL\text{-}2^+$ cells were also positive for TNFα, but that less than half of the TNF^+ cells were also positive for IL-2. This may suggest that IL-2 production is strictly associated with TNFα production, but that some T cells' TNFα production is independent of IL-2. Additionally, pairwise comparisons in FlowJo demonstrated that while 24% of the $CD8^+$ T cells were $IFN\gamma^+$,

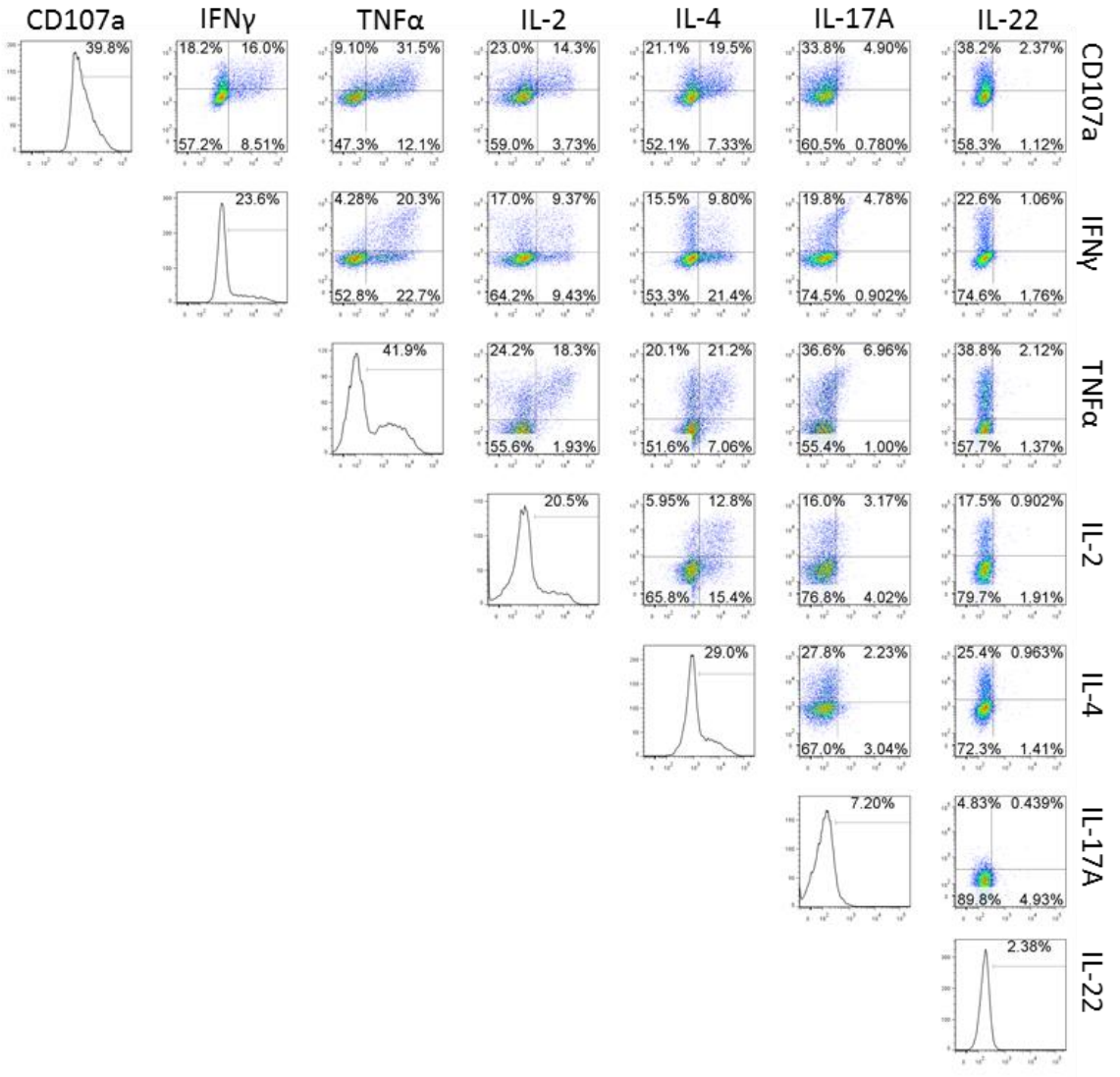

Figure 44. Seven-parameter comparative analysis in FlowJo. PBL-derived T cells from a normal donor were transduced with the HCV1406 TCR retroviral vector. TCR-transduced T cells were enriched using anti-CD34 immunomagnetic beads. T cells were co-cultured for 5 hr with T2 cells loaded with 10 µg/mL of HCV NS3:1406-1415 peptide or tyrosinase:368-376 peptide. Cells were stained for CD3, CD4, CD8, CD34 and surface CD107a and intracellular IFN-γ, TNFα, IL-2, IL-4, IL-17A, and IL-22 using immunofluorescence. Gating and analysis was performed in FlowJovX. Uni-dimensional histograms and biaxial dotplots depict single or pairwise functional comparisons in $CD34^{+}CD8^{+}$ HCV1406 TCR-transduced T cells. Gates set against background (tyrosinase) stimulation can be found in The Appendix, Figure 73.

nearly equally as many IFNγ$^-$ cells were positive for either CD107a or TNFα. This highlights the important point that evaluation for only IFNγ would incorrectly label a large proportion of the T cells as “non-reactive”. However, analysis in FlowJo does not easily display how many other cytokines might be expressed by IFNγ$^-$ cells.

Most surprising were T cell populations that expressed unexpected combinations of cytokines. IL-4, a type 2 cytokine, is generally thought to be restricted to type 2 T cells, whereas type 1 cytokines (IFNγ, TNFα, and IL-2) are restricted to type 1 T cells [64]. However, our analysis indicated that a substantial number of CD8$^+$ T cells are doubly positive for IL-4 and a type 1 cytokine. For example, of the 29% of IL-4$^+$ T cells, nearly one third were also positive for IFNγ, over one third also expressed IL-2, and nearly two thirds also stained for intracellular TNFα. These data contradict what is normally accepted and reported in the literature concerning type 1 and type 2 T cell populations. Perhaps evaluation of T cell function on similarly large scales could clarify the biology of T cell reactivity.

Portrayal of this data in FlowJo allows for simple comparisons, but would require an inordinate number of pairwise dotplots to compare variant peptide or tumor stimulations. In fact, it would require 756 dotplots to compare WT and mutant peptide and naturally processed antigen stimulation between CD4$^+$ and CD8$^+$ T cells. This makes meaningful interpretations of the data quite challenging. Limited to pairwise comparisons also does not resolve how many other non-type 2 cytokines IL-4$^+$ T cells may also express. Similarly, pairwise comparison does not easily reveal how many

cytokines are expressed by IFNγ$^-$ cells that would be "lost" in traditional assays. We attempted higher resolution of multi-dimensional analysis within FlowJo, by Boolean gating all 7 parameters to generate frequencies in each of the 128 phenotypes (2^n, n = number of parameters). FlowJo cannot easily accommodate these multi-parameter comparisons, so we summed the frequencies of populations into categories of 0 to 7 functional parameters positive. By categorizing phenotypes into pie charts according to the number of functional parameters expressed, we can make clearer comparisons between CD4$^+$ and CD8$^+$ T cell responses across mutant epitope stimulations (Fig 45).

We found that HCV TCR-transduced CD4$^+$ and CD8$^+$ T cells contained a similar percentage of antigen reactive T cells when stimulated with the WT HCV NS3:1406-1415 peptide (50.3% versus 56.5%, respectively). Both populations also exhibited a similar number of functional markers (1 marker-13.1% vs 14.4%; 2 markers-14.5% vs 13.3%; 3 markers-11.5% vs 14.6%; 4 markers-7.0% vs 9.4%; 5 markers-3.1% vs 3.8%, respectively). At this point, however, we still lack the resolution to detect what combinations of cytokines are present in each category. Despite similarities in between CD4$^+$ and CD8$^+$ TCR-transduced T cells upon WT peptide stimulation, there were observable differences between polyfunctional populations across altered TCR-pMHC interactions. For example, "moderate affinity" ligand I1412L exhibited only a slight decrease in antigen reactive CD8$^+$ T cells compared to WT stimulation (56.5% compared to 51.1%). But this mutation led to a dramatic decrease in antigen reactive CD4$^+$ T cells (50.3% to 33.2%) (Table 13). I1412L stimulation also induced relatively modest changes

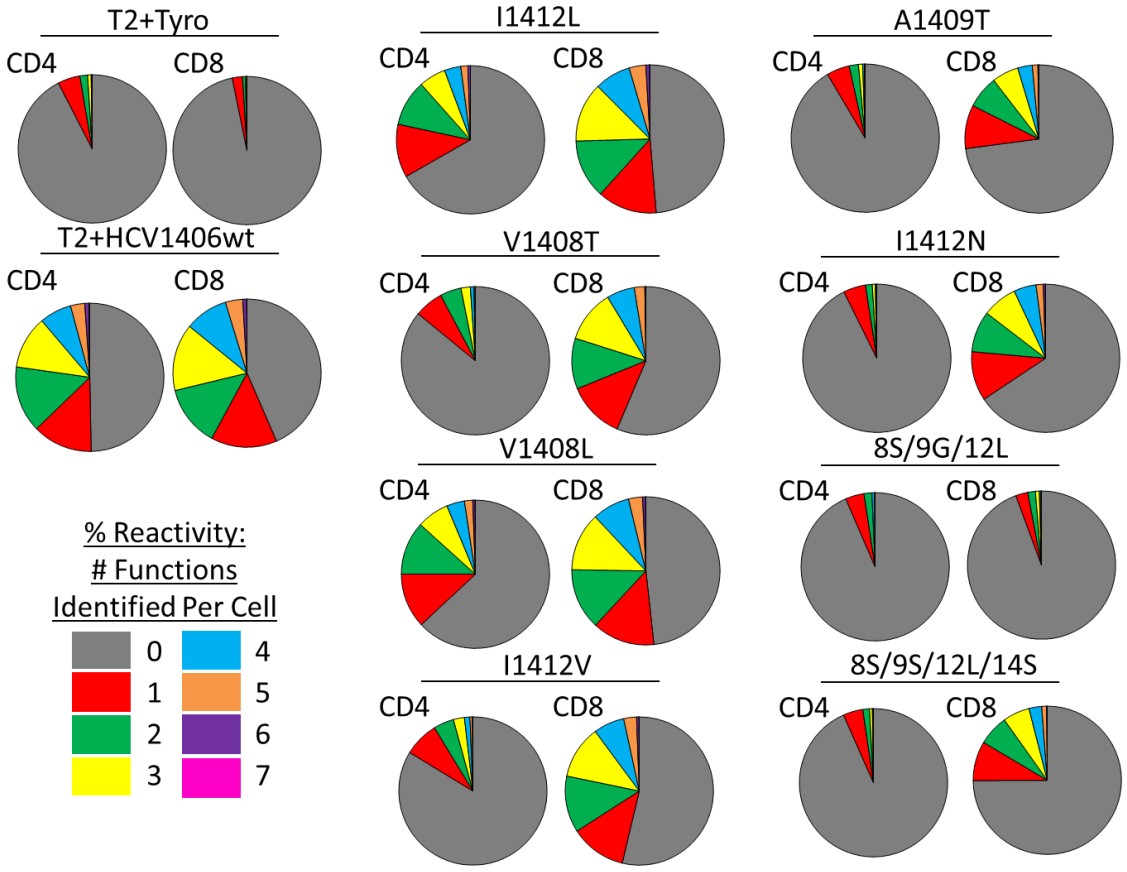

Figure 45. Number of functional markers produced by HCV 1406 TCR-transduced T cells when stimulated with naturally occurring mutant HCV NS3:1406-1415 peptides. Human PBL-derived T cells were transduced to express the HCV 1406 TCR. TCR-transduced T cells were enriched using anti-CD34 immunomagnetic beads. T cells were co-cultured for 5 hours with T2 cells loaded with 10 µg/mL of each peptide and stained for CD107a expression and intracellular IFN-γ, TNFα, IL-2, IL-4, IL-17A, and IL-22. Cells were also stained for CD3, CD4, CD8, and CD34 to measure the individual transduced T cell subsets. Each pie wedge represents the percent of cells producing no (gray), 1 (red), 2 (green), 3 (yellow), 4 (blue), 5 (orange), 6 (purple), or 7 (pink) functional markers. These data are representative of a single donor from three independent experiments using three different donors each.

Table 13. Frequencies of polyfunctional populations upon stimulation with HCV NS3:1406-1415 mutant peptides.

Epitope	CD4+ T cell Functional Markers (%+)*							
	0	1	2	3	4	5	6	7
WT	49.7	13.1	14.5	11.5	7.0	3.3	0.9	0.2
I1412L	66.8	11.6	10.1	5.9	3.6	1.5	0.5	0.0
V1408T	85.9	6.3	4.6	2.0	0.8	0.2	0.0	0.0
V1408L	63.1	11.9	11.7	7.0	3.9	1.8	0.5	0.1
I1412V	83.7	7.6	4.4	2.4	1.2	0.5	0.1	0.0
A1409T†	91.5	5.0	2.0	0.9	0.4	0.1	0.1	0.0
I1412N†	92.7	4.9	1.5	0.6	0.3	0.1	0.0	0.0
8S/9G/12L†	93.5	4.1	1.7	0.5	0.2	0.0	0.0	0.0
8S/9S/12L/14S†	93.4	4.3	1.5	0.6	0.2	0.1	0.0	0.0
Epitope	**CD8+ T cell Functional Markers (%+)***							
	0	1	2	3	4	5	6	7
WT	43.5	14.4	13.3	14.6	9.4	3.8	0.9	0.1
I1412L	48.7	13.0	12.9	13.0	7.9	3.7	0.8	0.1
V1408T	56.4	12.5	11.1	11.5	6.1	2.3	0.2	0.0
V1408L	48.3	13.7	13.3	12.8	8.2	3.1	0.7	0.1
I1412V	53.7	12.2	12.3	11.6	6.7	2.8	0.5	0.1
A1409T	72.9	9.5	7.1	5.8	3.2	1.2	0.2	0.0
I1412N	65.7	10.8	9.0	7.6	4.9	1.6	0.5	0.1
8S/9G/12L†	94.4	2.7	1.7	0.8	0.3	0.1	0.0	0.0
8S/9S/12L/14S	74.9	8.6	6.6	5.9	2.8	1.1	0.1	0.0

*Percentages reflect frequency of cells positive for only the number of parameters indicated in each column; †Non-reactive. These data are representative of a single donor from three independent experiments using three different donors each.

in polyfunctional frequencies compared to WT stimulation in $CD8^+$ T cells. Percentages differed anywhere from 1.6-0.1% in each category (1 marker-14.4% vs 13.0%; 2 markers-13.3% vs 12.9%; 3 markers-14.6% vs 13.0%; 4 markers-9.4% vs 7.9%); 5 markers-3.8% vs 3.7%). There was more of a dramatic decrease, however, in the number of polyfunctional markers among $CD4^+$ T cells. Percentages differed as much at nearly 50% compared to WT (1 marker-13.1% vs 11.6%; 2 markers-14.5% vs 10.1%; 3 markers-11.5% vs 5.9%; 4 markers-7.0% vs 3.6%; 5 markers-3.3% vs 1.5%) (Table 13). Interestingly, differences in polyfunctional percentages were more pronounced in higher order polyfunctional categories (3, 4, and 5 functional parameters). Additionally, differences in polyfunctional population frequencies were even more pronounced in $CD4^+$ T cells stimulated with V1408L and I1412L peptides. Although similar in affinity to that of V1408T and I1412V, their polyfunctional profiles were substantially reduced, to fewer than 2.5% of the cells producing 3, 4, or 5 functional makers. This is consistent with previous observations that variant TCR-pMHC interactions with similar affinities do not necessarily correlate with similar biologic outcomes.

A similar decrease in higher order polyfunctional categories (≥3 parameters) is seen in $CD8^+$ T cells stimulated with “lower affinity” mutants (A1409T, I1412N, 8S/9S/'12L/14S) compared to WT. These data support observations discussed earlier where “lower affinity” ligands had pronounced effects on bi-functional $CD107a^+IFN\gamma^+$ greater than either mono-functional population. This provides further evidence that perturbations in TCR-pMHC interactions have a biased effect on polyfunctional

populations. Taken together, these results indicate that multi-parameter per-cell analysis of T cell reactivity is able to resolve differences that standard assays fail to detect.

Despite these meaningful interpretations, analysis in FlowJo still lacked the ability to graphically portray individual polyfunctional phenotypes or display how altered TCR-pMHC interactions impact their relative abundance. We addressed this issue by evaluating a series of software packages in their ability to visualize and interpret our complex, high dimensional datasets. Software evaluated included GemStone [311], SPADE [312], FlowSOM [316], viSNE [317], and FLOCK [319]. Detailed analysis methods, advantages and disadvantages, and representative graphical output for each tool using our datasets are described in Chapter Two for your reference. Based on our extensive evaluation of these software packages, tandem analysis is Pestle/SPICE was the user-friendliest and provided the most interpretable graphical output. Thus, the rest of the discussion will focus on polyfunctional phenotypes analyzed with SPICE.

T Cell Polyfunctional Responses Are Extremely Diverse

Boolean gating within FlowJo followed by tandem analysis in Pestle/SPICE data processing software packages adequately visualized individual polyfunctional populations. One of the first observations was the heterogeneity in polyfunctional populations and their frequencies between $CD4^+$ and $CD8^+$ TCR-transduced T cells. Figure 46 quantitatively compares the frequencies of polyfunctional phenotypes of $CD4^+$ and $CD8^+$ TCR-transduced T cells stimulated with WT NS3:1406-1415 peptide-loaded T2

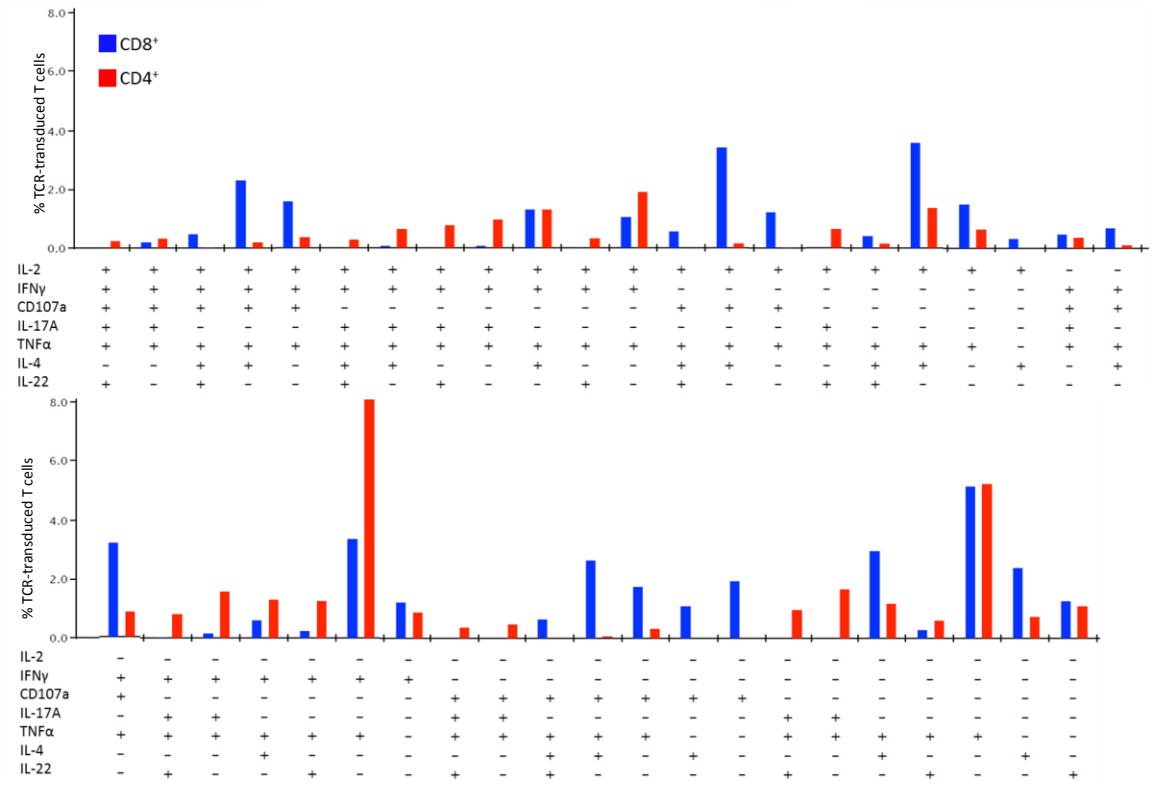

Figure 46. Polyfunctional heterogeneity between WT HCV NS3:1406-1415 peptide-stimulated CD4$^+$ and CD8$^+$ HCV1406 TCR-transduced T cells. Boolean-gated frequencies within FlowJo were formatted within Pestle and exported into SPICE. Bar heights compare frequencies of CD4$^+$ (red) and CD8$^+$ (blue) TCR-transduced T cell polyfunctional populations after stimulation with NS3:1406-1415 WT peptide-loaded T2 cells. The bar graph has been limited to include only populations above 0.25%. Please refer to The Appendix, Figure 74, for frequencies of all 128 possible phenotypes. These data are representative of three independent experiments using three different donors each.

cells. For simplicity, a cut off has been set to only display frequencies of at least 0.25% for either $CD4^+$ or $CD8^+$ T cells. Please refer to The Appendix for original output showing frequencies of all 128 combinatorial phenotypes. It is clearly evident how heterogeneous $CD4^+$ and $CD8^+$ T cells behave. For example, the two most dominant phenotypes for both $CD4^+$ and $CD8^+$ are $IFN\gamma^+TNF\alpha^+$ and $TNF\alpha^+$-only (remaining parameters negative). But a number of phenotypes exist in $CD4^+$ T cells that are not evident in $CD8^+$ T cells ($TNF\alpha^+IL\text{-}4^+$, $TNF\alpha^+IL\text{-}17A^+$, $IL\text{-}2^+IFN\gamma^+TNF\alpha^+IL\text{-}4^+$). Additionally, certain phenotypes were present in the $CD8^+$ T cell subsets but not in $CD4^+$ T Cells ($CD107a^+TNF\alpha^+IL\text{-}4^+$, $IL\text{-}2^+CD107a^+IL\text{-}17A^+$, $IL\text{-}2^+CD107a^+IL\text{-}4^+IL\text{-}22^+$). It is interesting how many phenotypes are actually present and how variable the frequencies are between $CD4^+$ and $CD8^+$ T cells. Analysis in SPICE finally provides us to resolution to make these highly complex observations.

Another useful comparison tool in SPICE is a heat-map-like feature, known as a cool plot. Cool plots allow us to compare changes in the frequencies of polyfunctional phenotypes in light of altered TCR-pMHC interactions. Figure 47 displays a complete cool plot showing frequencies (denoted by shade of blue) of polyfunctional phenotypes (read by +/- combinations of each of the 7 functional parameters in columns). Figure 47 specifically compares the changes in polyfunctional phenotype frequencies of HCV1406 TCR-transduced $CD8^+$ T cells after stimulation by WT and variant HCV NS3:1406-1415 peptide-loaded T2 cells. The respective cool plot for this PBL donor's TCR-transduced $CD4^+$ T cells can be found in The Appendix. This representation evaluates frequencies of

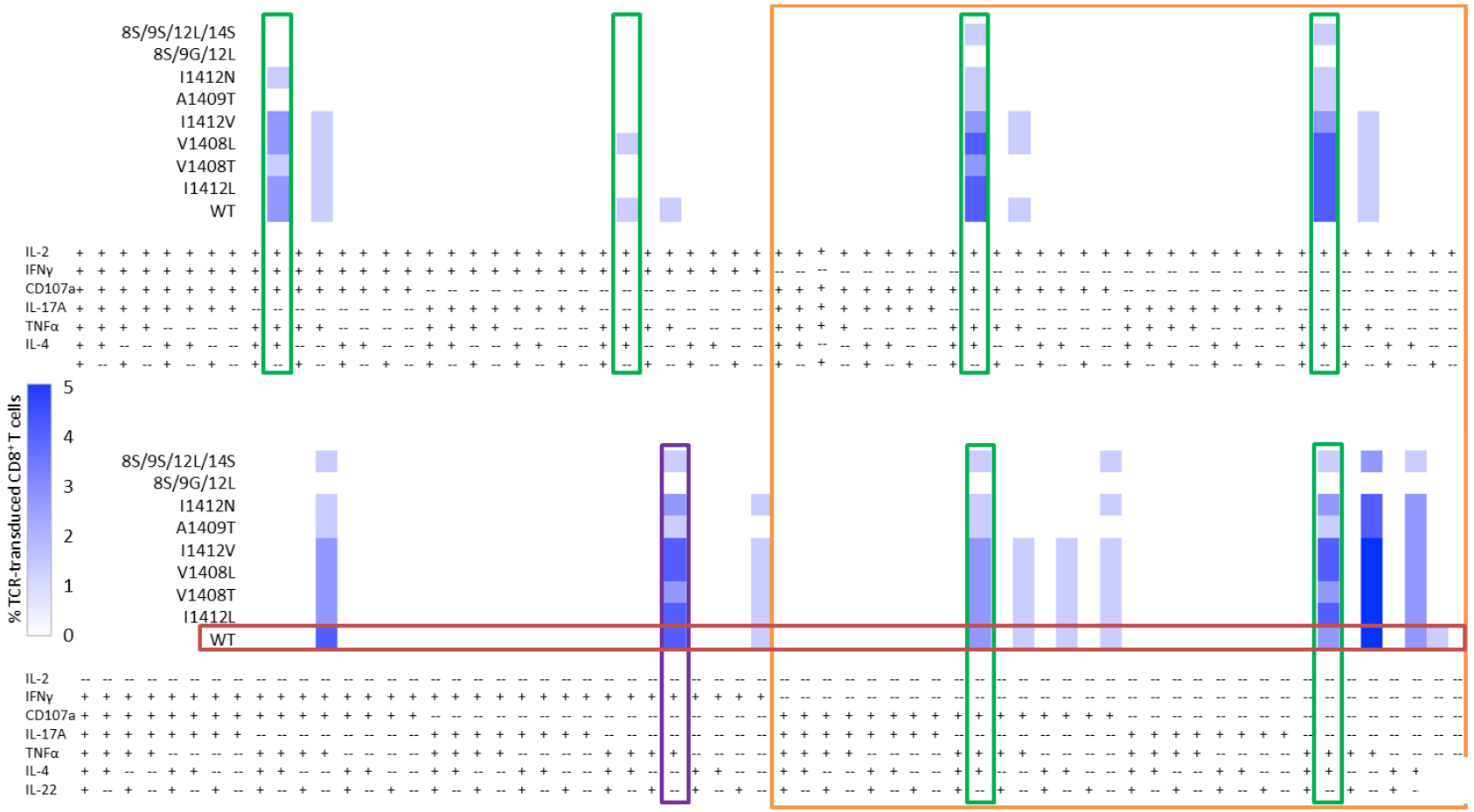

Figure 47. SPICE-generated cool plot comparing changing frequencies of T cell polyfunctional phenotypes in light of altered TCR-pMHC interactions. HCV 1406 TCR-transduced T cells were co-cultured for 5 hours with T2 cells loaded with 10 µg/mL of each WT and mutant HCV NS3:1406-1415 peptide. Cells were stained for CD3, CD4, CD8, CD34, and CD107a surface expression as well as intracellular IFN-γ, TNFα, IL-2, IL-4, IL-17A, and IL-22. Boolean gating for each functional marker was performed in FlowJo.

Resulting multivariate datasets were formatted and background subtracted (tryosinase stimulation) in Pestle, and cool plot overlay was generated in SPICE. Evaluation along the x-axis (red box) determines frequency (shade of blue) of TCR-transduced cells for each of the 128 phenotypes. Each column is a separate phenotype denoted by +/- for each functional parameter. Evaluation along the y-axis (purple box) determines changes in frequency upon variant peptide stimulation for a given phenotype. Unique populations of simultaneously type 1 and type 2 cytokine producing cells are denoted in green boxes. Populations negative for IFNγ are surround by an orange box. TCR-pMHC interactions are ranked from bottom to top by decreasing affinity. These data are representative of three independent experiments using three different donors each.

all 128 possible phenotypes for a given stimulation condition read across the x-axis (red box). It can also compare changing frequencies of an individual functional phenotype across mutant epitope stimulations in the y-direction (purple box). Alterations in TCR-pMHC interactions are ranked from bottom to top by decreasing TCR-pMHC affinities. We can finally gain a clearer picture of the polyfunctional potential of these gene-modified T cells and how polyfunctionality fluctuates with altered TCR-pMHC interactions. First, it is clear that while 128 phenotypes are possible given seven-parameter analysis, not all phenotypes are observed. Second, we again detect surprising cytokine combinations produced by individual cells. Highlighted in green boxes are IL-4^{+} cells (a type 2 cytokine) that also express at least one additional type 1 cytokine (IL-2, TNFα, or IFNγ) and/or are lytic. Third, we can start to delineate differences in polyfunctional responses in light of altered TCR-pMHC interactions by comparing changing frequencies in the y-direction. Fourth, is it clearly evident how many reactive T cells would be unaccounted for if only IFNγ were measured. IFNγ^{-} populations (surrounded by an orange box in Figure 47) accounted for surprisingly the majority of the $CD8^{+}$ T cells in the population. Once again, examining more cytokines than just IFNγ reveals a much more complete picture of a T cell culture. Polyfunctional analysis also suggests that the field's conception of T cell function and the classification of T cells into restricted cytokine-producing populations (type 1 vs type 2, etc.) may be drastically oversimplified.

A clearer interpretation is achieved when cool plots are condensed to display only detectable populations in each culture. Figure 48 shows condensed cool plots for both $CD4^+$ (Fig. 48a) and $CD8^+$ (Fig. 48b) HCV1406 TCR-transduced T cells stimulated with HCV NS3:1406-1415 mutant peptides. TCR-pMHC interactions are ordered from bottom to top by decreasing affinity. Condensed cool plots also highlight the heterogeneity between $CD4^+$ and $CD8^+$ T cell responses. Additionally, while lower affinity TCR-pMHC interactions yield overall lower frequencies, not each polyfunctional population is affected equally, nor are changes in polyfunctional responses directly correlated with affinity. For example, $TNF\alpha^+$-only population fluctuated much more in $CD4^+$ TCR-transduced T cells despite the strength of the mutant TCR-pMHC interactions (I1412L, V1408T, V1408L, I1412V) being relatively similar (32-63 μM) (Fig. 48a). Higher order phenotypes (3 or 4 functional markers) were also restricted to WT, I1412L, and V1408L peptide stimulations. These results suggest that certain pMHC ligands may be recognized differently by the TCR (despite similar affinities) leading to a less diverse polyfunctional response.

A similar trend is seen when comparing functional frequencies of $CD8^+$ TCR-transduced T cells (Fig. 48b). For example, the frequencies of the $CD107a^+$-only population were very consistent with roughly 5% of $CD8^+$ T cells present in nearly all mutant peptide stimulations. However, $IFN\gamma^+TNF\alpha^+$ (all other parameters negative) $CD8^+$ TCR-transduced T cells exhibit a higher degree of change. There was less variability in response to the “moderate affinity” group of TCR-pMHC interactions, but V1408L

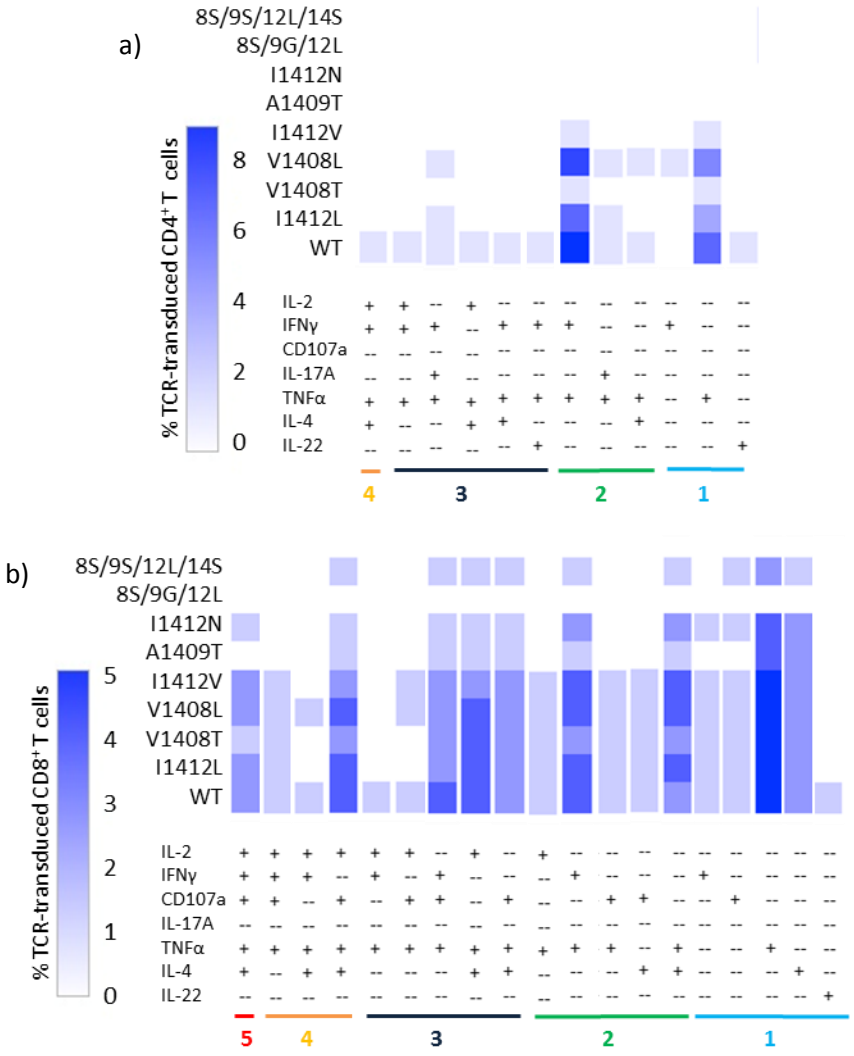

Figure 48. Polyfunctional phenotypes are heterogeneous and fluctuate with altered TCR-pMHC interactions. Human PBL-derived T cells were transduced to express the HCV1406 TCR. T cells were co-cultured for 5 hours with T2 cells loaded with 10 µg/mL of each WT and mutant HCV NS3:1406-1415 peptide. Cells were stained for CD3, CD4, CD8, CD34, and CD107a surface expression as well as intracellular IFN-γ, TNFα, IL-2, IL-4, IL-17A, and IL-22. Multivariate analysis was performed using FlowJo, Pestle, and SPICE software packages. Condensed cool plots display frequencies of polyfunctional populations of **(a)** $CD4^+$ or **(b)** $CD8^+$ TCR-transduced T cells shown in increasing order of polyfunctionality (right to left). Each column is a separate phenotype denoted by +/- for each functional parameter. TCR-pMHC interactions are ranked from bottom to top by decreasing affinity. Complete cool plots are shown in Figures 47 and 75. These data are representative of three independent experiments using three different donors each.

induced lower frequencies of reactive T cells in almost all phenotypes compared to I1412L, V1408L, or I1412V. Interestingly, "lower affinity" pMHC (A1409T, I1412N, and 8S/9S/12L/14S) induced a fewer number of detected phenotypes overall. Generally, the absence of higher order polyfunctional populations (4 or 5 functional markers) correlated with lower TCR-pMHC affinity. Furthermore, the frequency of all functional phenotypes was decreased when T cells were stimulated with lower affinity compared to moderate affinity ligands. Overall, portraying data in SPICE-generated cool plots provided a remarkable tool to characterize the polyfunctionality of T cells. We can very easily observe the polyfunctional heterogeneity between $CD4^+$ and $CD8^+$ T cells and the varying impact that alterations in TCR-pMHC interactions have on the spectrum and frequency of polyfunctional populations.

Heterogeneity in Polyfunctional Responses Exists Among PBL Donors

We examined whether polyfunctional phenotypes against our panel of mutant pMHC were donor-dependent by evaluating polyfunctionality in HCV TCR-transduced T cells derived from PBL of additional donors. Representative condensed cool plot of $CD4^+$ or $CD8^+$ HCV TCR-transduced T cells from two different donors are displayed in Figures 49-50, respectively. Full cool plots for these and other donors can be found in The Appendix. Interestingly, functional T cell phenotypes were not the same between different donors despite being transduced with the same TCR and stimulated with the same ligands. For example, Figure 48 displays cool plots highlighting differences between T cell functional phenotypes of two donors' $CD4^+$ TCR-transduced T cells

against HCV NS3:1406-1415 peptide-loaded T2 cells. Compared to Donor 2, Donor 1's TCR-transduced $CD4^+$ T cells (Fig. 49a) were less reactive overall (56.5% vs 78.2% total reactive T cells) and less heterogeneous (fewer functional phenotypes present; 12 vs 18) (Fig. 49b). Additionally, Donor 1 exhibited functional phenotypes lacking in Donor 2 (i.e. $TNF\alpha^+IL\text{-}4^+$ (approximately 8% of WT peptide-stimulated)). Similarly, certain phenotypes were absent in Donor 1 that were present in Donor 2 (i.e. $IL\text{-}22^+TNF\alpha^+IL\text{-}17A^+$ (approximately 4% of WT peptide-stimulated)). Donor 2 was also more polyfunctional upon stimulation with WT peptide. For example, donor 2 exhibited 8 quad-functional populations compared to Donor 1 having only 1 quad-functional population. Polyfunctional profiles of additional donors have been evaluated and representative cool plots can be found in The Appendix. These observations suggest that the number and type of functional phenotypes between PBL donors are not necessarily consistent.

Similar trends were observed between TCR-transduced $CD8^+$ T cells of Donor 1 (Fig. 50a) and Donor 2 (Fig. 50b). Donor 1 also had polyfunctional $CD8^+$ TCR-transduced T cell populations missing in Donor 2 (bi-functional $TNFa^+IL\text{-}2^+$ (approximately 2% of WT and "moderate affinity"-stimulated T cells)). Conversely, Donor 2 quad-functional $TNF\alpha^+IL\text{-}17A^+CD107a^+IFN\gamma^+$ population (ranging from 2-6% of total cells) was absent in Donor 1. These donors exhibited similar numbers of individual polyfunctional populations present (equal at 19), but varied in the number of simultaneous parameters detected. For example, Donor 1 had fewer higher order polyfunctional (3 parameters or less) populations (5 mono-functional, 5 bi-functional, 5 tri-functional, 3 quad-functional,

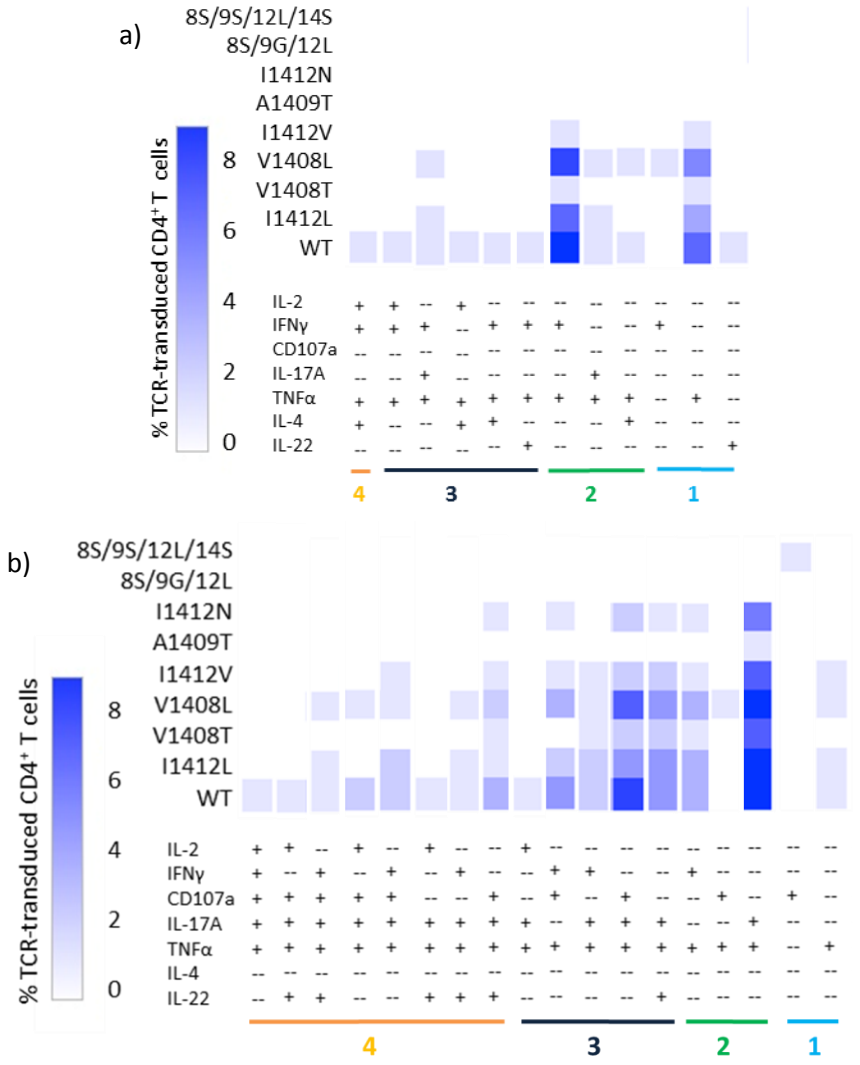

Figure 49. Heterogeneity of HCV1406 TCR-transduced CD4$^+$ T cells in two PBL donors. T cells from two PBL donors were transduced to express the HCV 1406 TCR. T cells were co-cultured for 5 hours with T2 cells loaded with 10 µg/mL of each WT and mutant HCV NS3:1406-1415 peptide. Cells were stained for CD3, CD4, CD8, CD34, and CD107a surface expression as well as intracellular IFN-γ, TNFα, IL-2, IL-4, IL-17A, and IL-22. Multivariate analysis was performed using FlowJo, Pestle, and SPICE software packages. Condensed cool plots display frequencies of polyfunctional populations CD4$^+$ TCR-transduced T cells of **(a)** Donor 1 and **(b)** Donor 2 shown in increasing order of polyfunctionality (right to left). Each column is a separate phenotype denoted by +/- for each functional parameter. TCR-pMHC interactions are ranked from bottom to top by decreasing affinity. Complete cool plots are shown in The Appendix, Figures 75-76.

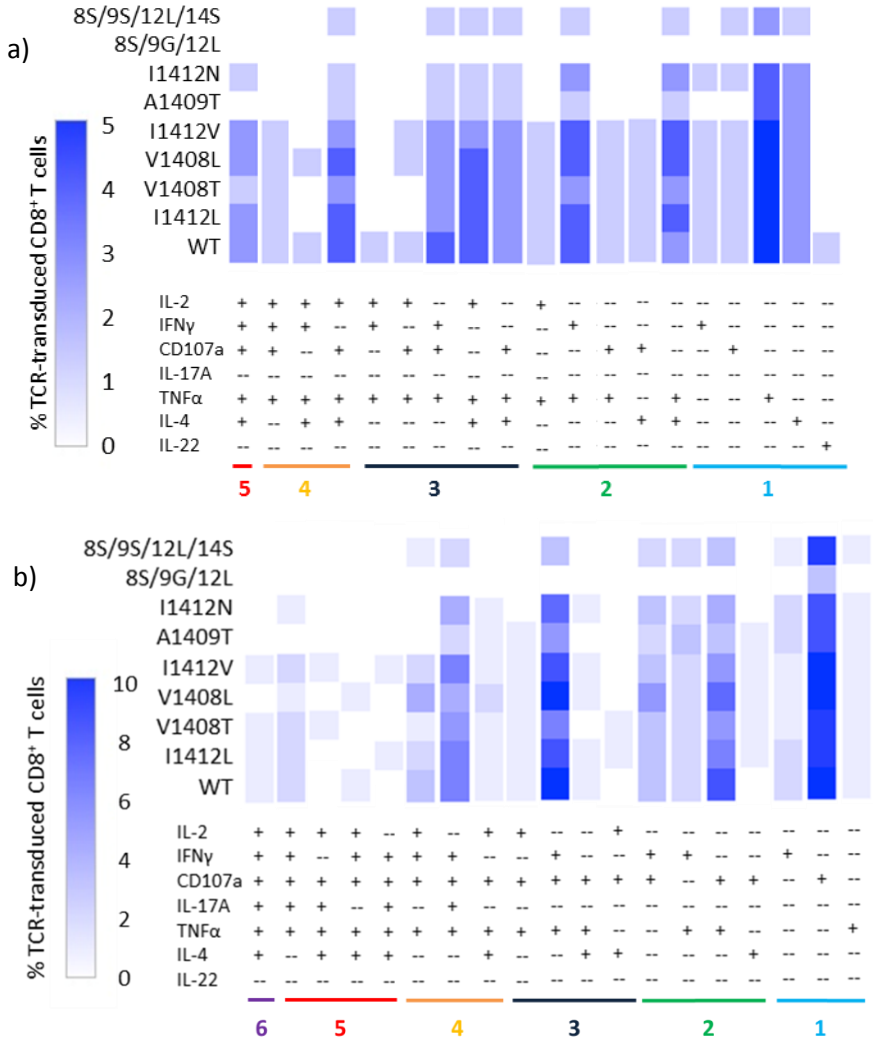

Figure 50. Heterogeneity of HCV1406 TCR-transduced CD8$^+$ T cells in two PBL donors. T cells from a second PBL donor were transduced to express the HCV 1406 TCR. T cells were co-cultured for 5 hours with T2 cells loaded with 10 µg/mL of each WT and mutant HCV NS3:1406-1415 peptide. Cells were stained for CD3, CD4, CD8, CD34, and CD107a surface expression as well as intracellular IFN-γ, TNFα, IL-2, IL-4, IL-17A, and IL-22. Multivariate analysis was performed using FlowJo, Pestle, and SPICE software packages. Condensed cool plots display frequencies of polyfunctional populations CD8$^+$ TCR-transduced T cells of **(a)** Donor 1 and **(b)** Donor 2 shown in increasing order of polyfunctionality (right to left). Each column is a separate phenotype denoted by +/- for each functional parameter. TCR-pMHC interactions are ranked from bottom to top by decreasing affinity. Complete cool plots are shown in Figure 47 and in The Appendix, Figure 77.

and 1 penta-functional phenotypes), whereas Donor 2 demonstrated much more higher order (4 or greater parameters) populations (3 mono-functional, 4 bi-functional, 4 tri-functional, 3 quad-functional, 4 penta-functional, and 1 hexa-functional phenotypes). These observations suggest that PBL can be comprised of very heterogeneous T cell populations within a single culture and between donors. Despite being engineered with the same TCR and stimulated with the same pMHC, both number and frequency of polyfunctional populations can dramatically differ but general trends between altered ligand reactivity remained the same.

Such heterogeneity is difficult to explain, but may begin to offer explanations for different patients responses to therapies. For instance, if a more polyfunctional response is more advantageous, than Donor 2's T cells may perform better therapeutically. However, if a certain individual phenotype is a "better" anti-tumor phenotype (i.e. IL-2^{+}TNFα^{+}IL-4^{+}) Donor 1 may have the advantage because this population is present in approximately 5% of reactive $CD8^{+}$ T cells against WT and multiple mutant antigens, but is absent all together in Donor 2. This inherent heterogeneity between donors is an interesting observation and concept, but further investigation into identifying which functional populations are "better" for anti-tumor or anti-viral responses is needed.

Reduced Ligand Density Dampens Polyfunctional Responses

Earlier, we described that reduced ligand density had a dramatic effect on T cell function. As a follow up to this concept, we evaluated if there were altered

polyfunctional responses against HepG2 cells engineered to express naturally processed NS3 variants (Fig. 51). Similar to previous experiments, $CD4^+$ T cells were non-reactive against this "lowest density" naturally processed antigen, but $CD8^+$ T cells demonstrated polyfunctional responses against WT and "moderate affinity" ligands I1412L, V1408T, V1408L, and I1412V (Fig. 52a). Remarkably, there was a dramatic reduction in polyfunctional phenotypes compared to peptide-stimulated $CD8^+$ T cells (Fig. 52b). Peptide-stimulated cells exhibited a robust response comprised of 19 different functional phenotypes ranging from mono-functional to hexa-functional (6 simultaneous parameters). Conversely, tumor-stimulated $CD8^+$ T cells were restricted to only 9 different functional phenotypes, the majority (6/9) being limited to mono- or bi-functional. There were only 2 tri- and 1 quad-functional populations present. Penta-and hexa-functional populations that made up roughly 25% of peptide-stimulated phenotypes were now completely absent. Tumor stimulation also seemed to preferentially reduce higher order polyfunctional populations and restricted the heterogeneity of responses. This suggests that a lower level of antigen density may result in incomplete T cell activation.

To further evaluate the effects of decreasing antigen density on polyfunctional T cell responses, we stimulated HCV TCR-transduced T cells with T2 cells loaded with the WT NS3:1406-1415 peptide at concentrations ranging from 10 µg/mL to 10^{-11} µg/mL. We also stimulated HepG2 cells expressing naturally processed WT NS3 ("lowest density" of ligand) or HepG2 cells exogenously loaded with 10 µg/mL WT peptide to

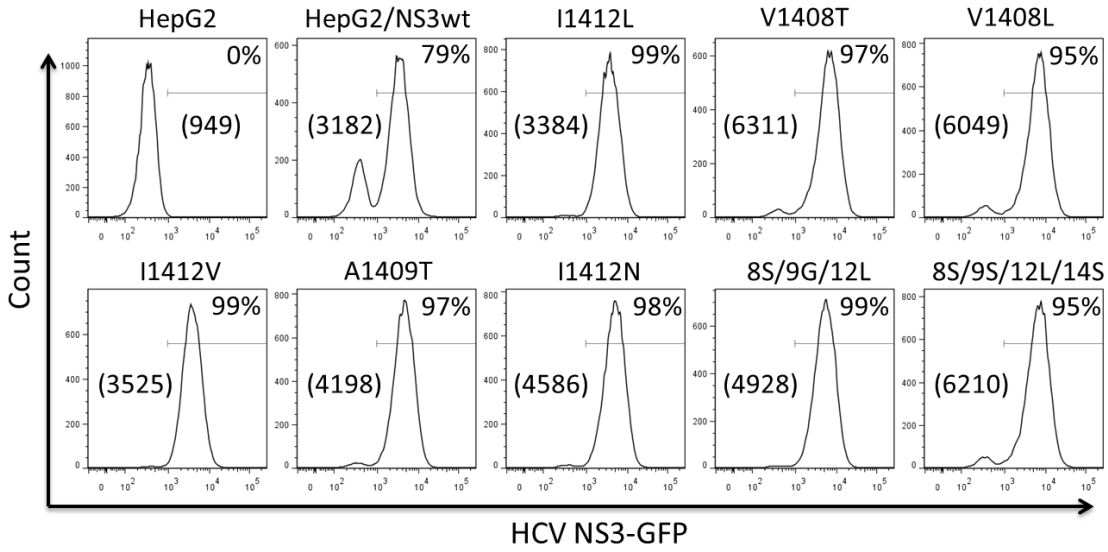

Figure 51. Generation of HepG2 cells expressing naturally processed HCV NS3 with WT and naturally occurring mutant NS3:1406-1415 epitopes. HepG2 cells were transduced retroviral vectors encoding full length HCV NS3 protein containing WT or variant NS3:1406-1415 epitopes fused to GFP by a T2A linker. Cells were sorted for high and uniform GFP expression. WT antigen was slightly downregulated after multiple passages. Mean fluorescence intensity of each population is listed in parentheses.

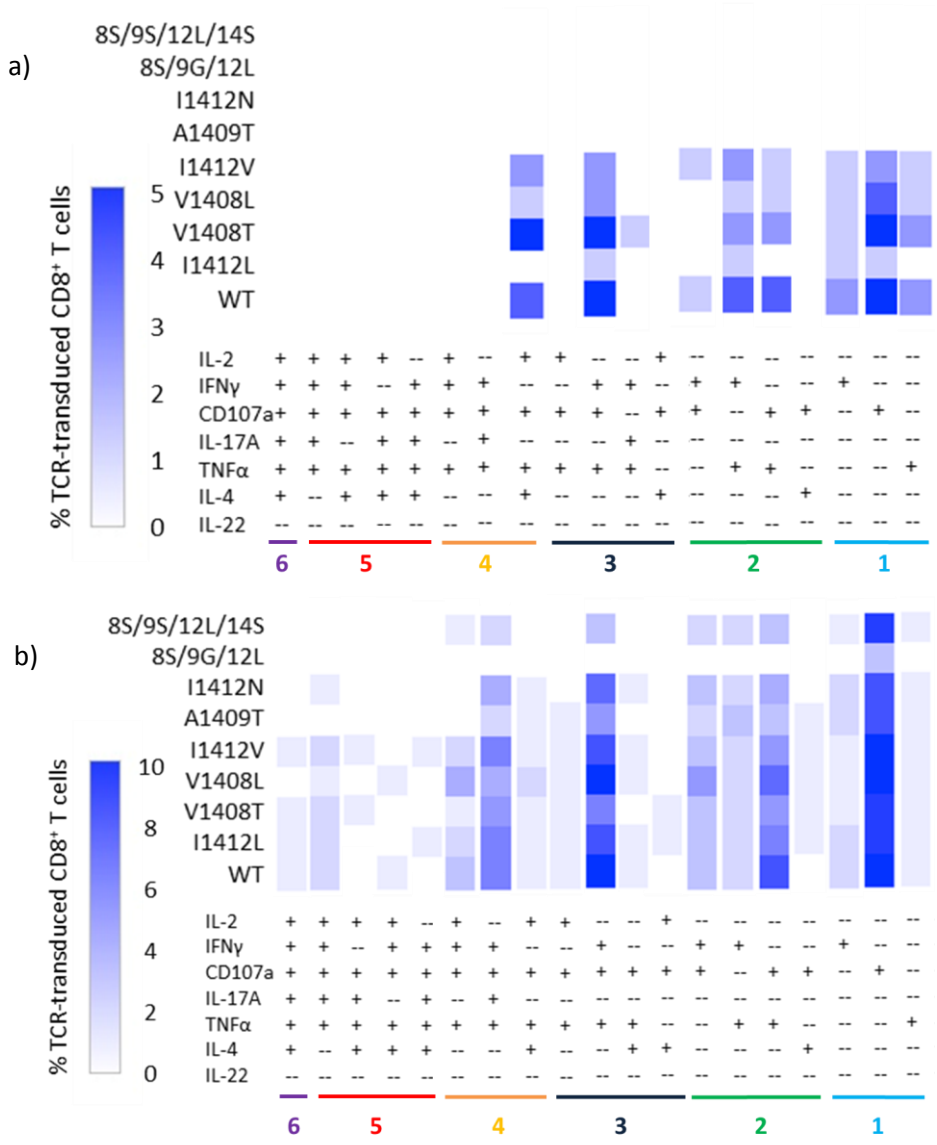

Figure 52. NS3$^+$ HepG2 stimulation reveals a markedly reduced polyfunctional response. T cells from two PBL donors were transduced to express the HCV 1406 TCR. T cells were co-cultured for 5 hours with HepG2 cells engineered to express full length HCV NS3 with WT of variant 1406-1415 epitopes. Cells were stained for CD3, CD4, CD8, CD34, and CD107a surface expression as well as intracellular IFN-γ, TNFα, IL-2, IL-4, IL-17A, and IL-22. Multivariate analysis was performed using FlowJo, Pestle, and SPICE software packages. Condensed cool plots display frequencies of polyfunctional populations CD8$^+$ TCR-transduced T cells stimulated by **(a)** HCV NS3$^+$ HepG2 cells or **(b)** Peptide-loaded T2 cells. Functional phenotypes are shown in increasing order of polyfunctionality (right to left). Complete cool plots are in The Appendix, Figures 77,79. Data are representative of three independent experiments using three different donors.

augment ligand density (Fig. 53). We found that a reduction in ligand concentration from 10 to 10^{-3} μg/mL eliminated nearly all functional responses in $CD4^+$ TCR-transduced T cells. Interestingly, the IL-4^+-only population maintained prevalence throughout, which might suggest that production of IL-4 has lowest the threshold of TCR-pMHC contacts for initiation. $CD8^+$ TCR-transduced T cells on the other hand exhibited a greater tolerance for reduced antigen density, with gradual reductions in frequency across multiple functional phenotypes. Interestingly, higher order polyfunctional populations (4 or 5 parameters positive) were more susceptible to changes in ligand density as they were eliminated when stimulated with lower concentrations (10^{-5}-10^{-7} μg/mL) compared to mono- or bi-functional populations that were still present when stimulated with 10^{-11} μg/mL of antigen.

$NS3^+$ HepG2 cells expressing naturally processed antigen, on the other hand, stimulated minimal polyfunctional responses, suggesting the density of ligand may be less than that of 10^{-11} μg/mL peptide-loaded T2 cells. Remarkably, exogenously loading HepG2 cells with 10 μg/mL peptide, increasing relative ligand density, rescued the frequency and range of polyfunctional phenotypes. Polyfunctional responses were now comparable to stimulation by “highest density” T2 cells. Increasing antigen density on HepG2 cells even restored polyfunctional responses in $CD4^+$ T cells that had minimal reactivity against naturally processed antigen. Overall, these data support the notion that ligand density not only plays a role in binary T cell reactivity, but highly influences polyfunctional responses, especially higher order polyfunctional T cells.

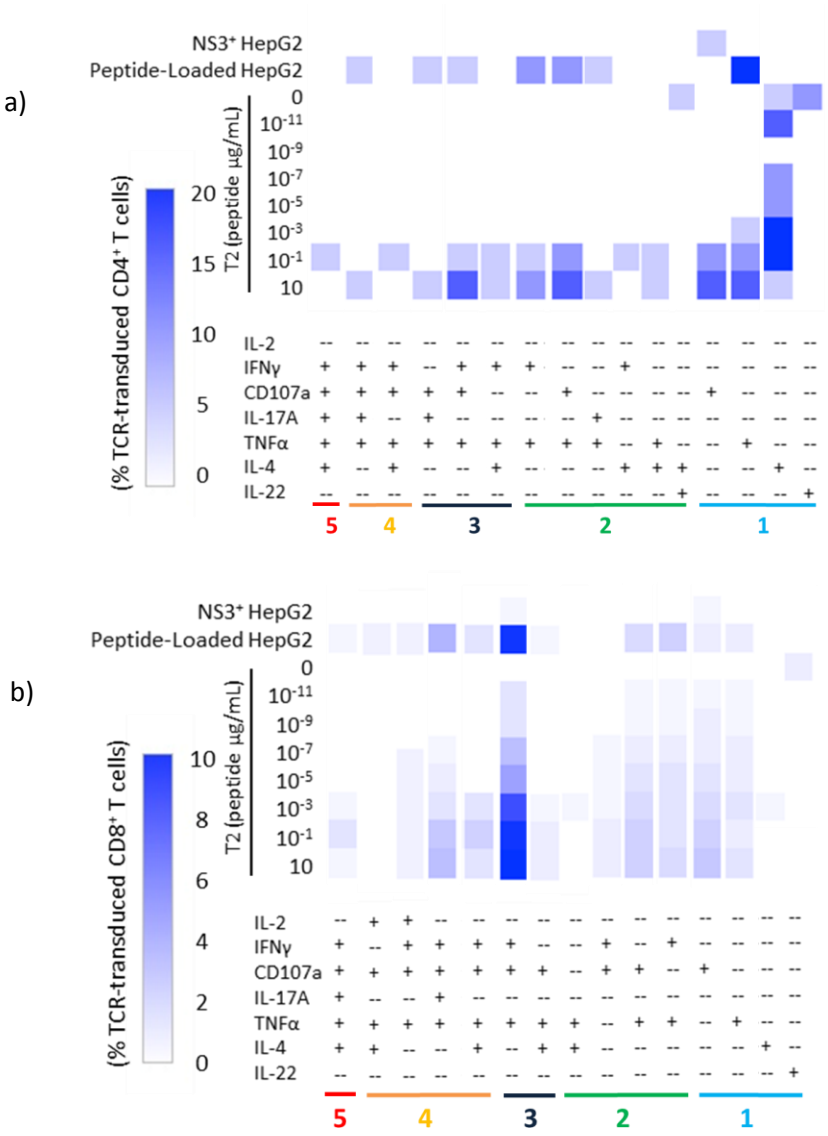

Figure 53. Influence of ligand density on polyfunctional phenotypes. PBL-derived T cells transduced with the HCV1406 TCR retroviral vector were co-cultured with T2 cells loaded with WT HCV NS3:1406-1415 peptide ranging from 10 – 10^{-11} µg/mL. T cells were also co-cultured with HepG2 cells expressing naturally processed full length NS3 protein or HepG2 cells exogenously loaded with 10 µg/mL NS3:1406-1415 peptide. Cells were stained for extracellular markers and intracellular cytokines; multivariate analysis was performed in FlowJo, Pestle, and SPICE software packages. Condensed SPICE-generated cool plots display frequencies of polyfunctional populations for **(a)** $CD4^+$ and **(b)** $CD8^+$ TCR-transduced T cells. Complete cool plots are shown in The Appendix, Figures 84-85. These data are representative of independent experiments using two different donors.

Hierarchical Clustering Relates Polyfunctional Phenotypes to Alterations in TCR-pMHC Interactions

While it is clear that there are differences in polyfunctional phenotypes against our panel of naturally occurring HCV NS3:1406-1415 variants, it would be helpful to relate these changes to alterations in TCR-pMHC affinity. To do this, we utilized a classical bioinformatic approach known as hierarchical clustering analysis, which clusters phenotypic patterns which are most similar to each other. It was made popular in the era of gene expression microarray data analysis where both tissue samples and genes would be clustered to identify genes that could distinguish between tissue subtypes [321]. In our experimental data, hierarchical clustering ranked the frequencies of T cell functional phenotypes as well as their relatability using dendograms. Phenotype patterns that do not occur are in a sense relegated to the bottom of the clustering analysis output, providing an easy way to focus on pertinent data.

The hierarchical clustering analysis shown here is a tailored version, visualizing only the phenotypes present in a $CD8^+$ TCR-transduced T cell culture stimulated with T2 cells, loaded with each HCV NS3:1406-1415 peptide (Fig. 54), corresponding to Donor 1 cool plots shown in Figures 47-48. Complete hierarchical clustering for multiple donors' $CD4^+$ and $CD8^+$ TCR-transduced T cell stimulations can be found in The Appendix. Hierarchical clustering also relates pMHC ligands by their induced functional phenotypes. So, ligands that stimulated a similar intensity or number of functional phenotypes are represented closer together in the dendogram than pMHC ligands that

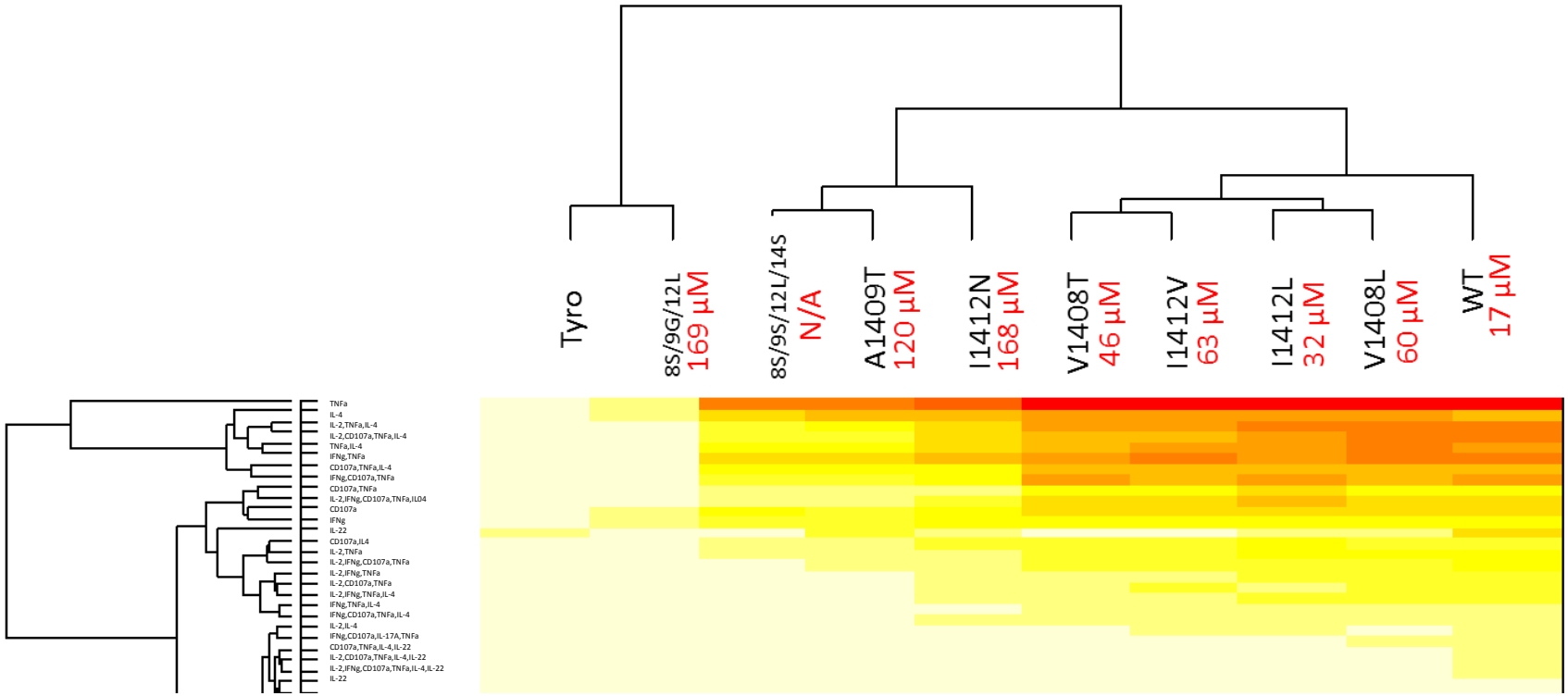

Figure 54. Bioinformatic hierarchical clustering relates polyfunctional responses to TCR-pMHC affinity. A hierarchical clustering analysis using FlowJo Boolean gated frequencies organizes polyfunctional phenotype by frequency and relatedness (left dendograms) by peptide-stimulated TCR-transduced $CD8^+$ T cells. This analysis can also demonstrate response relatedness between HCV NS3:1406-1415 peptide stimulations (top dendograms). An affinity value for each variant TCR-pMHC interaction is denoted in red. Output has been modified to portray only positively identified phenotypes. Please refer to The Appendix, Figure 88 for complete output.

stimulated less intense or more dissimilar functional phenotypes. Comparing hierarchical clustering of pMHC ligands with TCR-pMHC affinity measurements (red font) demonstrated that the strength or diversity of a T cell response is not necessary dependent on affinity. While “moderate” and “lower” affinity variants tended to be related in larger groups, dendograms did not order individual mutant pMHC ligands strictly by their K_D values. This relatedness (grouping) of pMHC ligands was conserved in multiple peptide-stimulated donors (Figs. 54-55). Interestingly, the relatedness (grouping) of pMHC ligands changed upon tumor stimulation (Fig. 56), suggesting that the alterations in TCR-pMHC interactions can have a different impact on functional outcomes at lower densities. While TCR-pMHC affinity is routinely thought to be the most influential factor governing antigen recognition, we demonstrate yet again, that this is not entirely true.

Significance

It is clear that the evaluation of T cell reactivity based on a single cytokine readout is not a completely accurate representation of the biology of the T cell culture. We first established this by evaluating two distinct functions, lytic activity and cytokine production, by measuring surface CD107a and intracellular IFNγ by flow cytometry. We were able to observe functional heterogeneity between $CD4^+$ and $CD8^+$ HCV TCR-transduced T cells. We also established that alterations in TCR-pMHC interactions and changes in ligand density preferentially decreased bi-functional $CD107a^+IFN\gamma^+$

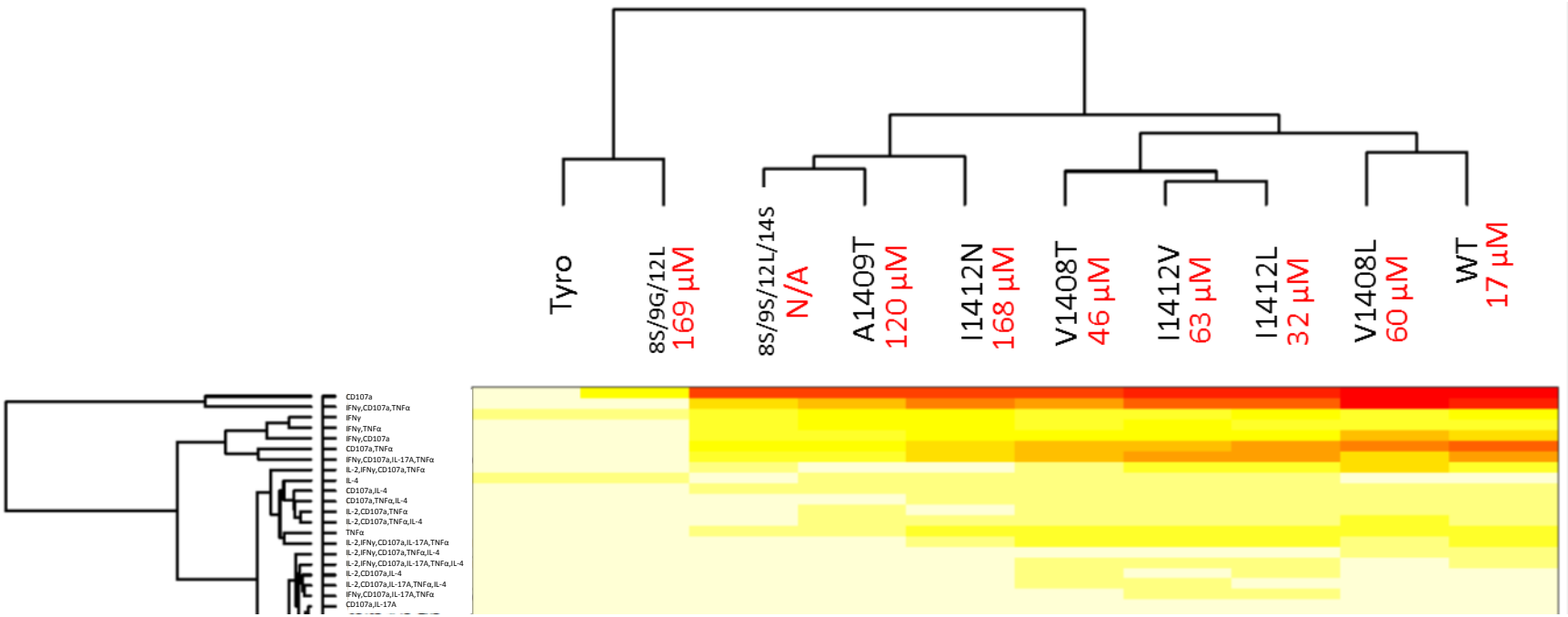

Figure 55. A second PBL donor relates mutant peptide responses similarly but with different clustering of polyfunctional phenotypes. A hierarchical clustering analysis using FlowJo Boolean gated frequencies organizes polyfunctional phenotype by frequency and relatedness (left dendograms) by peptide-stimulated TCR-transduced $CD8^+$ T cells in a second PBL donor. This analysis portrays the same relatedness between HCV NS3:1406-1415 peptide stimulations evaluated in a previous donor (top dendogram). Affinity values for each variant TCR-pMHC interaction are denoted in red. Output has been modified to portray only positively identified phenotypes. Please refer to Appendix, Figure 90 for complete output.

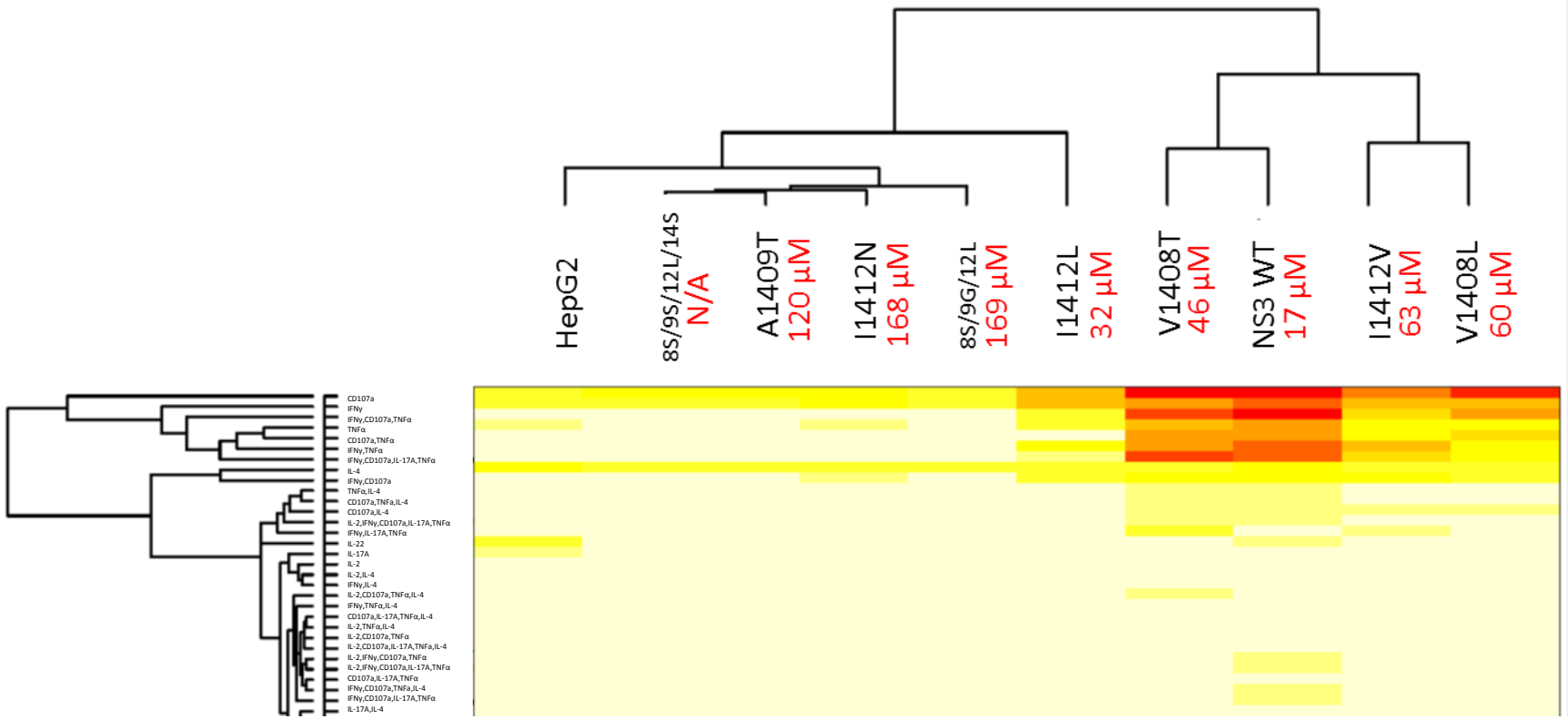

Figure 56. Hierarchical clustering also relates tumor-stimulated responses. A hierarchical clustering analysis using FlowJo Boolean gated frequencies organizes polyfunctional phenotype by frequency and relatedness (left dendograms) by HepG2 or $NS3^+$ HepG2 cell-stimulated TCR-transduced $CD8^+$ T cells in a second PBL donor (peptide response displayed in Figure 55). This analysis portrays the relatedness between naturally processed antigen stimulations (top dendograms). An affinity value for each variant TCR-pMHC interaction is denoted in red. Output has been modified to portray only positively identified phenotypes. Please refer to The Appendix, Figure 92 for complete output.

populations over either mono-functional phenotype. Large changes in total reactivity and individual phenotype frequencies occurred, in some cases, despite similar TCR-pMHC affinities. These data provided further evidence that affinity does not entirely dictate antigen recognition.

We then expanded our assessment of T cell polyfunctionality to include additional cytokines TNFα, IL-2, IL-4, IL-17A, and IL-22, which yielded highly complex multi-dimensional data sets. Analysis in software packages FlowJo, Pestle, and SPICE allowed us to graphically compare functional responses of HCV TCR-transduced T cells against our panel of naturally occurring mutant peptides. We found that $CD4^+$ and $CD8^+$ TCR-transduced T cells exhibited a much greater degree of phenotypic and functional complexity than previously appreciated. It was also clear that altered TCR-pMHC interactions influenced these diverse responses. This observed large degree of functional diversity may give T cells a remarkable degree of flexibility in responding to pathogens or tumor. Furthermore, at a single cell level, most of the traditional functional classifications (type 1, type 2, etc.) do not always hold true. These results suggest that polyfunctional analysis of T cells was able to perceive differences that standard assays fail to detect. Observations using human TCR-transduced T cells are intriguing because they represent the kinds of T cell populations we transfer to patients. Heterogeneity between PBL donors demonstrated differences in phenotypes identified as well as overall polyfunctionality. Expansive evaluation of T cell polyfunctionality in the context of anti-viral or anti-tumor responses may allow for better treatment

correlations, biomarkers for predictive outcomes, or the ability to select for or design an "optimal" phenotype of T cells to be used in ACT.

However, it is still unclear how alterations in TCR-pMHC interactions dictate changes in polyfunctional phenotypes. While hierarchical clustering analysis supports our hypothesis that TCR-pMHC affinity is not necessarily correlated with antigen recognition, we still lack a firm explanation for this phenomenon. The next chapter attempts to give weight to all these data in light of what is accepted in the field. We will speculate on structural observations that may help rationalize discrepancies in polyfunctional outcomes. We will also discuss how our novel observations may influence what should be considered when optimizing TCRs for gene-modification of T cells used in ACT.

CHAPTER SEVEN

CONCLUSIONS

Introduction

Adoptive cell transfer using TCR gene-modified T cells is an exciting and rapidly evolving field. Numerous *in vitro* and *in vivo* studies discussed in Chapter One have demonstrated various levels of feasibility, safety, and efficacy using TCR-engineered T cells to treat cancer and viral infections. Although evidence suggests their use can be effective, how effective and how to improve these therapeutics are still remaining questions.

Various means of improving the efficacy of TCR-engineered T cells, previously discussed, include cytokine and chemokine support, modifying retroviral vectors to promote pairing of introduced TCR α and β chains, and affinity-enhancement of the TCR. Because the affinity of TCR-pMHC interaction is thought to play the central role in defining T cell specificity and sensitivity , most of the field has adopted the theory that creating affinity-enhanced TCRs results in better functioning T cells. Although physiologic TCR-pMHC affinities traditionally range anywhere from 1-100 μM [11], the use of yeast and phage display can generate TCRs with affinities in the nM to pM range [3, 4]. However, enhanced affinity creates the opportunity for cross-reactivity. In fact, it has been shown *in vitro* that high affinity TCRs are much more tolerant of TCR contact

residue substitutions and dramatically increase the number of stimulatory peptides [407]. Additionally, a clinical trial using a MART-1-specific TCR with a K_D of only 30 μM demonstrated serious adverse events due to on-target/off-tumor activity [184]. Moreover, a murine-derived, affinity-enhanced MAGE-3-specific TCR caused lethality in another clinical trial due to off-target cross-reactivity with structurally similar epitopes [211, 213].

While TCR cross-reactivity was unwanted and detrimental in these cases, cross-reactive TCRs may offer therapeutic benefits if the antigens targeted are susceptible to mutation from genomic instability. Thus, the proper choice and design of therapeutic TCRs mandates a broader understanding of the basic principles governing antigen recognition by a T cell. In light of what is known about TCRs and T cell function, numerous factors still need to be addressed. These include: (1) what kinetic or cellular factors are most important in facilitating antigen recognition; (2) how is T cell function affected by alterations in TCR-pMHC interactions; (3) how can we structurally rationalize the cross-reactivity of a TCR; and (4) how might such cross-reactivity augment or inhibit therapeutic benefit.

The studies discussed in this dissertation aimed to address the above questions. Below we revisit key findings identified in each chapter and discuss how they contribute to an enhanced understanding of antigen recognition and T cell function. We also point out what questions are still unanswered and what needs to be addressed to advance the development of safe and efficacious TCR-engineered T cells for ACT.

HCV1406 TCR Displays Anti-Tumor Activity *In Vivo*

For any adoptive immunotherapy to be a viable treatment option, it must be clearly evident that antigen-reactive T cells are capable of being generated. Additionally, physiologically relevant targets need to be recognized by functional T cells. We believe that we have fulfilled these criteria. We demonstrated that we can engineer T cells with an HLA-A2-restricted, HCV NS3:1406-1415-reactive, CD8-independent TCR (HCV1406 TCR). We also showed that PBL-derived T cells engineered to express HCV1406 TCR are capable of recognizing naturally processed HCV NS3 antigen presented by HCC cell lines *in vitro* and can mediate the regression of established HCV^+ tumors *in vivo*.

To date, only a limited number of naturally occurring CD8-independent TCRs have been cloned and characterized. The ability of the HCV1406 TCR to transfer reactivity to both effector and helper T cells is advantageous for an effective immunotherapy candidate. HCV1406 TCR-transduced $CD4^+$ and $CD8^+$ PBL-derived T cells recognized both peptide-loaded targets and a variety of HCV^+ tumor cells lines. Our *in vivo* tumor regression model further supports our *in vitro* data that this TCR is capable of recognizing HCV^+ tumors. Further analysis of differential adoptive transfer of $CD8^+$ T cells with and without $CD4^+$ T cells may better distinguish the importance of generating $CD4^+$-reactive T cells for eliminating tumor, which may influence treatment modality in patients. Since one of the fundamental problems typical of chronic or recurrent HCV infections is a weak or absent HCV-specific $CD4^+$ T cell response [363, 364, 408, 409], the ability to engineer $CD4^+$ T cells capable of secreting cytokines and exhibiting cytolytic

activity may be extremely beneficial for an effective treatment. Taken together, we have established a proof-of-principle that we can generate TCR gene-modified $CD4^+$ and $CD8^+$ PBL-derived T cells capable of impacting on the growth of HCV^+ tumor targets and may be a useful tool to treat patients with HCV-associated diseases, such as HCC.

While other studies have examined AFP [410-412], ferritin [413], NY-ESO-1 [414-418] or Glypican 3 [417, 419-424] as biomarkers or therapeutic targets for HCC, we have chosen to investigate HCV for its nonself nature, its immunogenicity, and the fact that HCV is a major risk factor for the development of HCC. While the role of HCV proteins in hepatocarcinogenesis is not well described, HCV is mainly thought to cause HCC via indirect pathways including chronic inflammation, cell death, proliferation, and cirrhosis [425-428]. Consequently, it is possible that HCV TCR-transduced T cells would target both normal and malignant hepatocytes, potentially leading to severe adverse events, as noted by another group investigating HCV TCR-redirected T cells [222]. This accompanied with cirrhosis and liver dysfunction in many HCC patients may limit a systemic infusion of HCV TCR-transduced T cells. Thus, clinical trials for this immunotherapy are designed to involve CT or ultrasound guided intratumoral injection in a manner similar to transarterial chemoembolization or radioembolization. A similar intratumoral technique was used successfully in one of our previous clinical trials [207]. Such carefully thought approaches would help preclude significant exposure of normal hepatocytes to the HCV TC- transduced T cells and minimize adverse events.

In summary, our results are encouraging that HCV1406 TCR gene-modified T cells could serve as an immunotherapeutic candidate for HCV-associated HCC. However, the propensity for HCV to generate immune escape variants due to its genomic instability [279, 352-356] may require an effective TCR to recognize mutated epitopes. Therefore, it is important to assess the cross-reactivity of HCV-reactive TCRs against naturally occurring and epidemiologically relevant mutant epitopes to better evaluate their therapeutic benefit. Characterizing TCRs cross-reactive against mutagenic HCV antigens not only serves as a model for designing therapeutics against diseases with genomic instability, but also serves as a model to study the kinetic and biologic principles governing antigen recognition.

Cross-Reactive TCRs May Be Therapeutic Against

Diseases with Genomic Instability

Immune evasion by viruses and cancer cells has been a critical barrier to mounting effective host immune responses and has been problematic for the development of successful immunotherapies including ACT. A combination of viral/cancer genomic instability and immense selective pressure by successful immune effectors can lead to such escape variants. Manipulating the immune system to selectively eliminate its target while maintaining flexibility to combat genomic instability, a driving force behind immune escape, is the ultimate therapeutic goal. As discussed, we hypothesize that TCRs flexible enough to facilitate T cell recognition of mutated epitopes may serve as a vehicle to achieve this goal.

We addressed this hypothesis by establishing a model to evaluate the therapeutic benefit of cross-reactive TCRs to combat diseases with genomic instability. As discussed, the HCV genome contains several regions that are genetically unstable and mutate readily [357, 358], making HCV an excellent model for genomic instability. To create our model, we selected panels of naturally occurring and epidemiologically relevant mutants of two immunogenic epitopes to assess the cross-reactivity of a pair of HCV-reactive TCRs. The cross-reactivity observed by two independently isolated TCRs against two different, but highly antigenic HCV epitopes argues strongly that the ability of a TCR to be cross-reactive against a spectrum of mutant antigens is a generalizable phenomenon.

We were originally interested in the cross-reactive potential of HCV1406 TCR because it was an allo-reactive TCR [302]. Interestingly, we found that HCV1406 TCR-transduced T cells recognized numerous naturally occurring HCV NS31406-1415 epitopes identified in the GenBank. Aside from being naturally occurring, it is important to evaluate the epidemiologic prevalence of these mutations in infected individuals. Such validation would enhance the clinical relevance of the HCV1406 TCR, and would be an important point to consider for establishing the therapeutic merit of any cross-reactive TCR. A QuickAlign search of the Los Alamos HCV Sequence Database, which houses 918 recorded worldwide HCV genome sequences from infected individuals, provided a tool to perform this analysis.

While the WT and eight variant epitope sequences studied for NS3:1406-1415 account for 42.38% of all recorded sequences in the Los Alamos HCV Sequence Database, they comprise 80.38% of the recorded genotype 1a sequences, most applicable to the United States [373]. As discussed, cross-reactivity against seven out of the eight mutant epitopes by TCR-transduced $CD8^+$ effectors nearly doubled the amount of recorded sequences recognized compared to the prevalence of the WT epitope (43.46%). Additionally, CD8-independent recognition of WT and four mutant epitopes suggests HCV1406 TCR is a high affinity receptor and may facilitate $CD4^+$ T cell cytokine support against 78.42% of recorded sequences. Thus, HCV1406 TCR's cross-reactivity profile greatly enhances coverage against observed mutant epitopes. Furthermore, the generation of both helper and effector T cells allows for a novel population of MHC-class I restricted T helper cells to contribute to a broadened immune response.

We also characterized the cross-reactivity of a second, non-allo-restricted, TCR against a second immunodominant HCV epitope NS3:1073-1081. Gene transfer of HCV1073 TCR into T cells also facilitated CD8-independent recognition of multiple naturally occurring and epidemiologically relevant mutant epitopes. As discussed, the NS3:1073-1081 epitope for genotype 1a is well conserved with 90.2% of the recorded genomes in the Los Alamos Database exhibiting the WT CINGVCWTV epitope. However, genotype 1b is dominated by the I1074V mutant at 45.57% , WT comprising only 41.59% of recorded sequences. Cross-reactivity of the HCV1073 TCR against WT and I1074V epitopes alone could provide enhanced coverage for 94.46% and 89.3% of genotypes 1a

and 1b, respectively, most relevant to the United States' and Europe's viral prevalence [373]. Based on the prevalence of mutations studied, our HCV model suggests T cells engineered with such cross-reactive TCRs may provide therapeutic benefit while limiting selection for escape variants [365].

In light of observations that cross-reactive TCRs might enhance recognition against epidemiologically prevalent mutant targets, it is important to understand the biology behind TCR cross-reactivity. How peptide amino acid changes are tolerated or weaken the ability of the T cell to recognize pMHC are important points to consider when identifying or designing an immunotherapeutic candidate.

In our model for genomic instability, we have combined our functional studies with TCR-pMHC structural modeling. Our structural models allowed us to generate rational hypotheses for cross-reactivity by the HCV1406 and HCV1073 TCRs. Generally, we found amino acid substitutions that do not impact function occur in regions with few or no TCR or MHC contacts, or alternatively, are conservative substitutions that are not predicted to alter contacts.

Presumably, other TCRs in patients from which the viruses harboring the various NS3 mutant sequences propagated made more crucial TCR contacts at these positions, permitting viral escape. It is logical to predict that HCV1406 and HCV1073 TCRs exhibit a greater flexibility than TCRs in patients that would have allowed these immune escape variants to exist and persist. However, because HCV14073 TCR was isolated in a patient with a chronic HCV infection [166] this may not always be the case. Such TCRs may also

not be able to accommodate every possible mutation (i.e. HCV1406 TCR non-reactivity against variant 8S/9G/12L). However, if immune pressure is cross-reactive enough or there are multiple clonal cross-reactive T cell responses in an infected individual, it may limit the ability for a virus to avoid such a diverse immune pressure.

One might predict viral mutations affecting proteosomal processing or peptide binding to MHC (namely anchor residues) would be most beneficial for immune evasion should it reduce or eliminate the ability of the peptide to be properly presented by MHC-I. However, in the case of NS3:1406-1415, there were only 6 out of 918 recorded substitutions involving anchor positions 2 or 10. What would seemingly be an advantageous mutation for the virus may have been restricted if these residues are important for NS3 function or necessary for overall viral fitness. Verification of our structure-based hypotheses as well as a more detailed examination of potential structural alterations not predicted by our modeling would be helpful to understand implications of altered pMHC on T cell function.

Overall, in our HCV model for genomic instability, we have characterized CD8-independent recognition of multiple naturally occurring mutant epitopes for two HCV-cross-reactive TCRs. The reported HCV genome sequence data greatly adds clinical relevance to the potential therapeutic use of either or both of these receptors in ACT. Furthermore, preliminary experiments evaluating cross-reactivity of T cell clones raised from chronically infected versus spontaneously resolved patients support the hypothesis that HCV-cross-reactive TCRs could have an impact on clearance of HCV

infection or its associated disease. Aside from therapeutic implications for HCV and its associated disease, this approach serves as a helpful roadmap to identify or develop therapeutic cross-reactive TCRs. It may also allow us to better understand our immune response towards diseases with genomic instability.

TCR-pMHC Affinity Does Not Necessarily Dictate T Cell Function

Although our structural modeling of HCV1406- and HCV1073 TCR-pMHC interactions helped explain altered T cell reactivity against naturally occurring mutant epitopes, it does not provide a true mechanism for what facilitates antigen recognition. It is important to consider what kinetic and/or cellular parameters help facilitate antigen recognition in light of altered TCR-pMHC interactions. A better understanding of what influences antigen recognition may help modify TCRs to specifically enhance or inhibit TCR cross-reactivity to improve efficacy and maximize safety.

TCR-pMHC affinity is generally thought to play the most central role driving T cell specificity and reactivity [1]; therefore, it was logical to compare T cell reactivity against each variant pMHC with the affinity of each TCR-pMHC interaction. Because the two cysteine residues in NS3:1073-1081 peptides inhibited biochemical characterization, we proceeded with analysis of only HCV1406 TCR with WT and variant NS3:1406-1415 epitopes. To correlate TCR-pMHC affinity with T cell function, we compared the equilibrium K_D for each TCR-pMHC to the magnitude of IFNγ release by TCR-transduced $CD4^+$ or $CD8^+$ T cells. Measurable affinities grouped the peptides into categories of "moderate affinity" compared to 17 μM for WT (I1412L, V1408T, V1408L, and I1412V,

ranging from 32-63 μM) and "lower affinity" (A1409T, I1412L, and 8s/9G/12L, ranging from 120-169 μM). The TCR-pMHC affinity for mutant 8S/9S/12L/14S was unable to be measured but was grouped into this category based on predicted affinity from its amino acid substitutions and its CD8-dependent recognition.

We found that affinity seemed to trend with antigen recognition, as WT and "moderate affinity" mutants were CD8-independent, and "lower affinity" variants were generally CD8-dependent. These observations seemed consistent with the field's interpretation of affinity's importance on antigen recognition. However, the magnitude of T cell responses did not completely agree with this theory. As discussed, TCR-transduced $CD4^+$ T cells secreted less IFNγ against V1408T and I1412L compared to mutants with similar affinites. Furthermore, I1412N and 8S/9G/12L have virtually identical affinity measurements (168 and 169 μM, respectively), but recognition of I1412N was CD8-dependent and 8S/9G/12L was not recognized. These functional observations are quite inconsistent with what would have been predicted based solely on affinity measurements.

Responses by $CD8^-$ T cells should more accurately reflect affinity's influence on functional recognition because SPR measurements take place in the absence of CD8. However, the functional avidity of HCV1406 TCR-transduced $CD4^+$ T cells against mutant NS3:1406-1415 epitopes did not always correlate with the affinity of the TCR-pMHC interactions. This discord between TCR-pMHC affinity and T cell reactivity contradicts

what is accepted by many in the field and surprisingly suggests that TCR-pMHC affinity may not be the most important influence on T cell function.

One potential explanation for these inconsistencies is that affinity measurements by SPR may not necessary necessarily reflect the true affinity of the physiologic TCR-pMHC interaction. SPR is performed in three-dimensional (3D) space with soluble TCRs and pMHCs. However, physiologically the TCR and pMHC are anchored on two-dimensional (2D) membranes of opposing cells [429]. One major caveat of 3D measurements by SPR is that soluble TCRs fail to account for the possible regulations imposed by the complex T-cell membrane environment. These include reduced spatial degrees of freedom of molecular motion and the presence of co-receptors [430]. Consequently, affinity rates in physiologic 2D may be vastly different from what is measured in typical 3D assays.

To overcome the limitation of 3D affinity measurements, methods have been developed to establish binding partners anchored onto 2D surfaces These include the mechanically based micropipette adhesion frequency assay [431], the thermal fluctuation assay [431], biomembrane force probes [432], as well as FRET-based single-molecule microscopy [433]. Mechanically-based 2D binding measurements of TCR-pMHC interactions revealed dramatically different kinetic parameters than 3D measurements, and 2D measurements displayed a better correlation with T cell responses [431, 434]. In addition, 2D techniques enable the measurement of TCR-pMHC-CD8 tri-molecular interactions. Such analysis revealed signaling-dependent

cooperation between the TCR and CD8 for pMHC binding, which synergistically enhanced discrimination of peptides of varying potencies [435]. Implementation of 2D methodologies to generate refined binding data may serve as a better correlative marker for understanding HCV1406 TCR cross-reactivity. Additionally, 2D techniques should be seriously considered when evaluating all therapeutic TCRs as more evidence suggests 3D affinity measurements do not accurately correlate with T cell function or predict TCR cross-reactivity.

It is also important to point out that differences in peptide-MHC affinity are also thought to have an effect on antigen recognition and the effectiveness of an immune response [436], but to what degree is unclear. All HCV NS3:1406-1415 peptides evaluated bound HLA-A2 similarly, but not identically. Additionally, thermal stability measurements generated by CD used to evaluate peptide-MHC binding is a proxy for affinity. Further studies in the field are necessary to improve the evaluation peptide-MHC-I binding interactions and to relate small changes in peptide-MHC binding to differences in T cell functional responses.

CD8 Co-Receptor Expression and Signaling, Antigen Density, and TCR Density Impact T Cell Function and Cross-Reactivity

It is also possible that TCR-pMHC affinity, whether measured in 3D or 2D, is not the most important parameter governing T cell reactivity. Weak correlations between TCR-pMHC affinity and T cell function led us evaluate the importance of other parameters that may influence antigen recognition. Because there seemed to be a

cutoff in CD8-dependence relative to affinity (somewhere between 63 μM (I1412L) and 120 μM (A1409T)), we further evaluated the influence of CD8 on antigen recognition and TCR cross-reactivity.

It is generally accepted that CD8 enhances T cell sensitivity by stabilizing, or affinity-enhancing, the TCR-pMHC interaction [378]. However, others have shown that lck-recruitment to the TCR/CD3 complex by CD8 is essential for T cell function [305]. To test the importance of both structural stabilization and signaling by CD8, we compared mutant antigen recognition by TCR-transduced Jurkat cells expressing no CD8, full length CD8 (CD8αβ), or a truncated version (CD8α'β') which lacks the intracellular lck-binding domain. Interestingly, these cell lines exhibited unanticipated cross-reactive profiles. Mutant epitopes characterized as CD8-independent by primary T cell functional studies elicited similar cytokine release in Jurkat cells regardless of the CD8 function. However, recognition of "lower affinity" CD8-dependent variants required both the extracellular portion and intracellular lck-binding domain of CD8. Thus, it is not only the TCR-pMHC stabilization by CD8 that dictates T cell function, but the recruitment of lck augmenting TCR/CD3 signaling also plays an important role. This further supports the notion that TCR-pMHC affinity is not necessarily the most influential parameter driving T cell function.

The importance of CD8's individual functions has been highly debated. One study concluded that only the extracellular domains of CD8αβ are sufficient for HLA class I-restricted TCR-transduced $CD4^+$ T cells to have optimal antigen recognition [437].

However, others argued that CD8 signaling can be required for antigen recognition depending on the strength of the TCR [305]. Additionally, a gp100-reactive T cell clone designated T4H2 was a $CD4^-/CD8^-$ T cell that efficiently recognized HLA-$A2^+$ $gp100^+$ human melanoma cells *in vitro* [44, 164]. However, when the T4H2 TCR was cloned and expressed in human T cells, it surprisingly required CD8 expression for tumor cell recognition [44]. Perhaps each TCR may need to be independently evaluated for its reliance on individual functional components of CD8 to assess its specific requirements for antigen recognition.

It is important to recognize that in addition to the CD8 co-receptor, the sensitivity of T cells is known to be modulated by varied expression of other accessory and/or co-stimulatory molecules including CD28, LFA-1, ICAM-1, OX40, CD80 and TNF family members like 4-1BB [438]. It is also possible that upregulated expression of key early signal transduction molecules such as lck and ZAP70 could lower the threshold for T-cell triggering [384]. Alternatively, molecules such as CD45 or SHP-1 that negatively regulate signal transduction [439] could also alter the level of antigen density required for full T-cell activation [440, 441]. Thus, it is important to investigate how surface, adhesion, and signaling molecules other than CD8 can influence antigen recognition and cross-reactivity.

In addition to CD8, we also wanted to evaluate the importance of antigen density on TCR cross-reactivity. Antigen density may influential because clinical reports of on-target/off-tumor or off-target effects by high affinity TCR-gene modified T cells

have been attributed to the detection of low levels of antigen [184, 211]. Additionally, peptide-loaded T2 cells do not represent physiologic levels of antigen a T cell would encounter on a tumor or virally-infected cell. To evaluate the influence of antigen density on TCR cross-reactivity, we arbitrarily defined three levels of antigen density. We consider peptide-loaded TAP^- T2 cells to be the "highest" antigen density because exogenously loaded peptides saturate surface MHC-I in the absence of endogenously processed peptides. TAP^+ HepG2 cells expressing HCV NS3:1406-1415 epitopes as minigenes require the epitopes to be expressed, minimally processed, and to compete for MHC-I with all other endogenously processed peptides, serving as our "lowest" density. Exogenously loading peptide onto TAP^+ HepG2 cells eliminates any internal processing, but the peptide has to outcompete endogenous peptides occupying surface MHC-I. Peptide-loaded HepG2 cells serve as our "intermediate" density between peptide-loaded T2 cells and antigen-expressing HepG2 cells. Comparing reactivity against these three systems allows for an arbitrary evaluation of the influence of antigen density on TCR cross-reactivity.

As described, cross-reactive profiles were markedly reduced against lower antigen levels. For example, at an "intermediate" density of antigen, $CD4^+$ TCR-transduced T cells secreted 100-fold less IFNγ against HepG2 cells peptide-loaded with V1408L compared to I1412V, despite having virtually identical TCR-pMHC affinities (60 and 63 μM, respectively). However, there was only a consistent 2-fold difference in IFNγ release between V1408L and I1412V peptide-loaded T2 cells. Recognition of antigen-

expressing HepG2 cells (our “lowest” antigen density) was reduced even more. For example, $CD4^+$ TCR-transduced T cells secreted IFNγ when stimulated with the WT HCV^+ HepG2 cells but lost reactivity against any mutant epitope; $CD8^+$ T cells were only reactive against “moderate affinity” mutants that were CD8-independent in a high antigen density T2 cell system. These observations suggest antigen density can have a profound effect on antigen recognition, and that differences in IFNγ secretion are not always reconciled by differences in TCR-pMHC affinity.

Because antigen density exhibited an important influence on TCR cross-reactivity, we wanted to evaluate if TCR density has a similar impact on antigen recognition. We first evaluated the impact of TCR density on antigen recognition by taking advantage of the CD34 cassette in our retroviral vectors. CD34 expression represents a surrogate marker for TCR transgene expression (Foley, unpublished, [304]). Evaluation of IFNγ expression in high, medium, and low transgene-expressing T cells by flow cytometry revealed a TCR density-dependent response in $CD8^+$ T cells. Highest TCR expression correlated with high expression of IFNγ, and lowest levels of TCR expression correlated with low, but still above background, IFNγ production. Conversely, $CD4^+$ T cells were much more dependent on high levels of TCR expression to produce IFNγ against most CD8-independent variant peptides, which have comparable affinities to WT. These findings further support that affinity measurements do not predict the requirement for TCR expression for function. These data also suggest that TCR density

also plays an important role in antigen recognition, sometimes independent of TCR-pMHC affinity.

A potential explanation for TCR density-dependence is provided by the biology of a TCR-gene-modified T cell. In TCR-engineered T cells and Jurkat cells, endogenously expressed TCRs limit the functional expression of introduced TCRs through mismatched chain pairing between endogenous and introduced TCR α and β chains. Additionally, the introduced receptor is limited by available CD3ζ for which it competes with the endogenous TCR. Thus, the nature of a TCR-engineered T cells limits optimal density of an introduced TCR. Because it is thought that the occupancy of a TCR may determine the magnitude of the T cell response [2], situations of inefficient TCR pairing may be detrimental to T cell function and may influence TCR cross-reactivity. So, if an altered peptide ligand requires a greater number of TCRs to be occupied by pMHC to generate a strong enough signal to induce activation, variations in TCR density may play key a role in its recognition.

To test this hypothesis, we performed parallel experiments using TCR-transduced Jurkat76 cells, which lack an endogenous TCR. This allows us to directly assess the impacts of TCR chain mispairing and competition for CD3 on antigen recognition. Jurkat76 cells were also engineered to express no CD8, full length CD8αβ, or truncated CD8α'β' to simultaneously assess the importance of the co-receptor in light of absent chain pairing competition. Surprisingly, "lower affinity" CD8-dependent ligands were now recognized in the absence of CD8. This suggests that enhancing

introduced TCR chain pairing can alleviate the requirement of CD8 and can enhance TCR cross-reactivity. The most surprising observation was that CD8αβ Jurkat76 cells (exhibiting high TCR density and fully functional CD8) were reactive against never-before-recognized mutant 8S/9G/12L. This key observation highlights the important interplay between TCR density, TCR-pMHC stabilization by CD8, and CD8-dependent signaling and how these factors directly influence antigen recognition irrespective of affinity.

Overall, the influence of TCR density on antigen recognition suggests that affinity measurements measured by SPR (a system that lacks TCR pairing competition) may not accurately reflect TCR-pMHC interactions in TCR-gene-modified T cells. Furthermore, modification of TCR pairing, without altering its affinity, can have dramatic effects on cross-reactivity and the requirement for co-receptors. This is an important point to reflect on because many approaches refining TCR engineered T cells involves modification of the retroviral vector or the TCR itself to enhance expression, chain pairing, and/or association with CD3. As discussed in Chapter One, techniques used to enhance uniform TCR expression include introduction of 2A self-cleaving viral sequences to promote stoichiometric TCR chain expression or codon optimization to improve mRNA translation [192, 193]. Additionally, a host of approaches used to modify the TCR to promote chain pairing include, but are not limited to, introducing additional disulfide bridges into the constant regions of each chain [176], adding leucine zippers at end of the cytoplasmic tails [174], or murinization of the constant regions [170, 198-202].

While these approaches are thought to make better effectors by enhancing the pairing of introduced TCRs, it has not been considered how modifying pairing efficiency could induce or alter the cross-reactivity of TCRs. Yet, our data suggest that enhancing the pairing of an introduced TCR could have a dramatic impact on the recognition of related antigens. Certainly, this may not be a desired result and could cause unwanted toxicities in patients treated with pairing-enhanced TCRs. Conversely, such strategies to enhance pairing that would also enhance cross-reactivity could be advantageous in diseases with genomic instability. Thus, the importance of TCR chain pairing on cross-reactivity should now be considered when designing TCRs for ACT.

Antigen Recognition Cannot Be Assessed

Based on a Single Functional Parameter

As described earlier, T cells are often classified by their functional profile (type 1 vs type 2, etc.), which have been related to therapeutic efficacy [395-399]. Specifically, T cells with type 1 responses are considered to facilitate better anti-tumor efficacy [395, 396], and play an important role in T-cell mediated viral clearance [400-402]. However, emerging other T cell subsets have been implicated in enhancing anti-tumor and anti-viral immunity [401-404]. In light of these generalizations, immune monitoring primarily evaluates one type 1 cytokine, namely IFNγ, to characterize the reactivity of bulk T cell cultures. In fact, up until this point, our analyses concerning the importance of affinity, CD8, ligand density, and TCR density on antigen recognition have been performed by

evaluating the release of a single cytokine. It may be important, however, to evaluate more than one functional parameter to appropriately characterize T cell reactivity.

Our simultaneously evaluation of intracellular IFNγ and surface CD107a revealed a much different biologic message than single cytokine release by a bulk T cell culture. We described that $CD4^+$ and $CD8^+$ T cells behave in different functional proportions and that changes in pMHC ligands, sometimes independently of affinity, disproportionately affected bi-functional $IFN\gamma^+CD107a^+$ populations. These preliminary observations suggested that the evaluation of a single cytokine might underestimate the complexity of T cell function and misrepresent the impact of altered TCR-pMHC interactions on T cell responses.

To evaluate the importance of assessing multiple functional parameters, we expanded our evaluation of T cell polyfunctionality by flow cytometry to include CD107a and six cytokines (IFNγ, TNFα, IL-2, IL-4, IL-17A, and IL-22). The resulting multi-dimensional datasets were immensely difficult to analyze by standard analysis software. Comparing combinations of seven functional parameters generated 128 discrete functional phenotypes for a single antigen stimulation. Increasing the number of stimulation conditions or T cell subsets ($CD4^+$ vs $CD8^+$) only complicated this analysis. Comparisons of over half a dozen software packages enabled us to generate simple and interpretable graphical output using SPICE which allowed us to draw meaningful conclusions. While no software package is perfect, the field is continuously developing and evaluating new tools equipped to analyze such complex datasets [442].

Initial comparisons of $CD4^+$ and $CD8^+$ TCR-transduced T cell reactivity against WT NS3:1406-1415 peptide-loaded targets revealed a much greater degree of phenotypic and functional complexity than is appreciated by the field, suggesting T cell responses have been oversimplified. Furthermore, we noticed that traditional functional classifications of type 1 vs type 2 responses do not always hold true. For example, certain populations of $CD4^+$ or $CD8^+$ TCR-transduced T cells produced unexpected combinations of cytokines, including IFNγ, IL-2, TNFα, and IL-4 in a single cell. Comparing T cell functional responses against altered pMHC ligands revealed that the frequency of polyfunctional populations did not always correlate with changes in affinity. Additionally, alterations in TCR-pMHC interactions seemed to preferentially affect higher order polyfunctional populations (≥3 simultaneous functions). Furthermore, we observed that higher order polyfunctional phenotypes are completely lost when T cells were stimulated by HCV^+ tumor cells. A stark contrast in polyfunctional phenotypes between peptide- and naturally processed antigen-stimulations further highlights the importance of ligand density on the quality of the T cell response. It would be interesting to evaluate if modifications to the TCR that enhanced chain pairing (increasing TCR density) could compensate for lower densities of antigen. This may offer a solution to restore a robust polyfunctional response against tumor cells expressing lower levels of antigen. It may also, however, inadvertently increase the risk of off-target effects.

Overall, these observations using human TCR-transduced T cells are intriguing because they represent the kinds of T cell populations we transfer into patients. Heterogeneity in polyfunctional populations among PBL donors demonstrated that different donors had different functional phenotypes as well as different ranges in numbers of functional parameters per cell. Expansive evaluation of T cell polyfunctionality in the context of individuals' anti-viral or anti-tumor responses may allow for better treatment correlations or biomarkers for predictive outcomes. It might be predicted that a T cell performing multiple functions may provide a more effective immune response. However, if a T cell is performing additional functions at the expense of the overall magnitude of a given response, a more polyfunctional phenotype may be less advantageous. For instance, if a T cell is restricted to producing ten functional units and secretes five different cytokines, the magnitude of a response (two units of each cytokine) might be lower compared to a T cell secreting only two different cytokines (five units of each). If the strength of the response is more important than the its diversity, a T cell with a less diverse functional phenotype may be more therapeutic. However, if the diversity of a response is more important than magnitude of respective functions, a T cell producing more cytokines may be more therapeutic.

In vivo modeling will be helpful in testing these hypotheses. TCR-engineered T cells adoptively transferred into tumor-bearing mice can be isolated from tumors or lymphoid compartments, assessed for functional profiles *ex vivo,* and compared to the tumor status of each animal. If T cells isolated from regressing tumors have distinctly

different functional phenotypes than those isolated from stable or growing tumors, this may indicate which functional phenotypes are providing better anti-tumor activity. Additionally, T cells can be isolated into individual functional phenotypes using cytokine affinity matrices [443-446]. T cells with certain functional phenotypes can be selectively adoptively transferred into tumor-bearing mice and evaluated for which functional phenotype(s) are most effective at reducing tumor growth. The strategies described above may help elucidate the importance of certain functional phenotypes and how they can contribute to effective immune responses.

Together, incorporation of multiple functional parameters in immune monitoring may better assess the true biology of T cell cultures. This level of functional characterization could also allow us to isolate cells with certain polyfunctional phenotypes to test *in vivo* which functional profiles are better for anti-tumor or anti-viral immunity. A more complete understanding of the different populations of T cells delivered to patients might also enable us to select for or design T cells with an "optimal" polyfunctional profile. This would be an immensely powerful tool to enhance the efficacy and safety of TCR-engineered T cells used in ACT.

It is important to point out that these observations would have never been established had we limited our characterization of T cell reactivity to standard assays evaluating a single cytokine. While evaluation of T cell polyfunctionality by multi-parameter flow cytometry is not necessarily a novel concept, most evaluations, however, have been limited to 2-4 parameters [447-451]. Very few studies have

assessed up to seven functional parameters, but advancement in reagents, instrumentation and multivariate data analysis is making this more feasible [452]. Some groups are evaluating larger numbers of fluorescent markers to evaluate T cell populations, but studies focusing on functionality are limited. A novel technology surpassing the practical limitations of flow cytometry, cytometry by time-of-flight (CyTOF), uses metal-labeled probes and mass spectrometric analysis to facilitate the measurement of 36 or more parameters in a single-cell with minimal crosstalk between channels [453]. Implementation of CyTOF has enabled researchers to evaluate previously unfeasible numbers of cellular parameters simultaneously. One study used the simultaneous detection of 16 surface markers, 6 tetramers, and 10 intracellular stains to evaluate combinatorial cytokine expression in virus-specific $CD8^+$ T cells within the continuum of cellular differentiation [454]. Others have used this approach to evaluate differential immune and drug responses across a human hematopoietic continuum [455]. Expansion of our functional panel using CyTOF to include lineage, memory, and effector markers, as well as phospho-signaling proteins or transcriptions factors may help provide explanations for unexpected cytokine combinations, but would admittedly exponentially complicate the analysis. Furthermore, scarcity of available instrumentation, cost of reagents, and careful optimization required make CyTOF analysis currently a less feasible approach. Nonetheless, our multi-parameter flow cytometric analysis of T cell polyfunctionality greatly alters the interpretation of antigen recognition compared to standard single parameter evaluations.

A More Complete Understanding of Antigen Recognition and TCR Cross-Reactivity May Rely on Structural Interpretation of the TCR-pMHC Interface

As a whole, we have evaluated various kinetic and cellular parameters driving antigen recognition, TCR cross-reactivity, and T cell polyfunctionality. We have also come to the realization that while affinity is thought to play the most important role, it may be quite overvalued. In light of these observations, we still lack a complete understanding of (1) what is truly different about the altered ligand interactions, and (2) how that translates into varied polyfunctional responses.

The concept of altered peptide ligands having differential effects on T cell function was first described by Evavold and Allen [456]. In this seminal report, a conservative substitution (E73D), removing one methylene group of an amino acid anchoring side chain impaired proliferation but not IL-4 production in T cells. Subsequent studies involving additional T cell clones indicated that TCRs have the capacity of differential signaling, leading to a spectrum of functional responses and events [296, 457-460]. Many of the explanations of altered T cell function were initially rationalized by changes in affinity due to small changes in pMHC topology [461]. Yet, in our studies, changes in TCR-pMHC affinity (or even interactions with similar affinities) were not always correlative with polyfunctional responses. Others have since suggested that altered peptides may induce small conformational changes in the TCR engaging altered pMHC, leading to ranges of TCR-initiated signals, sometimes independent of

measurable affinity [462-464]. Thus, structural studies highlighting the TCR-pMHC interface may provide a better explanation for unanticipated functional outcomes.

Efforts to better understand functional effects of altered peptide ligands have relied heavily on solving crystal structures of TCR-pMHC interactions. These evaluations provide the resolution necessary to detect important TCR contact points with peptide and/or MHC, identifying key hydrogen bonds or van der Waals contacts thought to influence antigen recognition. Comparing crystal structures of TCRs engaged with altered peptide ligands have revealed obvious or subtle changes in pMHC topography, resulting in altered TCR conformations thought to be responsible for profound biological effects [465-467].

It is important to realize that the true mechanism behind altered T cell function lies at the origin of the interaction, the interface of the TCR-pMHC. Therefore, we cannot begin to fully understand how HCV1406 TCR cross-reactivity dictates functional outcome without evaluating structurally what happens at this TCR-pMHC interface. We have previously provided computational modeling of the interactions between our HCV TCRs and WT pMHCs to help explain changes in binary function and potency of response influenced by the CD8 co-receptor. Since then we have discussed at length many parameters other than affinity we feel are involved in dictating T cell activation and polyfunctionality. But as mentioned, to identify the true mechanism calls for crystal structure analysis. Thus, to visualize the TCR-pMHC interface and rationalize functional

effects upon alteration of the peptide, we turned to the solved the crystal structure of HCV1406 TCR with WT HCV NS3:1406-1415/HLA-A*0201.

The crystal structure of the TCR-pMHC now allows us to highlight TCR contact residues important for a productive interaction. Figure 57 illustrates the crystal structure overview of the TCR interaction with pMHC as well as the pMHC topology with HCV1406 TCR's CDR loop footprint. A closer examination of hydrogen bonds and van der Waals contacts with TCR and WT peptide is shown in Figure 58 and summarized in Table 14. Interestingly, only CDRα loops are involved in hydrogen bond-mediated recognition of the peptide itself (Fig. 58). CDR1α loop residue S33 interacts strongly with the lysine residue at position one, which explains why an alanine substitution at this position abrogated functional responses by TCR-transduced PBL and Jurkat cells (See Appendix). Additionally, CDR3α loop residue D102 forms hydrogen bonds with peptide positions 4, 6, and 7 (A1409T, G1411, and I1412, respectively). The importance of these interactions may help resolve differences in recognition of mutants A1409T, I1412L, I1412V, and I1412N. If this S33-p4 interaction is important for TCR recognition of pMHC, an amino acid class substitution from a nonpolar alanine to a polar threonine (A1409T) could require TCR and/or peptide rearrangements to resolve atomic clashes. If this were to only weaken the TCR-pMHC interaction, CD8-dependence would only require the extracellular domain stabilizing TCR-pMHC. But because recognition of A1409T also requires the lck-binding domain of CD8, perhaps an interface rearrangement induces a conformational change in the TCR leads to differential TCR/CD3 signaling requirements.

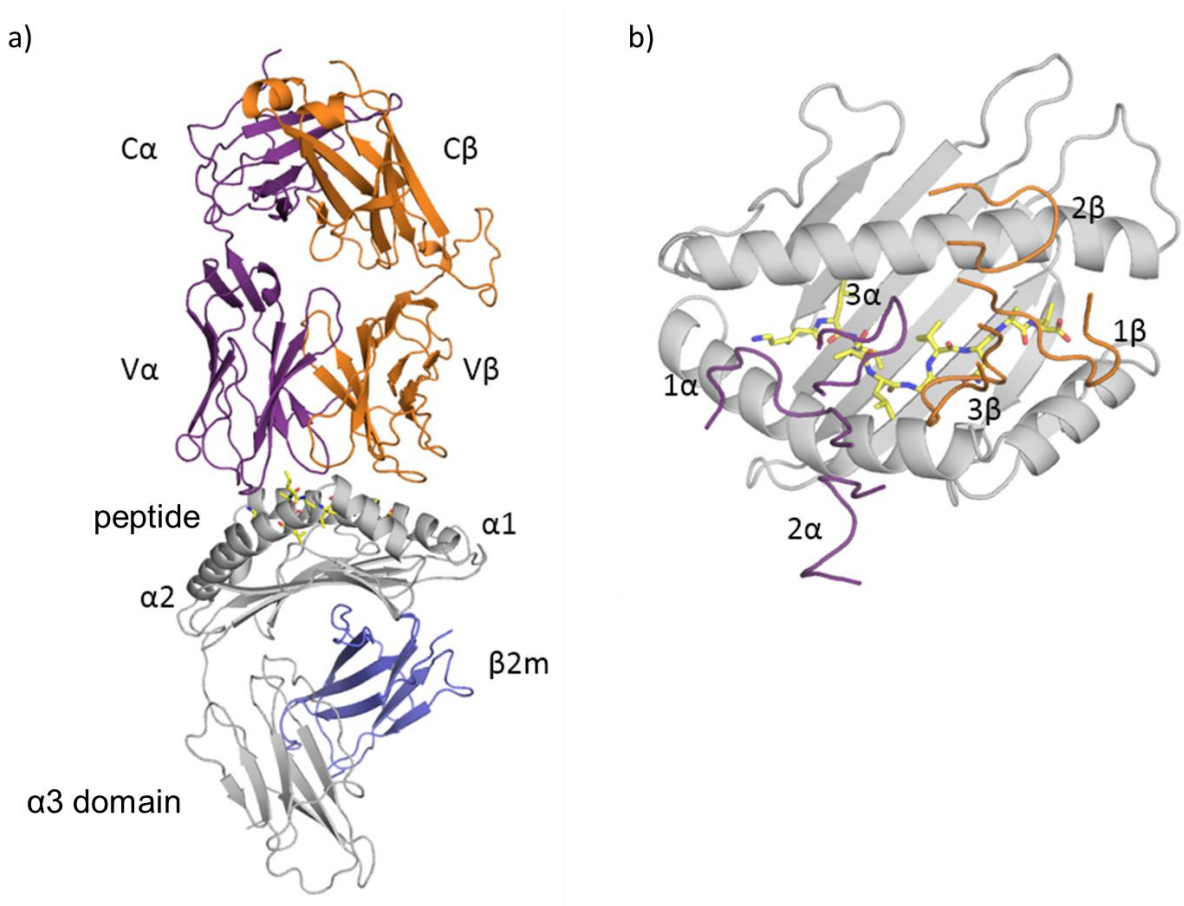

Figure 57. Crystal structure overview of HCV1406 TCR : WT HCV NS3:1406-1415 / HLA-A2. (a) Side view of the TCR-pMHC complex (ribbond diagram). TCRα chain (orange); TCRβ chain (purple); HLA-A2 heavy chain (gray); β2m chain (blue); WT peptide is drawn in stick representation with carbon atoms in yellow, nitrogen atoms in blue, and oxygen atoms in red. **(b)** Footprint of the HCV1406 TCR CDR loops over the WT HCV NS3:1406-1415 peptide. Same color scheme as part a. Crystal structure data was kindly provided by Yuan Wang in the Baker Lab (University of Notre Dame).

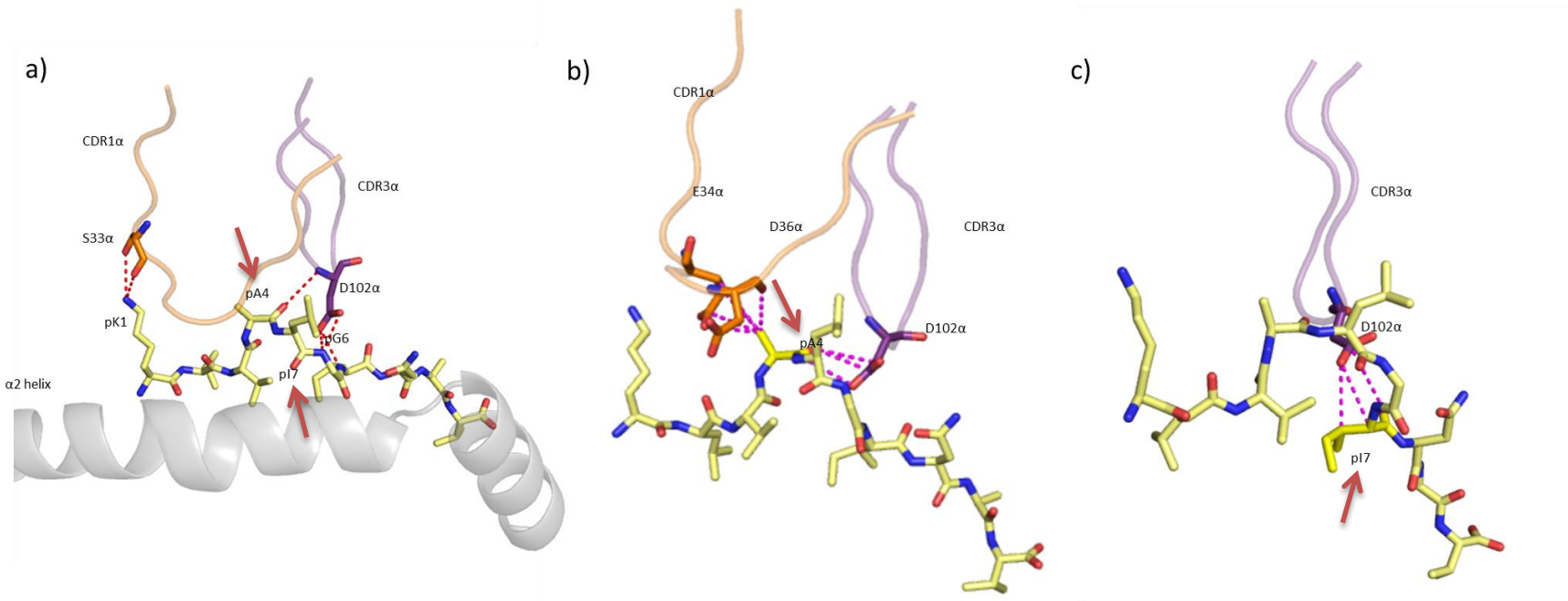

Figure 58. Hydrogen bonds and van der Waals contacts between HCV1406 TCR CDR loops and WT HCV NS3:1406-1415 / HLA-A2. **(a)** Hydrogen bonds between TCR and pMHC. Only CDRα loops are involved into peptide recognition. CDR1α (orange), CDR3α (purple); hydrogen bonds are represented by red dotted lines; TCR residues are identified by a one-letter amino acid designation followed by position number and chain designation. **(b)** van der Waals contacts (purpled dotted lines) between HCV1406 TCR CDR loops with pA4 (A1409). Same color scheme as in part a. **(c)** van der Waals contacts (purple dotted lines) between HCV1406 TCR CD$ loops with pI7 (I1412L). Same color scheme as in part a. Red arrows highlight altered residues in naturally occurring mutant epitopes. Crystal structure data was kindly provided by Yuan Wang in the Baker Lab (University of Notre Dame).

Table 14. Interactions between HCV1406 TCR CDR loops and WT HCV NS3:1406-1415 peptide in the TCR-pMHC complex.

TCR CDR loop residue		Hydrogen bonds/ salt bridges (bold)	van der Waals contacts
CDR1α	S33	O:pK1(N^{ζ}) O^{γ}:pK1(N^{ζ})	pK1
	E34		pK1 pA4
	D36		pA4
	Y37		pL5
	Y38		pL5
CDR3α	D102	N:pA4(O) $O^{\delta1}$:pG6(N) $O^{\delta2}$:pG6(N) $O^{\delta2}$:pI7(N)	pA4 pA5 pG6 pI7
CDR3β	G96		pN8
	P97		pL5 pN8

Crystal structure data was kindly provided by Yuan Wang in the Baker Lab (University of Notre Dame).

That being said, in the absence of receptor pairing competition, $CD8^-$ Jurkat76 cells can recognize this mutant, suggesting that augmentation of TCR density can overcome or accommodate for any structural changes associated with this substitution.

Similarly, we studied three altered pMHC ligands with substitutions at position 7. I1412L and I1412V are both CD8-independent with similar K_D measurements and conservative substitutions. Yet I1412L, with a 2-fold higher affinity, consistently blunted $CD4^+$ T cell responses. It is less clear how the subtraction of a single methyl group (I1412V) could have a greater detrimental affect than the same number of hydrocarbons but in different branching orientation (I1412L) despite similar (yet two-fold higher) affinity. As these residues are hydrophobic and buried in the binding groove of HLA-A2, it is plausible that the orientation of the hydrocarbon side chains could alter the overall topology of the pMHC. Because hydrogen bonds' energetic dependence on the stereochemistry and geometry of the bond is crucial [468], a minor change in a single hydrocarbon side chain orientation could have a significant effect on TCR conformational change. Thus, identification of important TCR-peptide hydrogen bonds helps rationalize differential antigen recognition, but a complete explanation is not yet clear.

TCR and peptide interactions are also influenced by van der Waals contacts between CDR3α loop residue D102 with peptide positions 4-7 (Fig. 58b-c). While individually weaker compared to hydrogen bonds, van der Waals interactions when presented in large numbers across broad interfaces "sum" to substantial binding

energies between TCR and pMHC [469]. Thus, variants with substitutions at positions 4 (A1409) and 7 (I1412) could disrupt the integrity of van der Waals forces, leading to conformational changes and differences in functional responses without a large impact on affinity. Similarly, while variants I1412N and 8S/9G/12L have essentially the same affinity, 8S/9G/12L remains unrecognized by HCV1406 TCR-transduced T cells. Perhaps despite identical affinities, the number of mutations or the position in which they occur could dramatically alter the conformation of the pMHC topography, not predicted by 3D affinity. In fact, it is reasonable to predict an altered conformation could affect the efficiency of TCR signaling, or require a greater threshold of TCR contacts or number of occupied TCR for functional recognition. This might explain why CD8αβ Jurkat76 cells (enhancing introduced TCR chain pairing and TCR signaling) could overcome structural perturbations and mediate T cell recognition of 8S/9G/12L.

Additionally, TCR interactions with HLA-A2, including hydrogen bonds, salt bridges, and van der Waals contacts are also important (summarized in Table 15). Two CDRs of the α chain and all three CDRs of the β chain contact a myriad of residues throughout HLA-A2. It is plausible that variant peptides could alter pMHC conformation and disrupt TCR interaction with MHC independently of peptide contacts. Taken together, information gathered from crystal structure analysis offer us the opportunity to explain the structural importance of certain residues' influence on downstream function.

Table 15. Interactions between HCV1406 TCR CDR loops and HLA-A2 in the TCR-pMHC complex.

TCR CDR loop residue		Hydrogen bonds/ salt bridges (bold)	van der waals contacts
CDR1α	E34	**$O^{\varepsilon 1}$:K66(N^{ζ})** **$O^{\varepsilon 2}$:K66(N^{ζ})**	K66α1
	S35		T163α2
	D36	$O^{\delta 1}$:T163(O^{γ}) $O^{\delta 2}$:T163(O^{γ})	Y159α2 T163α2
	Y38		Q155α2
CDR2α	Y59		E154α2 Q155α2 A158α2
	K60	**N^{ζ}:E154($O^{\varepsilon 2}$)**	E154α2
CDR2α	D103		R65α1
CDR1β	D30	**$O^{\delta 1}$:K146(N^{ζ})**	K146α2
CDR2β	Y50		A69α1 Q72α1
	G51		V76α1
	V52		V76α1
	N53		R75α1
	S54		V76α1
	E56		Q72α1
CDR3β	R95	$N^{\eta 1}$:A149(O)	
	P97		Q155α2
	Y98	O^{η}:A150(O) O^{η}:Q155($N^{\zeta 2}$)	A150α2 H151α2 Q155α2

Crystal structure data was kindly provided by Yuan Wang in the Baker Lab (University of Notre Dame).

However, it is still not clear how conservative (i.e. I1412L vs I1412V) or more radical (I1412N vs 8S/9G/12L) mutations resulting in similarly paired affinities can induce modestly or starkly different polyfunctional outcomes. To confirm our predictions, comparison of crystal structures of HCV1406 TCR with each mutant peptide bound to HLA-A2 is required. While out of the scope of this dissertation, this is a logical next step to discern any true conformational changes that might induce differential T cell functions. Even so, based on some mutants' minor and conservative amino acid changes (some with merely the addition or change in place of a single hydrocarbon), such conformational changes might be so subtle that a crystal structure may not provide enough resolution to detect them. But combining a series of crystal structures with alternative 2D kinetic and thermodynamic analyses may help determine what changes at the TCR-pMHC interface influence TCR cross-reactivity and ultimately T cell function. Nonetheless, structure-function studies like the ones outlined here are important to better understand the principles behind antigen recognition and the consequences of alterations in TCR-pMHC. Appreciation of important TCR-pMHC contact points and their impact on downstream function might allow for structure-guided design of TCRs enhancing or limiting contacts with peptide or MHC in order to enhance or limit a T cells specificity [266, 270, 470].

Concluding Remarks

To improve T cell-based immunotherapy, we need to better understand the basic requirements for antigen recognition and what parameters govern antigen

specificity, TCR cross-reactivity, and T cell function. Experimental questions addressed in this dissertation utilized traditional and novel approaches to characterize (1) the requirements for cross-reactive antigen recognition by HCV1406 TCR gene-modified T cells and (2) the functional consequences of altered TCR-pMHC interactions. The characterization of HCV1406 TCR cross-reactivity against naturally occurring mutant HCV NS3:1406-1415 epitopes fundamentally serves as a model to study antigen recognition. While it is important to acknowledge that because HCV1406 TCR was allo-restricted, it was by definition cross-reactive. But this should not limit any value from the work as a whole because in a sense all T cells are inherently cross-reactive. As thymic education requires antigen recognition by a T cell for positive selection, certainly pathogenic peptides with which TCRs engage in the periphery are not presented in the thymus. The principles behind thymic education as well as the existence of allo-specific T cells [471, 472] would suggest that TCRs must be cross-reactive to some extent and that the lock-and-key principle of TCR-specificity is outdated. Aside from characterization of TCR cross-reactivity, this dissertation examines the basic principles behind antigen recognition and how TCRs can facilitate drastically different functional responses against naturally occurring mutant peptides.

Overall, contrary to what is generally accepted in the field, we found that TCR-pMHC affinity is not necessarily the most important role dictating antigen recognition and T cell function. Other cellular parameters, including ligand density, TCR density, and co-receptor signaling greatly influenced recognition of altered ligands, providing a new

working model for antigen recognition (Fig. 59). Additionally, modifying any of these parameters could dramatically change functional responses, sometimes independently of affinity. We also found that the field's interpretation of TCR cross-reactivity or antigen recognition may be narrowed and misguided when evaluation of T cell function is limited to a single cytokine. Functional phenotyping by seven-parameter flow cytometry revealed that T cell functional profiles are more complex than were previously believed. Evaluation of a single functional phenotype, such as IFNγ, also does not accurately reflect the functional behavior of a T cell culture, especially when comparing altered TCR-pMHC interactions. But as the technology improves, the evaluation of seven functional parameters for any immune cell type will be inadequate. While more information may be learned from multi-parameter analyses, its analysis will inherently be more complex, but it will more accurately reflect the true nature of the immune response.

Together, these studies suggest that the field is grossly oversimplifying the biology of T cells and the fundamentals of antigen recognition. It is important to note, however, that the data presented in this dissertation challenge longstanding assumptions not because the field is ignorant of them, but rather that no one has evaluated these questions in as much detail as is presented here. A sound explanation of our observations may depend on a clearer understanding of what is happening structurally at the TCR-pMHC interface combined with novel, emerging strategies

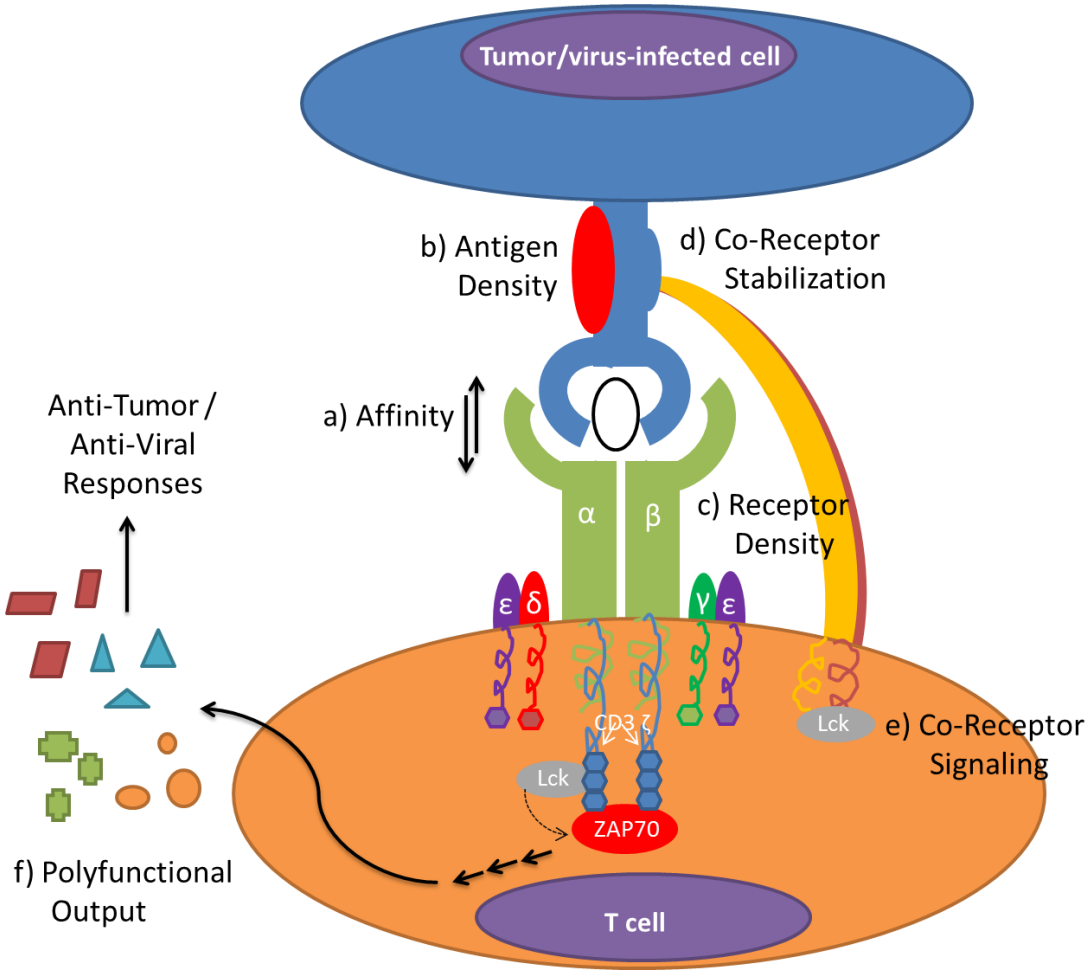

Figure 59. A new working model for kinetic and cellular parameters influencing antigen recognition and T cell function. Schematic diagram illustrating factors involved in T cell activation upon TCR-pMHC ligation. While **(a)** affinity of the TCR-pMHC interaction is thought be the most influential factor governing antigen recognition, studies in this dissertation suggest that is not the case. **(b)** Antigen and **(c)** TCR densities also play important roles, and augmentation of either one can modulate TCR cross-reactivity. Additionally, **(d)** CD8 co-receptor has been shown to stabilize the TCR-pMHC interaction, but its **(e)** ability to augment TCR/CD3 signaling by recruiting lck is essential for low affinity interactions. A complex interplay of these, and other factors, play a role in dictating the **(f)** polyfunctional output of T cells which facilitate anti-tumor and anti-viral immune responses. Evaluating single-cell polyfunctional response, rather than single cytokine release by a bulk T cell culture greatly enhances biologic interpretation.

evaluating TCR-pMHC binding. Only then can we truly rationalize how single amino acid substitutions relay such substantial changes in functional output. Once resolved, such comprehension will not only help steer rational, structure-guided design of TCRs to generate better functioning T cells, but it will also impact the way in which we study other immune cell and receptor types, approach epitope discovery, and evaluate vaccine design. In this way, we have provided a new foundation in which to evaluate the design and implementation of novel immunotherapies.

APPENDIX

ADDITIONAL FIGURES FOR REFERENCE

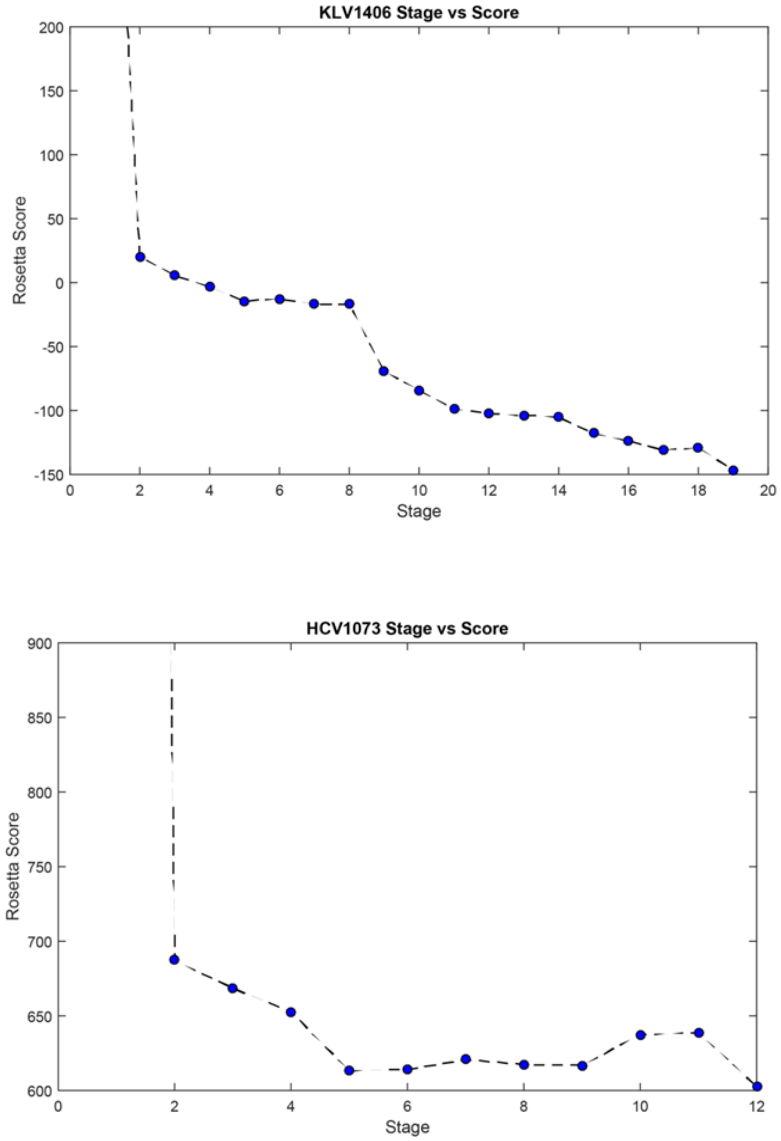

Figure 60. Rosetta score vs. modeling stage for modeling the HCV1406 (top) and HCV1073 (bottom) TCR-pMHC complexes.

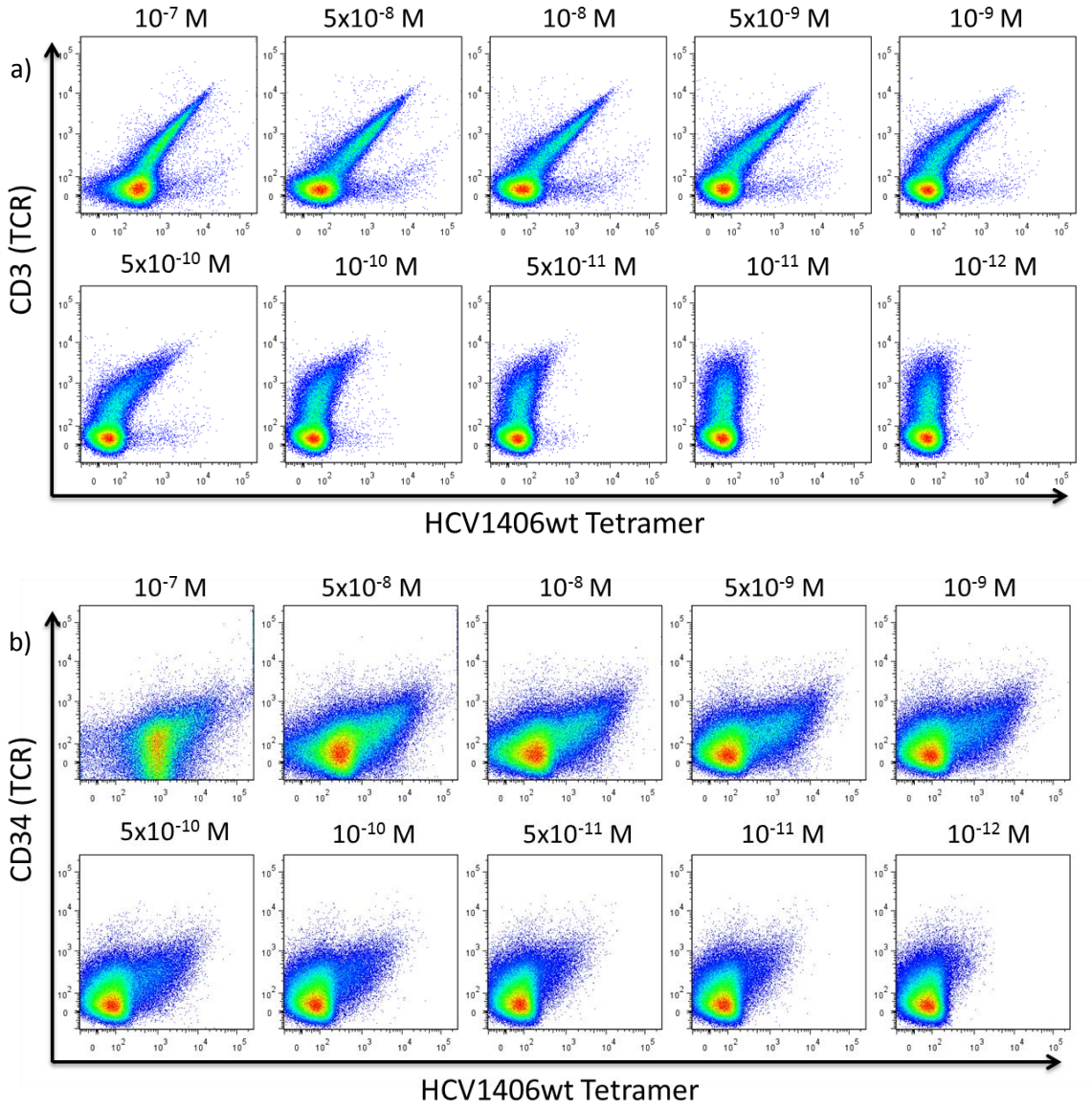

Figure 61. Comparison of TCR density and HCV NS3:1406-1415 (WT) tetramer staining by HCV1406 Jurkat and Jurkat76 cells. (a) CD3 serves as a surrogate marker for HCV1406 TCR expression in Jurkat76 cells. **(b)** CD34 serves as a surrogate marker for HCV1406 TCR exprssion in Jurkat cells. Concentrations indicate amount of tetramer used to stain $1x10^6$ cells.

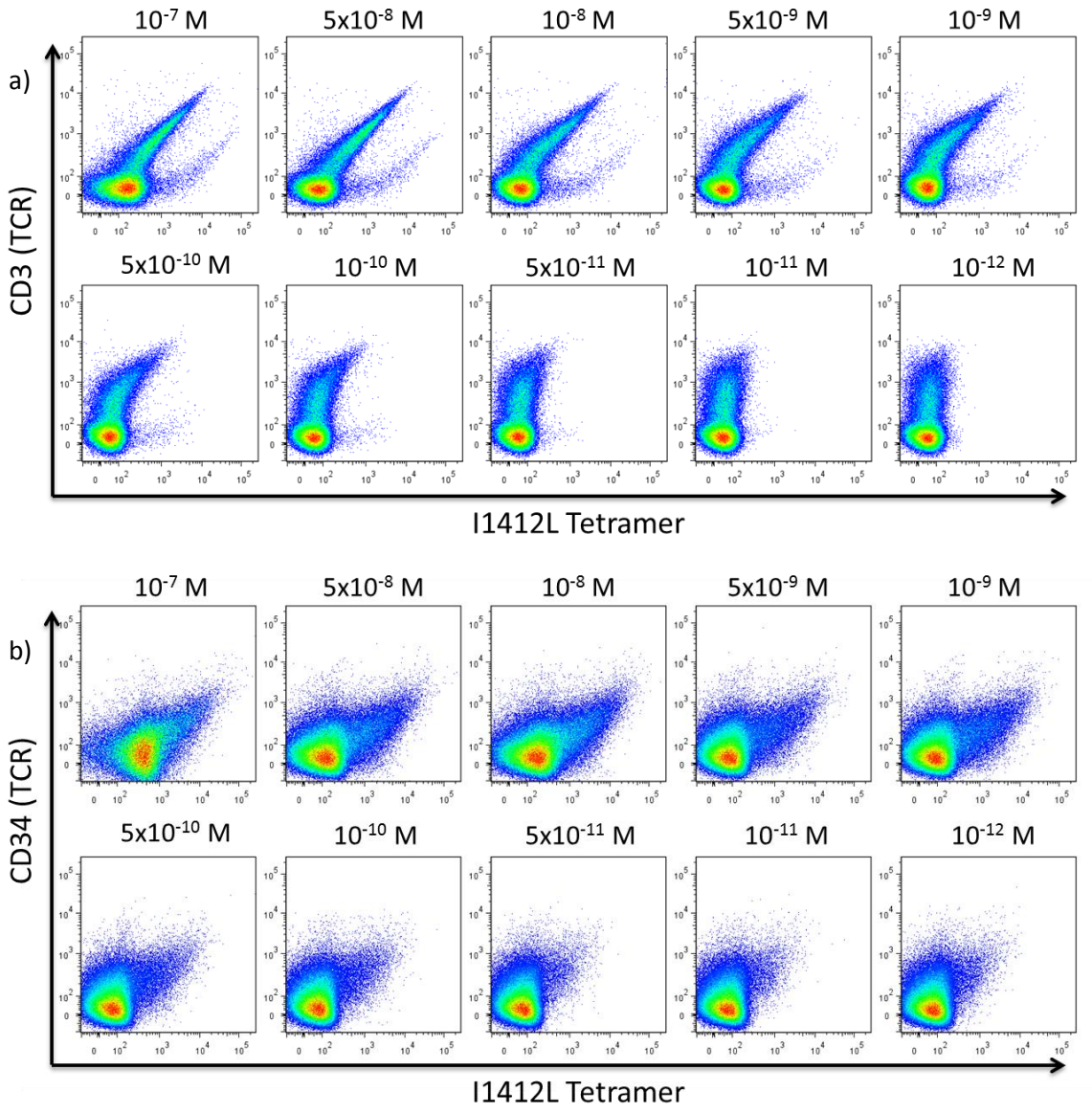

Figure 62. Comparison of TCR density and HCV NS3:1406-1415 (I1412L) tetramer staining by HCV1406 Jurkat and Jurkat76 cells. (a) CD3 serves as a surrogate marker for HCV1406 TCR expression in Jurkat76 cells. **(b)** CD34 serves as a surrogate marker for HCV1406 TCR exprssion in Jurkat cells. Concentrations indicate amount of tetramer used to stain $1x10^6$ cells.

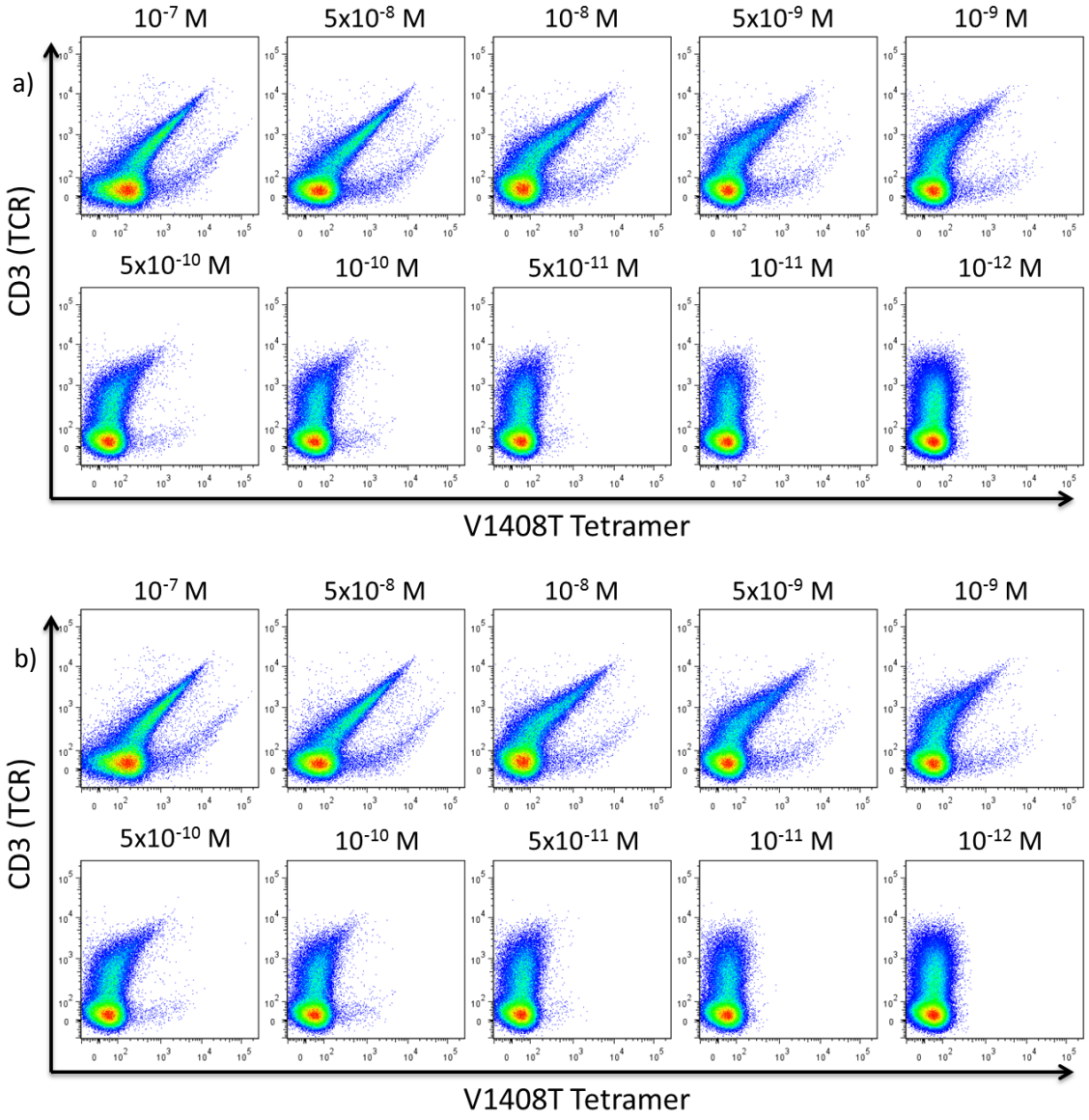

Figure 63. Comparison of TCR density and HCV NS3:1406-1415 (V1408T) tetramer staining by HCV1406 Jurkat and Jurkat76 cells. (a) CD3 serves as a surrogate marker for HCV1406 TCR expression in Jurkat76 cells. **(b)** CD34 serves as a surrogate marker for HCV1406 TCR exprssion in Jurkat cells. Concentrations indicate amount of tetramer used to stain $1x10^6$ cells.

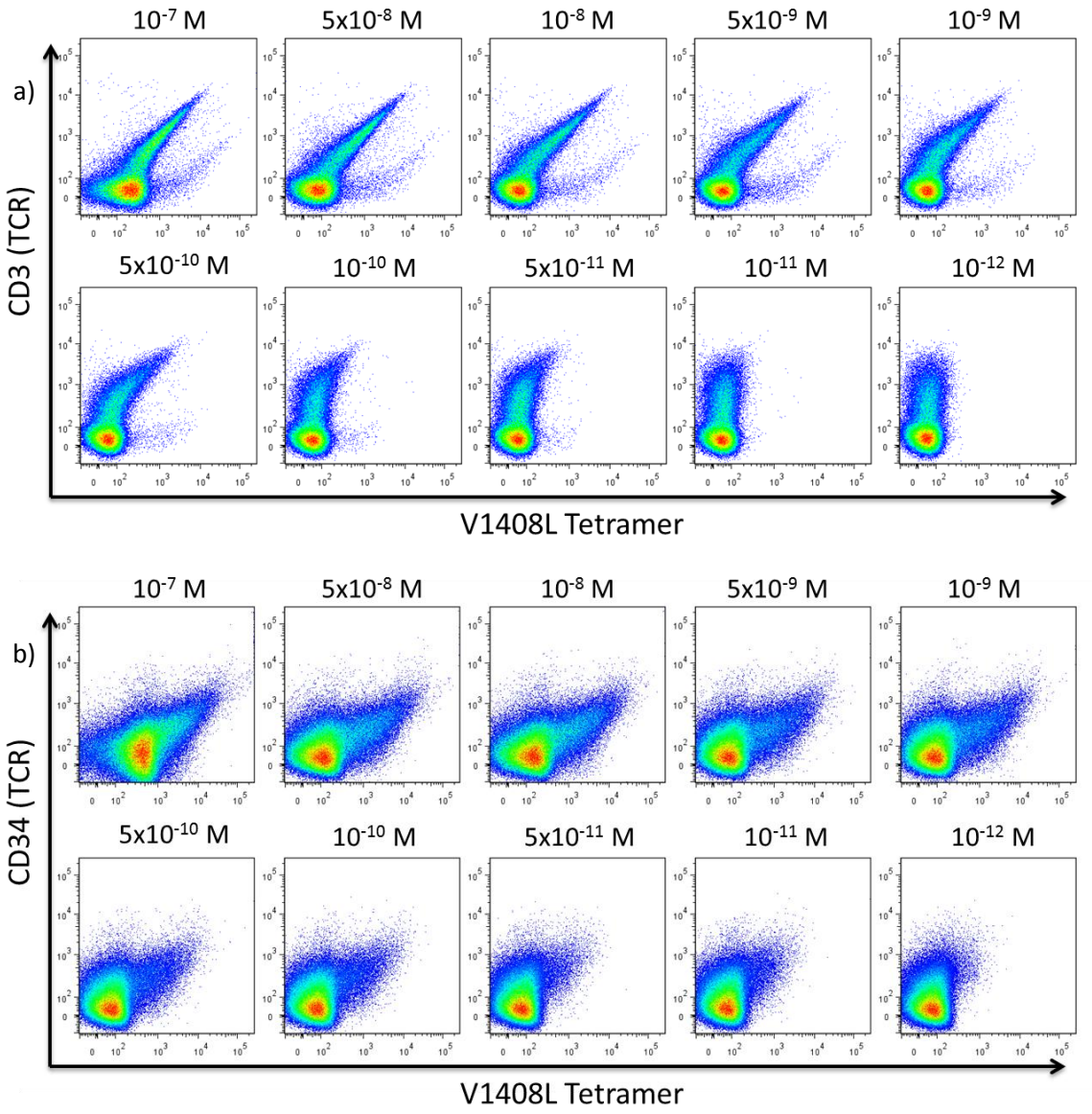

Figure 64. Comparison of TCR density and HCV NS3:1406-1415 (V1408L) tetramer staining by HCV1406 Jurkat and Jurkat76 cells. (a) CD3 serves as a surrogate marker for HCV1406 TCR expression in Jurkat76 cells. **(b)** CD34 serves as a surrogate marker for HCV1406 TCR exprssion in Jurkat cells. Concentrations indicate amount of tetramer used to stain $1x10^6$ cells.

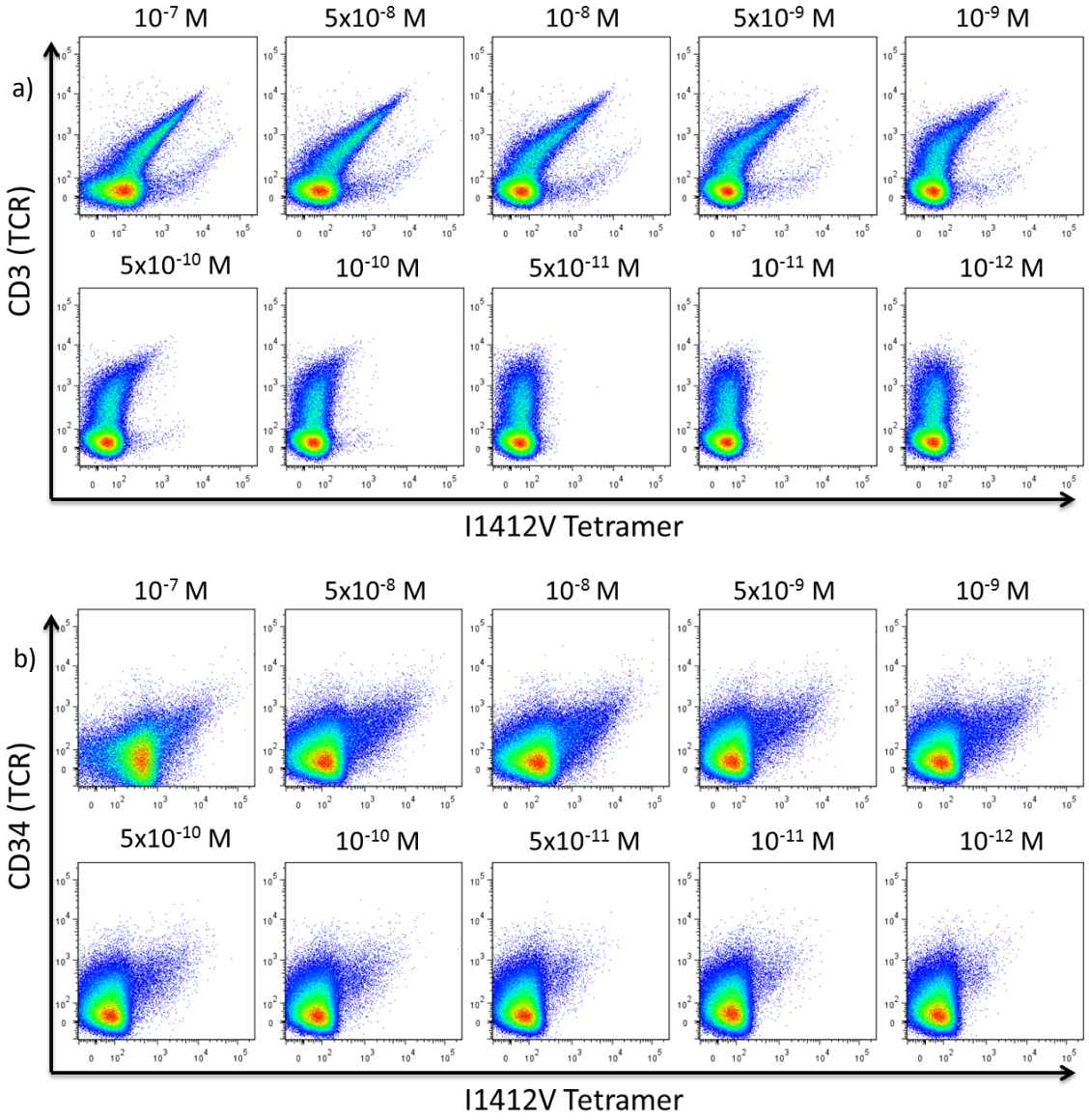

Figure 65. Comparison of TCR density and HCV NS3:1406-1415 (I1412V) tetramer staining by HCV1406 Jurkat and Jurkat76 cells. (a) CD3 serves as a surrogate marker for HCV1406 TCR expression in Jurkat76 cells. **(b)** CD34 serves as a surrogate marker for HCV1406 TCR exprssion in Jurkat cells. Concentrations indicate amount of tetramer used to stain $1x10^6$ cells.

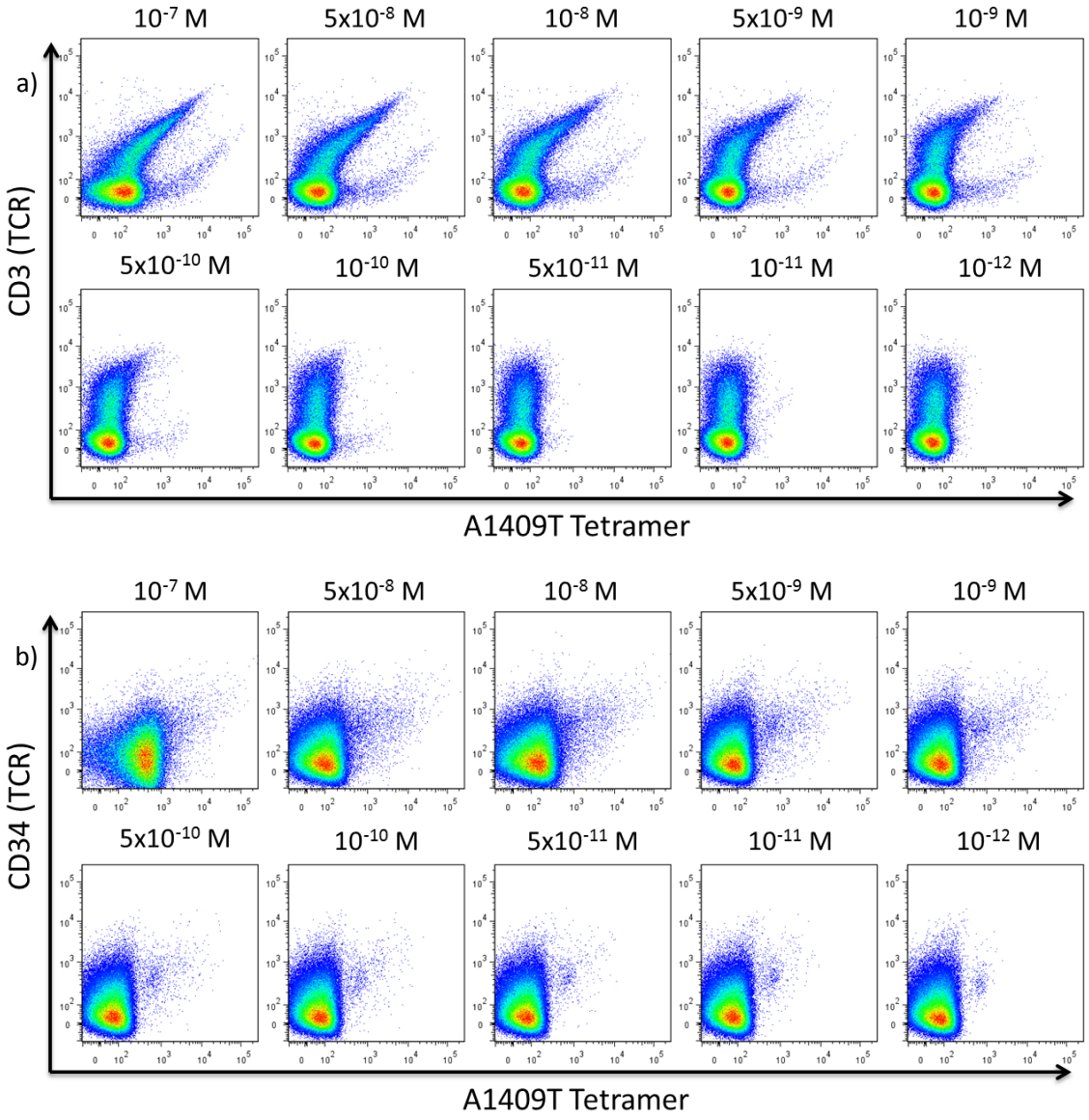

Figure 66. Comparison of TCR density and HCV NS3:1406-1415 (A1409T) tetramer staining by HCV1406 Jurkat and Jurkat76 cells. (a) CD3 serves as a surrogate marker for HCV1406 TCR expression in Jurkat76 cells. **(b)** CD34 serves as a surrogate marker for HCV1406 TCR exprssion in Jurkat cells. Concentrations indicate amount of tetramer used to stain $1x10^6$ cells.

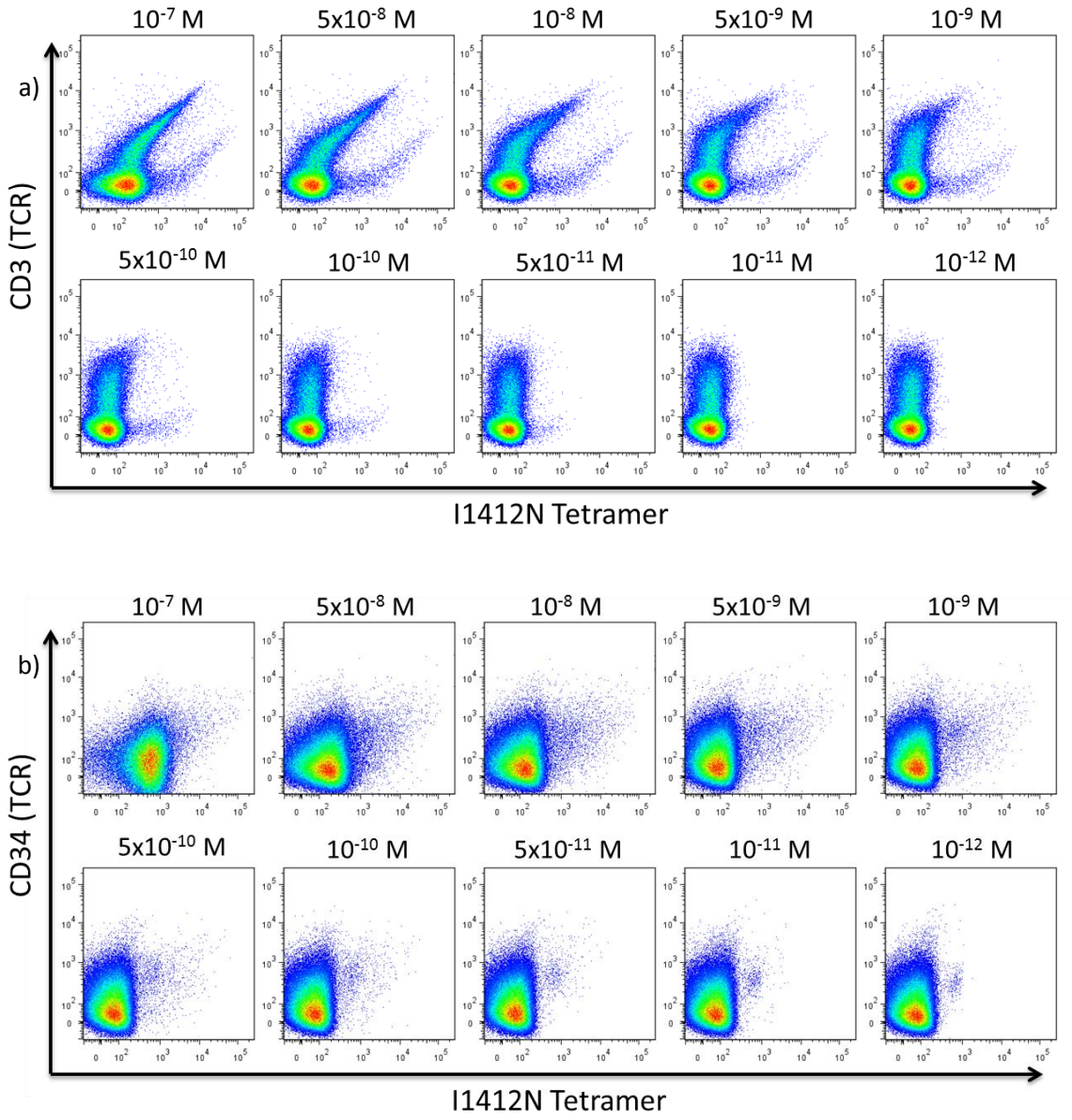

Figure 67. Comparison of TCR density and HCV NS3:1406-1415 (I1412N) tetramer staining by HCV1406 Jurkat and Jurkat76 cells. (a) CD3 serves as a surrogate marker for HCV1406 TCR expression in Jurkat76 cells. **(b)** CD34 serves as a surrogate marker for HCV1406 TCR exprssion in Jurkat cells. Concentrations indicate amount of tetramer used to stain $1x10^6$ cells.

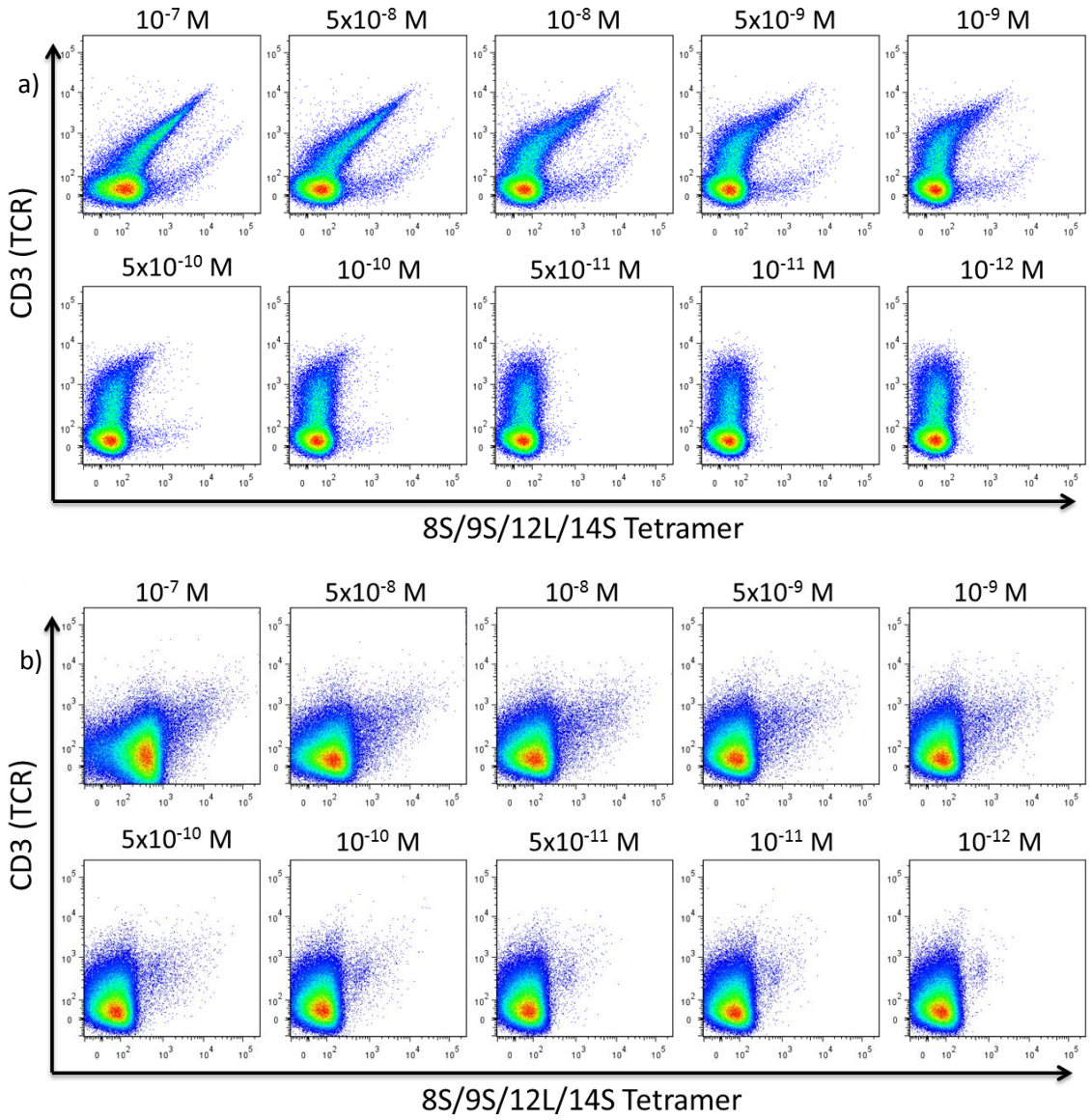

Figure 68. Comparison of TCR density and HCV NS3:1406-1415 (8S/9S/12L/14S) tetramer staining by HCV1406 Jurkat and Jurkat76 cells. (a) CD3 serves as a surrogate marker for HCV1406 TCR expression in Jurkat76 cells. **(b)** CD34 serves as a surrogate marker for HCV1406 TCR exprssion in Jurkat cells. Concentrations indicate amount of tetramer used to stain $1x10^6$ cells.

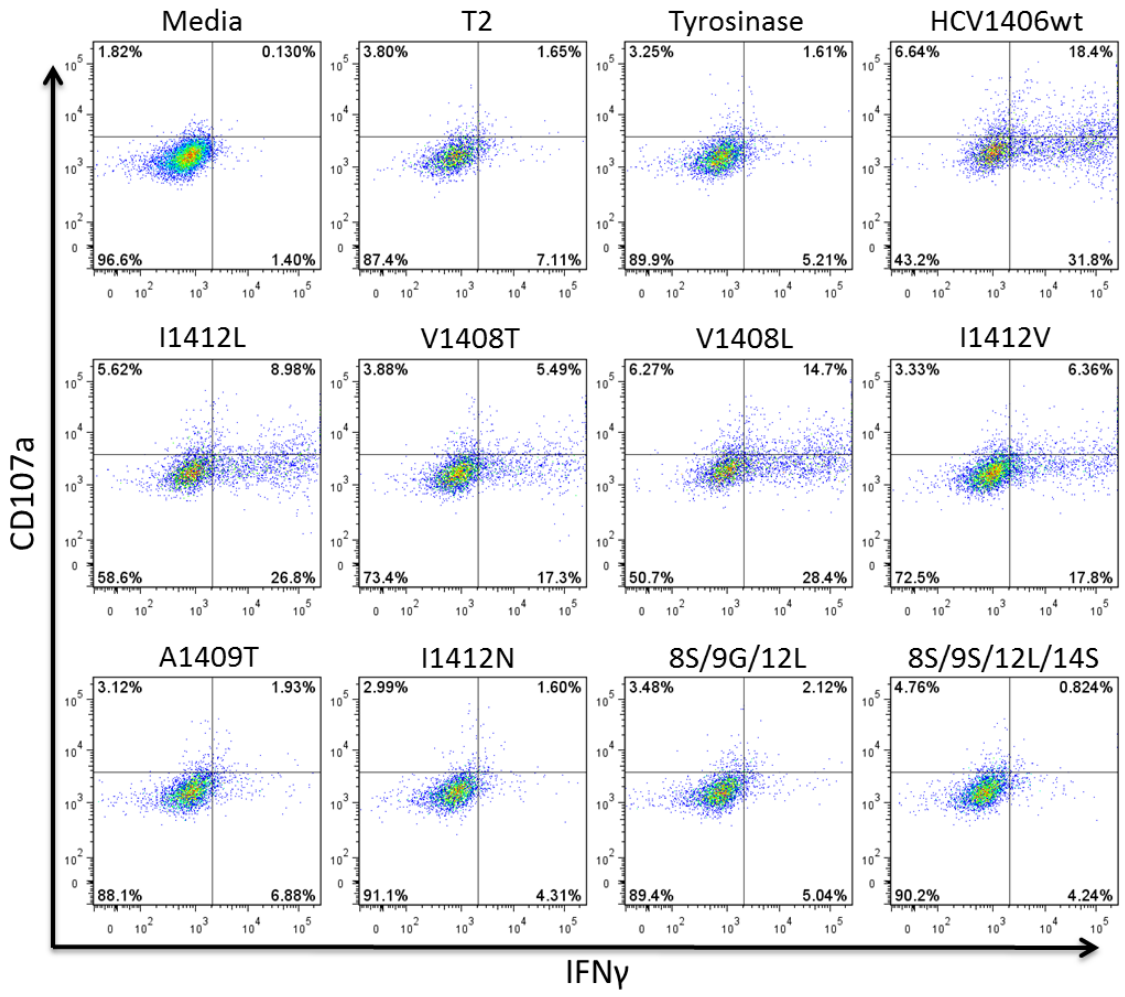

Figure 69. Evaluation of CD107a and intracellular IFNγ expression by $CD4^+$ HCV1406 TCR-transduced T cells stimulated with variant HCV NS3:1406-1415 peptides. HCV1406 TCR-transduced PBL were co-cultured for 5 hr with T2 cells loaded with WT and mutant HCV NS3:1406-1415 or tyrosinase:368-376 peptides and stained for immunofluorescence. $CD3^+CD34^+CD4^+CD8^-$ T cells were identified and evaluated for CD107a vs IFNγ expression. These data were used to create pie charts displayed in Figures 39.

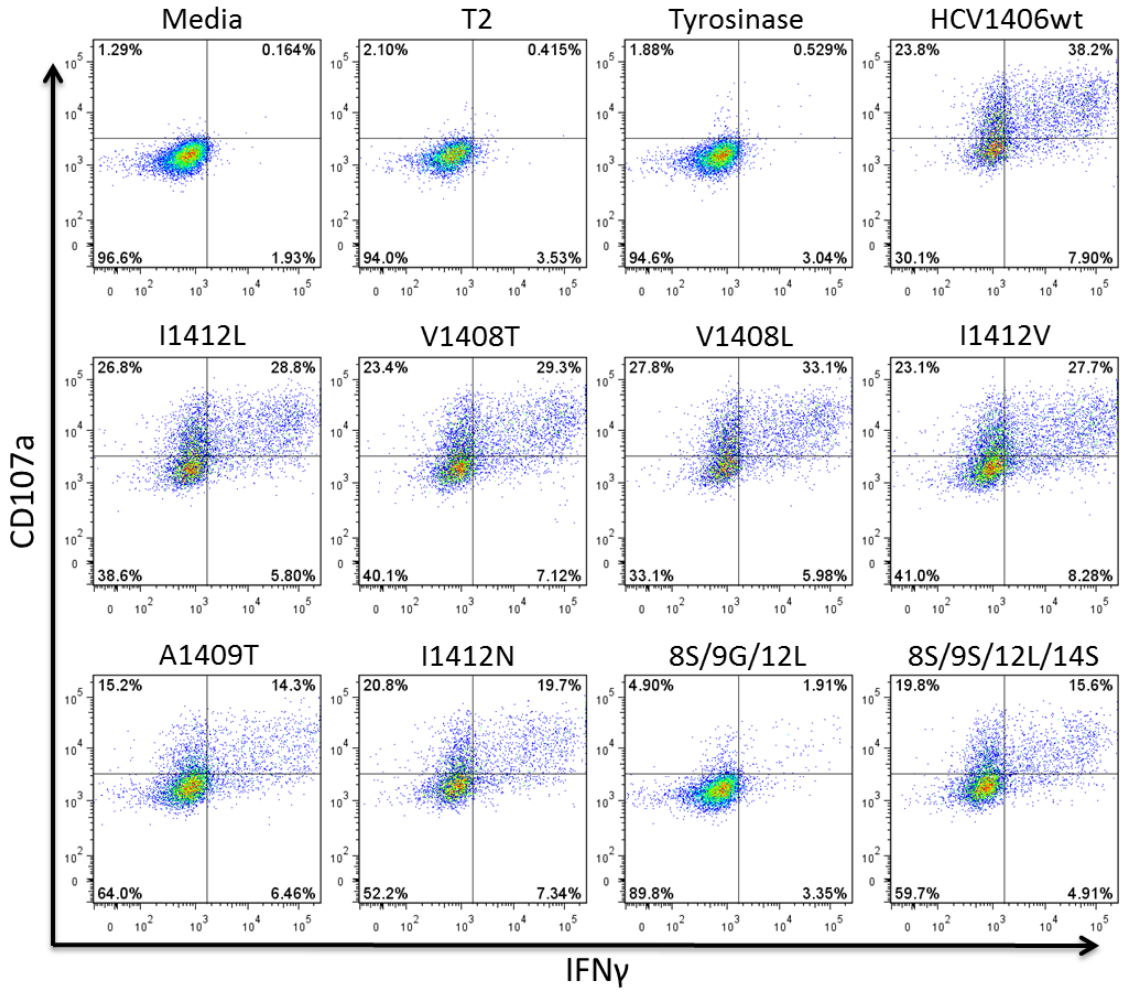

Figure 70. Evaluation of CD107a and intracellular IFNγ expression by $CD8^+$ HCV1406 TCR-transduced T cells stimulated with variant HCV NS3:1406-1415 peptides. HCV1406 TCR-transduced PBL were co-cultured for 5 hr with T2 cells loaded with WT and mutant HCV NS3:1406-1415 or tyrosinase:368-376 peptides and stained for immunofluorescence. $CD3^+CD34^+CD4^-CD8^+$ T cells were identified and evaluated for CD107a vs IFNγ expression. These data were used to create pie charts displayed in Figures 39-40.

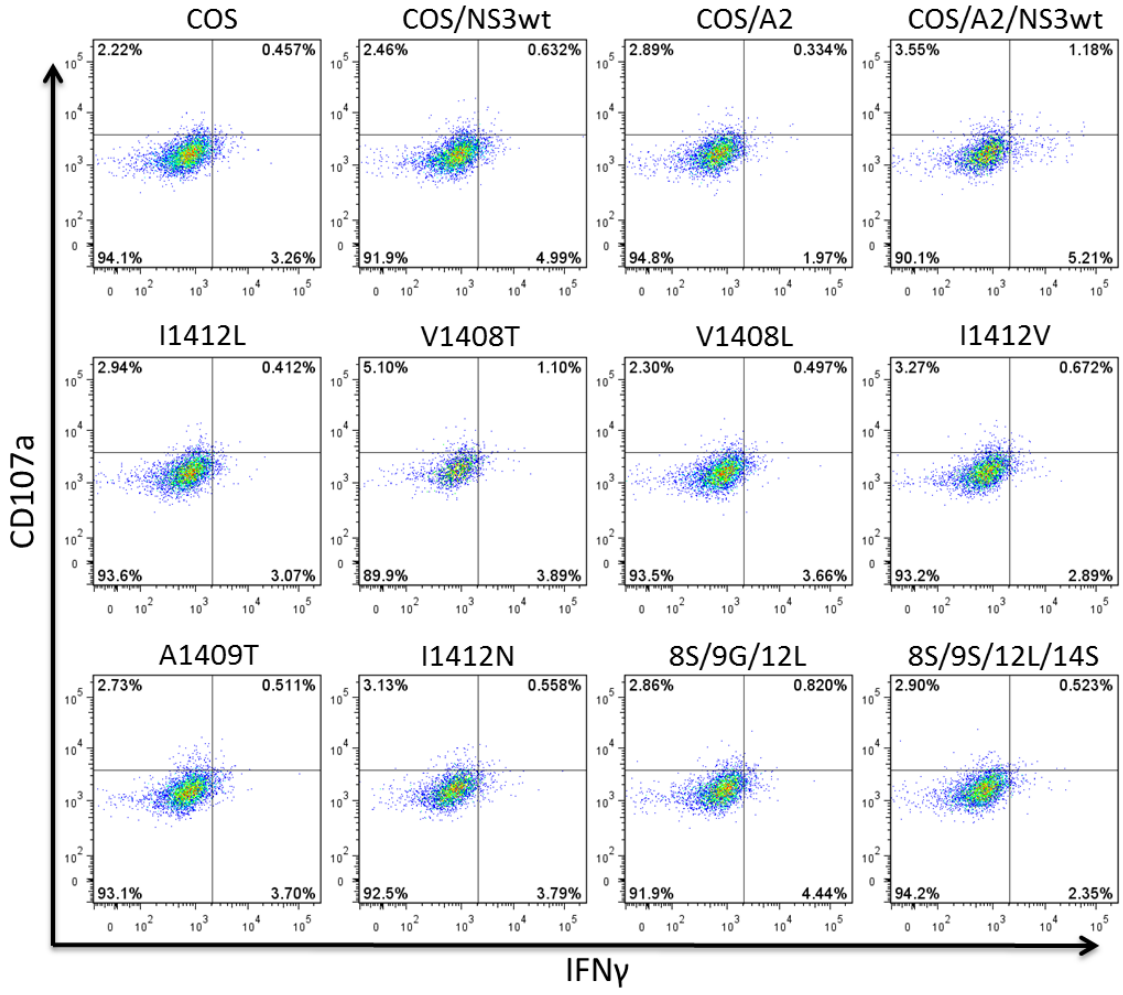

Figure 71. Evaluation of CD107a and intracellular IFNγ expression by $CD4^+$ HCV1406 TCR-transduced T cells stimulated with variant naturally processed HCV NS3. COS cells were transfected to express full length WT HCV NS3 and COS/A2 cells were transfected to express full length HCV NS3 with WT or variant 1406-1415 epitopes. HCV1406 TCR-transduced PBL were co-cultured with transfected COS cells for 5 hr and stained for immunofluorescence. $CD3^+CD34^+CD4^+CD8^-$ T cells were identified and evaluated for CD107a vs IFNγ expression. These data were used to create pie charts displayed in Figure 41.

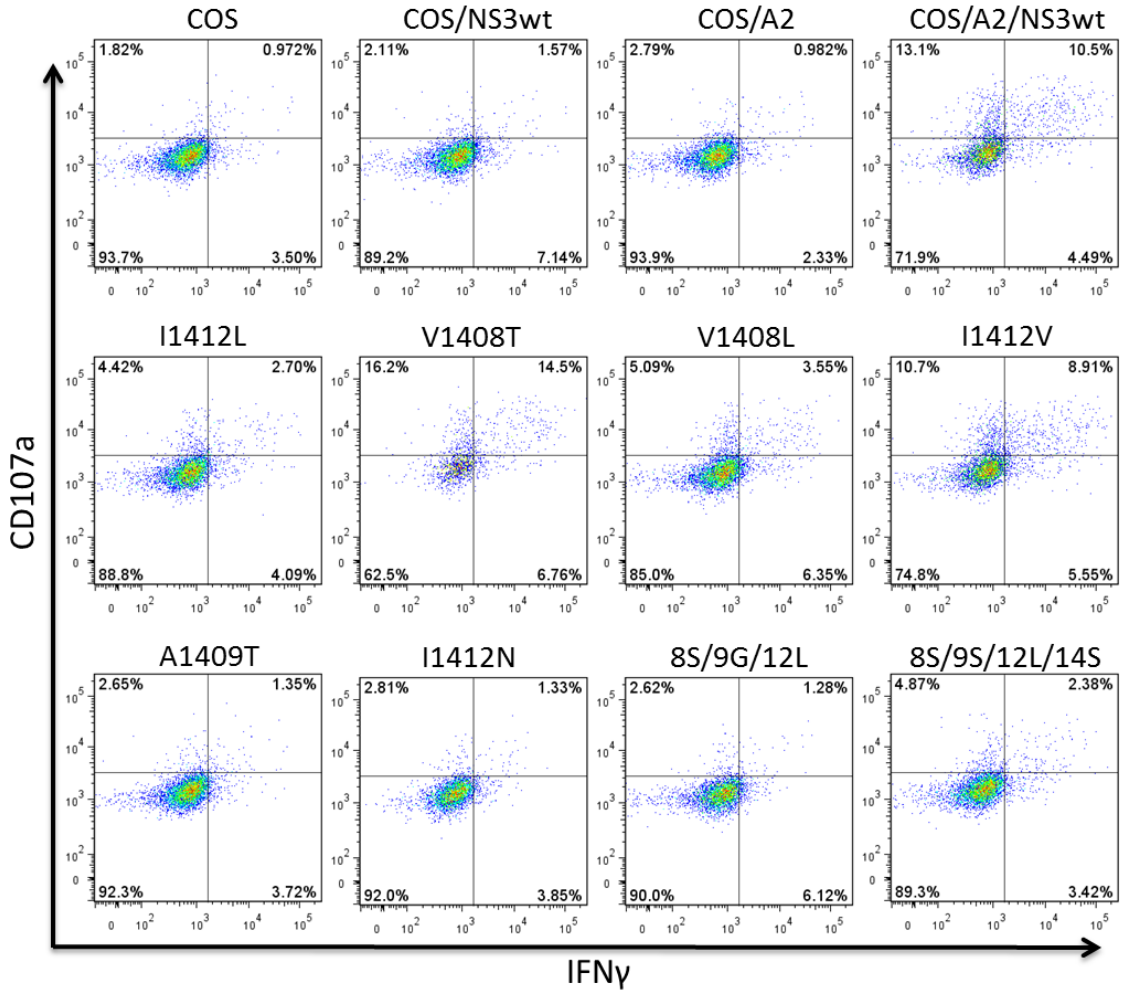

Figure 72. Evaluation of CD107a and intracellular IFNγ expression by $CD8^+$ HCV1406 TCR-transduced T cells stimulated with variant naturally processed HCV NS3. COS cells were transfected to express full length WT HCV NS3 and COS/A2 cells were transfected to express full length HCV NS3 with WT or variant 1406-1415 epitopes. HCV1406 TCR-transduced PBL were co-cultured with transfected COS cells for 5 hr and stained for immunofluorescence. $CD3^+CD34^+CD4^-CD8^+$ T cells were identified and evaluated for CD107a vs IFNγ expression. These data were used to create pie charts displayed in Figures 41-42.

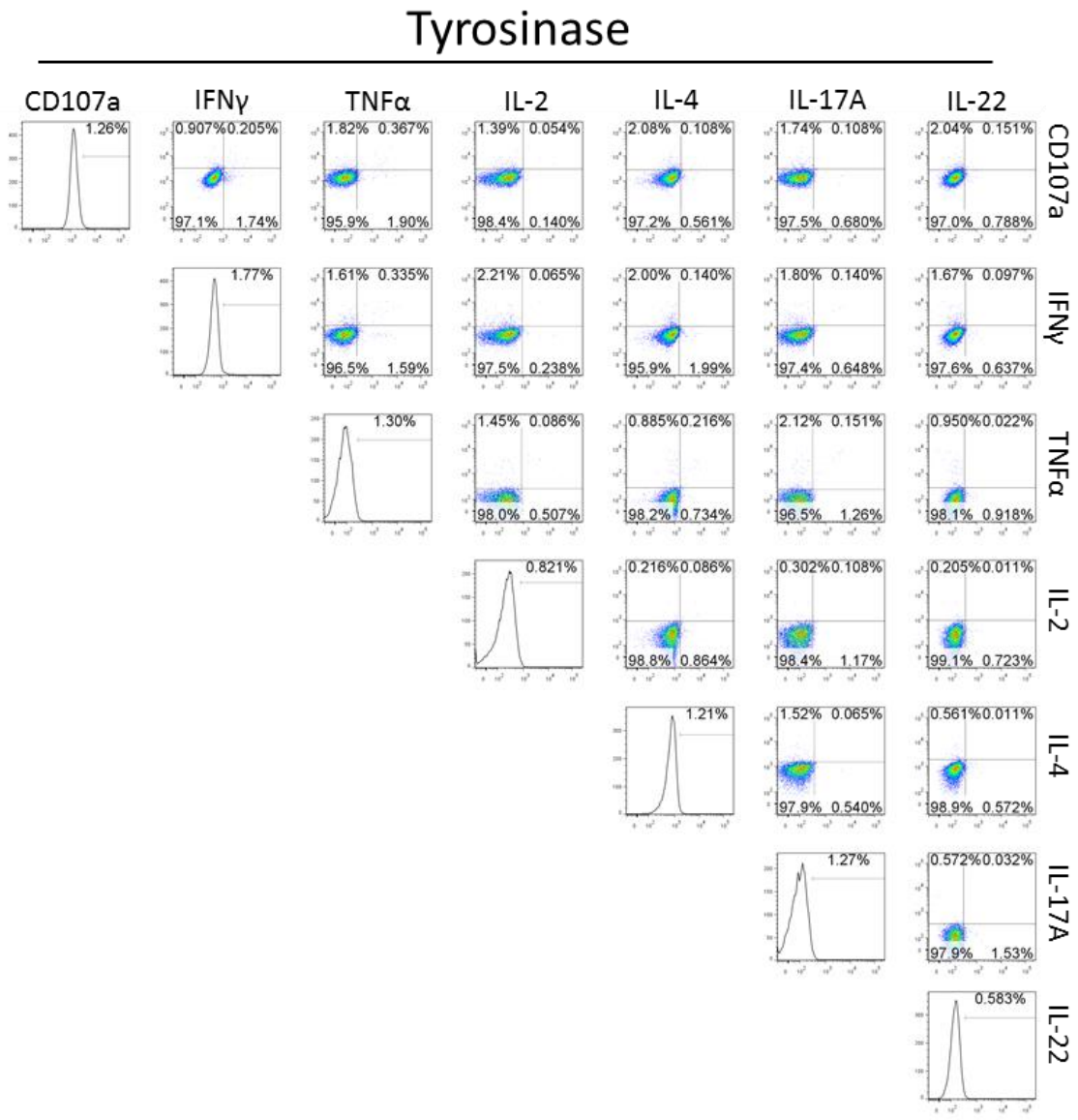

Figure 73. FlowJo-generated seven-parameter pairwise matrix displaying how gates are set against tyrosinase:368-376 peptide stimulation. Gates were set for non-specific (tyrsoinase) peptide stimulation and applied to HCV1406 TCR-transduced T cells stimulated WT HCV NS3:1405-1415 peptide-loaded T2 cells. Compare to Figure 44.

Figure 74. Polyfunctional profiles of CD4^{+} vs CD8^{+} HCV1406 TCR-transduced T cells after stimulation with WT HCV NS3:1405-1415 peptide-loaded T2 cells. Compare to Figure 46 for condensed SPICE-generated bar graph. Percentages represent frequencies after background subtraction from tyronsiase peptide stimulation.

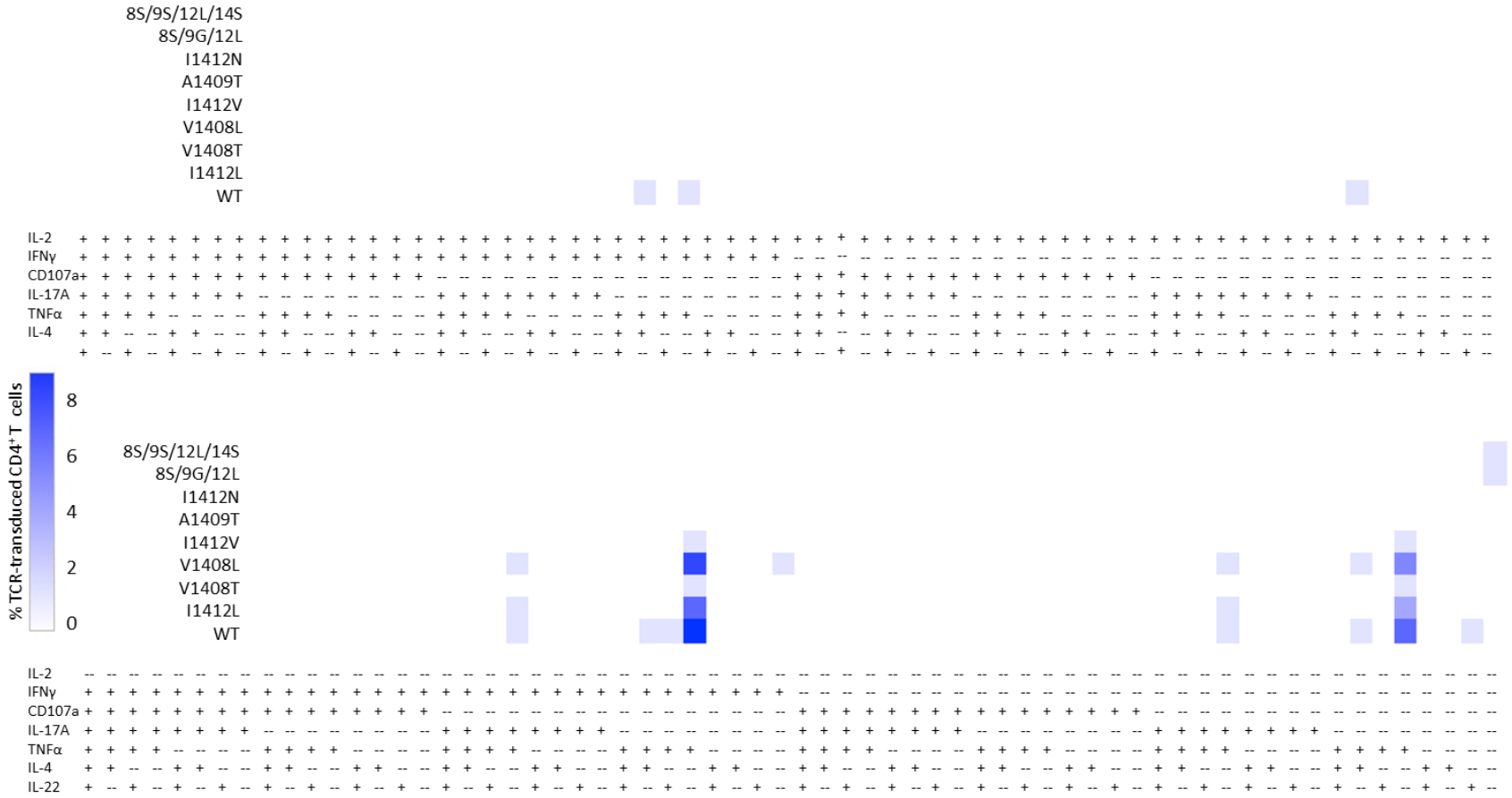

Figure 75. Polyfunctional profiles of CD4$^+$ HCV1406 TCR-transduced T cells after stimulation with WT and various mutant HCV NS3:1405-1415 peptide-loaded T2 cells (Donor 1). Compare to Figures 48-49 for condensed cool plots. Percentages represent frequencies after background subtraction from tyronsiase peptide stimulation.

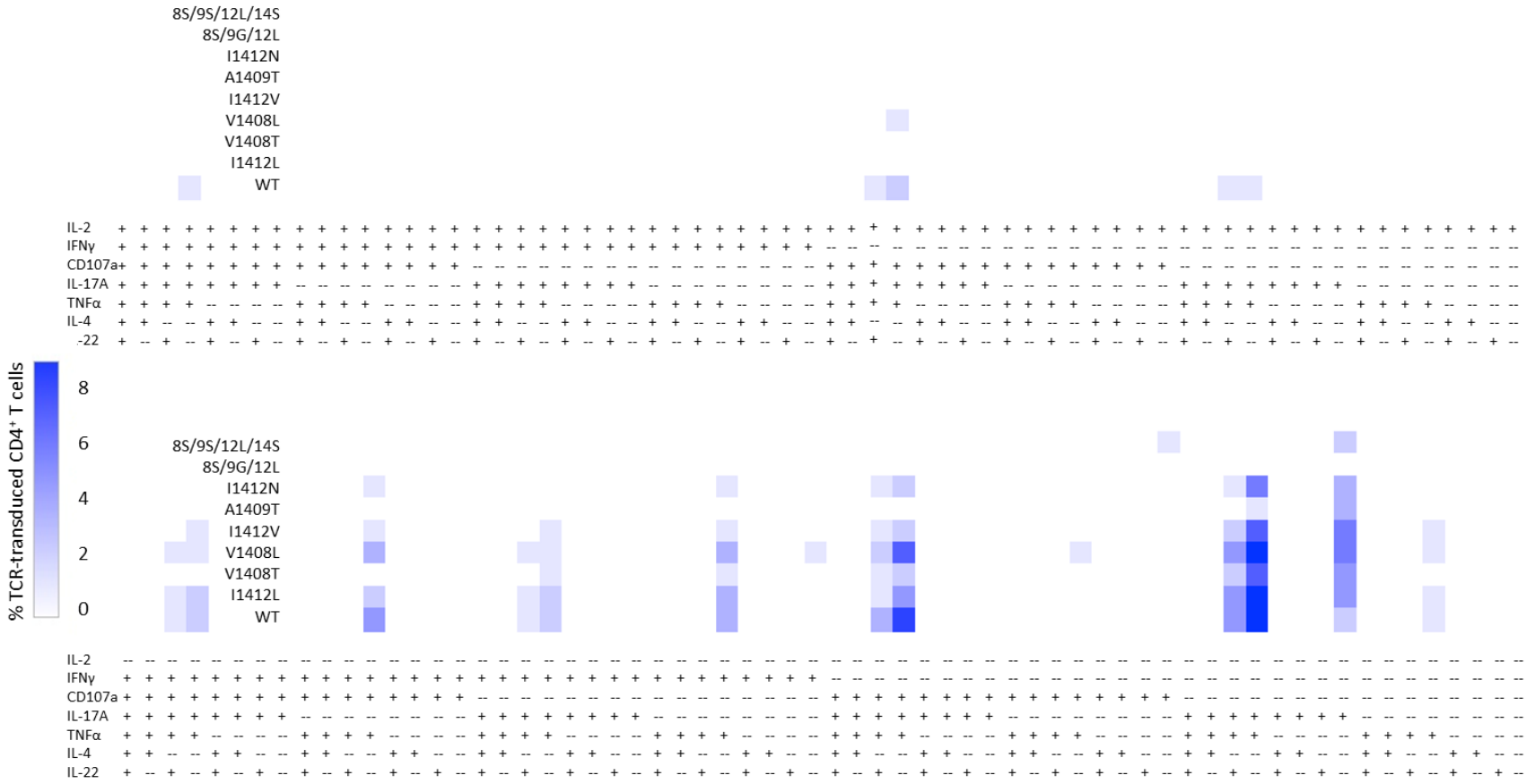

Figure 76. Polyfunctional profiles of CD4+ HCV1406 TCR-transduced T cells after stimulation with WT and various mutant HCV NS3:1405-1415 peptide-loaded T2 cells (Donor 2). Compare to Figure 49 for condensed cool plot. Percentages represent frequencies after background subtraction from tyronsiase peptide stimulation.

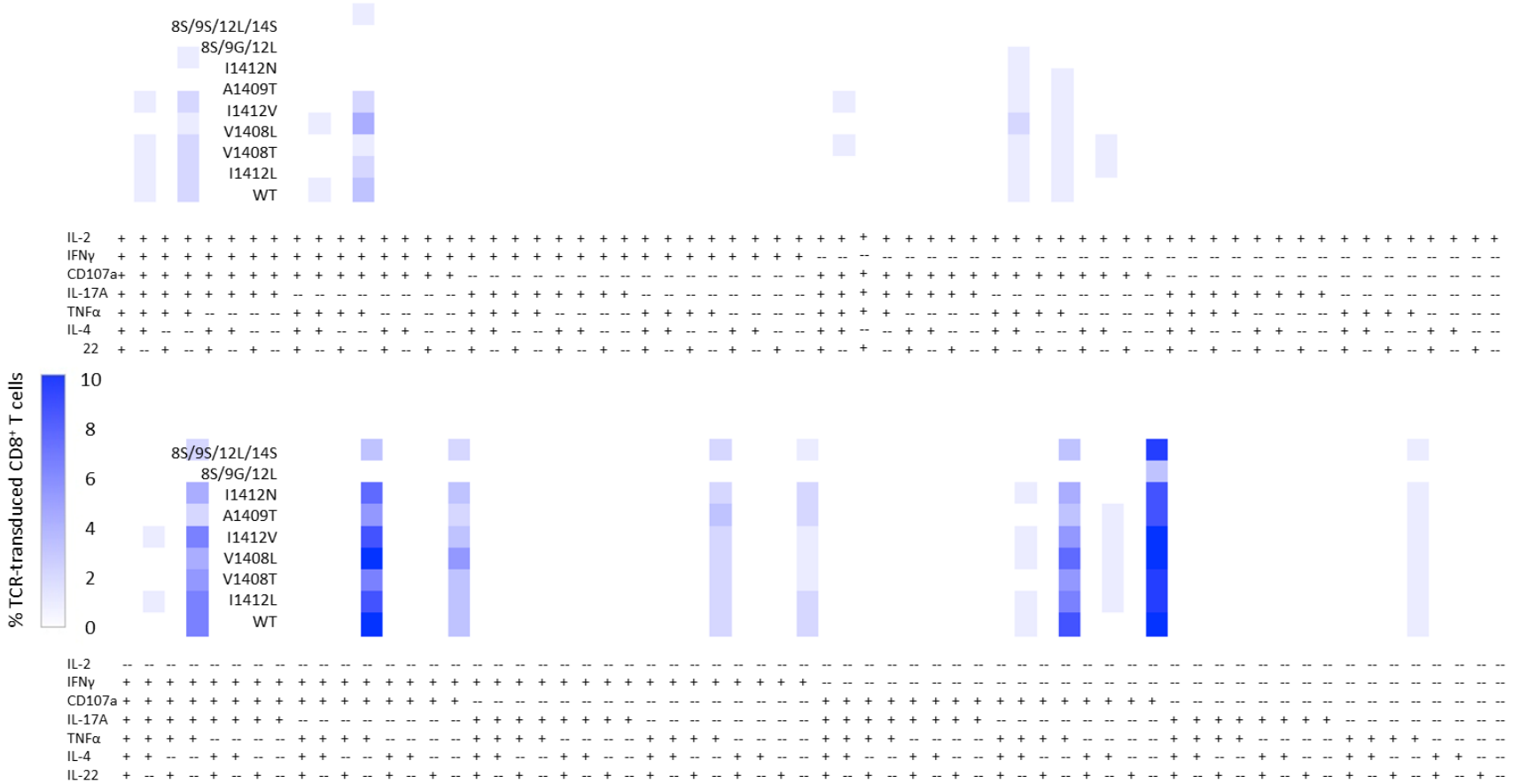

Figure 77. Polyfunctional profiles of CD8$^+$ HCV1406 TCR-transduced T cells after stimulation with WT and various mutant HCV NS3:1405-1415 peptide-loaded T2 cells (Donor 2). Compare to Figures 50-51 for condensed cool plots. Percentages represent frequencies after background subtraction from tyronsiase peptide stimulation.

Figure 78. Polyfunctional profiles of CD4$^+$ HCV1406 TCR-transduced T cells after stimulation with WT and various mutant HCV NS3 expressing HepG2 cells (Donor 2). T cells are non-reactive above background. Percentages represent frequencies after background subtraction from HCV$^-$ HepG2 peptide stimulation.

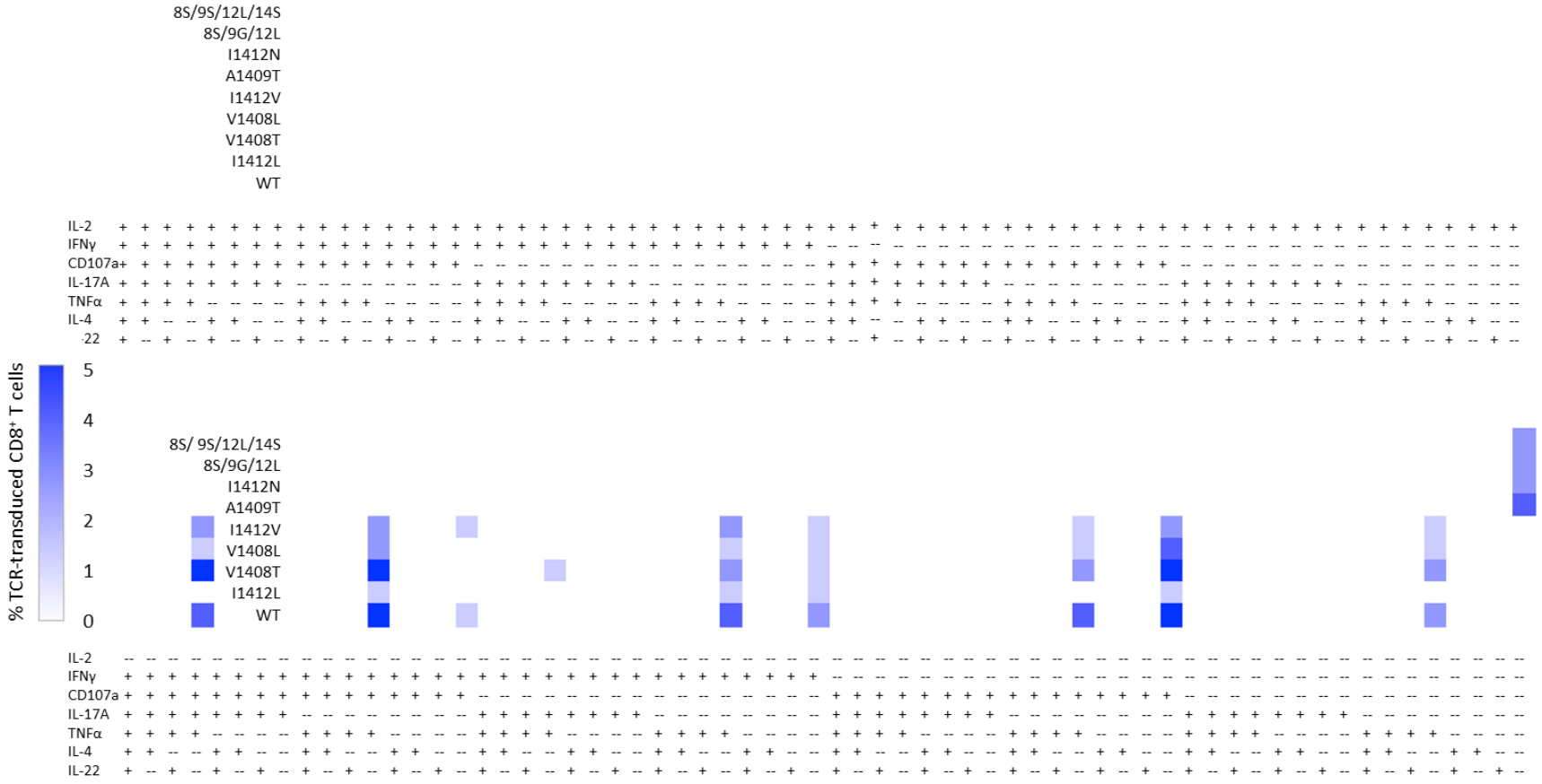

Figure 79. Polyfunctional profiles of CD8$^+$ HCV1406 TCR-transduced T cells after stimulation with WT and various mutant HCV NS3 expressing HepG2 cells (Donor 2). Compare to Figure 52 for condensed cool plot. Percentages represent frequencies after background subtraction from HCV$^-$ HepG2 peptide stimulation.

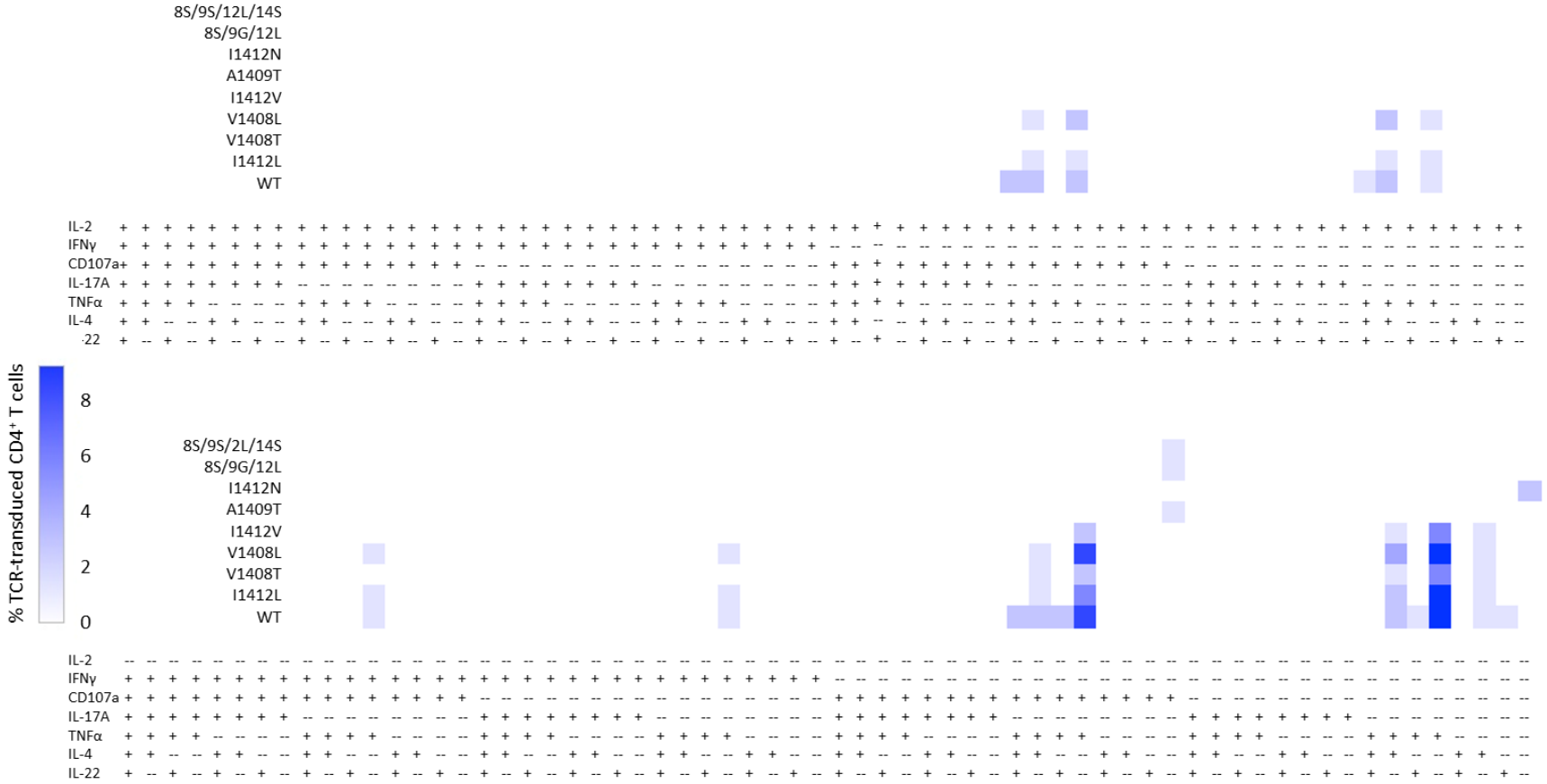

Figure 80. Polyfunctional profiles of CD4+ HCV1406 TCR-transduced T cells after stimulation with WT and various mutant HCV NS3:1405-1415 peptide-loaded T2 cells (Donor 3). Percentages represent frequencies after background subtraction from tyronsiase peptide stimulation.

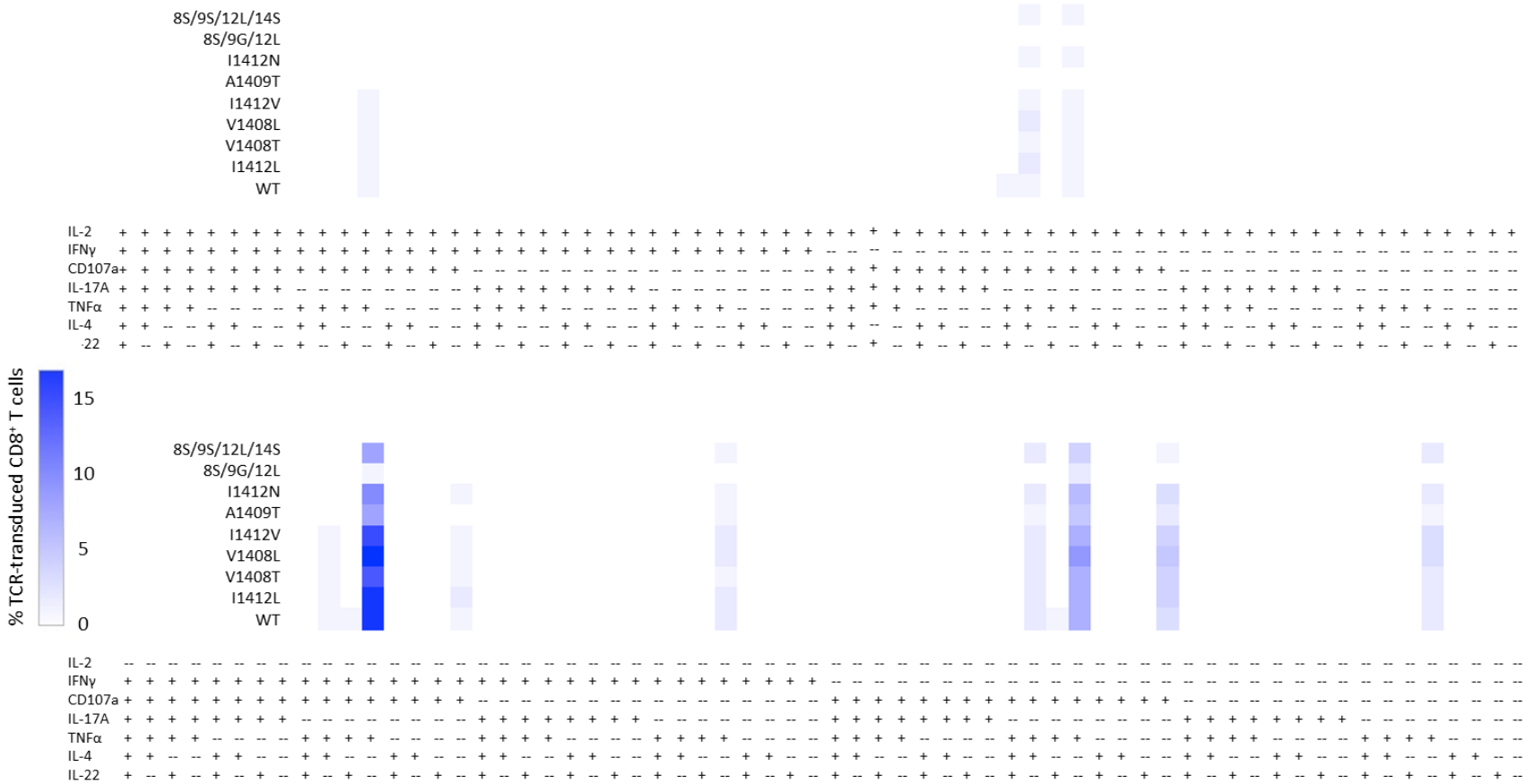

Figure 81. Polyfunctional profiles of CD8+ HCV1406 TCR-transduced T cells after stimulation with WT and various mutant HCV NS3:1405-1415 peptide-loaded T2 cells (Donor 3). Percentages represent frequencies after background subtraction from tyronsiase peptide stimulation.

Figure 82. Polyfunctional profiles of CD4$^+$ HCV1406 TCR-transduced T cells after stimulation with WT and various mutant HCV NS3 expressing HepG2 cells (Donor 3). Percentages represent frequencies after background subtraction from HCV$^-$ HepG2 peptide stimulation.

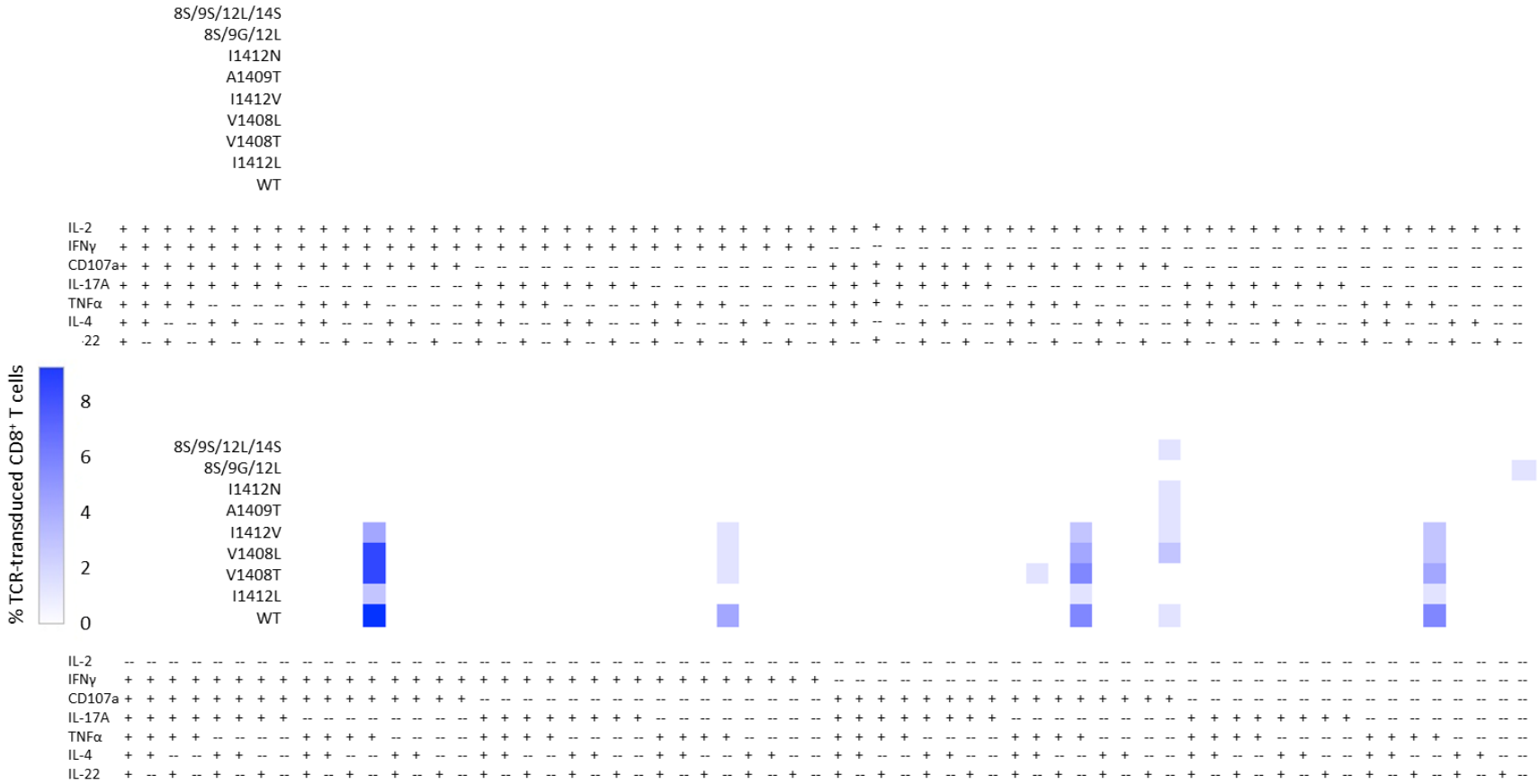

Figure 83. Polyfunctional profiles of CD8$^+$ HCV1406 TCR-transduced T cells after stimulation with WT and various mutant HCV NS3 expressing HepG2 cells (Donor 3). Percentages represent frequencies after background subtraction from HCV$^-$ HepG2 peptide stimulation.

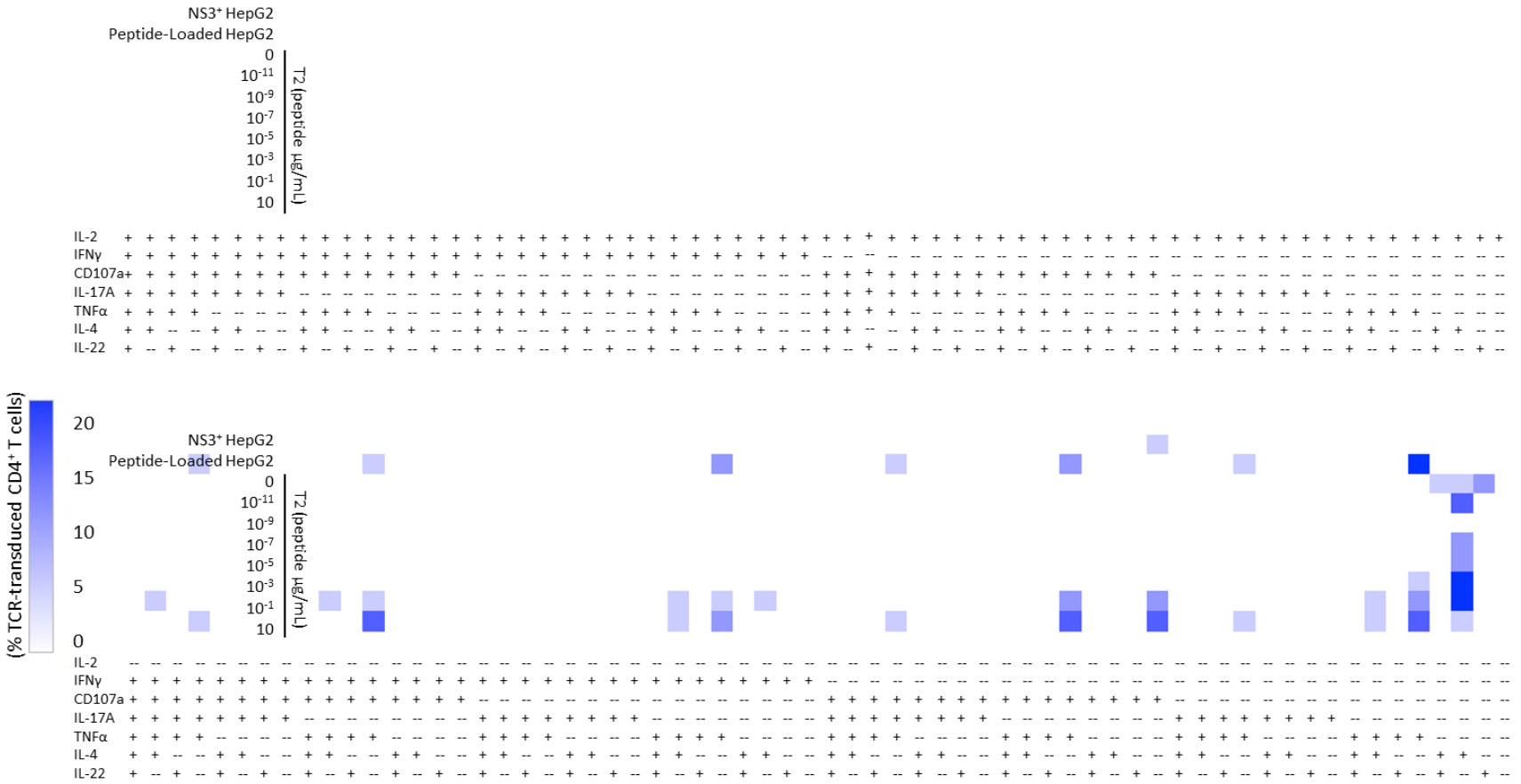

Figure 84. Polyfunctional profiles of CD4$^+$ HCV1406 TCR-transduced T cells after stimulation with a peptide titration of WT HCV NS3:1406-1415 (Donor 3). Compare to Figure 53. Percentages represent frequencies after background subtraction from tyronsiase peptide stimulation.

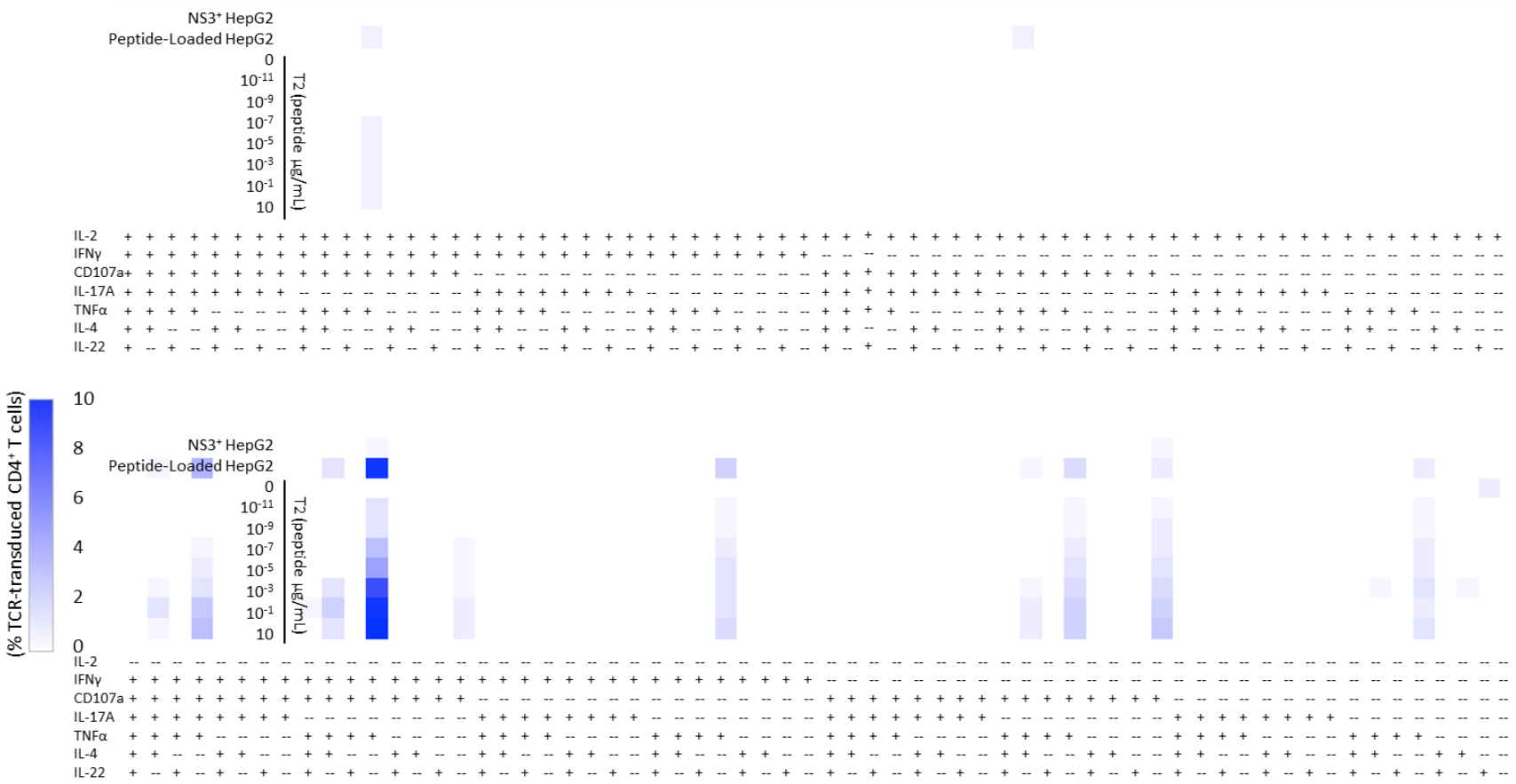

Figure 85. Polyfunctional profiles of CD8$^+$ HCV1406 TCR-transduced T cells after stimulation with a peptide titration of WT HCV NS3:1406-1415 (Donor 3). Compare to Figure 49. Percentages represent frequencies after background subtraction from tyronsiase peptide stimulation.

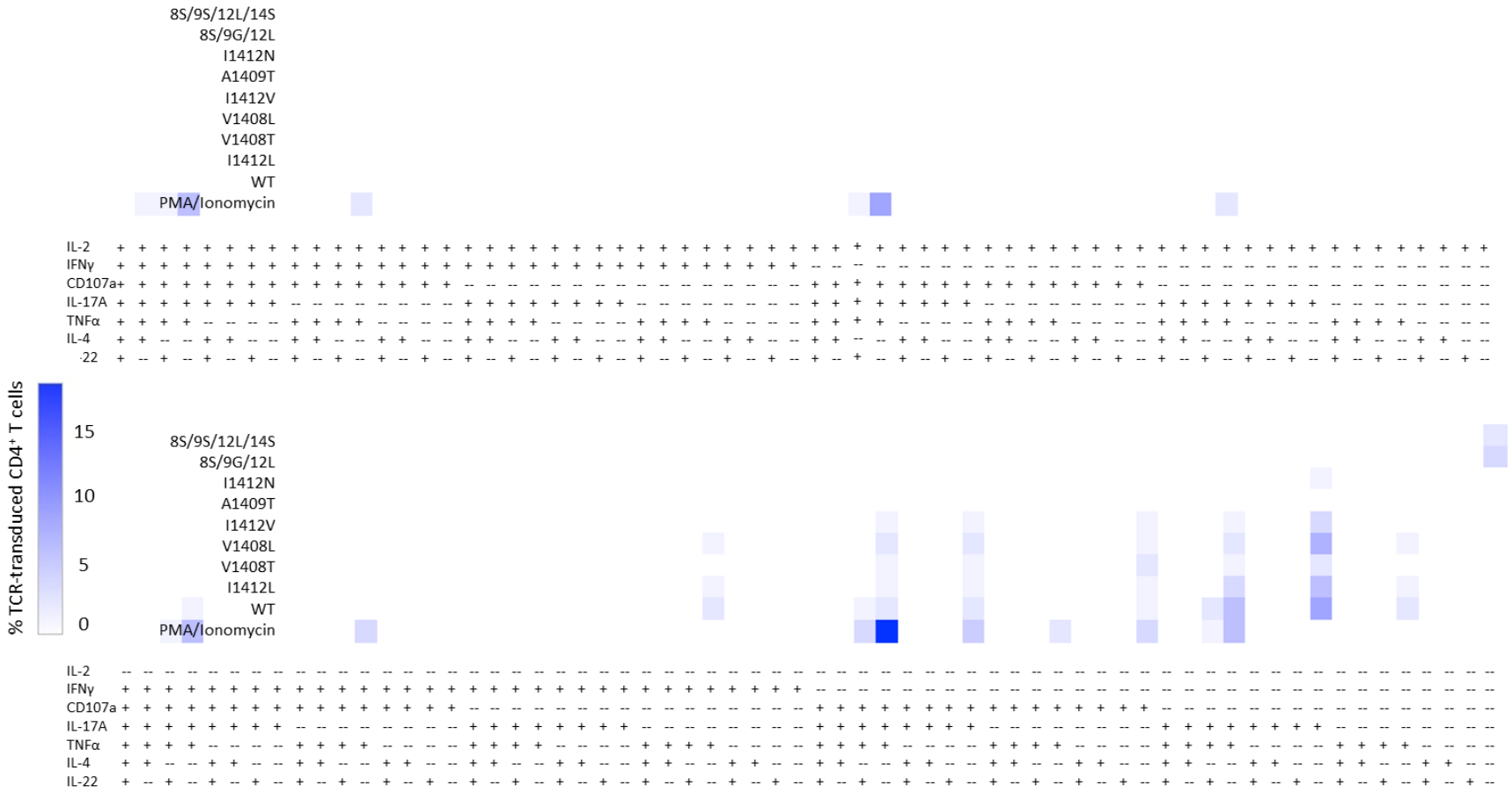

Figure 86. Comparison of CD4$^+$ T cell polyfunctional profiles between TCR-independent and TCR-dependent T cell activation (Donor 2). HCV1406 TCR-transduced CD4$^+$ T cells were stimulated with peptide-loaded T2 cells or PMA/Ionomycin. Percentages represent frequencies after background subtraction from tyronsiase peptide stimulation.

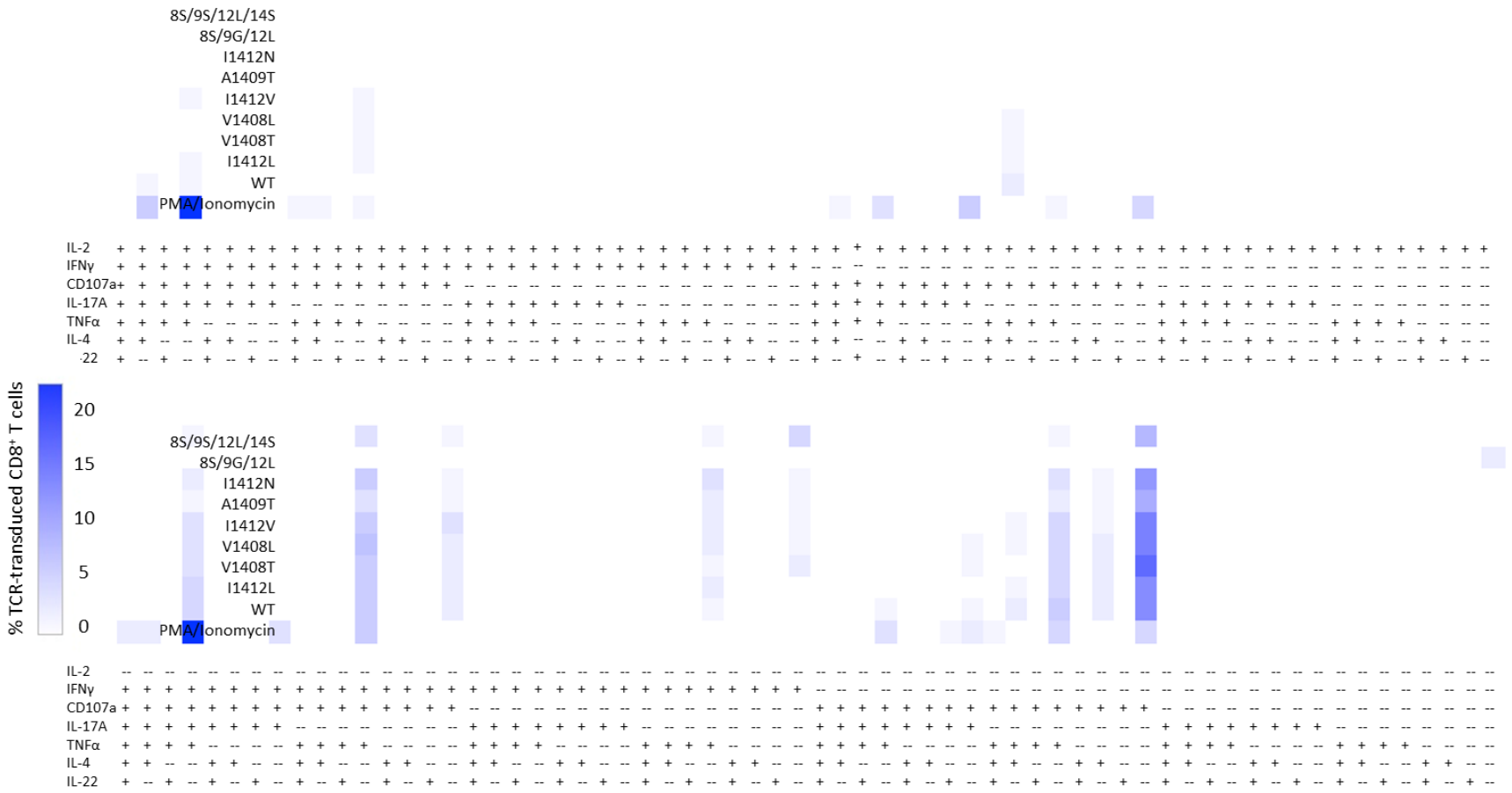

Figure 87. Comparison of CD8$^+$ T cell polyfunctional profiles between TCR-independent and TCR-dependent T cell activation (Donor 2). HCV1406 TCR-transduced CD8$^+$ T cells were stimulated with peptide-loaded T2 cells or PMA/Ionomycin. Percentages represent frequencies after background subtraction from tyronsiase peptide stimulation.

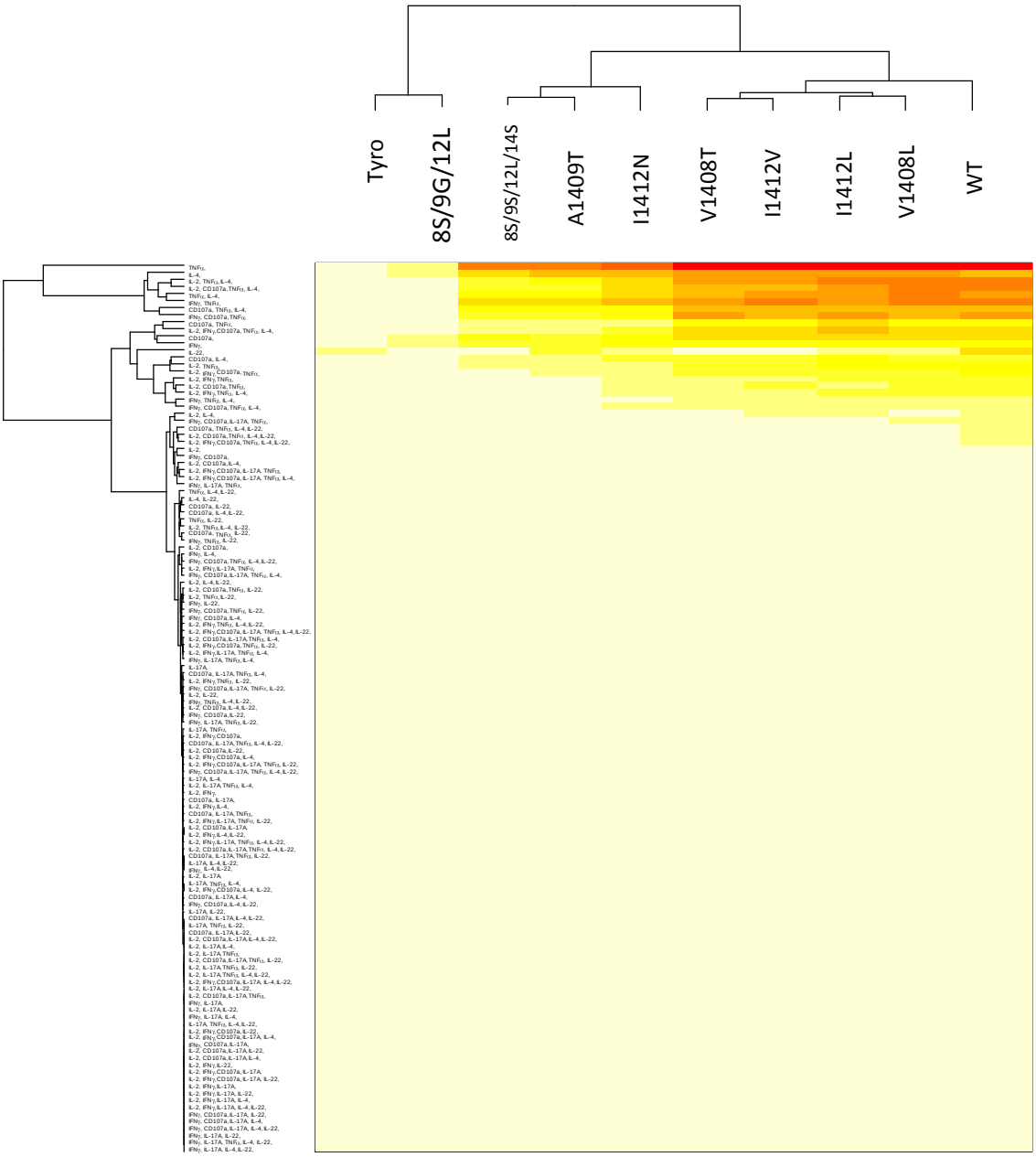

Figure 88. Hierarchical clustering of peptide-stimulated responses of TCR-transduced CD8$^+$ T cells (Donor 1).

Figure 89. Hierarchical clustering of peptide-stimulated repsonses of TCR-transduced CD4^{+} T cells (Donor 1).

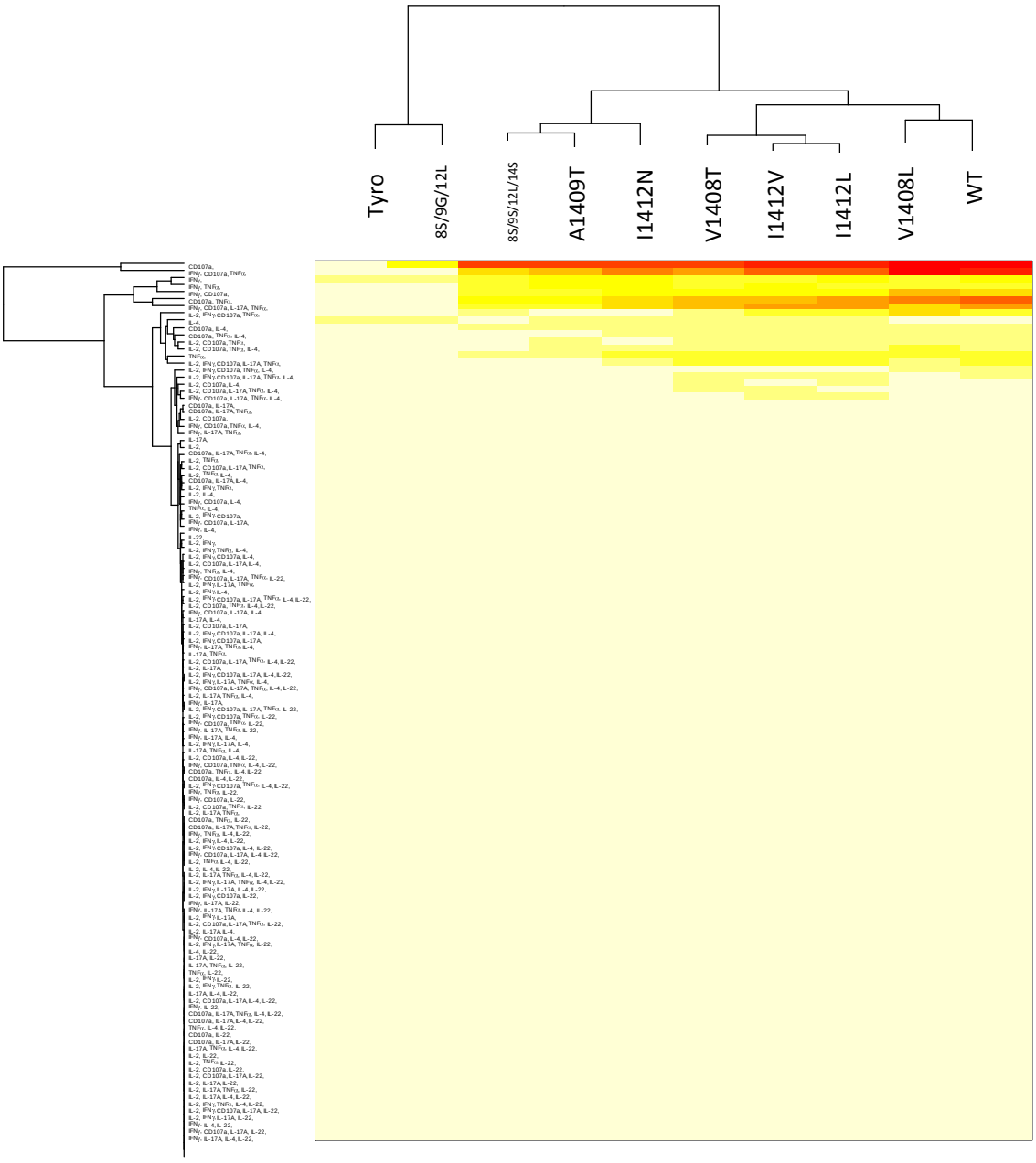

Figure 90. Hierarchical clustering of peptide-stimulated responses of TCR-transduced CD8$^+$ T cells (Donor 2).

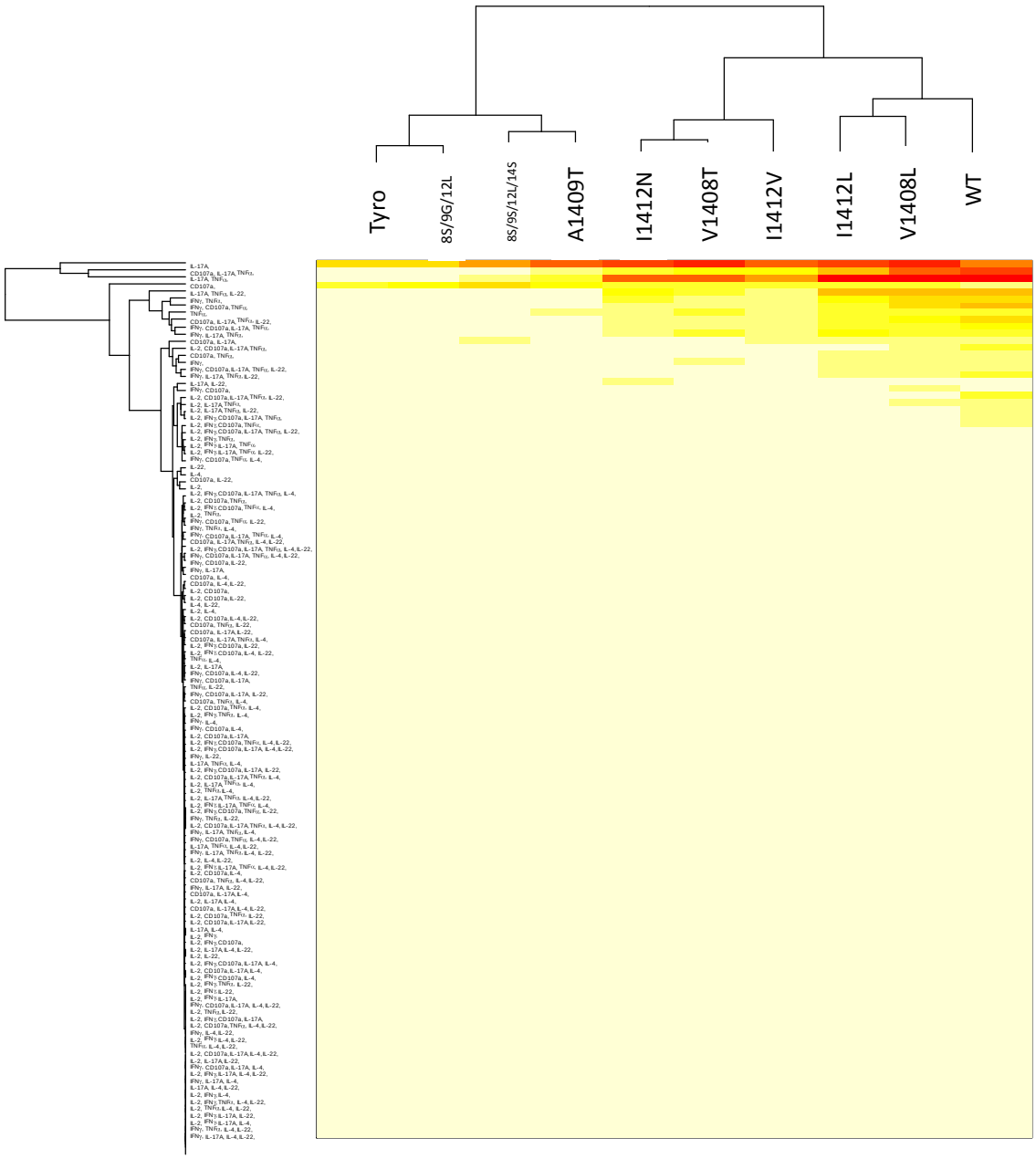

Figure 91. Hierarchical clustering of peptide-stimulated responses of TCR-transduced CD4^{+} T cells (Donor 2).

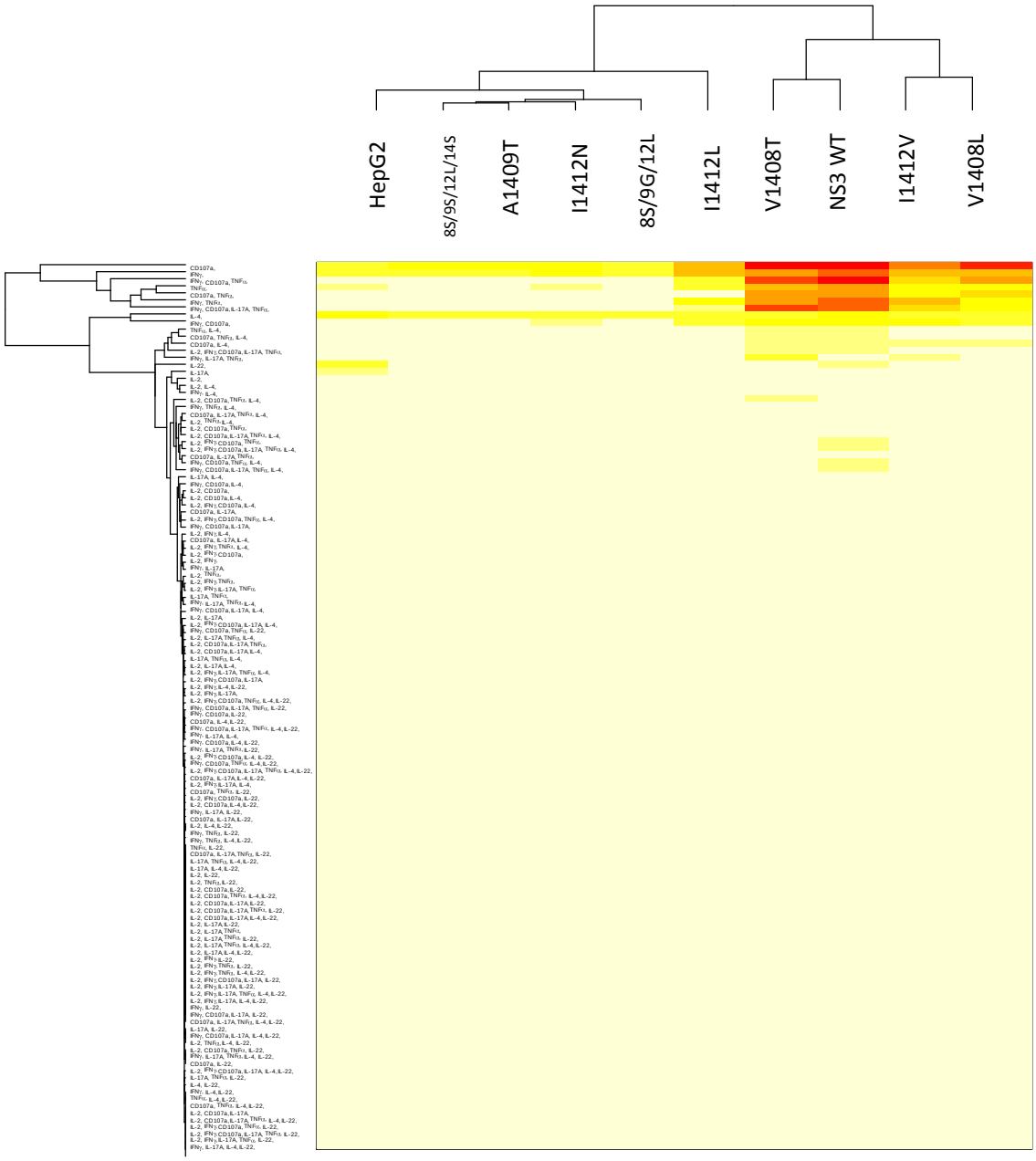

Figure 92. Hierarchical clustering of tumor-stimulated responses of TCR-transduced CD8^{+} T cells (Donor 2).

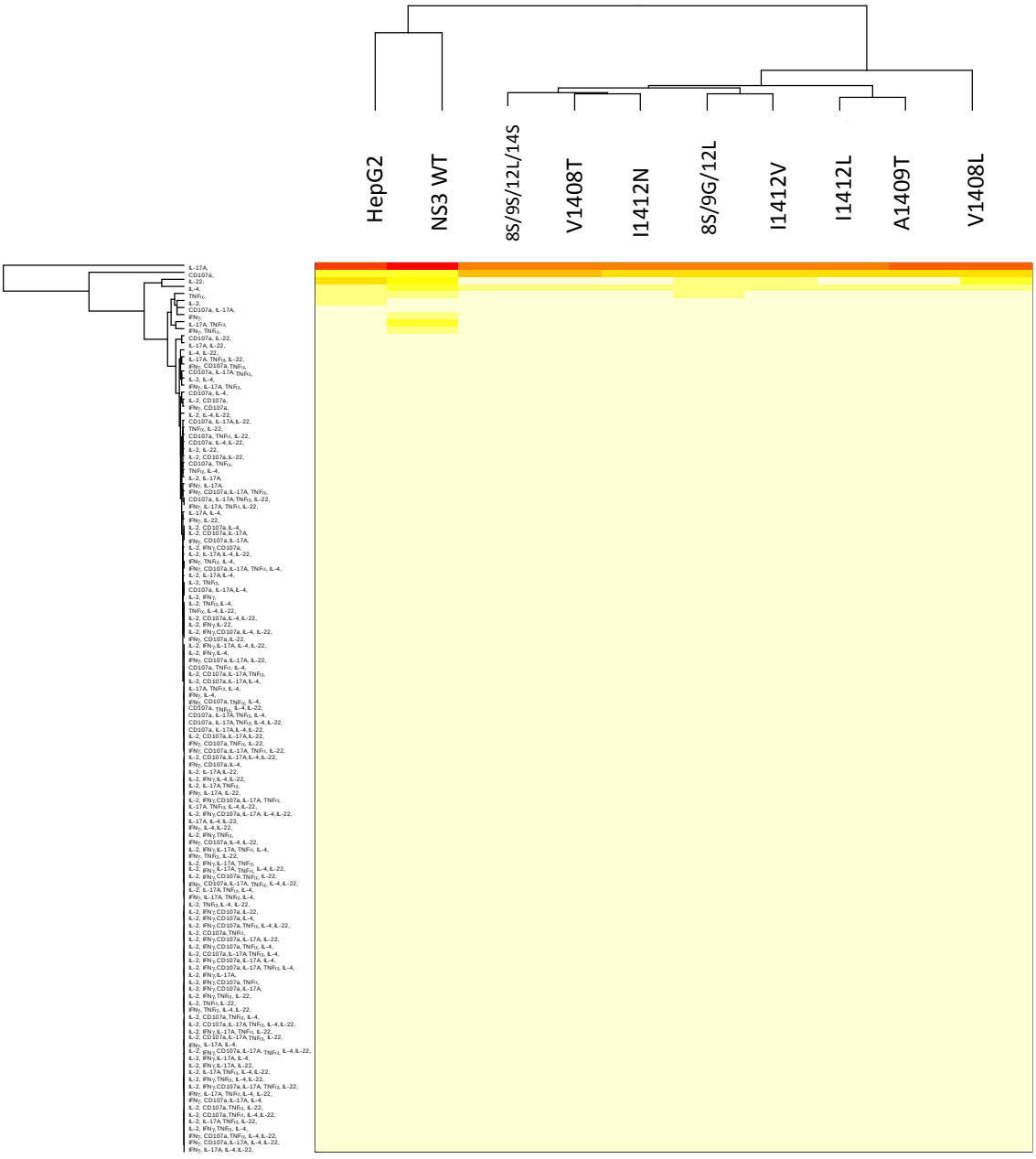

Figure 93. Hierarchical clustering of tumor-stimulated responses of TCR-transduced CD4$^+$ T cells (Donor 2).

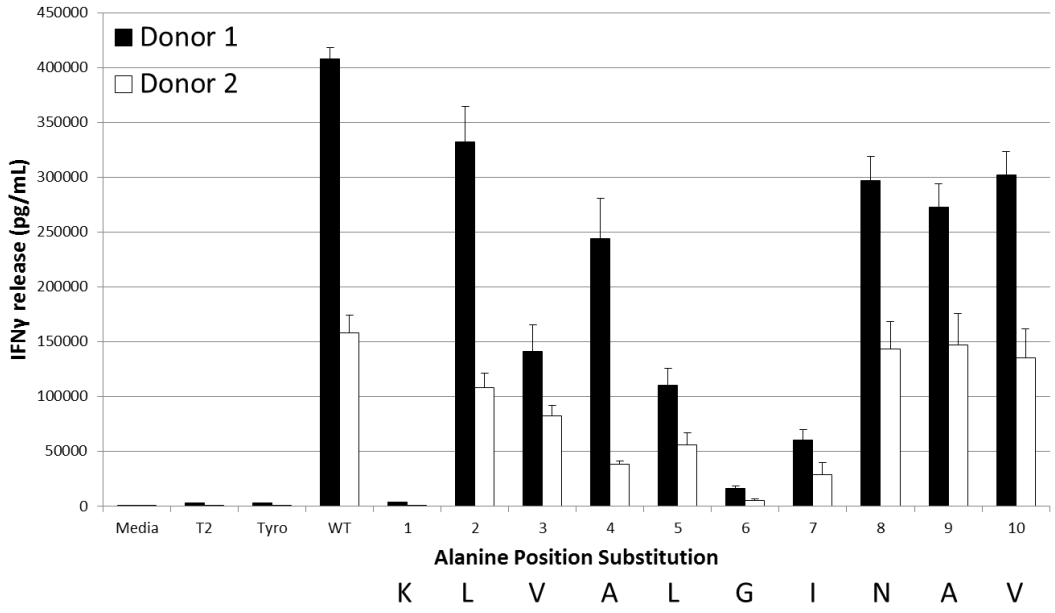

Figure 94. Cross-reactivity against alanine-substituted HCV NS3:1406-1415 peptides by HCV1406 TCR-transduced PBL-derived T cells. PBL from two normal donors were transduced with the HCV1406 TCR retroviral vector and were enriched for CD34-expressing cells. T2 cells were loaded with 10 µg/mL HCV NS3:1406-1415, alanine substituted peptides (isoleucine substitutions at positions 4 and 9), or tyrosinase:368-376. IFNγ release was determined by ELISA. Mean and standard deviation of triplicate measurements are shown. These data are a representative of two independent experiments using two donors each.

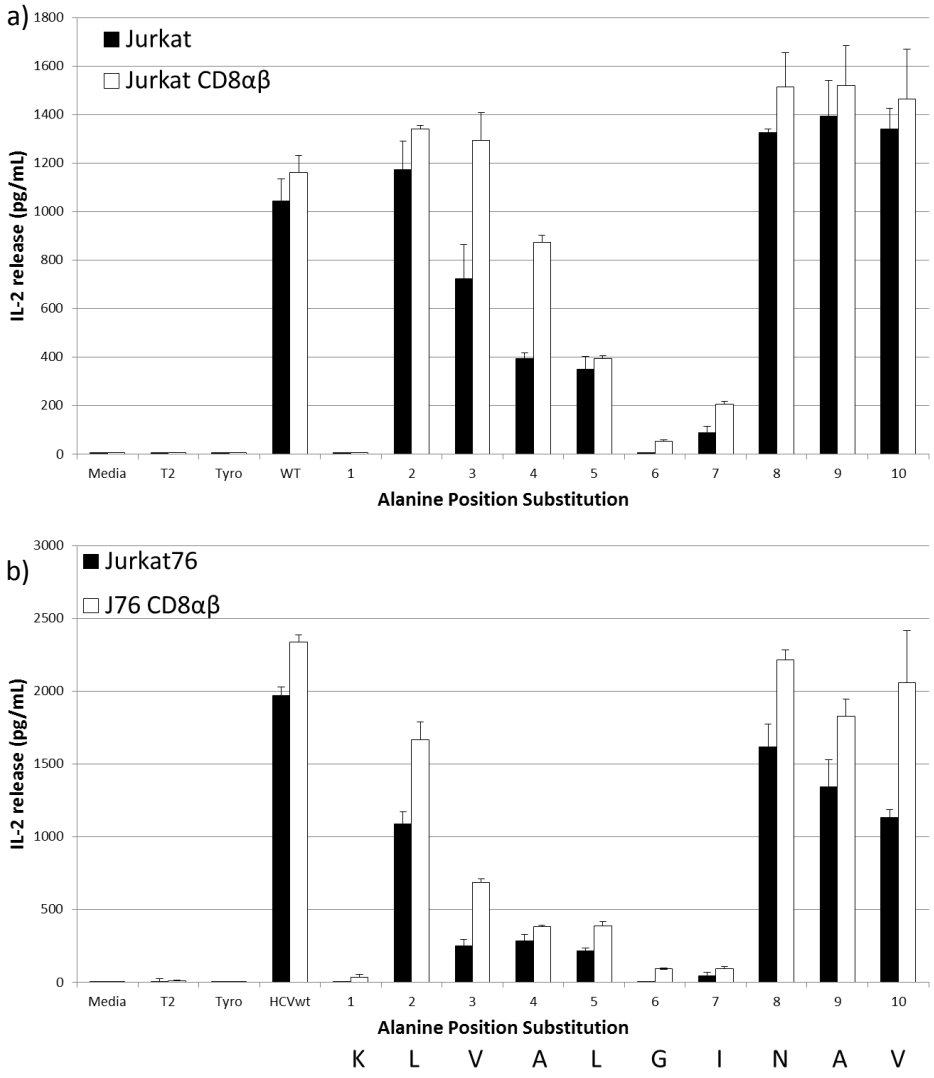

Figure 95. HCV1406 TCR-transduced Jurkat and Jurkat76 cells exhibit similar cross-reactive profiles against alanine-substituted HCV NS3:1406-1415 peptides. (a) Jurkat or **(b)** Jurkat76 cells were transduced with the HCV1406 TCR retroviral vector. Transduced cells were enriched for CD34-expression. T2 cells were loaded with 10 µg/mL HCV NS3:1406-1415, alanine substituted peptides (isoleucine substitutions at positions 4 and 9), or tyrosinase:368-376. IFNγ release was determined by ELISA. Mean and standard deviation of triplicate measurements are shown. These data are representative of two independent experiments.

Table 16. Comparison of cross-reactive profiles against alanine-substituted HCV NS3:1406-1415 peptides.

Epitope	Sequence	PBL*	WT Jurkat		Jurkat76	
			CD8–	CD8+	CD8–	CD8+
Tyrosinase	YMDGTMSQV		-	-	-	-
HCV1406wt	KLVALGINAV	+++	+++	+++	+++	+++
K1406A	**A**LVALGINAV	-	-	-	-	-
L1407A	K**A**VALGINAV	++	+++	+++	++	++
V1408A	KL**A**ALGINAV	++	++	+++	+	+
A1409I	KLV**I**LGINAV	++	+	++	+	++
L1410A	KLVA**A**GINAV	++	+	++	+	++
G1411A	KLVAL**A**INAV	-	-	-	-	-
I1412A	KLVALG**A**NAV	+	-	+	-	-
N1413A	KLVALGI**A**AV	+++	+++	+++	+++	+++
A1414I	KLVALGIN**I**V	+++	+++	+++	+++	+++
V1415A	KLVALGINA**A**	+++	+++	+++	+++	+++

*Two donor average

+++ = >75% WT reactivity; ++ = 25-75% WT reactivity; + = 25-5% WT reactivity; - <5% WT reactivity

These data portray comparisons of cytokine release shown in Figures 94-95 and are a representative of two independent experiments.

REFERENCES

1. Tian, S., et al., *CD8+ T cell activation is governed by TCR-peptide/MHC affinity, not dissociation rate.* J Immunol, 2007. **179**(5): p. 2952-60.

2. Stone, J.D., A.S. Chervin, and D.M. Kranz, *T-cell receptor binding affinities and kinetics: impact on T-cell activity and specificity.* Immunology, 2009. **126**(2): p. 165-76.

3. Holler, P.D., et al., *In vitro evolution of a T cell receptor with high affinity for peptide/MHC.* Proc Natl Acad Sci U S A, 2000. **97**(10): p. 5387-92.

4. Li, Y., et al., *Directed evolution of human T-cell receptors with picomolar affinities by phage display.* Nat Biotechnol, 2005. **23**(3): p. 349-54.

5. McIntyre, B.W. and J.P. Allison, *The mouse T cell receptor: structural heterogeneity of molecules of normal T cells defined by xenoantiserum.* Cell, 1983. **34**(3): p. 739-46.

6. Sangster, R.N., et al., *Rearrangement and expression of the alpha, beta, and gamma chain T cell receptor genes in human thymic leukemia cells and functional T cells.* J Exp Med, 1986. **163**(6): p. 1491-508.

7. Toyonaga, B. and T.W. Mak, *Genes of the T-cell antigen receptor in normal and malignant T cells.* Annu Rev Immunol, 1987. **5**: p. 585-620.

8. Bjorkman, P.J., et al., *The foreign antigen binding site and T cell recognition regions of class I histocompatibility antigens.* Nature, 1987. **329**(6139): p. 512-8.

9. Brown, J.H., et al., *Three-dimensional structure of the human class II histocompatibility antigen HLA-DR1.* Nature, 1993. **364**(6432): p. 33-9.

10. Davis, M.M. and P.J. Bjorkman, *A model for T cell receptor and MHC/peptide interaction.* Adv Exp Med Biol, 1989. **254**: p. 13-6.

11. Davis, M.M., et al., *Ligand recognition by alpha beta T cell receptors.* Annu Rev Immunol, 1998. **16**: p. 523-44.

ZRMHQN12. Davis, M.M., et al., *A possible basis for major histocompatibility complex-restricted T-cell recognition.* Philos Trans R Soc Lond B Biol Sci, 1989. **323**(1217): p. 521-4.

13. Stern, L.J., et al., *Crystal structure of the human class II MHC protein HLA-DR1 complexed with an influenza virus peptide.* Nature, 1994. **368**(6468): p. 215-21.

14. Cambier, J.C., *Antigen and Fc receptor signaling. The awesome power of the immunoreceptor tyrosine-based activation motif (ITAM).* J Immunol, 1995. **155**(7): p. 3281-5.

15. Clay, T.M., et al., *Efficient transfer of a tumor antigen-reactive TCR to human peripheral blood lymphocytes confers anti-tumor reactivity.* J Immunol, 1999. **163**(1): p. 507-13.

16. Curran, K.J., H.J. Pegram, and R.J. Brentjens, *Chimeric antigen receptors for T cell immunotherapy: current understanding and future directions.* J Gene Med, 2012. **14**(6): p. 405-15.

17. Jensen, M.C. and S.R. Riddell, *Designing chimeric antigen receptors to effectively and safely target tumors.* Curr Opin Immunol, 2015. **33**: p. 9-15.

18. Romeo, C., et al., *Activation of immune system effector function by T-cell or Fc receptor intracellular domains.* Cold Spring Harb Symp Quant Biol, 1992. **57**: p. 117-25.

19. Stancovski, I., et al., *Targeting of T lymphocytes to Neu/HER2-expressing cells using chimeric single chain Fv receptors.* J Immunol, 1993. **151**(11): p. 6577-82.

20. Weiss, A. and D.R. Littman, *Signal transduction by lymphocyte antigen receptors.* Cell, 1994. **76**(2): p. 263-74.

21. de Vries, J.E., H. Yssel, and H. Spits, *Interplay between the TCR/CD3 complex and CD4 or CD8 in the activation of cytotoxic T lymphocytes.* Immunol Rev, 1989. **109**: p. 119-41.

22. Emmrich, F., U. Strittmatter, and K. Eichmann, *Synergism in the activation of human CD8 T cells by cross-linking the T-cell receptor complex with the CD8 differentiation antigen.* Proc Natl Acad Sci U S A, 1986. **83**(21): p. 8298-302.

23. Swain, S.L., *T cell subsets and the recognition of MHC class.* Immunol Rev, 1983. **74**: p. 129-42.

24. Dialynas, D.P., et al., *Characterization of the murine antigenic determinant, designated L3T4a, recognized by monoclonal antibody GK1.5: expression of L3T4a by functional T cell clones appears to correlate primarily with class II MHC antigen-reactivity.* Immunol Rev, 1983. **74**: p. 29-56.

25. Veillette, A., et al., *The CD4 and CD8 T cell surface antigens are associated with the internal membrane tyrosine-protein kinase p56lck.* Cell, 1988. **55**(2): p. 301-8.

26. Barber, E.K., et al., *The CD4 and CD8 antigens are coupled to a protein-tyrosine kinase (p56lck) that phosphorylates the CD3 complex.* Proc Natl Acad Sci U S A, 1989. **86**(9): p. 3277-81.

27. Davis, M.M. and P.J. Bjorkman, *T-cell antigen receptor genes and T-cell recognition.* Nature, 1988. **334**(6181): p. 395-402.

28. Koop, B.F., et al., *The human T-cell receptor TCRAC/TCRDC (C alpha/C delta) region: organization, sequence, and evolution of 97.6 kb of DNA.* Genomics, 1994. **19**(3): p. 478-93.

29. Toyonaga, B., et al., *Organization and sequences of the diversity, joining, and constant region genes of the human T-cell receptor beta chain.* Proc Natl Acad Sci U S A, 1985. **82**(24): p. 8624-8.

30. Eisen, H.N., Y. Sykulev, and T.J. Tsomides, *Antigen-specific T-cell receptors and their reactions with complexes formed by peptides with major histocompatibility complex proteins.* Adv Protein Chem, 1996. **49**: p. 1-56.

31. Coulie, P.G., et al., *Tumour antigens recognized by T lymphocytes: at the core of cancer immunotherapy.* Nat Rev Cancer, 2014. **14**(2): p. 135-46.

32. Rosenberg, S.A., *Identification of cancer antigens: impact on development of cancer immunotherapies.* Cancer J, 2000. **6 Suppl 3**: p. S200-7.

33. Van Der Bruggen, P., et al., *Tumor-specific shared antigenic peptides recognized by human T cells.* Immunol Rev, 2002. **188**: p. 51-64.

34. Shilyansky, J., et al., *T-cell receptor usage by melanoma-specific clonal and highly oligoclonal tumor-infiltrating lymphocyte lines.* Proc Natl Acad Sci U S A, 1994. **91**(7): p. 2829-33.

35. Cole, D.J., et al., *T-cell receptor repertoire in matched MART-1 peptide-stimulated peripheral blood lymphocytes and tumor-infiltrating lymphocytes.* Cancer Res, 1997. **57**(23): p. 5320-7.

36. Cole, D.J., et al., *Identification of MART-1-specific T-cell receptors: T cells utilizing distinct T-cell receptor variable and joining regions recognize the same tumor epitope.* Cancer Res, 1994. **54**(20): p. 5265-8.

37. Kawakami, Y., et al., *T-cell recognition of human melanoma antigens.* J Immunother Emphasis Tumor Immunol, 1993. **14**(2): p. 88-93.

38. Nishimura, M.I., et al., *T cell-receptor V gene use by CD4+ melanoma-reactive clonal and oligoclonal T-cell lines.* J Immunother, 1998. **21**(5): p. 352-62.

39. Nishimura, M.I., et al., *T-cell receptor repertoire in tumor-infiltrating lymphocytes. Analysis of melanoma-specific long-term lines.* J Immunother Emphasis Tumor Immunol, 1994. **16**(2): p. 85-94.

40. Sensi, M., et al., *Two autologous melanoma-specific and MHC-restricted human T cell clones with identical intra-tumour reactivity do not share the same TCR V alpha and V beta gene families.* Melanoma Res, 1991. **1**(4): p. 261-71.

41. Loftus, D.J., et al., *Identification of epitope mimics recognized by CTL reactive to the melanoma/melanocyte-derived peptide MART-1(27-35).* J Exp Med, 1996. **184**(2): p. 647-57.

42. Dudley, M.E., et al., *Antitumor immunization with a minimal peptide epitope (G9-209-2M) leads to a functionally heterogeneous CTL response.* J Immunother, 1999. **22**(4): p. 288-98.

43. Foote, J. and H.N. Eisen, *Breaking the affinity ceiling for antibodies and T cell receptors.* Proc Natl Acad Sci U S A, 2000. **97**(20): p. 10679-81.

44. Moore, T.V., et al., *Relationship between CD8-dependent antigen recognition, T cell functional avidity, and tumor cell recognition.* Cancer Immunol Immunother, 2009. **58**(5): p. 719-28.

45. Kroger, C.J. and M.A. Alexander-Miller, *Cutting edge: CD8+ T cell clones possess the potential to differentiate into both high- and low-avidity effector cells.* J Immunol, 2007. **179**(2): p. 748-51.

46. Josefowicz, S.Z., L.F. Lu, and A.Y. Rudensky, *Regulatory T cells: mechanisms of differentiation and function.* Annu Rev Immunol, 2012. **30**: p. 531-64.

47. Kumar, V. and D.I. Gabrilovich, *Hypoxia-inducible factors in regulation of immune responses in tumour microenvironment.* Immunology, 2014. **143**(4): p. 512-9.

48. Leguern, C., *Regulatory T cells for tolerance therapy: revisiting the concept.* Crit Rev Immunol, 2011. **31**(3): p. 189-207.

49. Ostrand-Rosenberg, S., *Myeloid-derived suppressor cells: more mechanisms for inhibiting antitumor immunity.* Cancer Immunol Immunother, 2010. **59**(10): p. 1593-600.

50. Raber, P., A.C. Ochoa, and P.C. Rodriguez, *Metabolism of L-arginine by myeloid-derived suppressor cells in cancer: mechanisms of T cell suppression and therapeutic perspectives.* Immunol Invest, 2012. **41**(6-7): p. 614-34.

51. Carpenito, C., et al., *Control of large, established tumor xenografts with genetically retargeted human T cells containing CD28 and CD137 domains.* Proc Natl Acad Sci U S A, 2009. **106**(9): p. 3360-5.

52. Marigo, I., et al., *Tumor-induced tolerance and immune suppression by myeloid derived suppressor cells.* Immunol Rev, 2008. **222**: p. 162-79.

53. De Sanctis, F., et al., *The emerging immunological role of post-translational modifications by reactive nitrogen species in cancer microenvironment.* Front Immunol, 2014. **5**: p. 69.

54. Kono, K., et al., *Hydrogen peroxide secreted by tumor-derived macrophages down-modulates signal-transducing zeta molecules and inhibits tumor-specific T cell-and natural killer cell-mediated cytotoxicity.* Eur J Immunol, 1996. **26**(6): p. 1308-13.

55. Mao, Y., I. Poschke, and R. Kiessling, *Tumour-induced immune suppression: role of inflammatory mediators released by myelomonocytic cells.* J Intern Med, 2014. **276**(2): p. 154-70.

56. Kusmartsev, S., et al., *Antigen-specific inhibition of CD8+ T cell response by immature myeloid cells in cancer is mediated by reactive oxygen species.* J Immunol, 2004. **172**(2): p. 989-99.

57. Lu, T. and D.I. Gabrilovich, *Molecular pathways: tumor-infiltrating myeloid cells and reactive oxygen species in regulation of tumor microenvironment.* Clin Cancer Res, 2012. **18**(18): p. 4877-82.

58. Miyazaki, Y., et al., *Development of a novel redirected T-cell-based adoptive immunotherapy targeting human telomerase reverse transcriptase for adult T-cell leukemia.* Blood, 2013. **121**(24): p. 4894-901.

59. Pecht, I. and D.M. Gakamsky, *Spatial coordination of CD8 and TCR molecules controls antigen recognition by CD8+ T-cells.* FEBS Lett, 2005. **579**(15): p. 3336-41.

60. Cawthon, A.G. and M.A. Alexander-Miller, *Optimal colocalization of TCR and CD8 as a novel mechanism for the control of functional avidity.* J Immunol, 2002. **169**(7): p. 3492-8.

61. Nagaraj, S., et al., *Altered recognition of antigen is a mechanism of CD8+ T cell tolerance in cancer.* Nat Med, 2007. **13**(7): p. 828-35.

62. Brownlie, R.J. and R. Zamoyska, *T cell receptor signalling networks: branched, diversified and bounded.* Nat Rev Immunol, 2013. **13**(4): p. 257-69.

63. Acuto, O., V. Di Bartolo, and F. Michel, *Tailoring T-cell receptor signals by proximal negative feedback mechanisms.* Nat Rev Immunol, 2008. **8**(9): p. 699-712.

64. Broere, F., Apasov, S.G., Sitkovsky, M.V., and van Edn, W., *T cell subsets and T cell-mediated immunity*. 3rd ed. Principles of Immunopharmacology. 2011: Springer.

65. McKeithan, T.W., *Kinetic proofreading in T-cell receptor signal transduction.* Proc Natl Acad Sci U S A, 1995. **92**(11): p. 5042-6.

66. Regner, M., *Cross-reactivity in T-cell antigen recognition.* Immunol Cell Biol, 2001. **79**(2): p. 91-100.

67. Amin, A. and R.L. White, Jr., *High-dose interleukin-2: is it still indicated for melanoma and RCC in an era of targeted therapies?* Oncology (Williston Park), 2013. **27**(7): p. 680-91.

68. Hodi, F.S., et al., *Improved survival with ipilimumab in patients with metastatic melanoma.* N Engl J Med, 2010. **363**(8): p. 711-23.

69. Robert, C., et al., *Ipilimumab plus dacarbazine for previously untreated metastatic melanoma.* N Engl J Med, 2011. **364**(26): p. 2517-26.

70. Schadendorf, D., et al., *Pooled Analysis of Long-Term Survival Data From Phase II and Phase III Trials of Ipilimumab in Unresectable or Metastatic Melanoma.* J Clin Oncol, 2015. **33**(17): p. 1889-94.

71. Ribas, A., et al., *Pembrolizumab versus investigator-choice chemotherapy for ipilimumab-refractory melanoma (KEYNOTE-002): a randomised, controlled, phase 2 trial.* Lancet Oncol, 2015. **16**(8): p. 908-18.

72. Robert, C., et al., *Pembrolizumab versus Ipilimumab in Advanced Melanoma.* N Engl J Med, 2015. **372**(26): p. 2521-32.

73. Mule, J.J., et al., *Adoptive immunotherapy of established pulmonary metastases with LAK cells and recombinant interleukin-2.* Science, 1984. **225**(4669): p. 1487-9.

74. Rosenberg, S.A., et al., *Treatment of patients with metastatic melanoma with autologous tumor-infiltrating lymphocytes and interleukin 2.* J Natl Cancer Inst, 1994. **86**(15): p. 1159-66.

75. Sherry, R.M., S.A. Rosenberg, and J.C. Yang, *Relapse after response to interleukin-2-based immunotherapy: patterns of progression and response to retreatment.* J Immunother (1991), 1991. **10**(5): p. 371-5.

76. Dudley, M.E., et al., *Cancer regression and autoimmunity in patients after clonal repopulation with antitumor lymphocytes.* Science, 2002. **298**(5594): p. 850-4.

77. Mackensen, A., et al., *Phase I study of adoptive T-cell therapy using antigen-specific CD8+ T cells for the treatment of patients with metastatic melanoma.* J Clin Oncol, 2006. **24**(31): p. 5060-9.

78. Riddell, S.R., P. Reusser, and P.D. Greenberg, *Cytotoxic T cells specific for cytomegalovirus: a potential therapy for immunocompromised patients.* Rev Infect Dis, 1991. **13 Suppl 11**: p. S966-73.

79. Walter, E.A., et al., *Reconstitution of cellular immunity against cytomegalovirus in recipients of allogeneic bone marrow by transfer of T-cell clones from the donor.* N Engl J Med, 1995. **333**(16): p. 1038-44.

80. Muul, L.M., et al., *Identification of specific cytolytic immune responses against autologous tumor in humans bearing malignant melanoma.* J Immunol, 1987. **138**(3): p. 989-95.

81. Rosenberg, S.A., P. Spiess, and R. Lafreniere, *A new approach to the adoptive immunotherapy of cancer with tumor-infiltrating lymphocytes.* Science, 1986. **233**(4770): p. 1318-21.

82. Rosenberg, S.A., et al., *Use of tumor-infiltrating lymphocytes and interleukin-2 in the immunotherapy of patients with metastatic melanoma. A preliminary report.* N Engl J Med, 1988. **319**(25): p. 1676-80.

83. Yannelli, J.R., E. Hirscowitz, and J.M. Wroblewski, *Growth and functional reactivity of lymphocytes obtained from three anatomic compartments in patients with non-small-cell lung cancer (NSCLC).* Cancer Biother Radiopharm, 2003. **18**(5): p. 735-49.

84. Yannelli, J.R., et al., *Melanoma tumor-infiltrating lymphocytes derived from four distinct anatomic sites obtained from a single patient: comparison of functional reactivity and melanoma antigen recognition.* J Immunother Emphasis Tumor Immunol, 1995. **18**(4): p. 263-71.

85. Barrett, D.M., S.A. Grupp, and C.H. June, *Chimeric Antigen Receptor- and TCR-Modified T Cells Enter Main Street and Wall Street.* J Immunol, 2015. **195**(3): p. 755-61.

86. Barrett, D.M., et al., *Chimeric antigen receptor therapy for cancer.* Annu Rev Med, 2014. **65**: p. 333-47.

87. Gross, G., T. Waks, and Z. Eshhar, *Expression of immunoglobulin-T-cell receptor chimeric molecules as functional receptors with antibody-type specificity.* Proc Natl Acad Sci U S A, 1989. **86**(24): p. 10024-8.

88. Letourneur, F. and R.D. Klausner, *T-cell and basophil activation through the cytoplasmic tail of T-cell-receptor zeta family proteins.* Proc Natl Acad Sci U S A, 1991. **88**(20): p. 8905-9.

89. Hombach, A., et al., *T cell targeting of TAG72+ tumor cells by a chimeric receptor with antibody-like specificity for a carbohydrate epitope.* Gastroenterology, 1997. **113**(4): p. 1163-70.

90. Rossig, C., et al., *Targeting of G(D2)-positive tumor cells by human T lymphocytes engineered to express chimeric T-cell receptor genes.* Int J Cancer, 2001. **94**(2): p. 228-36.

91. Riddell, S.R., M.C. Jensen, and C.H. June, *Chimeric antigen receptor--modified T cells: clinical translation in stem cell transplantation and beyond.* Biol Blood Marrow Transplant, 2013. **19**(1 Suppl): p. S2-5.

92. Geldres, C., B. Savoldo, and G. Dotti, *Chimeric antigen receptor-redirected T cells return to the bench.* Semin Immunol, 2016.

93. Sadelain, M., R. Brentjens, and I. Riviere, *The basic principles of chimeric antigen receptor design.* Cancer Discov, 2013. **3**(4): p. 388-98.

94. Sadelain, M., R. Brentjens, and I. Riviere, *The promise and potential pitfalls of chimeric antigen receptors.* Curr Opin Immunol, 2009. **21**(2): p. 215-23.

95. Davis, M.M., *The evolutionary and structural 'logic' of antigen receptor diversity.* Semin Immunol, 2004. **16**(4): p. 239-43.

96. Lamers, C.H., et al., *Immune responses to transgene and retroviral vector in patients treated with ex vivo-engineered T cells.* Blood, 2011. **117**(1): p. 72-82.

97. Dao, T., et al., *Targeting the intracellular WT1 oncogene product with a therapeutic human antibody.* Sci Transl Med, 2013. **5**(176): p. 176ra33.

98. Muniappan, A., et al., *Ligand-mediated cytolysis of tumor cells: use of heregulin-zeta chimeras to redirect cytotoxic T lymphocytes.* Cancer Gene Ther, 2000. **7**(1): p. 128-34.

99. Niederman, T.M., et al., *Antitumor activity of cytotoxic T lymphocytes engineered to target vascular endothelial growth factor receptors.* Proc Natl Acad Sci U S A, 2002. **99**(10): p. 7009-14.

100. Zhang, T., M.R. Wu, and C.L. Sentman, *An NKp30-based chimeric antigen receptor promotes T cell effector functions and antitumor efficacy in vivo.* J Immunol, 2012. **189**(5): p. 2290-9.

101. Lehner, M., et al., *Redirecting T cells to Ewing's sarcoma family of tumors by a chimeric NKG2D receptor expressed by lentiviral transduction or mRNA transfection.* PLoS One, 2012. **7**(2): p. e31210.

102. Song, D.G., et al., *Chimeric NKG2D CAR-expressing T cell-mediated attack of human ovarian cancer is enhanced by histone deacetylase inhibition.* Hum Gene Ther, 2013. **24**(3): p. 295-305.

103. Zhang, T., A. Barber, and C.L. Sentman, *Generation of antitumor responses by genetic modification of primary human T cells with a chimeric NKG2D receptor.* Cancer Res, 2006. **66**(11): p. 5927-33.

104. Ramos, C.A. and G. Dotti, *Chimeric antigen receptor (CAR)-engineered lymphocytes for cancer therapy.* Expert Opin Biol Ther, 2011. **11**(7): p. 855-73.

105. Haynes, N.M., et al., *Single-chain antigen recognition receptors that costimulate potent rejection of established experimental tumors.* Blood, 2002. **100**(9): p. 3155-63.

106. Hombach, A., et al., *Tumor-specific T cell activation by recombinant immunoreceptors: CD3 zeta signaling and CD28 costimulation are simultaneously required for efficient IL-2 secretion and can be integrated into one combined CD28/CD3 zeta signaling receptor molecule.* J Immunol, 2001. **167**(11): p. 6123-31.

107. Maher, J., et al., *Human T-lymphocyte cytotoxicity and proliferation directed by a single chimeric TCRzeta /CD28 receptor.* Nat Biotechnol, 2002. **20**(1): p. 70-5.

108. Finney, H.M., et al., *Chimeric receptors providing both primary and costimulatory signaling in T cells from a single gene product.* J Immunol, 1998. **161**(6): p. 2791-7.

109. Imai, C., et al., *Chimeric receptors with 4-1BB signaling capacity provoke potent cytotoxicity against acute lymphoblastic leukemia.* Leukemia, 2004. **18**(4): p. 676-84.

110. Kowolik, C.M., et al., *CD28 costimulation provided through a CD19-specific chimeric antigen receptor enhances in vivo persistence and antitumor efficacy of adoptively transferred T cells.* Cancer Res, 2006. **66**(22): p. 10995-1004.

111. Krause, A., et al., *Antigen-dependent CD28 signaling selectively enhances survival and proliferation in genetically modified activated human primary T lymphocytes.* J Exp Med, 1998. **188**(4): p. 619-26.

112. Loskog, A., et al., *Addition of the CD28 signaling domain to chimeric T-cell receptors enhances chimeric T-cell resistance to T regulatory cells.* Leukemia, 2006. **20**(10): p. 1819-28.

113. Milone, M.C., et al., *Chimeric receptors containing CD137 signal transduction domains mediate enhanced survival of T cells and increased antileukemic efficacy in vivo.* Mol Ther, 2009. **17**(8): p. 1453-64.

114. Moeller, M., et al., *A functional role for CD28 costimulation in tumor recognition by single-chain receptor-modified T cells.* Cancer Gene Ther, 2004. **11**(5): p. 371-9.

115. Wang, J., et al., *Optimizing adoptive polyclonal T cell immunotherapy of lymphomas, using a chimeric T cell receptor possessing CD28 and CD137 costimulatory domains.* Hum Gene Ther, 2007. **18**(8): p. 712-25.

116. Yvon, E., et al., *Immunotherapy of metastatic melanoma using genetically engineered GD2-specific T cells.* Clin Cancer Res, 2009. **15**(18): p. 5852-60.

117. Zhao, Y., et al., *A herceptin-based chimeric antigen receptor with modified signaling domains leads to enhanced survival of transduced T lymphocytes and antitumor activity.* J Immunol, 2009. **183**(9): p. 5563-74.

118. Liu, L., M. Sun, and Z. Wang, *Adoptive T-cell therapy of B-cell malignancies: conventional and physiological chimeric antigen receptors.* Cancer Lett, 2012. **316**(1): p. 1-5.

119. Wang, J., et al., *Cellular immunotherapy for follicular lymphoma using genetically modified CD20-specific CD8+ cytotoxic T lymphocytes.* Mol Ther, 2004. **9**(4): p. 577-86.

120. Wilkie, S., et al., *Retargeting of human T cells to tumor-associated MUC1: the evolution of a chimeric antigen receptor.* J Immunol, 2008. **180**(7): p. 4901-9.

121. Zhong, X.S., et al., *Chimeric antigen receptors combining 4-1BB and CD28 signaling domains augment PI3kinase/AKT/Bcl-XL activation and CD8+ T cell-mediated tumor eradication.* Mol Ther, 2010. **18**(2): p. 413-20.

122. Morgan, R.A., et al., *Case report of a serious adverse event following the administration of T cells transduced with a chimeric antigen receptor recognizing ERBB2.* Mol Ther, 2010. **18**(4): p. 843-51.

123. Kershaw, M.H., et al., *A phase I study on adoptive immunotherapy using gene-modified T cells for ovarian cancer.* Clin Cancer Res, 2006. **12**(20 Pt 1): p. 6106-15.

124. Lamers, C.H., et al., *Treatment of metastatic renal cell carcinoma with autologous T-lymphocytes genetically retargeted against carbonic anhydrase IX: first clinical experience.* J Clin Oncol, 2006. **24**(13): p. e20-2.

125. Brentjens, R.J., et al., *Safety and persistence of adoptively transferred autologous CD19-targeted T cells in patients with relapsed or chemotherapy refractory B-cell leukemias.* Blood, 2011. **118**(18): p. 4817-28.

126. Jensen, M.C., et al., *Antitransgene rejection responses contribute to attenuated persistence of adoptively transferred CD20/CD19-specific chimeric antigen receptor redirected T cells in humans.* Biol Blood Marrow Transplant, 2010. **16**(9): p. 1245-56.

127. Kalos, M., et al., *T cells with chimeric antigen receptors have potent antitumor effects and can establish memory in patients with advanced leukemia.* Sci Transl Med, 2011. **3**(95): p. 95ra73.

128. Kochenderfer, J.N., et al., *B-cell depletion and remissions of malignancy along with cytokine-associated toxicity in a clinical trial of anti-CD19 chimeric-antigen-receptor-transduced T cells.* Blood, 2012. **119**(12): p. 2709-20.

129. Kochenderfer, J.N., et al., *Eradication of B-lineage cells and regression of lymphoma in a patient treated with autologous T cells genetically engineered to recognize CD19.* Blood, 2010. **116**(20): p. 4099-102.

130. Porter, D.L., et al., *Chimeric antigen receptor-modified T cells in chronic lymphoid leukemia.* N Engl J Med, 2011. **365**(8): p. 725-33.

131. Savoldo, B., et al., *CD28 costimulation improves expansion and persistence of chimeric antigen receptor-modified T cells in lymphoma patients.* J Clin Invest, 2011. **121**(5): p. 1822-6.

132. Brentjens, R.J., et al., *CD19-targeted T cells rapidly induce molecular remissions in adults with chemotherapy-refractory acute lymphoblastic leukemia.* Sci Transl Med, 2013. **5**(177): p. 177ra38.

133. Grupp, S.A., et al., *Chimeric antigen receptor-modified T cells for acute lymphoid leukemia.* N Engl J Med, 2013. **368**(16): p. 1509-18.

134. Lee, D.W., et al., *T cells expressing CD19 chimeric antigen receptors for acute lymphoblastic leukaemia in children and young adults: a phase 1 dose-escalation trial.* Lancet, 2015. **385**(9967): p. 517-28.

135. Nellan, A. and D.W. Lee, *Paving the road ahead for CD19 CAR T-cell therapy.* Curr Opin Hematol, 2015. **22**(6): p. 516-20.

136. Ahmed, N., et al., *Human Epidermal Growth Factor Receptor 2 (HER2) -Specific Chimeric Antigen Receptor-Modified T Cells for the Immunotherapy of HER2-Positive Sarcoma.* J Clin Oncol, 2015. **33**(15): p. 1688-96.

137. Miao, H., et al., *EGFRvIII-specific chimeric antigen receptor T cells migrate to and kill tumor deposits infiltrating the brain parenchyma in an invasive xenograft model of glioblastoma.* PLoS One, 2014. **9**(4): p. e94281.

138. Brentjens, R.J., et al., *Eradication of systemic B-cell tumors by genetically targeted human T lymphocytes co-stimulated by CD80 and interleukin-15.* Nat Med, 2003. **9**(3): p. 279-86.

139. Rossig, C., et al., *Epstein-Barr virus-specific human T lymphocytes expressing antitumor chimeric T-cell receptors: potential for improved immunotherapy.* Blood, 2002. **99**(6): p. 2009-16.

140. Lo, A.S., et al., *Anti-GD3 chimeric sFv-CD28/T-cell receptor zeta designer T cells for treatment of metastatic melanoma and other neuroectodermal tumors.* Clin Cancer Res, 2010. **16**(10): p. 2769-80.

141. Yun, C.O., et al., *Targeting of T lymphocytes to melanoma cells through chimeric anti-GD3 immunoglobulin T-cell receptors.* Neoplasia, 2000. **2**(5): p. 449-59.

142. Willemsen, R.A., et al., *T cell retargeting with MHC class I-restricted antibodies: the CD28 costimulatory domain enhances antigen-specific cytotoxicity and cytokine production.* J Immunol, 2005. **174**(12): p. 7853-8.

143. Burns, W.R., et al., *A high molecular weight melanoma-associated antigen-specific chimeric antigen receptor redirects lymphocytes to target human melanomas.* Cancer Res, 2010. **70**(8): p. 3027-33.

144. James, S.E., et al., *Antigen sensitivity of CD22-specific chimeric TCR is modulated by target epitope distance from the cell membrane.* J Immunol, 2008. **180**(10): p. 7028-38.

145. Jensen, M.C., et al., *Engineered CD20-specific primary human cytotoxic T lymphocytes for targeting B-cell malignancy.* Cytotherapy, 2003. **5**(2): p. 131-8.

146. Till, B.G., et al., *CD20-specific adoptive immunotherapy for lymphoma using a chimeric antigen receptor with both CD28 and 4-1BB domains: pilot clinical trial results.* Blood, 2012. **119**(17): p. 3940-50.

147. Yu, K., et al., *Immunotherapy of lymphomas with T cells modified by anti-CD20 scFv/CD28/CD3zeta recombinant gene.* Leuk Lymphoma, 2008. **49**(7): p. 1368-73.

148. Giordano Attianese, G.M., et al., *In vitro and in vivo model of a novel immunotherapy approach for chronic lymphocytic leukemia by anti-CD23 chimeric antigen receptor.* Blood, 2011. **117**(18): p. 4736-45.

149. Di Stasi, A., et al., *T lymphocytes coexpressing CCR4 and a chimeric antigen receptor targeting CD30 have improved homing and antitumor activity in a Hodgkin tumor model.* Blood, 2009. **113**(25): p. 6392-402.

150. Hombach, A., et al., *T cells engrafted with a recombinant anti-CD30 receptor target autologous CD30(+) cutaneous lymphoma cells.* Gene Ther, 2001. **8**(11): p. 891-5.

151. Savoldo, B., et al., *Epstein Barr virus specific cytotoxic T lymphocytes expressing the anti-CD30zeta artificial chimeric T-cell receptor for immunotherapy of Hodgkin disease.* Blood, 2007. **110**(7): p. 2620-30.

152. Ma, Q., et al., *Anti-prostate specific membrane antigen designer T cells for prostate cancer therapy.* Prostate, 2004. **61**(1): p. 12-25.

153. Moritz, D., et al., *Cytotoxic T lymphocytes with a grafted recognition specificity for ERBB2-expressing tumor cells.* Proc Natl Acad Sci U S A, 1994. **91**(10): p. 4318-22.

154. Darcy, P.K., et al., *Expression in cytotoxic T lymphocytes of a single-chain anti-carcinoembryonic antigen antibody. Redirected Fas ligand-mediated lysis of colon carcinoma.* Eur J Immunol, 1998. **28**(5): p. 1663-72.

155. Hombach, A., et al., *A chimeric receptor that selectively targets membrane-bound carcinoembryonic antigen (mCEA) in the presence of soluble CEA.* Gene Ther, 1999. **6**(2): p. 300-4.

156. Nolan, K.F., et al., *Bypassing immunization: optimized design of "designer T cells" against carcinoembryonic antigen (CEA)-expressing tumors, and lack of suppression by soluble CEA.* Clin Cancer Res, 1999. **5**(12): p. 3928-41.

157. Daly, T., et al., *Recognition of human colon cancer by T cells transduced with a chimeric receptor gene.* Cancer Gene Ther, 2000. **7**(2): p. 284-91.

158. Chinnasamy, D., et al., *Gene therapy using genetically modified lymphocytes targeting VEGFR-2 inhibits the growth of vascularized syngenic tumors in mice.* J Clin Invest, 2010. **120**(11): p. 3953-68.

159. Wang, S., et al., *[The specific cytotoxic effect of tumor infiltrating lymphocytes transfected with chimeric T cell receptor on cells which express KDR].* Zhonghua Zhong Liu Za Zhi, 2004. **26**(2): p. 82-4.

160. Chekmasova, A.A., et al., *Successful eradication of established peritoneal ovarian tumors in SCID-Beige mice following adoptive transfer of T cells genetically targeted to the MUC16 antigen.* Clin Cancer Res, 2010. **16**(14): p. 3594-606.

161. Brentjens, R., et al., *Treatment of chronic lymphocytic leukemia with genetically targeted autologous T cells: case report of an unforeseen adverse event in a phase I clinical trial.* Mol Ther, 2010. **18**(4): p. 666-8.

162. Xu, X.J. and Y.M. Tang, *Cytokine release syndrome in cancer immunotherapy with chimeric antigen receptor engineered T cells.* Cancer Lett, 2014. **343**(2): p. 172-8.

163. Orentas, R.J., et al., *Retroviral transduction of a T cell receptor specific for an Epstein-Barr virus-encoded peptide.* Clin Immunol, 2001. **98**(2): p. 220-8.

164. Voelkl, S., et al., *Characterization of MHC class-I restricted TCRalphabeta+ CD4- CD8- double negative T cells recognizing the gp100 antigen from a melanoma patient after gp100 vaccination.* Cancer Immunol Immunother, 2009. **58**(5): p. 709-18.

165. Callender, G.G., et al., *Identification of a hepatitis C virus-reactive T cell receptor that does not require CD8 for target cell recognition.* Hepatology, 2006. **43**(5): p. 973-81.

166. Zhang, Y., et al., *Transduction of human T cells with a novel T-cell receptor confers anti-HCV reactivity.* PLoS Pathog, 2010. **6**(7): p. e1001018.

167. Lyons, G.E., et al., *T-cell receptor tetramer binding or the lack there of does not necessitate antigen reactivity in T-cell receptor transduced T cells.* Cancer Immunol Immunother, 2006. **55**(9): p. 1142-50.

168. Cole, D.J., et al., *Characterization of the functional specificity of a cloned T-cell receptor heterodimer recognizing the MART-1 melanoma antigen.* Cancer Res, 1995. **55**(4): p. 748-52.

169. Roszkowski, J.J., et al., *Simultaneous generation of CD8+ and CD4+ melanoma-reactive T cells by retroviral-mediated transfer of a single T-cell receptor.* Cancer Res, 2005. **65**(4): p. 1570-6.

170. Roszkowski, J.J., et al., *CD8-independent tumor cell recognition is a property of the T cell receptor and not the T cell.* J Immunol, 2003. **170**(5): p. 2582-9.

171. Deng, L., et al., *Structural basis for the recognition of mutant self by a tumor-specific, MHC class II-restricted T cell receptor.* Nat Immunol, 2007. **8**(4): p. 398-408.

172. Matsuzaki, J., et al., *Direct tumor recognition by a human CD4(+) T-cell subset potently mediates tumor growth inhibition and orchestrates anti-tumor immune responses.* Sci Rep, 2015. **5**: p. 14896.

173. van der Veken, L.T., et al., *HLA class II restricted T-cell receptor gene transfer generates CD4+ T cells with helper activity as well as cytotoxic capacity.* Gene Ther, 2005. **12**(23): p. 1686-95.

174. Chang, H.C., et al., *A general method for facilitating heterodimeric pairing between two proteins: application to expression of alpha and beta T-cell receptor extracellular segments.* Proc Natl Acad Sci U S A, 1994. **91**(24): p. 11408-12.

175. Johnson, L.A., et al., *Gene transfer of tumor-reactive TCR confers both high avidity and tumor reactivity to nonreactive peripheral blood mononuclear cells and tumor-infiltrating lymphocytes.* J Immunol, 2006. **177**(9): p. 6548-59.

176. Kuball, J., et al., *Facilitating matched pairing and expression of TCR chains introduced into human T cells.* Blood, 2007. **109**(6): p. 2331-8.

177. Kuball, J., et al., *Increasing functional avidity of TCR-redirected T cells by removing defined N-glycosylation sites in the TCR constant domain.* J Exp Med, 2009. **206**(2): p. 463-75.

178. Tsuji, T., et al., *Generation of tumor-specific, HLA class I-restricted human Th1 and Tc1 cells by cell engineering with tumor peptide-specific T-cell receptor genes.* Blood, 2005. **106**(2): p. 470-6.

179. Voss, R.H., et al., *Molecular design of the Calphabeta interface favors specific pairing of introduced TCRalphabeta in human T cells.* J Immunol, 2008. **180**(1): p. 391-401.

180. Wilde, S., et al., *Dendritic cells pulsed with RNA encoding allogeneic MHC and antigen induce T cells with superior antitumor activity and higher TCR functional avidity.* Blood, 2009. **114**(10): p. 2131-9.

181. Willemsen, R.A., et al., *CD8 alpha coreceptor to improve TCR gene transfer to treat melanoma: down-regulation of tumor-specific production of IL-4, IL-5, and IL-10.* J Immunol, 2006. **177**(2): p. 991-8.

182. Combadiere, B., et al., *Differential TCR signaling regulates apoptosis and immunopathology during antigen responses in vivo.* Immunity, 1998. **9**(3): p. 305-13.

183. Lenardo, M.J., et al., *Autocrine feedback death and the regulation of mature T lymphocyte antigen responses.* Int Rev Immunol, 1995. **13**(2): p. 115-34.

184. Johnson, L.A., et al., *Gene therapy with human and mouse T-cell receptors mediates cancer regression and targets normal tissues expressing cognate antigen.* Blood, 2009. **114**(3): p. 535-46.

185. Mehrotra, S., et al., *A coreceptor-independent transgenic human TCR mediates anti-tumor and anti-self immunity in mice.* J Immunol, 2012. **189**(4): p. 1627-38.

186. Parkhurst, M.R., et al., *T cells targeting carcinoembryonic antigen can mediate regression of metastatic colorectal cancer but induce severe transient colitis.* Mol Ther, 2011. **19**(3): p. 620-6.

187. Bicknell, D.C., A. Rowan, and W.F. Bodmer, *Beta 2-microglobulin gene mutations: a study of established colorectal cell lines and fresh tumors.* Proc Natl Acad Sci U S A, 1994. **91**(11): p. 4751-5.

188. Hicklin, D.J., F.M. Marincola, and S. Ferrone, *HLA class I antigen downregulation in human cancers: T-cell immunotherapy revives an old story.* Mol Med Today, 1999. **5**(4): p. 178-86.

189. Leisegang, M., et al., *Enhanced functionality of T cell receptor-redirected T cells is defined by the transgene cassette.* J Mol Med (Berl), 2008. **86**(5): p. 573-83.

190. Scholten, K.B., et al., *Codon modification of T cell receptors allows enhanced functional expression in transgenic human T cells.* Clin Immunol, 2006. **119**(2): p. 135-45.

191. Yang, S., et al., *Development of optimal bicistronic lentiviral vectors facilitates high-level TCR gene expression and robust tumor cell recognition.* Gene Ther, 2008. **15**(21): p. 1411-23.

192. Leisegang, M., et al., *T-cell receptor gene-modified T cells with shared renal cell carcinoma specificity for adoptive T-cell therapy.* Clin Cancer Res, 2010. **16**(8): p. 2333-43.

193. Meyerhuber, P., et al., *Targeting the epidermal growth factor receptor (HER) family by T cell receptor gene-modified T lymphocytes.* J Mol Med (Berl), 2010. **88**(11): p. 1113-21.

194. Hart, D.P., et al., *Retroviral transfer of a dominant TCR prevents surface expression of a large proportion of the endogenous TCR repertoire in human T cells.* Gene Ther, 2008. **15**(8): p. 625-31.

195. Bendle, G.M., et al., *Lethal graft-versus-host disease in mouse models of T cell receptor gene therapy.* Nat Med, 2010. **16**(5): p. 565-70, 1p following 570.

196. van Loenen, M.M., et al., *Mixed T cell receptor dimers harbor potentially harmful neoreactivity.* Proc Natl Acad Sci U S A, 2010. **107**(24): p. 10972-7.

197. Rosenberg, S.A., *Of mice, not men: no evidence for graft-versus-host disease in humans receiving T-cell receptor-transduced autologous T cells.* Mol Ther, 2010. **18**(10): p. 1744-5.

198. Cohen, C.J., et al., *Enhanced antitumor activity of murine-human hybrid T-cell receptor (TCR) in human lymphocytes is associated with improved pairing and TCR/CD3 stability.* Cancer Res, 2006. **66**(17): p. 8878-86.

199. Sommermeyer, D. and W. Uckert, *Minimal amino acid exchange in human TCR constant regions fosters improved function of TCR gene-modified T cells.* J Immunol, 2010. **184**(11): p. 6223-31.

200. Voss, R.H., et al., *Coexpression of the T-cell receptor constant alpha domain triggers tumor reactivity of single-chain TCR-transduced human T cells.* Blood, 2010. **115**(25): p. 5154-63.

201. Blank, U., et al., *Analysis of tetanus toxin peptide/DR recognition by human T cell receptors reconstituted into a murine T cell hybridoma.* Eur J Immunol, 1993. **23**(12): p. 3057-65.

202. Hastings, A.E., et al., *Molecular interactions between transfected human TCR, immunodominant myelin basic protein peptide 152-165, and HLA-DR13.* J Immunol, 1996. **157**(8): p. 3460-71.

203. Aggen, D.H., et al., *Single-chain ValphaVbeta T-cell receptors function without mispairing with endogenous TCR chains.* Gene Ther, 2012. **19**(4): p. 365-74.

204. Okamoto, S., et al., *Improved expression and reactivity of transduced tumor-specific TCRs in human lymphocytes by specific silencing of endogenous TCR.* Cancer Res, 2009. **69**(23): p. 9003-11.

205. Provasi, E., et al., *Editing T cell specificity towards leukemia by zinc finger nucleases and lentiviral gene transfer.* Nat Med, 2012. **18**(5): p. 807-15.

206. Dembic, Z., et al., *Transfer of specificity by murine alpha and beta T-cell receptor genes.* Nature, 1986. **320**(6059): p. 232-8.

207. Duval, L., et al., *Adoptive transfer of allogeneic cytotoxic T lymphocytes equipped with a HLA-A2 restricted MART-1 T-cell receptor: a phase I trial in metastatic melanoma.* Clin Cancer Res, 2006. **12**(4): p. 1229-36.

208. Morgan, R.A., et al., *Cancer regression in patients after transfer of genetically engineered lymphocytes.* Science, 2006. **314**(5796): p. 126-9.

209. Hammarstrom, S., *The carcinoembryonic antigen (CEA) family: structures, suggested functions and expression in normal and malignant tissues.* Semin Cancer Biol, 1999. **9**(2): p. 67-81.

210. Robbins, P.F., et al., *Tumor regression in patients with metastatic synovial cell sarcoma and melanoma using genetically engineered lymphocytes reactive with NY-ESO-1.* J Clin Oncol, 2011. **29**(7): p. 917-24.

211. Morgan, R.A., et al., *Cancer regression and neurological toxicity following anti-MAGE-A3 TCR gene therapy.* J Immunother, 2013. **36**(2): p. 133-51.

212. Cameron, B.J., et al., *Identification of a Titin-derived HLA-A1-presented peptide as a cross-reactive target for engineered MAGE A3-directed T cells.* Sci Transl Med, 2013. **5**(197): p. 197ra103.

213. Linette, G.P., et al., *Cardiovascular toxicity and titin cross-reactivity of affinity-enhanced T cells in myeloma and melanoma.* Blood, 2013. **122**(6): p. 863-71.

214. Schub, A., et al., *CMV-specific TCR-transgenic T cells for immunotherapy.* J Immunol, 2009. **183**(10): p. 6819-30.

215. van Lent, A.U., et al., *Functional human antigen-specific T cells produced in vitro using retroviral T cell receptor transfer into hematopoietic progenitors.* J Immunol, 2007. **179**(8): p. 4959-68.

216. Yang, D., et al., *Evaluation of Epstein-Barr virus latent membrane protein 2 specific T-cell receptors driven by T-cell specific promoters using lentiviral vector.* Clin Dev Immunol, 2011. **2011**: p. 716926.

217. Zheng, Y., et al., *Human Leukocyte Antigen (HLA) A*1101-Restricted Epstein-Barr Virus-Specific T-cell Receptor Gene Transfer to Target Nasopharyngeal Carcinoma.* Cancer Immunol Res, 2015.

218. Hofmann, C., et al., *Human T cells expressing two additional receptors (TETARs) specific for HIV-1 recognize both epitopes.* Blood, 2011. **118**(19): p. 5174-7.

219. Ueno, T., et al., *Reconstitution of anti-HIV effector functions of primary human CD8 T lymphocytes by transfer of HIV-specific alphabeta TCR genes.* Eur J Immunol, 2004. **34**(12): p. 3379-88.

220. Varela-Rohena, A., et al., *Control of HIV-1 immune escape by CD8 T cells expressing enhanced T-cell receptor.* Nat Med, 2008. **14**(12): p. 1390-5.

221. Cooper, L.J., et al., *Transfer of specificity for human immunodeficiency virus type 1 into primary human T lymphocytes by introduction of T-cell receptor genes.* J Virol, 2000. **74**(17): p. 8207-12.

222. Pasetto, A., et al., *TCR-redirected human T cells inhibit hepatitis C virus replication: hepatotoxic potential is linked to antigen specificity and functional avidity.* J Immunol, 2012. **189**(9): p. 4510-9.

223. Scholten, K.B., et al., *Generating HPV specific T helper cells for the treatment of HPV induced malignancies using TCR gene transfer.* J Transl Med, 2011. **9**: p. 147.

224. Chhabra, A., et al., *CD4+CD25- T cells transduced to express MHC class I-restricted epitope-specific TCR synthesize Th1 cytokines and exhibit MHC class I-restricted cytolytic effector function in a human melanoma model.* J Immunol, 2008. **181**(2): p. 1063-70.

225. Ray, S., et al., *MHC-I-restricted melanoma antigen specific TCR-engineered human CD4+ T cells exhibit multifunctional effector and helper responses, in vitro.* Clin Immunol, 2010. **136**(3): p. 338-47.

226. Brusko, T.M., et al., *Human antigen-specific regulatory T cells generated by T cell receptor gene transfer.* PLoS One, 2010. **5**(7): p. e11726.

227. Rees, W., et al., *An inverse relationship between T cell receptor affinity and antigen dose during CD4(+) T cell responses in vivo and in vitro.* Proc Natl Acad Sci U S A, 1999. **96**(17): p. 9781-6.

228. Wilkie, S., et al., *Dual targeting of ErbB2 and MUC1 in breast cancer using chimeric antigen receptors engineered to provide complementary signaling.* J Clin Immunol, 2012. **32**(5): p. 1059-70.

229. Fedorov, V.D., M. Themeli, and M. Sadelain, *PD-1- and CTLA-4-based inhibitory chimeric antigen receptors (iCARs) divert off-target immunotherapy responses.* Sci Transl Med, 2013. **5**(215): p. 215ra172.

230. Liu, K. and S.A. Rosenberg, *Transduction of an IL-2 gene into human melanoma-reactive lymphocytes results in their continued growth in the absence of exogenous IL-2 and maintenance of specific antitumor activity.* J Immunol, 2001. **167**(11): p. 6356-65.

231. Kerkar, S.P., et al., *Tumor-specific CD8+ T cells expressing interleukin-12 eradicate established cancers in lymphodepleted hosts.* Cancer Res, 2010. **70**(17): p. 6725-34.

232. Spear, P., et al., *Chimeric antigen receptor T cells shape myeloid cell function within the tumor microenvironment through IFN-gamma and GM-CSF.* J Immunol, 2012. **188**(12): p. 6389-98.

233. Kerkar, S.P., et al., *IL-12 triggers a programmatic change in dysfunctional myeloid-derived cells within mouse tumors.* J Clin Invest, 2011. **121**(12): p. 4746-57.

234. Koneru, M., et al., *A phase I clinical trial of adoptive T cell therapy using IL-12 secreting MUC-16(ecto) directed chimeric antigen receptors for recurrent ovarian cancer.* J Transl Med, 2015. **13**: p. 102.

235. Craddock, J.A., et al., *Enhanced tumor trafficking of GD2 chimeric antigen receptor T cells by expression of the chemokine receptor CCR2b.* J Immunother, 2010. **33**(8): p. 780-8.

236. Kershaw, M.H., et al., *Redirecting migration of T cells to chemokine secreted from tumors by genetic modification with CXCR2.* Hum Gene Ther, 2002. **13**(16): p. 1971-80.

237. Chinnasamy, D., et al., *Local delivery of interleukin-12 using T cells targeting VEGF receptor-2 eradicates multiple vascularized tumors in mice.* Clin Cancer Res, 2012. **18**(6): p. 1672-83.

238. Legler, D.F., et al., *The alpha v beta 3 integrin as a tumor homing ligand for lymphocytes.* Eur J Immunol, 2004. **34**(6): p. 1608-16.

239. Buckanovich, R.J., et al., *Endothelin B receptor mediates the endothelial barrier to T cell homing to tumors and disables immune therapy.* Nat Med, 2008. **14**(1): p. 28-36.

240. Gattinoni, L., et al., *Removal of homeostatic cytokine sinks by lymphodepletion enhances the efficacy of adoptively transferred tumor-specific CD8+ T cells.* J Exp Med, 2005. **202**(7): p. 907-12.

241. Cho, B.K., et al., *Homeostasis-stimulated proliferation drives naive T cells to differentiate directly into memory T cells.* J Exp Med, 2000. **192**(4): p. 549-56.

242. Kedl, R.M., et al., *T cells compete for access to antigen-bearing antigen-presenting cells.* J Exp Med, 2000. **192**(8): p. 1105-13.

243. Antony, P.A., et al., *CD8+ T cell immunity against a tumor/self-antigen is augmented by CD4+ T helper cells and hindered by naturally occurring T regulatory cells.* J Immunol, 2005. **174**(5): p. 2591-601.

244. Dudley, M.E., et al., *Adoptive cell therapy for patients with metastatic melanoma: evaluation of intensive myeloablative chemoradiation preparative regimens.* J Clin Oncol, 2008. **26**(32): p. 5233-9.

245. Besser, M.J., et al., *Adoptive transfer of tumor-infiltrating lymphocytes in patients with metastatic melanoma: intent-to-treat analysis and efficacy after failure to prior immunotherapies.* Clin Cancer Res, 2013. **19**(17): p. 4792-800.

246. Ellebaek, E., et al., *Adoptive cell therapy with autologous tumor infiltrating lymphocytes and low-dose Interleukin-2 in metastatic melanoma patients.* J Transl Med, 2012. **10**: p. 169.

247. Ciceri, F., et al., *Infusion of suicide-gene-engineered donor lymphocytes after family haploidentical haemopoietic stem-cell transplantation for leukaemia (the TK007 trial): a non-randomised phase I-II study.* Lancet Oncol, 2009. **10**(5): p. 489-500.

248. Recchia, A., et al., *Retroviral vector integration deregulates gene expression but has no consequence on the biology and function of transplanted T cells.* Proc Natl Acad Sci U S A, 2006. **103**(5): p. 1457-62.

249. Berger, C., et al., *Analysis of transgene-specific immune responses that limit the in vivo persistence of adoptively transferred HSV-TK-modified donor T cells after allogeneic hematopoietic cell transplantation.* Blood, 2006. **107**(6): p. 2294-302.

250. Riddell, S.R., et al., *T-cell mediated rejection of gene-modified HIV-specific cytotoxic T lymphocytes in HIV-infected patients.* Nat Med, 1996. **2**(2): p. 216-23.

251. Budde, L.E., et al., *Combining a CD20 chimeric antigen receptor and an inducible caspase 9 suicide switch to improve the efficacy and safety of T cell adoptive immunotherapy for lymphoma.* PLoS One, 2013. **8**(12): p. e82742.

252. Di Stasi, A., et al., *Inducible apoptosis as a safety switch for adoptive cell therapy.* N Engl J Med, 2011. **365**(18): p. 1673-83.

253. Hoyos, V., et al., *Engineering CD19-specific T lymphocytes with interleukin-15 and a suicide gene to enhance their anti-lymphoma/leukemia effects and safety.* Leukemia, 2010. **24**(6): p. 1160-70.

254. Straathof, K.C., et al., *An inducible caspase 9 safety switch for T-cell therapy.* Blood, 2005. **105**(11): p. 4247-54.

255. Griffioen, M., et al., *Retroviral transfer of human CD20 as a suicide gene for adoptive T-cell therapy.* Haematologica, 2009. **94**(9): p. 1316-20.

256. Wang, X., et al., *A transgene-encoded cell surface polypeptide for selection, in vivo tracking, and ablation of engineered cells.* Blood, 2011. **118**(5): p. 1255-63.

257. Vitiello, A., et al., *Analysis of the HLA-restricted influenza-specific cytotoxic T lymphocyte response in transgenic mice carrying a chimeric human-mouse class I major histocompatibility complex.* J Exp Med, 1991. **173**(4): p. 1007-15.

258. Parkhurst, M.R., et al., *Characterization of genetically modified T-cell receptors that recognize the CEA:691-699 peptide in the context of HLA-A2.1 on human colorectal cancer cells.* Clin Cancer Res, 2009. **15**(1): p. 169-80.

259. Kuball, J., et al., *Cooperation of human tumor-reactive CD4+ and CD8+ T cells after redirection of their specificity by a high-affinity p53A2.1-specific TCR.* Immunity, 2005. **22**(1): p. 117-29.

260. Wilde, S., et al., *Generation of allo-restricted peptide-specific T cells using RNA-pulsed dendritic cells: A three phase experimental procedure.* Oncoimmunology, 2012. **1**(2): p. 129-140.

261. Schmitt, T.M., et al., *Enhanced-affinity murine T-cell receptors for tumor/self-antigens can be safe in gene therapy despite surpassing the threshold for thymic selection.* Blood, 2013. **122**(3): p. 348-56.

262. Chlewicki, L.K., et al., *High-affinity, peptide-specific T cell receptors can be generated by mutations in CDR1, CDR2 or CDR3.* J Mol Biol, 2005. **346**(1): p. 223-39.

263. Gostick, E., et al., *Functional and biophysical characterization of an HLA-A*6801-restricted HIV-specific T cell receptor.* Eur J Immunol, 2007. **37**(2): p. 479-86.

264. Purbhoo, M.A., et al., *The HLA A*0201-restricted hTERT(540-548) peptide is not detected on tumor cells by a CTL clone or a high-affinity T-cell receptor.* Mol Cancer Ther, 2007. **6**(7): p. 2081-91.

265. Jones, L.L., et al., *Engineering and characterization of a stabilized alpha1/alpha2 module of the class I major histocompatibility complex product Ld.* J Biol Chem, 2006. **281**(35): p. 25734-44.

266. Malecek, K., et al., *Specific increase in potency via structure-based design of a TCR.* J Immunol, 2014. **193**(5): p. 2587-99.

267. Malecek, K., et al., *Engineering improved T cell receptors using an alanine-scan guided T cell display selection system.* J Immunol Methods, 2013. **392**(1-2): p. 1-11.

268. Dunn, S.M., et al., *Directed evolution of human T cell receptor CDR2 residues by phage display dramatically enhances affinity for cognate peptide-MHC without increasing apparent cross-reactivity.* Protein Sci, 2006. **15**(4): p. 710-21.

269. Zhao, Y., et al., *High-affinity TCRs generated by phage display provide CD4+ T cells with the ability to recognize and kill tumor cell lines.* J Immunol, 2007. **179**(9): p. 5845-54.

270. Haidar, J.N., et al., *Structure-based design of a T-cell receptor leads to nearly 100-fold improvement in binding affinity for pepMHC.* Proteins, 2009. **74**(4): p. 948-60.

271. Khong, H.T. and N.P. Restifo, *Natural selection of tumor variants in the generation of "tumor escape" phenotypes.* Nat Immunol, 2002. **3**(11): p. 999-1005.

272. Lucas, M., et al., *Viral escape mechanisms--escapology taught by viruses.* Int J Exp Pathol, 2001. **82**(5): p. 269-86.

273. Protzer, U. and H. Schaller, *Immune escape by hepatitis B viruses.* Virus Genes, 2000. **21**(1-2): p. 27-37.

274. Rosenberg, W., *Mechanisms of immune escape in viral hepatitis.* Gut, 1999. **44**(5): p. 759-64.

275. Kim, D., et al., *Number of mutations within CTL-defined epitopes of the hepatitis B Virus (HBV) core region is associated with HBV disease progression.* J Med Virol, 2011. **83**(12): p. 2082-7.

276. Moorman, J.P., M. Joo, and Y.S. Hahn, *Evasion of host immune surveillance by hepatitis C virus: potential roles in viral persistence.* Arch Immunol Ther Exp (Warsz), 2001. **49**(3): p. 189-94.

277. Quarleri, J.F. and J.R. Oubina, *Hepatitis C virus strategies to evade the specific-T cell response: a possible mission favoring its persistence.* Ann Hepatol, 2015. **15**(1): p. 17-26.

278. Walker, A., et al., *Distinct escape pathway by HCV genotype 1a from a dominant CD8+ T cell response by selection of altered epitope processing.* J Virol, 2015.

279. Kolls, J.K. and G. Szabo, *The genetics of hepatitis C virus underlie its ability to escape humoral immunity.* J Clin Invest, 2015. **125**(1): p. 97-8.

280. McMichael, A.J. and R.E. Phillips, *Escape of human immunodeficiency virus from immune control.* Annu Rev Immunol, 1997. **15**: p. 271-96.

281. Wolinsky, S.M., et al., *Adaptive evolution of human immunodeficiency virus-type 1 during the natural course of infection.* Science, 1996. **272**(5261): p. 537-42.

282. Phillips, R.E., et al., *Human immunodeficiency virus genetic variation that can escape cytotoxic T cell recognition.* Nature, 1991. **354**(6353): p. 453-9.

283. de Campos-Lima, P.O., et al., *HLA-A11 epitope loss isolates of Epstein-Barr virus from a highly A11+ population.* Science, 1993. **260**(5104): p. 98-100.

284. de Campos-Lima, P.O., et al., *T cell responses and virus evolution: loss of HLA A11-restricted CTL epitopes in Epstein-Barr virus isolates from highly A11-positive populations by selective mutation of anchor residues.* J Exp Med, 1994. **179**(4): p. 1297-305.

285. Bertoletti, A., et al., *Natural variants of cytotoxic epitopes are T-cell receptor antagonists for antiviral cytotoxic T cells.* Nature, 1994. **369**(6479): p. 407-10.

286. Restifo, N.P., et al., *Identification of human cancers deficient in antigen processing.* J Exp Med, 1993. **177**(2): p. 265-72.

287. Cromme, F.V., et al., *Loss of transporter protein, encoded by the TAP-1 gene, is highly correlated with loss of HLA expression in cervical carcinomas.* J Exp Med, 1994. **179**(1): p. 335-40.

288. Johnsen, A.K., et al., *Deficiency of transporter for antigen presentation (TAP) in tumor cells allows evasion of immune surveillance and increases tumorigenesis.* J Immunol, 1999. **163**(8): p. 4224-31.

289. Ossendorp, F., et al., *A single residue exchange within a viral CTL epitope alters proteasome-mediated degradation resulting in lack of antigen presentation.* Immunity, 1996. **5**(2): p. 115-24.

290. Stackpole, C.W., et al., *Antigenic modulation as a mechanism for tumor escape from immune destruction: identification of modulation-positive and modulation-*

negative mouse lymphomas with xenoantisera to murine leukemia virus gp70. J Immunol, 1980. **125**(4): p. 1715-23.

291. Jerne, N.K., *THE NATURAL-SELECTION THEORY OF ANTIBODY FORMATION.* Proc Natl Acad Sci U S A, 1955. **41**(11): p. 849-57.

292. Jerne, N.K., *The somatic generation of immune recognition.* Eur J Immunol, 1971. **1**(1): p. 1-9.

293. Mason, D., *A very high level of crossreactivity is an essential feature of the T-cell receptor.* Immunol Today, 1998. **19**(9): p. 395-404.

294. Sewell, A.K., *Why must T cells be cross-reactive?* Nat Rev Immunol, 2012. **12**(9): p. 669-77.

295. Robinson, J., et al., *IMGT/HLA and IMGT/MHC: sequence databases for the study of the major histocompatibility complex.* Nucleic Acids Res, 2003. **31**(1): p. 311-4.

296. Arstila, T.P., et al., *A direct estimate of the human alphabeta T cell receptor diversity.* Science, 1999. **286**(5441): p. 958-61.

297. Ignatowicz, L., J. Kappler, and P. Marrack, *The repertoire of T cells shaped by a single MHC/peptide ligand.* Cell, 1996. **84**(4): p. 521-9.

298. Ignatowicz, L., et al., *T cells can be activated by peptides that are unrelated in sequence to their selecting peptide.* Immunity, 1997. **7**(2): p. 179-86.

299. Hiemstra, H.S., et al., *Quantitative determination of TCR cross-reactivity using peptide libraries and protein databases.* Eur J Immunol, 1999. **29**(8): p. 2385-91.

300. Maynard, J., et al., *Structure of an autoimmune T cell receptor complexed with class II peptide-MHC: insights into MHC bias and antigen specificity.* Immunity, 2005. **22**(1): p. 81-92.

301. Wooldridge, L., et al., *A single autoimmune T cell receptor recognizes more than a million different peptides.* J Biol Chem, 2012. **287**(2): p. 1168-77.

302. Rosen, H.R., et al., *Cutting edge: identification of hepatitis C virus-specific CD8+ T cells restricted by donor HLA alleles following liver transplantation.* J Immunol, 2004. **173**(9): p. 5355-9.

303. Treisman, J., et al., *Interleukin-2-transduced lymphocytes grow in an autocrine fashion and remain responsive to antigen.* Blood, 1995. **85**(1): p. 139-45.

304. Norell, H., et al., *CD34-based enrichment of genetically engineered human T cells for clinical use results in dramatically enhanced tumor targeting.* Cancer Immunol Immunother, 2010. **59**(6): p. 851-62.

305. Lyons, G.E., et al., *Influence of human CD8 on antigen recognition by T-cell receptor-transduced cells.* Cancer Res, 2006. **66**(23): p. 11455-61.

306. Garboczi, D.N., D.T. Hung, and D.C. Wiley, *HLA-A2-peptide complexes: refolding and crystallization of molecules expressed in Escherichia coli and complexed with single antigenic peptides.* Proc Natl Acad Sci U S A, 1992. **89**(8): p. 3429-33.

307. Pierce, B.G., et al., *Computational design of the affinity and specificity of a therapeutic T cell receptor.* PLoS Comput Biol, 2014. **10**(2): p. e1003478.

308. Clement, M., et al., *Anti-CD8 antibodies can trigger CD8+ T cell effector function in the absence of TCR engagement and improve peptide-MHCI tetramer staining.* J Immunol, 2011. **187**(2): p. 654-63.

309. Wooldridge, L., et al., *Anti-CD8 antibodies can inhibit or enhance peptide-MHC class I (pMHCI) multimer binding: this is paralleled by their effects on CTL activation and occurs in the absence of an interaction between pMHCI and CD8 on the cell surface.* J Immunol, 2003. **171**(12): p. 6650-60.

310. Wooldridge, L., et al., *Anti-coreceptor antibodies profoundly affect staining with peptide-MHC class I and class II tetramers.* Eur J Immunol, 2006. **36**(7): p. 1847-55.

311. Bagwell, C.B., et al., *Probability state modeling theory.* Cytometry A, 2015. **87**(7): p. 646-60.

312. Qiu, P., et al., *Extracting a cellular hierarchy from high-dimensional cytometry data with SPADE.* Nat Biotechnol, 2011. **29**(10): p. 886-91.

313. Diggins, K.E., P.B. Ferrell, Jr., and J.M. Irish, *Methods for discovery and characterization of cell subsets in high dimensional mass cytometry data.* Methods, 2015. **82**: p. 55-63.

314. Jobin, C., et al., *Heterogeneity of in vitro-cultured CD34+ cells isolated from peripheral blood.* Cytotherapy, 2015.

315. Qiu, P., *Inferring phenotypic properties from single-cell characteristics.* PLoS One, 2012. **7**(5): p. e37038.

316. Van Gassen, S., et al., *FlowSOM: Using self-organizing maps for visualization and interpretation of cytometry data.* Cytometry A, 2015. **87**(7): p. 636-45.

317. Amir el, A.D., et al., *viSNE enables visualization of high dimensional single-cell data and reveals phenotypic heterogeneity of leukemia.* Nat Biotechnol, 2013. **31**(6): p. 545-52.

318. Lin, L., et al., *Identification and visualization of multidimensional antigen-specific T-cell populations in polychromatic cytometry data.* Cytometry A, 2015. **87**(7): p. 675-82.

319. Qian, Y., et al., *Elucidation of seventeen human peripheral blood B-cell subsets and quantification of the tetanus response using a density-based method for the automated identification of cell populations in multidimensional flow cytometry data.* Cytometry B Clin Cytom, 2010. **78 Suppl 1**: p. S69-82.

320. Roederer, M., J.L. Nozzi, and M.C. Nason, *SPICE: exploration and analysis of post-cytometric complex multivariate datasets.* Cytometry A, 2011. **79**(2): p. 167-74.

321. Garrett, E.S., *Overview of Standard Clustering Approaches for Gene Microarray Data Analysis*, in *DNA Microarrays and Statistical Genomic Techniques: Design, Analyis, and Interpretation of Experiments*, M.B. D. Allison, J. Edwards, G. Page, Editor. 2006, Marcel-Dekker: New York.

322. Gagnon, S.J., et al., *Unraveling a hotspot for TCR recognition on HLA-A2: evidence against the existence of peptide-independent TCR binding determinants.* J Mol Biol, 2005. **353**(3): p. 556-73.

323. Khan, A.R., et al., *The structure and stability of an HLA-A*0201/octameric tax peptide complex with an empty conserved peptide-N-terminal binding site.* J Immunol, 2000. **164**(12): p. 6398-405.

324. Riley, T., et al., *Computational modeling of TCR-pMHC complexes*, in *Methods Mol Biol*, B.L. Stoddard, Editor. 2016, Springer: New Yor, New York.

325. Borbulevych, O.Y., et al., *TCRs used in cancer gene therapy cross-react with MART-1/Melan-A tumor antigens via distinct mechanisms.* J Immunol, 2011. **187**(5): p. 2453-63.

326. Ding, Y.H., et al., *Two human T cell receptors bind in a similar diagonal mode to the HLA-A2/Tax peptide complex using different TCR amino acids.* Immunity, 1998. **8**(4): p. 403-11.

327. Chaudhury, S., S. Lyskov, and J.J. Gray, *PyRosetta: a script-based interface for implementing molecular modeling algorithms using Rosetta.* Bioinformatics, 2010. **26**(5): p. 689-91.

328. Kaufmann, K.W., et al., *Practically useful: what the Rosetta protein modeling suite can do for you.* Biochemistry, 2010. **49**(14): p. 2987-98.

329. Leaver-Fay, A., et al., *Scientific benchmarks for guiding macromolecular energy function improvement.* Methods Enzymol, 2013. **523**: p. 109-43.

330. Mandell, D.J., E.A. Coutsias, and T. Kortemme, *Sub-angstrom accuracy in protein loop reconstruction by robotics-inspired conformational sampling.* Nat Methods, 2009. **6**(8): p. 551-2.

331. Adams, P.D., et al., *PHENIX: a comprehensive Python-based system for macromolecular structure solution.* Acta Crystallogr D Biol Crystallogr, 2010. **66**(Pt 2): p. 213-21.

332. Murshudov, G.N., et al., *REFMAC5 for the refinement of macromolecular crystal structures.* Acta Crystallogr D Biol Crystallogr, 2011. **67**(Pt 4): p. 355-67.

333. Emsley, P., et al., *Features and development of Coot.* Acta Crystallogr D Biol Crystallogr, 2010. **66**(Pt 4): p. 486-501.

334. Rosati, S.F., et al., *A novel murine T-cell receptor targeting NY-ESO-1.* J Immunother, 2014. **37**(3): p. 135-46.

335. Stanislawski, T., et al., *Circumventing tolerance to a human MDM2-derived tumor antigen by TCR gene transfer.* Nat Immunol, 2001. **2**(10): p. 962-70.

336. Chodon, T., et al., *Adoptive transfer of MART-1 T-cell receptor transgenic lymphocytes and dendritic cell vaccination in patients with metastatic melanoma.* Clin Cancer Res, 2014. **20**(9): p. 2457-65.

337. WHO. *Hepatitis C fact sheet*. 2015 [cited 2015 July]; Available from: http://www.who.int/mediacentre/factsheets/fs164/en/.

338. *Hepatitis C FAQs*. 2015 [cited 2015 July]; Available from: http://www.cdc.gov/hepatitis/hcv/hcvfaq.htm.

339. Campos-Varela, I., et al., *Hepatitis C genotype influences post-liver transplant outcomes.* Transplantation, 2015. **99**(4): p. 835-40.

340. Hézode, C., et al., *Telaprevir and Peginterferon with or without Ribavirin for Chronic HCV Infection.* New England Journal of Medicine, 2009. **360**(18): p. 1839-1850.

341. Kwo, P.Y., et al., *Efficacy of boceprevir, an NS3 protease inhibitor, in combination with peginterferon alfa-2b and ribavirin in treatment-naive patients with genotype 1 hepatitis C infection (SPRINT-1): an open-label, randomised, multicentre phase 2 trial.* Lancet, 2010. **376**(9742): p. 705-16.

342. Manns, M., et al., *Simeprevir with pegylated interferon alfa 2a or 2b plus ribavirin in treatment-naive patients with chronic hepatitis C virus genotype 1 infection (QUEST-2): a randomised, double-blind, placebo-controlled phase 3 trial.* Lancet, 2014. **384**(9941): p. 414-26.

343. Berger, K.L., et al., *Baseline Polymorphisms and Emergence of Drug Resistance in the NS3/4A Protease of HCV Genotype-1 Following Treatment with Faldaprevir plus Pegylated Interferon Alfa-2a and Ribavirin in Phase 2 and Phase 3 Studies.* Antimicrob Agents Chemother, 2015.

344. De Luca, A., et al., *Two Distinct Hepatitis C Virus Genotype 1a Clades Have Different Geographical Distribution and Association With Natural Resistance to NS3 Protease Inhibitors.* Open Forum Infect Dis, 2015. **2**(2): p. ofv043.

345. Nagpal, N., et al., *Molecular principles behind Boceprevir resistance due to mutations in hepatitis C NS3/4A protease.* Gene, 2015. **570**(1): p. 115-21.

346. Lechmann, M. and T.J. Liang, *Vaccine development for hepatitis C.* Semin Liver Dis, 2000. **20**(2): p. 211-26.

347. Trujillo-Murillo Kdel, C., et al., *Experimental models for hepatitis C virus (HCV): new opportunities for combating hepatitis C.* Ann Hepatol, 2004. **3**(2): p. 54-62.

348. Freeman, M.L., et al., *CD4 T cells specific for a latency-associated gamma-herpesvirus epitope are polyfunctional and cytotoxic.* J Immunol, 2014. **193**(12): p. 5827-34.

349. Keesen, T.S., et al., *Characterization of CD4(+) cytotoxic lymphocytes and apoptosis markers induced by Trypanossoma cruzi infection.* Scand J Immunol, 2012. **76**(3): p. 311-9.

350. Kitano, S., et al., *Enhancement of tumor-reactive cytotoxic CD4+ T cell responses after ipilimumab treatment in four advanced melanoma patients.* Cancer Immunol Res, 2013. **1**(4): p. 235-44.

351. Morales, O., et al., *EBV Latency II-derived peptides induce a specific CD4+ cytotoxic T-cell activity and not a CD4+ regulatory T-cell response.* J Immunother, 2012. **35**(3): p. 254-66.

352. Campo, D.S., et al., *Next-generation sequencing reveals large connected networks of intra-host HCV variants.* BMC Genomics, 2014. **15 Suppl 5**: p. S4.

353. Cusick, M.F., et al., *Naturally occurring CD4+ T-cell epitope variants act as altered peptide ligands leading to impaired helper T-cell responses in hepatitis C virus infection.* Hum Immunol, 2011. **72**(5): p. 379-85.

354. Gededzha, M.P., M.J. Mphahlele, and S.G. Selabe, *Characterization of HCV genotype 5a envelope proteins: implications for vaccine development and therapeutic entry target.* Hepat Mon, 2014. **14**(11): p. e23660.

355. Skums, P., L. Bunimovich, and Y. Khudyakov, *Antigenic cooperation among intrahost HCV variants organized into a complex network of cross-immunoreactivity.* Proc Natl Acad Sci U S A, 2015. **112**(21): p. 6653-8.

356. Ulsenheimer, A., et al., *Lack of variant specific CD8+ T-cell response against mutant and pre-existing variants leads to outgrowth of particular clones in acute hepatitis C.* Virol J, 2013. **10**: p. 295.

357. Rehermann, B., *Interaction between the hepatitis C virus and the immune system.* Semin Liver Dis, 2000. **20**(2): p. 127-41.

358. Seifert, U., et al., *Hepatitis C virus mutation affects proteasomal epitope processing.* J Clin Invest, 2004. **114**(2): p. 250-9.

359. Jazwinski, A.B. and A.J. Muir, *Direct-acting antiviral medications for chronic hepatitis C virus infection.* Gastroenterol Hepatol (N Y), 2011. **7**(3): p. 154-62.

360. Salvatierra, K., et al., *Hepatitis C virus resistance to new specifically-targeted antiviral therapy: A public health perspective.* World J Virol, 2013. **2**(1): p. 6-15.

361. Barth, H., *Hepatitis C virus: Is it time to say goodbye yet? Perspectives and challenges for the next decade.* World J Hepatol, 2015. **7**(5): p. 725-37.

362. Ogishi, M., et al., *Deconvoluting the composition of low-frequency hepatitis C viral quasispecies: comparison of genotypes and NS3 resistance-associated variants between HCV/HIV coinfected hemophiliacs and HCV monoinfected patients in Japan.* PLoS One, 2015. **10**(3): p. e0119145.

363. Missale, G., et al., *Different clinical behaviors of acute hepatitis C virus infection are associated with different vigor of the anti-viral cell-mediated immune response.* J Clin Invest, 1996. **98**(3): p. 706-14.

364. Thimme, R., et al., *Determinants of viral clearance and persistence during acute hepatitis C virus infection.* J Exp Med, 2001. **194**(10): p. 1395-406.

365. Rosen, H.R., *Emerging concepts in immunity to hepatitis C virus infection.* J Clin Invest, 2013. **123**(10): p. 4121-30.

366. Rehermann, B., *Hepatitis C virus versus innate and adaptive immune responses: a tale of coevolution and coexistence.* J Clin Invest, 2009. **119**(7): p. 1745-54.

367. Oniangue-Ndza, C., et al., *Compensatory mutations restore the replication defects caused by cytotoxic T lymphocyte escape mutations in hepatitis C virus polymerase.* J Virol, 2011. **85**(22): p. 11883-90.

368. Dazert, E., et al., *Loss of viral fitness and cross-recognition by CD8+ T cells limit HCV escape from a protective HLA-B27-restricted human immune response.* J Clin Invest, 2009. **119**(2): p. 376-86.

369. Yerly, D., et al., *Increased cytotoxic T-lymphocyte epitope variant cross-recognition and functional avidity are associated with hepatitis C virus clearance.* J Virol, 2008. **82**(6): p. 3147-53.

370. Alexander-Miller, M.A., G.R. Leggatt, and J.A. Berzofsky, *Selective expansion of high- or low-avidity cytotoxic T lymphocytes and efficacy for adoptive immunotherapy.* Proc Natl Acad Sci U S A, 1996. **93**(9): p. 4102-7.

371. Spear, T.T., Callender, G.G., Roszkowski, J.J., Moxley, K.M., Simms, P.E., Foley, K.C., Murray, D.C., Scurti, G.M., Li, M., Thomas, J.T., Langerman, A., Garrett-Mayer, E., Zhang, Y., and Nishimura, M.I., *TCR gene-modified T cells can efficiently treat established hepatitis C-associated hepatocellular carcinoma tumors.* Cancer Immunology, Immunotherapy, 2016. **In Press.**

372. King, C., et al., *Removing T-cell epitopes with computational protein design.* Proc Natl Acad Sci U S A, 2014. **111**(23): p. 8577-82.

373. Messina, J.P., et al., *Global distribution and prevalence of hepatitis C virus genotypes.* Hepatology, 2015. **61**(1): p. 77-87.

374. Rudolph, M.G., R.L. Stanfield, and I.A. Wilson, *How TCRs bind MHCs, peptides, and coreceptors.* Annu Rev Immunol, 2006. **24**: p. 419-66.

375. Insaidoo, F.K., et al., *Loss of T cell antigen recognition arising from changes in peptide and major histocompatibility complex protein flexibility: implications for vaccine design.* J Biol Chem, 2011. **286**(46): p. 40163-73.

376. Borbulevych, O.Y., et al., *Increased immunogenicity of an anchor-modified tumor-associated antigen is due to the enhanced stability of the peptide/MHC complex: implications for vaccine design.* J Immunol, 2005. **174**(8): p. 4812-20.

377. Madden, D.R., *The three-dimensional structure of peptide-MHC complexes.* Annu Rev Immunol, 1995. **13**: p. 587-622.

378. Wooldridge, L., et al., *Interaction between the CD8 coreceptor and major histocompatibility complex class I stabilizes T cell receptor-antigen complexes at the cell surface.* J Biol Chem, 2005. **280**(30): p. 27491-501.

379. Turner, J.M., et al., *Interaction of the unique N-terminal region of tyrosine kinase p56lck with cytoplasmic domains of CD4 and CD8 is mediated by cysteine motifs.* Cell, 1990. **60**(5): p. 755-65.

380. Cebecauer, M., et al., *Soluble MHC-peptide complexes induce rapid death of CD8+ CTL.* J Immunol, 2005. **174**(11): p. 6809-19.

381. Purbhoo, M.A., et al., *The human CD8 coreceptor effects cytotoxic T cell activation and antigen sensitivity primarily by mediating complete phosphorylation of the T cell receptor zeta chain.* J Biol Chem, 2001. **276**(35): p. 32786-92.

382. Wooldridge, L., et al., *Enhanced immunogenicity of CTL antigens through mutation of the CD8 binding MHC class I invariant region.* Eur J Immunol, 2007. **37**(5): p. 1323-33.

383. Heemskerk, M.H., et al., *Redirection of antileukemic reactivity of peripheral T lymphocytes using gene transfer of minor histocompatibility antigen HA-2-specific T-cell receptor complexes expressing a conserved alpha joining region.* Blood, 2003. **102**(10): p. 3530-40.

384. Wooldridge, L., et al., *Tricks with tetramers: how to get the most from multimeric peptide-MHC.* Immunology, 2009. **126**(2): p. 147-64.

385. Bestard, O., et al., *Pretransplant immediately early-1-specific T cell responses provide protection for CMV infection after kidney transplantation.* Am J Transplant, 2013. **13**(7): p. 1793-805.

386. Kirkwood, J.M., et al., *Immunogenicity and antitumor effects of vaccination with peptide vaccine+/-granulocyte-monocyte colony-stimulating factor and/or IFN-alpha2b in advanced metastatic melanoma: Eastern Cooperative Oncology Group Phase II Trial E1696.* Clin Cancer Res, 2009. **15**(4): p. 1443-51.

387. Lee, K.H., et al., *Increased vaccine-specific T cell frequency after peptide-based vaccination correlates with increased susceptibility to in vitro stimulation but does not lead to tumor regression.* J Immunol, 1999. **163**(11): p. 6292-300.

388. Reynolds, S.R., et al., *Stimulation of CD8+ T cell responses to MAGE-3 and Melan A/MART-1 by immunization to a polyvalent melanoma vaccine.* Int J Cancer, 1997. **72**(6): p. 972-6.

389. Salgaller, M.L., et al., *Report of immune monitoring of prostate cancer patients undergoing T-cell therapy using dendritic cells pulsed with HLA-A2-specific peptides from prostate-specific membrane antigen (PSMA).* Prostate, 1998. **35**(2): p. 144-51.

390. Scheibenbogen, C., et al., *Long-term freedom from recurrence in 2 stage IV melanoma patients following vaccination with tyrosinase peptides.* Int J Cancer, 2002. **99**(3): p. 403-8.

391. Scheibenbogen, C., et al., *Phase 2 trial of vaccination with tyrosinase peptides and granulocyte-macrophage colony-stimulating factor in patients with metastatic melanoma.* J Immunother, 2000. **23**(2): p. 275-81.

392. Schreiber, S., et al., *Immunotherapy of metastatic malignant melanoma by a vaccine consisting of autologous interleukin 2-transfected cancer cells: outcome of a phase I study.* Hum Gene Ther, 1999. **10**(6): p. 983-93.

393. Tey, S.K., et al., *Clinical assessment of anti-viral CD8+ T cell immune monitoring using QuantiFERON-CMV(R) assay to identify high risk allogeneic hematopoietic stem cell transplant patients with CMV infection complications.* PLoS One, 2013. **8**(10): p. e74744.

394. Khader, S.A. and R. Gopal, *IL-17 in protective immunity to intracellular pathogens.* Virulence, 2010. **1**(5): p. 423-7.

395. Tada, T., et al., *Two distinct types of helper T cells involved in the secondary antibody response: independent and synergistic effects of Ia- and Ia+ helper T cells.* J Exp Med, 1978. **147**(2): p. 446-58.

396. Mosmann, T.R. and R.L. Coffman, *TH1 and TH2 cells: different patterns of lymphokine secretion lead to different functional properties.* Annu Rev Immunol, 1989. **7**: p. 145-73.

397. Harrington, L.E., et al., *Interleukin 17-producing CD4+ effector T cells develop via a lineage distinct from the T helper type 1 and 2 lineages.* Nat Immunol, 2005. **6**(11): p. 1123-32.

398. Jager, A., et al., *Th1, Th17, and Th9 effector cells induce experimental autoimmune encephalomyelitis with different pathological phenotypes.* J Immunol, 2009. **183**(11): p. 7169-77.

399. Li, H. and A. Rostami, *IL-9: basic biology, signaling pathways in CD4+ T cells and implications for autoimmunity.* J Neuroimmune Pharmacol, 2010. **5**(2): p. 198-209.

400. Kang, W., et al., *Dynamic analysis of Th1/Th2 cytokine concentration during antiretroviral therapy of HIV-1/HCV co-infected patients.* BMC Infect Dis, 2012. **12**: p. 102.

401. Price, P., et al., *A T2 cytokine environment may not limit T1 responses in human immunodeficiency virus patients with a favourable response to antiretroviral therapy.* Immunology, 2006. **119**(1): p. 74-82.

402. Villacres, M.C., et al., *Reduced type 1 and type 2 cytokines in antiviral memory T helper function among women coinfected with HIV and HCV.* J Clin Immunol, 2005. **25**(2): p. 134-41.

403. Lu, Y., et al., *Th9 cells promote antitumor immune responses in vivo.* J Clin Invest, 2012. **122**(11): p. 4160-71.

404. Foster, R.G., et al., *Interleukin (IL)-17/IL-22-producing T cells enriched within the liver of patients with chronic hepatitis C viral (HCV) infection.* Dig Dis Sci, 2012. **57**(2): p. 381-9.

405. Maraveyas, A., et al., *Possible improved survival of patients with stage IV AJCC melanoma receiving SRL 172 immunotherapy: correlation with induction of increased levels of intracellular interleukin-2 in peripheral blood lymphocytes.* Ann Oncol, 1999. **10**(7): p. 817-24.

406. Zaritskaya, L., et al., *New flow cytometric assays for monitoring cell-mediated cytotoxicity.* Expert Rev Vaccines, 2010. **9**(6): p. 601-16.

407. Donermeyer, D.L., et al., *The study of high-affinity TCRs reveals duality in T cell recognition of antigen: specificity and degeneracy.* J Immunol, 2006. **177**(10): p. 6911-9.

408. Gerlach, J.T., et al., *Recurrence of hepatitis C virus after loss of virus-specific CD4(+) T-cell response in acute hepatitis C.* Gastroenterology, 1999. **117**(4): p. 933-41.

409. Semmo, N. and P. Klenerman, *CD4+ T cell responses in hepatitis C virus infection.* World J Gastroenterol, 2007. **13**(36): p. 4831-8.

410. Cedrone, A., et al., *Utility of alpha-fetoprotein (AFP) in the screening of patients with virus-related chronic liver disease: does different viral etiology influence AFP levels in HCC? A study in 350 western patients.* Hepatogastroenterology, 2000. **47**(36): p. 1654-8.

411. Li, W., et al., *Development of a gene therapy strategy to target hepatocellular carcinoma based inhibition of protein phosphatase 2A using the alpha-fetoprotein promoter enhancer and pgk promoter: an in vitro and in vivo study.* BMC Cancer, 2012. **12**: p. 547.

412. Ohashi, M., et al., *Target gene therapy for alpha-fetoprotein-producing hepatocellular carcinoma by E1B55k-attenuated adenovirus.* Biochem Biophys Res Commun, 2001. **282**(2): p. 529-35.

413. Fan, Z., et al., *Radioiodinated anti-hepatocellular carcinoma (HCC) ferritin. Targeting therapy, tumor imaging and anti-antibody response in HCC patients with hepatic arterial infusion.* J Cancer Res Clin Oncol, 1992. **118**(5): p. 371-6.

414. Flecken, T., et al., *Immunodominance and functional alterations of tumor-associated antigen-specific CD8+ T-cell responses in hepatocellular carcinoma.* Hepatology, 2014. **59**(4): p. 1415-26.

415. Schmidt, N., T. Flecken, and R. Thimme, *Tumor-associated antigen specific CD8 T cells in hepatocellular carcinoma - a promising target for immunotherapy.* Oncoimmunology, 2014. **3**(9): p. e954919.

416. Shang, X.Y., et al., *The spontaneous CD8+ T-cell response to HLA-A2-restricted NY-ESO-1b peptide in hepatocellular carcinoma patients.* Clin Cancer Res, 2004. **10**(20): p. 6946-55.

417. Sideras, K., et al., *Tumour antigen expression in hepatocellular carcinoma in a low-endemic western area.* Br J Cancer, 2015. **112**(12): p. 1911-20.

418. Xu, H., et al., *NY-ESO-1 expression in hepatocellular carcinoma: A potential new marker for early recurrence after surgery.* Oncol Lett, 2012. **3**(1): p. 39-44.

419. Gao, W., H. Kim, and M. Ho, *Human Monoclonal Antibody Targeting the Heparan Sulfate Chains of Glypican-3 Inhibits HGF-Mediated Migration and Motility of Hepatocellular Carcinoma Cells.* PLoS One, 2015. **10**(9): p. e0137664.

420. Geramizadeh, B. and N. Seirfar, *Diagnostic Value of Arginase-1 and Glypican-3 in Differential Diagnosis of Hepatocellular Carcinoma, Cholangiocarcinoma and Metastatic Carcinoma of Liver.* Hepat Mon, 2015. **15**(7): p. e30336.

421. Hanaoka, H., et al., *Glypican-3 targeted human heavy chain antibody as a drug carrier for hepatocellular carcinoma therapy.* Mol Pharm, 2015. **12**(6): p. 2151-7.

422. Wang, L., et al., *Glypican-3 is a biomarker and a therapeutic target of hepatocellular carcinoma.* Hepatobiliary Pancreat Dis Int, 2015. **14**(4): p. 361-6.

423. Wu, Y., et al., *Glypican-3 promotes epithelial-mesenchymal transition of hepatocellular carcinoma cells through ERK signaling pathway.* Int J Oncol, 2015. **46**(3): p. 1275-85.

424. Dargel, C., et al., *T Cells Engineered to Express a T-Cell Receptor Specific for Glypican-3 to Recognize and Kill Hepatoma Cells In Vitro and in Mice.* Gastroenterology, 2015.

425. But, D.Y., C.L. Lai, and M.F. Yuen, *Natural history of hepatitis-related hepatocellular carcinoma.* World J Gastroenterol, 2008. **14**(11): p. 1652-6.

426. de Oliveria Andrade, L.J., et al., *Association between hepatitis C and hepatocellular carcinoma.* J Glob Infect Dis, 2009. **1**(1): p. 33-7.

427. Koike, K., *Hepatitis C virus contributes to hepatocarcinogenesis by modulating metabolic and intracellular signaling pathways.* J Gastroenterol Hepatol, 2007. **22 Suppl 1**: p. S108-11.

428. Pawlotsky, J.M., *Pathophysiology of hepatitis C virus infection and related liver disease.* Trends Microbiol, 2004. **12**(2): p. 96-102.

429. Dustin, M.L., et al., *Identification of self through two-dimensional chemistry and synapses.* Annu Rev Cell Dev Biol, 2001. **17**: p. 133-57.

430. Wu, Y., et al., *Transforming binding affinities from three dimensions to two with application to cadherin clustering.* Nature, 2011. **475**(7357): p. 510-3.

431. Huang, J., et al., *The kinetics of two-dimensional TCR and pMHC interactions determine T-cell responsiveness.* Nature, 2010. **464**(7290): p. 932-6.

432. Liu, B., et al., *Accumulation of dynamic catch bonds between TCR and agonist peptide-MHC triggers T cell signaling.* Cell, 2014. **157**(2): p. 357-68.

433. Huppa, J.B., et al., *TCR-peptide-MHC interactions in situ show accelerated kinetics and increased affinity.* Nature, 2010. **463**(7283): p. 963-7.

434. Adams, J.J., et al., *T cell receptor signaling is limited by docking geometry to peptide-major histocompatibility complex.* Immunity, 2011. **35**(5): p. 681-93.

435. Jiang, N., et al., *Two-stage cooperative T cell receptor-peptide major histocompatibility complex-CD8 trimolecular interactions amplify antigen discrimination.* Immunity, 2011. **34**(1): p. 13-23.

436. Engels, B., et al., *Relapse or eradication of cancer is predicted by peptide-major histocompatibility complex affinity.* Cancer Cell, 2013. **23**(4): p. 516-26.

437. van Loenen, M.M., et al., *Extracellular domains of CD8alpha and CD8ss subunits are sufficient for HLA class I restricted helper functions of TCR-engineered CD4(+) T cells.* PLoS One, 2013. **8**(5): p. e65212.

438. Stephan, M.T., et al., *T cell-encoded CD80 and 4-1BBL induce auto- and transcostimulation, resulting in potent tumor rejection.* Nat Med, 2007. **13**(12): p. 1440-9.

439. Plas, D.R. and M.L. Thomas, *Negative regulation of antigen receptor signaling in lymphocytes.* J Mol Med (Berl), 1998. **76**(8): p. 589-95.

440. Johnson, K.G., et al., *TCR signaling thresholds regulating T cell development and activation are dependent upon SHP-1.* J Immunol, 1999. **162**(7): p. 3802-13.

441. Sathish, J.G., et al., *Loss of Src homology region 2 domain-containing protein tyrosine phosphatase-1 increases CD8+ T cell-APC conjugate formation and is associated with enhanced in vivo CTL function.* J Immunol, 2007. **178**(1): p. 330-7.

442. Lugli, E., M. Roederer, and A. Cossarizza, *Data analysis in flow cytometry: the future just started.* Cytometry A, 2010. **77**(7): p. 705-13.

443. Ayyoub, M., et al., *An immunodominant SSX-2-derived epitope recognized by CD4+ T cells in association with HLA-DR.* J Clin Invest, 2004. **113**(8): p. 1225-33.

444. Oelke, M., et al., *Generation and purification of CD8+ melan-A-specific cytotoxic T lymphocytes for adoptive transfer in tumor immunotherapy.* Clin Cancer Res, 2000. **6**(5): p. 1997-2005.

445. Manz, R., et al., *Analysis and sorting of live cells according to secreted molecules, relocated to a cell-surface affinity matrix.* Proc Natl Acad Sci U S A, 1995. **92**(6): p. 1921-5.

446. Assenmacher, M., et al., *Sequential production of IL-2, IFN-gamma and IL-10 by individual staphylococcal enterotoxin B-activated T helper lymphocytes.* Eur J Immunol, 1998. **28**(5): p. 1534-43.

447. Hodge, G., et al., *Garlic compounds selectively kill childhood pre-B acute lymphoblastic leukemia cells in vitro without reducing T-cell function: Potential therapeutic use in the treatment of ALL.* Biologics, 2008. **2**(1): p. 143-9.

448. Horton, H., et al., *Optimization and validation of an 8-color intracellular cytokine staining (ICS) assay to quantify antigen-specific T cells induced by vaccination.* J Immunol Methods, 2007. **323**(1): p. 39-54.

449. McKinnon, L.R., et al., *Characterization of a human cervical CD4+ T cell subset coexpressing multiple markers of HIV susceptibility.* J Immunol, 2011. **187**(11): p. 6032-42.

450. Shulman, N., et al., *Development of an automated analysis system for data from flow cytometric intracellular cytokine staining assays from clinical vaccine trials.* Cytometry A, 2008. **73**(9): p. 847-56.

451. Tanaka, Y., et al., *Multiparameter flow cytometric approach for simultaneous evaluation of proliferation and cytokine-secreting activity in T cells responding to allo-stimulation.* Immunol Invest, 2004. **33**(3): p. 309-24.

452. Chattopadhyay, P.K. and M. Roederer, *Cytometry: today's technology and tomorrow's horizons.* Methods, 2012. **57**(3): p. 251-8.

453. Ornatsky, O., et al., *Multiple cellular antigen detection by ICP-MS.* J Immunol Methods, 2006. **308**(1-2): p. 68-76.

454. Newell, E.W., et al., *Cytometry by time-of-flight shows combinatorial cytokine expression and virus-specific cell niches within a continuum of CD8+ T cell phenotypes.* Immunity, 2012. **36**(1): p. 142-52.

455. Bendall, S.C., et al., *Single-cell mass cytometry of differential immune and drug responses across a human hematopoietic continuum.* Science, 2011. **332**(6030): p. 687-96.

456. Evavold, B.D. and P.M. Allen, *Separation of IL-4 production from Th cell proliferation by an altered T cell receptor ligand.* Science, 1991. **252**(5010): p. 1308-10.

457. Evavold, B.D., et al., *Separation of T helper 1 clone cytolysis from proliferation and lymphokine production using analog peptides.* J Immunol, 1993. **150**(8 Pt 1): p. 3131-40.

458. Evavold, B.D., et al., *Complete dissection of the Hb(64-76) determinant using T helper 1, T helper 2 clones, and T cell hybridomas.* J Immunol, 1992. **148**(2): p. 347-53.

459. Kersh, G.J. and P.M. Allen, *Essential flexibility in the T-cell recognition of antigen.* Nature, 1996. **380**(6574): p. 495-8.

460. Sloan-Lancaster, J. and P.M. Allen, *Altered peptide ligand-induced partial T cell activation: molecular mechanisms and role in T cell biology.* Annu Rev Immunol, 1996. **14**: p. 1-27.

461. Persaud, S.P., et al., *High-affinity T cell receptor differentiates cognate peptide-MHC and altered peptide ligands with distinct kinetics and thermodynamics.* Mol Immunol, 2010. **47**(9): p. 1793-801.

462. Baker, B.M., et al., *Conversion of a T cell antagonist into an agonist by repairing a defect in the TCR/peptide/MHC interface: implications for TCR signaling.* Immunity, 2000. **13**(4): p. 475-84.

463. Ding, Y.H., et al., *Four A6-TCR/peptide/HLA-A2 structures that generate very different T cell signals are nearly identical.* Immunity, 1999. **11**(1): p. 45-56.

464. Garboczi, D.N., et al., *Structure of the complex between human T-cell receptor, viral peptide and HLA-A2.* Nature, 1996. **384**(6605): p. 134-41.

465. Degano, M., et al., *A functional hot spot for antigen recognition in a superagonist TCR/MHC complex.* Immunity, 2000. **12**(3): p. 251-61.

466. Kalergis, A.M. and S.G. Nathenson, *Altered peptide ligand-mediated TCR antagonism can be modulated by a change in a single amino acid residue within the CDR3 beta of an MHC class I-restricted TCR.* J Immunol, 2000. **165**(1): p. 280-5.

467. Thomson, C.T., et al., *A structural difference limited to one residue of the antigenic peptide can profoundly alter the biological outcome of the TCR-peptide/MHC class I interaction.* J Immunol, 2001. **166**(6): p. 3994-7.

468. Schreiber, G. and A.R. Fersht, *Energetics of protein-protein interactions: analysis of the barnase-barstar interface by single mutations and double mutant cycles.* J Mol Biol, 1995. **248**(2): p. 478-86.

469. Garcia, K.C., et al., *The molecular basis of TCR germline bias for MHC is surprisingly simple.* Nat Immunol, 2009. **10**(2): p. 143-7.

470. Piepenbrink, K.H., et al., *Fluorine substitutions in an antigenic peptide selectively modulate T-cell receptor binding in a minimally perturbing manner.* Biochem J, 2009. **423**(3): p. 353-61.

471. Lechler, R., R. Batchelor, and G. Lombardi, *The relationship between MHC restricted and allospecific T cell recognition.* Immunol Lett, 1991. **29**(1-2): p. 41-50.

472. Amrolia, P.J., et al., *Allorestricted cytotoxic T cells specific for human CD45 show potent antileukemic activity.* Blood, 2003. **101**(3): p. 1007-14.

VITA

Timothy T. Spear attended the University of Notre Dame in Notre Dame, Indiana where he earned a Bachelor's of Science, *cum laude*, in Biological Sciences. After graduation, Timothy matriculated into the Loyola University Chicago Stritch School of Medicine MD/PhD Program. After completing two years of medical school, he began his graduate education in the Integrative Cell Biology Program under the mentorship of Dr. Michael I. Nishimura.

Timothy's dissertation work on the impact of altered TCR-pMHC interactions on antigen recognition and T cell function was supported by a Predoctoral Ruth L. Kirchstein National Research Service Award from the National Cancer Institute of the National Institutes of Health. After completion of his graduate studies, Timothy will pursue a one year Postdoctoral Fellowship in the lab of Michael I. Nishimura before returning to medical school.